UNIVERSITY OF CANTERBURY

Department of Physics and Astronomy

CHRISTCHURCH NEW ZEALAND

Ca II absorption in the circumstellar disk of β Pictoris and 51 Ophiuchi

---

A thesis submitted in
partial fulfilment of the
requirements for the degree of
Master of Science in Astronomy
at the
University of Canterbury

by
Stephen Persson

University of Canterbury
1998

Ca II absorption in the circumstellar disk of β Pictoris and 51 Ophiuchi

Stephen I. Persson

MSc Thesis 1998
Supervisor: Dr William Tobin

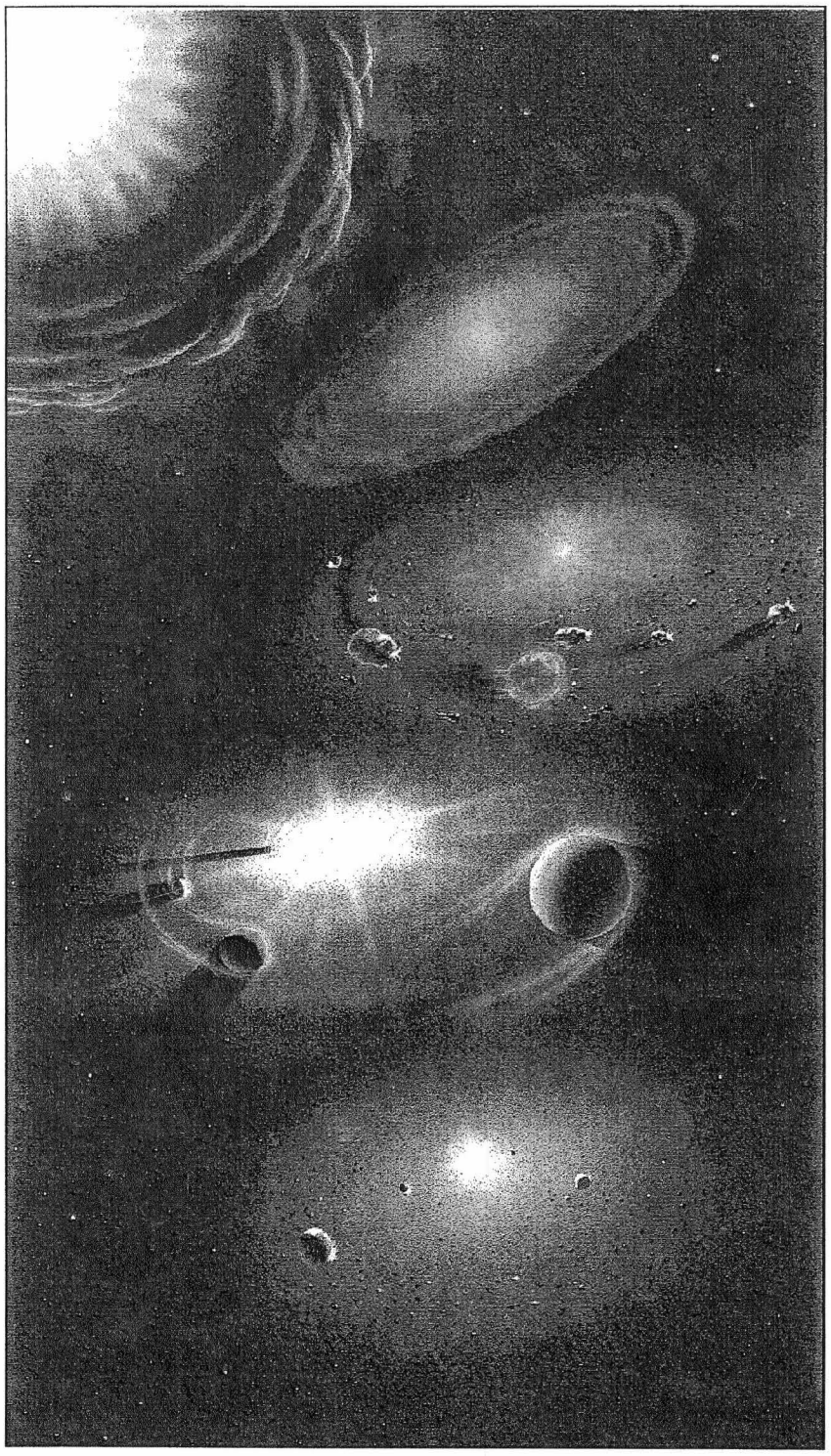

He, who through vast immensity can pierce, See worlds on worlds comprise one universe, Observe how system into system runs, What other planets circle other suns... May tell us why Heaven has made us as we are.
ALEXANDER POPE (1688-1744) English poet.

Abstract

Presented here are the results of observations made of the Ca II H and K absorption lines in the spectrum of the A5V star β Pictoris, a probable protoplanetary system surrounded by an edge-on circumstellar disc. At times when β Pic was low in the sky, observations were carried out on 51 Ophiuchi, which has been suggested as a possible β Pic like system. Observations were made to further test the Falling Evaporating Bodies (FEB) scenario.

Significant activity was again observed, with the bulk of the spectra containing absorptions in a number of different velocity regimes, confirming the clumpy nature of the orbiting gas. The variable absorptions include a very large number of blue-shifted features generally at low relative velocities, appearing to persist for timescales of many days. A large number of long-lived low velocity red-shifted features were also observed, probably largely due to the increased instrumental stability that has been achieved.

Many features were observed to last over timescales far longer than the crossing time, in the line of sight, of a single body, lending support to the idea of an infalling stream of comet-like bodies. These long-lived features were generally limited to the low-velocity features (LVFs), although a high-velocity feature at $\sim$200 kms^{-1} was observed to last over 2 days.

Simultaneous observations of the H and K lines have been able to confirm the presence of very high-velocity features (HVFs) lasting only the duration of a single exposure. These are also found to be narrow, shallow features rather than the broader features previously observed and predicted for HVFs.

Despite the simultaneity of the H and K line observations, no unequivocal case was observed of the H line being stronger than the K line, as has been suggested when the ionic cloud occults the region of the star rotating away from us.

The FEB scenario well explains most of the variable features observed. However the long-lived HVFs seen (as well as some of the LVFs) are not well explained by this scenario. The ability for a feature to last long periods of time requires either a very large number of comets on similar orbits to pass the line of sight continuously for many days or even weeks, otherwise another explanation other than solely the FEB scenario is required to explain the origin of the variations.

Contents

Figures

Tables

Chapter 1

Aims of this Thesis

This thesis looks into the variations of the Ca II H and K absorption lines in the spectrum of the A5V star β Pictoris, a probable protoplanetary system surrounded by an edge-on circumstellar disc. At times when β Pic was low in the sky, observations were carried out on 51 Ophiuchi, which has been suggested as a possible β Pic like system. The absorptions show two types of features in β Pic: Deep, narrow, low-velocity features (LVFs) lasting days or even weeks, and shallow, broad, high-velocity features (HVFs) lasting only a matter of hours. Many aspects of these absorptions can be explained in terms of the Falling Evaporating Bodies (FEB) scenario; however their observational characterisation is far from complete and the FEB hypothesis is not definitively established. This thesis follows the same approach and addresses the same questions in Lagrange *et al.* 'The β Pictoris circumstellar disc XXI. Results from the December 1992 spectroscopic campaign' [1] and in Orlon Petterson's 1996 MSc work [2], but with the following improvements:

- The installation of a focal reducer and Series 200 CCD system (with a larger SITe chip), which allowed simultaneous observations to be made of the H and K lines.

- Since there were no changes to the spectrograph settings, the profiles of the underlying wide photospheric Ca II absorptions were recorded with improved stability. The instrumental response was calibrated against the profiles of the absorptions in Canopus, which is angularly close to β Pic. The measurement of the broad, shallow HVFs in particular was improved.

- The wavelength scale was determined more accurately. In consequence it became possible (i) to remove the ambiguity between broad features centred near zero velocity and simultaneous red and blue-shifted narrower features flanking the stable circumstellar absorption, and (ii) to test the stability of the sharp, central circumstellar feature which has recently been hypothesised as due to the passage of Ca II ions through a distant circumstellar ring of neutral hydrogen.

- The almost doubled quantum efficiency of the SITe chip allowed shorter exposures and thus better characterisation of short timescale features.

- Sequential H and K observations made in 1992 suggest that the variable H absorptions can be stronger than the K ones. At first glance, this is surprising because the K line has the larger oscillator strength, but the phenomenon has been explained theoretically as deriving from the Doppler shifting of the underlying photospheric continuum due to the rotation of the star. However, since the fast features evolve on a timescale similar to the exposure durations with the PM3000 CCD system, the reality of the phenomenon was not clearly established. It was hoped that simultaneous H and K spectra would provide confirmation of the effect (if real) and this

was a principal goal of this thesis. Simultaneous H and K observations also result in more credible determination of covering factors.

- The spectra are less subject to disturbance by cosmic rays because the SITe chip is thinned.

Chapter 2

Review of β Pictoris

β Pictoris has in the past decade been the subject of many investigations since its discovery as an IR excess star by the IRAS satellite as a result of observations made in 1983 [3]. A circumstellar disk of dust was then successfully imaged by Smith and Terrile in 1984 [4], showing a disk viewed nearly edge-on from Earth and extending out 400AU. As a result of these and other observations β Pictoris has been intensely studied as the most promising candidate for an extra-solar planetary system orbiting a main sequence star.

2.1 Evolutionary Status and Stellar Parameters

Table 2.1 shows the stellar parameters of β Pictoris.

The evolutionary status of the star is an important parameter to evaluate. The age of the system has been studied but no definitive conclusion has been reached. The availability now of the Hipparcos satellite data has meant a lower limit has now been set on the age of the system, as well as the distance, luminosity, position on the HR diagram, and circumstellar extinction being more precisely evaluated. During the three years the Hipparcos satellite was in operation β Pic has was observed 102 times. The data obtained have quite considerably changed our understanding of the physical parameters of the star and its disk [5].

After reduction the final parallax of β Pic is:

$$\pi_{\mathrm{Hipp}} = 0.05187 \pm 0.00051 \text{ arc-seconds}$$

This value being somewhat smaller than the values previously derived, means β Pic is more distant and luminous than originally thought.

As a result of the greater accuracy in the distance determinations of β Pic, as well as the advances made in the sensitivity of detectors, the circumstellar disk has been detected extending out to 1400AU, compared to 400AU when first detected in 1984.

Using the observed visual magnitude of V = 3.85, also derived from the Hipparcos data [5], the revised absolute and bolometric magnitudes obtained are:

$$M_V = 2.42 \pm 0.03 \text{ and } M_{\mathrm{bol}} = 2.43$$

In order to more precisely evaluate the age of the system it is necessary to place β Pic on the HR diagram in which stellar evolutionary tracks are present. Taking an effective

Name	β Pictoris
HR	2020
HD	39060
RA (1997.5) h m s	5 47 13.6
Dec (1997.5) ° ′ ″	−51 04 02
Galactic longitude (2000)	258.37
Galactic latitude (2000)	−30.61
Spectral type	A5V
Parallax ″ (Hipparcos)	0.05187 ± 0.00051
Distance pc	19.28 ± 0.19
T_{eff}	8200 K
Age	>0.8 10^7 yrs
Mass	1.7-1.8 $M_\odot$
$\log g$	4.38 (if M=1.75 $M_\odot$)
Absolute magnitude, M_V	2.42
Bolometric magnitude	2.43
V	3.85
$B-V$	+0.17
$U-B$	+0.10
$R-I$	+0.16
PM (α) ″ yr^{-1} (Hipparcos)	+0.00465 ± 0.00053
PM (δ) ″ yr^{-1} (Hipparcos)	+0.08196 ± 0.00061
RV (kms^{-1})	+20V
$v \sin i$ (kms^{-1})	139

Table 2.1: β Pic parameters. Note that the Bright Star Catalogue gives RV = 20V? This is assumed to have been constant in reductions and analysis, but if indeed variable, this would affect the reference profile division.

temperature of 8200K [6], the new position of β Pic, bearing in mind the uncertainties of the stellar parameters, can be considered to be if not on the ZAMS then extremely close to it. Being so close to, or on the ZAMS, also removes the need for the 0.5 magnitude extinction originally thought necessary to account for the difference between the average magnitude of a A5V star and that of β Pic.

Fig.2.1 shows the evolutionary tracks, and position of β Pic on the HR diagram. From comparison with these evolutionary tracks the mass of β Pic is 1.7-1.8 $M_\odot$, with the estimate of gravity ($\log g$) being 4.38 if M=1.75$M_\odot$ (This is estimated after having inferred the radius from the luminosity, $\log(L_*/L_\odot)$ and the effective temperature) [5].

With these stellar parameters taken into account the pre-main sequence evolutionary tracks can be used to estimate the age of the system, by its position on the HR diagram. According to the computations of Palla and Stahler (1993) [7], the duration of the pre-main sequence phase for a star with mass of the order of that of β Pic is at least 0.8×10^7 years, as can be seen in Fig.2.1(b) [5]. A useful (in terms of planetary formation), upper

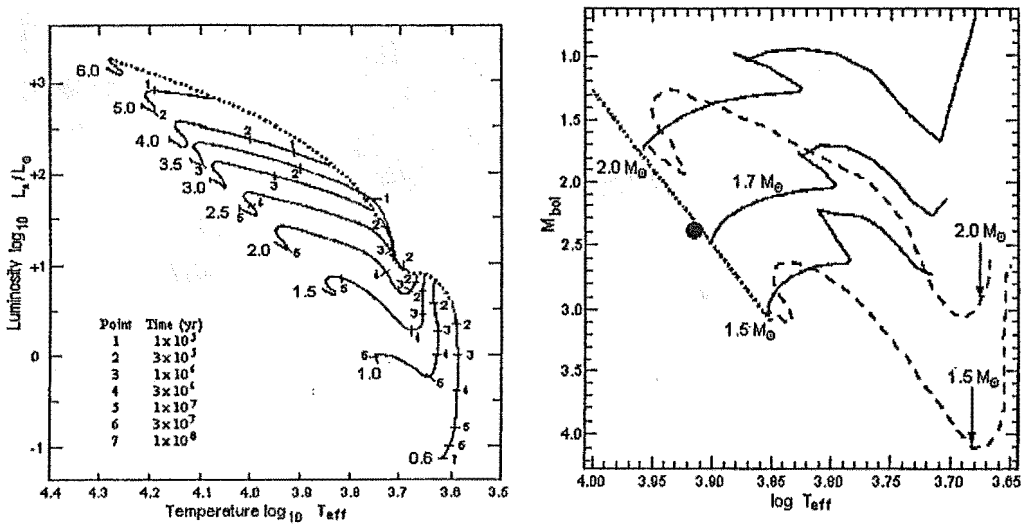

(a) (b)

Figure 2.1: Plot (a) shows evolutionary tracks in the HR diagram, labelled by their solar masses, for pre-main sequence stars. The tick marks along the track indicate evolutionary times, starting from the birth-line (dotted curve) and ending at the ZAMS [7]. Plot (b) shows the region of (a) corresponding to the position of β Pic, shown as the large circle. The solid lines are the post-main sequence tracks [8], and the dashed lines the pre-main sequence tracks [7].

limit of the age is not possible since the star is so close to the ZAMS. A limit can however be obtained using the Geneva isochrones [8], for the time taken before a β Pic mass star evolves off the ZAMS. This gives an upper limit for the age of β Pic as $\sim 30 \times 10^7$ years.

2.2 Model of the circumstellar disk

One of the most exciting and largely unexpected discoveries of the IRAS, is that many nearby stars are surrounded by disks of dust and material much like what is assumed to have been present within our own solar system. With the exception of β Pic, this dust can only be seen at infrared wavelengths and not in the visible.

The infrared radiation is a result of particles with sizes of a millimetre of more, in contrast to the dust particles within the interstellar medium with sizes of the order of a few microns. These particles absorb the visible and ultraviolet radiation from the star causing the particles to heat up. This warming up releases large amounts of infrared radiation easily detected by IRAS.

Fig. 2.2 shows the circumstellar dust disk (in false colours) as seen in the near-infrared (1.25μm) as obtained on January 6th, 1996, using the ESO 3.6m telescope at La Silla, Chile.

Modelling of the IRAS data suggests that these disks are made up of particles ranging

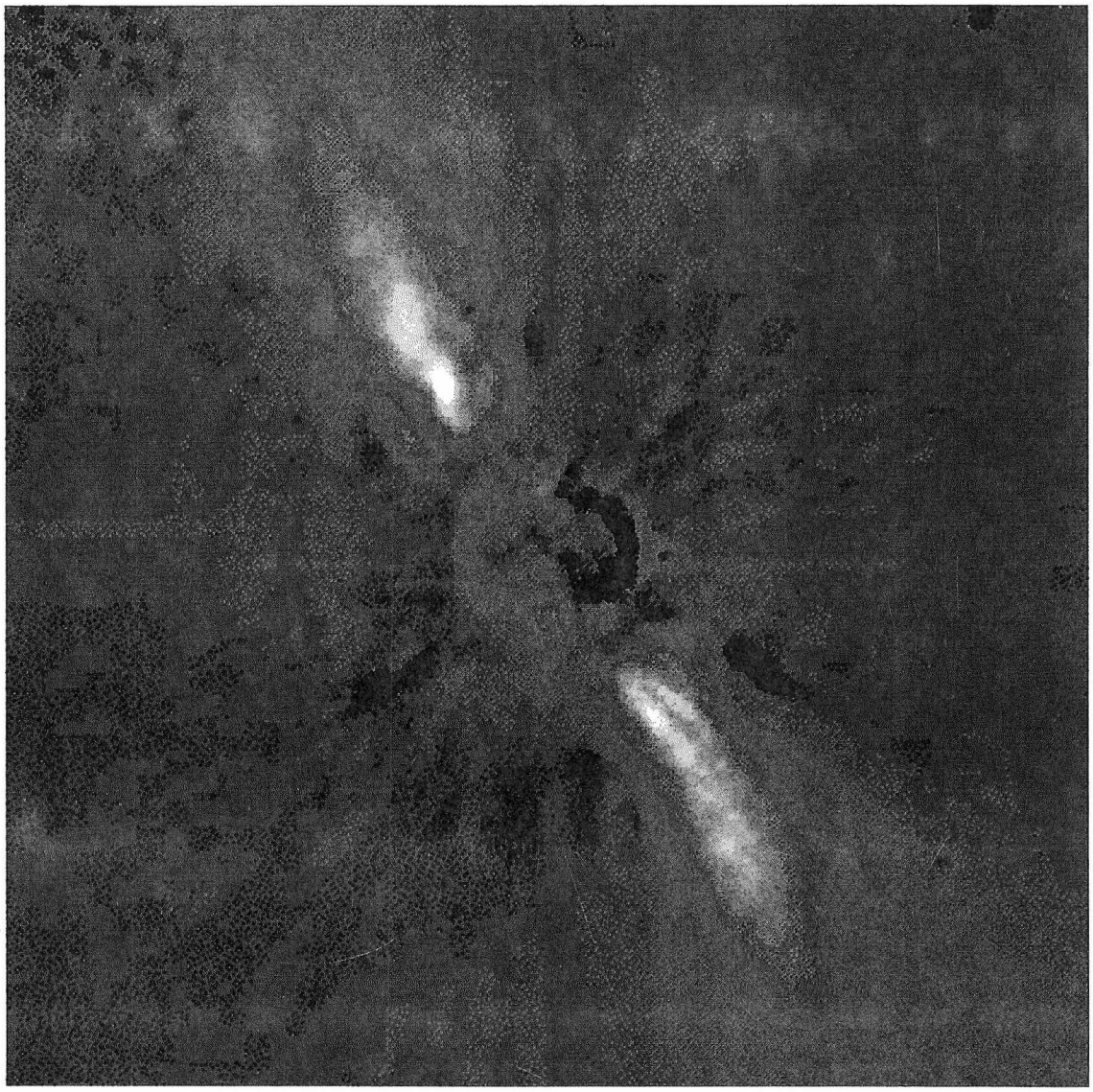

Figure 2.2: Near-infrared corongraphical image of the circumstellar disk of β Pic (J.-L. Beuzit *et al.* Grenoble Obs.,ESO); obtained from the Internet, `http://antwrp.gsfc.nasa.gov/apod/image/9711/beta-pic_eso_big.jpg`

in sizes from $\sim 1\mu$m up to bodies as large as comets and asteroids, with some arguments suggestive of larger planet-sized objects (Section 2.3).

As can be seen in Fig. 2.2, β Pic contains an outer surrounding disk of material but an inner region that is largely clear of material, extending out to ~30AU, roughly the size of our solar system. Within this region silicate emissions have been detected by observations from 8-12μm, suggesting particle sizes of $\leq 1\mu$m [9] near the star.

Within the region from ~30-100AU smaller particles near 1μm size are required for thermal modelling of the region [10]. However, since the ratio of dust to gas is observed to be small, the lifetime of these particles against being swept away must be small due to the high radiation pressure and the low probability of collisions due to their small size [11].

Larger and more stable particles are therefore required to obtain the orbital stability of the gas, with the smaller particles being continually replenished by collisions of these larger particles. The presence of silicate grains ($\leq 3\mu$m) has been confirmed by 8-13μm spectroscopy [12]. The disk is therefore a relatively evolved one in which larger objects such as comets and planetesimals may already exist [13] or even fully-formed planets [14].

In the outer region of the disk from ~100-1000AU, polarisation observations (~17±3%), as well as the known colours of the disk, suggest the presence of large ($\geq 10\mu$m) dust grains. This grain size is typical of that of cometary dust rather than interstellar dust, indicating that the dust is in some way processed (accretion or conversely evaporation), rather than resulting from stellar formation processes. Additional support for the presence of comets also comes from the detection of carbon monoxide absorption in the UV [15].

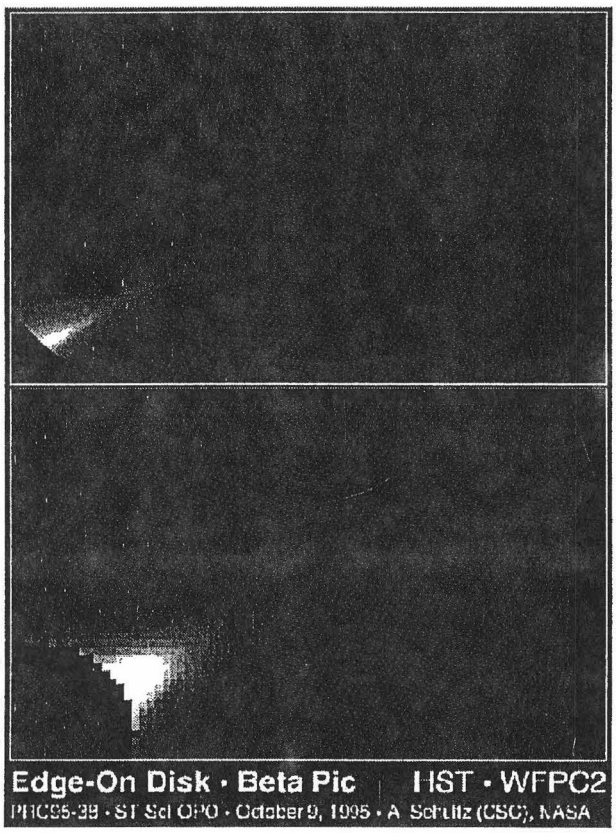

Figure 2.3: Circumstellar disk as seen at visible wavelengths by the HST (above) and from the University of Hawaii 2.2m telescope (below).

Fig. 2.3 shows the disk at visible wavelengths as seen from space and the ground. HST observations of the disk have put estimates of the disk width at no more than one billion miles (~11AU), about 1/4 of that of the ground observation shown in the same figure. The thinner, more flattened disk implies the disk has had more time to settle and is therefore older than previously estimated, increasing the likelihood of comet-sized or larger bodies, or even a fully-developed planetary system, formed through accretion within the disk.

Fig. 2.4 shows a model of how the circumstellar disk around β Pic is expected to be, as inferred from GHRS spectra [16]. The insert at the upper left shows the outer part of the disk, lying exterior to the central gaseous region. The small green rectangle marks the region expanded in the large drawing.

It is thought that the infalling streams of gas shown are the result of evaporation of dust in the disk. If the outer disk is similar to the Kuiper belt around our own Sun, then the observed gas is thought to originate from comet-like bodies entering the inner regions of the circumstellar disk and being evaporated by the increased temperature and radiation. This explanation, termed the grain evaporation hypothesis [17] is the most commonly held explanation as the source of the inner dust and gas. The radiation pressure from

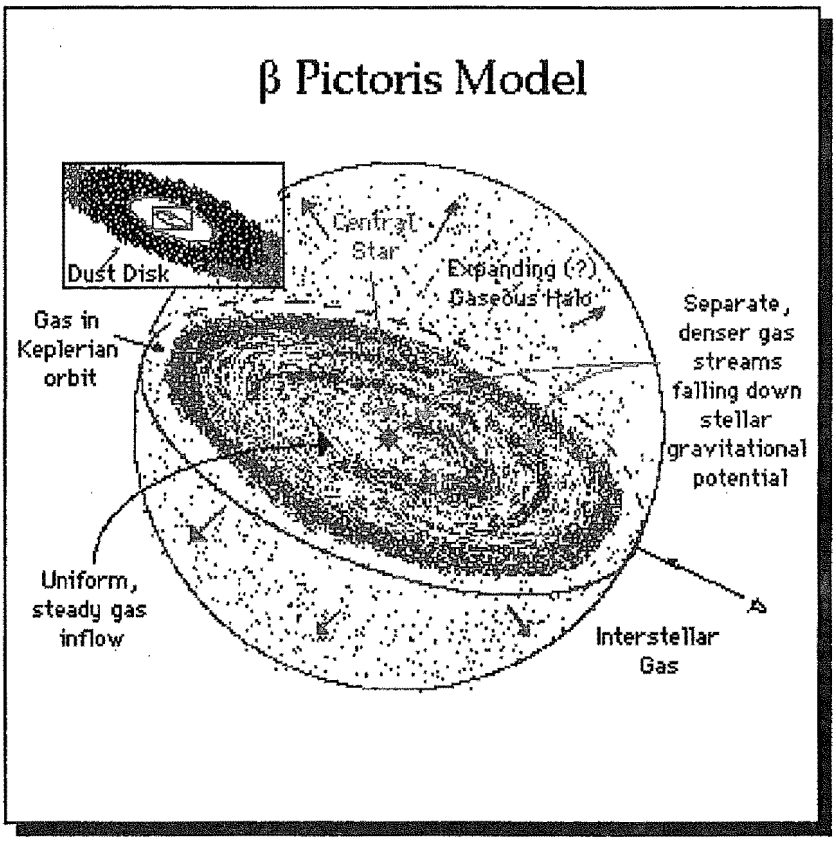

Figure 2.4: Model of the inner region (~2AU) of the circumstellar disk surrounding β Pic.

the star is then thought to blow the ions out, although some mechanism is required to slow down this outflow velocity in order to produce the stable circumstellar feature in the spectrum of β Pic. This is thought to be a ring of neutral hydrogen farther than 0.5AU from the star, causing collisions with the Ca II ions, such that the transit time through this ring is ~1000 days [18]. This process ensures there is a constant supply of material to maintain the stable absorption lines observed. It does also however suggest that while the circumstellar feature is stable over short timespans it may in actual fact vary over a period of years.

The bulk of absorption within the spectra of β Pic is due to the circumstellar gases [19], with a temperature $T_K \leq 4200K$ and a typical density $n_H \simeq 10^5 cm^{-3}$ [20] which contains a mass of less than 1% of our own planetary system, rising to $n_H \geq 10^6 cm^{-3}$ [17] in the inner parts of the disk.

The most abundant circumstellar gases so far observed are Na I, Fe I, C I, Fe II, Mn II, Ca II, Zn II, Mg II and Al III. These gases all display not only a stable circumstellar absorption feature, but also variable features caused by the infalling streams of gas being evaporated off the comet-like bodies passing into our line of sight.

By examining the Na I and Ca II lines, the absorptions can be ruled out as interstellar on four grounds:

1. For stars at a similar distance, the interstellar K line is far weaker than that observed in β Pic.

2. A ratio of $n(\mathrm{Ca\,II})/n(\mathrm{Na\,I}) \gg 1$ can be found only in interstellar lines that arise in high-velocity gas. This is in contrast to the case for β Pic.

3. β Pic contains narrow Fe II absorption lines for which no interstellar absorption has yet been detected.

4. The circumstellar K line is fully saturated, yet no interstellar K line has ever been observed to be saturated.

The different gases within the circumstellar disk are observed to have stable absorptions within different regions, depending on the intensity of the radiation. This is especially apparent for Ca II and Na I. The Na I is found in the outer region containing nearly all the mass of the disk, but where Ca II is under-abundant by a factor of $\sim 10^4$ [17]. The Ca II ions have been determined to lie in an inner region much closer to the stellar surface ($\sim$0.4AU), and are prevented from leaving the system by collisions creating a stable gaseous torus around the star producing the circumstellar feature seen in spectroscopic observations [15].

The large amount of observations made of the dust and gases within the circumstellar disk of β Pictoris lead to the modelling of the disk parameters, which raises many questions regarding the age of the system. Is the observed disk a remnant of a proto-stellar system, or is it more advanced to the extent that it may already possess a well-formed planetary system?

2.3 Planets within the circumstellar disk

There are four main arguments for the existence of planets within the circumstellar disk of β Pic:

1. The dust distribution falls (Fig. 2.2) within the inner $\sim$100AU of the disk, which is proposed to have been swept clear by a planet. After planets form they are expected to rapidly clear the visible disk in their vicinity. An alternative explanation for this clear region, however, is the result of the sublimation of ices.

2. Fig. 2.2 and Fig. 2.5 show examples of an image where it is evident that there is warp in the inner part of the disk, on both sides of the star. If the warp was present when the star was formed, it would long since have flattened out, unless it is produced and maintained by the gravitational pull of a planet. This planet would lie within the inner clear region of the disk, although it is not possible to see the planet directly because of the overwhelming brightness of the star [21]. The planet could be anywhere from 1/20th to 20$\times$ the mass of Jupiter depending on its distance from the star. If the suspected planet were as far from β Pic as Jupiter is from our Sun, it would also have about the same mass as Jupiter. The planet must also be moving along an inclined orbit ($\sim 3^\circ$) within 20AU of the star, which is typical of the inclinations of the orbits of planets within our own solar system. A closer

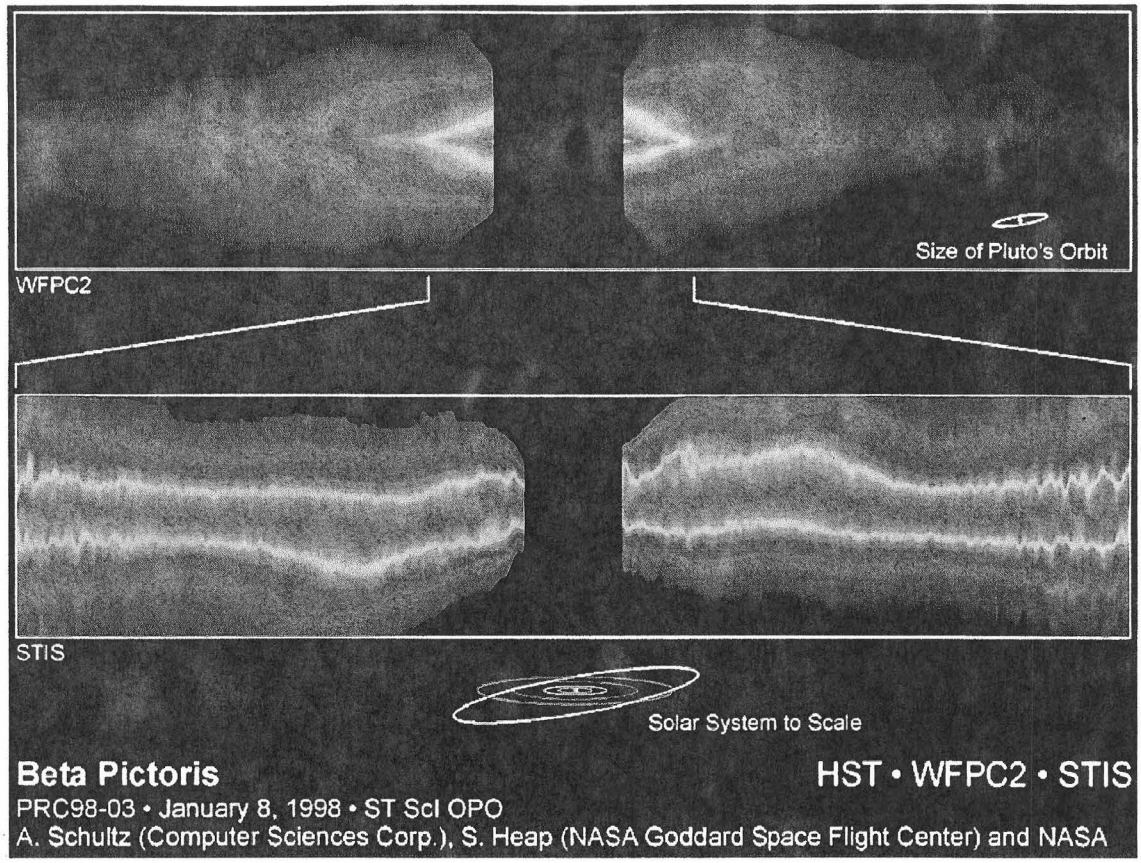

Figure 2.5: Visible light (false-colour enhanced) images taken from NASA's HST showing clearly the warping of the circumstellar disk. The top figure shows the full extend of the disk spanning 1500AU. The bottom figure is a more detailed image of the inner region of the disk, reaching into $\pm$15AU, showing the presence of a warp, supporting the presence of one or more planets orbiting the star. Images courtesy of Al Schultz (CSC/STScI and NASA) and Sally Heap (GSFC/NASA).

inspection of the circumstellar disk also reveals that the two sides are not mirror images of each other, but rather one is brighter, longer and thinner. A gravitational perturbation is also thought responsible for this asymmetry [22].

Fig. 2.5 (*Upper image*) also shows a warp in the outer disk (top right). This has been proposed to have been caused either by the passing of a nearby star, although the favoured idea is that β Pic may have a companion brown dwarf which may be orbiting at large distances from the star [23].

3. Variable circumstellar absorption features are observed to be mostly red-shifted implying a preferential infall direction of the comet-like bodies. Simulations, as detailed in Sections 4.2 and 4.3, have produced synthetic spectra much like observed, supporting a preferential infall direction. Secular resonances from neighbouring planets are proposed to be able to align the orbits of the comets to produce the type of features observed [24].

4. Photometric measurements of β Pic have shown variations in the brightness of the star with no colour dependency [25]. On short time-scales several peculiar variations

were observed, although the variations were regular, symmetrical and centred on a particular day for which the variations reached $0^m.04$. These variations could be explained by an occultation of the star by a planet or group of planets which cover an area slightly bigger than Jupiter [25].

Chapter 3

51 Ophiuchi

Since the 1980s and the discovery of IR excesses around a number of nearby A-F type stars, much work has been done to find other stars similar to β Pic with the existence of a circumstellar dust disc. The presence of an unusual IR excess around 51 Oph was first noted by Coté & Waters (1987) [26]. Of the 101 stars they looked at, 51 Oph was the only Be star to show clear evidence of a circumstellar disk.

Infrared excesses of $3^{m}.67$, $4^{m}.82$ and $4^{m}.33$ at 12μm, 25μm and 60μm respectively, have been measured for 51 Oph [26] which are a factor of 3-4 times larger than those typically found for B8-B9 emission stars. Attempts to explain the observed *far*-IR colours of 51 Oph have resulted in disk temperatures of 200-300K. This temperature however is far too low to explain the *near*-IR excesses, which requires disk temperatures of the order of 1000K [27]. Assuming the dust particles are in thermal equilibrium, the range of temperatures can be used to estimate the size of the disk to be of the order of 400AU [27].

Recent IUE observations of the star 51 Oph [28], have shown there to be variable accreting gas present within the system with relative speeds of up to $100\,\mathrm{kms}^{-1}$. The electron number density of the circumstellar disc was also found to be comparable to that of β Pic. In addition to the cooler gases present in the disk, absorptions from Al III, Si IV and C IV are present, providing evidence for collisional ionisation ($T_{\mathrm{exc}} > T_{\mathrm{eff}}$) of the circumstellar gas as found in β Pic.

Of the variable absorptions identified, they were found to evolve on timescales of $\sim$1 week, comparable to long-term changes with β Pic, but no short-term variations were observed [28].

The inclination of the 51 Oph system is able to be estimated from the Hα profiles, the presence of accreting gas and the transient mass ejection. Double-peaked Hα emission is typically present superimposed on the photospheric absorption (broadened by stellar rotation). By comparing the red (R) and visual (V) emission peaks, estimates can then be made of the inclination angle [29]. This method suggests the circumstellar disk is inclined within 10-15° of the equatorial plane.

The data collected implies that the 51 Oph system is very similar to the β Pic system both in its constituents and orientation, and possibly similar in its evolutionary state, making it a good candidate as a β Pic type protoplanetary system.

51 Oph is separated from β Pic by $\sim$12 hours, making it easily observable during times when β Pic is too low in the sky. For this reason 51 Oph was selected to make observations on during the times of the year when β Pic was unobservable.

Table 3.1 [30] shows the stellar parameters of 51 Oph.

Name	51 Ophiuchi
HR	6519
HD	158643
RA (2000) h m s	17 31 24.8
Dec (2000) ° ′ ″	−23 57 44.3
Galactic longitude (2000)	2.52
Galactic latitude (2000)	+5.34
Spectral type	B9.5Ve
Parallax ″ (Hipparcos)	0.00765 ± 0.00087
Distance pc	25
T_{eff}	10480 K
Mass	$1.64 M_{\odot}$
$\log g$	4.1 (if $M=1.64\,M_{\odot}$)
V	4.81
$B-V$	+0.00
$U-B$	−0.06
$R-I$	+0.02
PM (α) ″ yr^{-1} (Hipparcos)	+0.00491 ± 0.00082
PM (δ) ″ yr^{-1} (Hipparcos)	−0.02590 ± 0.00051
RV (kms^{-1})	−20V
$v \sin i$ (kms^{-1})	267

Table 3.1: 51 Ophiuchi parameters.

Chapter 4

Falling Evaporating Bodies Scenario

The Falling Evaporating Bodies (FEB) scenario was formed to explain the variations seen in the absorption profiles in some of the metallic lines in the spectrum of β Pic. It was suggested that the variations were caused by the presence of comet-like bodies orbiting the star and passing into our line of sight to the star. The edge-on orientation of the disk greatly increases the possibility of an orbiting comet being seen in the line of sight, since it is assumed that they are confined to the plane of the circumstellar disk. The idea is by no means unreasonable given the age of the system, and that observations of our own solar system show craters and remnants indicative of the intense bombardment of comets and meteorites during the early stages of planetary formation. β Pic being a relatively young protoplanetary system is therefore thought likely to be undergoing the same intense bombardment of comets and planetesimals, making the idea of the FEB scenario very appealing.

A model of this FEB scenario was developed by Beust *et al.* (1989) [31] to explain the cause of these variations. It proposes that the evaporation of dust off the cometary body, and the subsequent evaporation and ionisation of the dust by the stellar flux, is what causes the variation in the line profiles. It is observed that these features are predominantly red-shifted, implying the orbiting material is moving towards the star when it crosses the line of sight. Hence the model is termed the Falling Evaporating Bodies scenario.

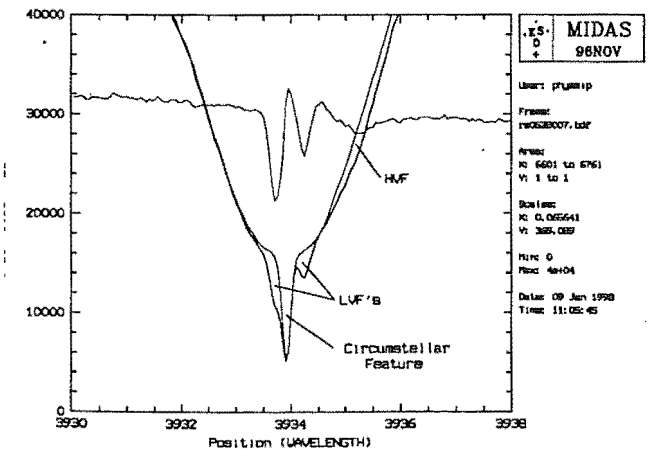

Figure 4.1: Type of variations seen in the absorption profile of the Ca II K line. The red line shows a profile with little or no absorption, while absorptions are present in the spectrum plotted in black. The blue trace shows the result of dividing the absorbed spectrum by the unabsorbed one.

For the purpose of this thesis the line variations are only observed for Ca II ions although the line profiles of Mg II, Fe II and Al III (accessible only from satellites) also exhibit temporally varying absorption features, for which comet-like bodies have been interpreted as the cause.

Fig. 4.1 shows the type of variations observed in the Ca II K line. Three features are observed in addition to the broad photospheric absorption:

- Central circumstellar feature at the radial velocity of the star.
- Low velocity features, LVFs,

which tend to feature deep and narrow absorption lines, close to the central peak, lasting from hours to months.

- High velocity features, HVFs, which are broad shallow lines away from the central peak varying rapidly (in hours).

All three of these features can be clearly seen in Fig. 4.1. The red line represents the K line reference profile, and the blue line the divided profile, clearly showing the two LVFs and the HVF.

4.1 Modelling of the Falling Evaporating Bodies Scenario

Testing and modelling of the FEB scenario has been performed by Beust *et al.* (1989) [31] who simulated the evaporation of comet-like bodies grazing the star on parabolic orbits with a periastron of 5-30 stellar radii. It is assumed that the observed variable features result from atoms or ions evaporated from the nucleus of the infalling body, and moving in the surrounding gas. In a first approximation there are three kinds of interactions that affect these ions:

- gravitation - towards star
- radiation pressure - away from star
- collisions.

The effect of stellar winds can be neglected: stellar winds in normal A5 stars are usually very weak, and their effect on ions or atoms can be assumed to be negligible.

Since the ions ejected from a infalling body move at relatively small velocities, it can be assumed that in the absence of any other interactions they would move towards the star at the free-fall velocity. However the stellar flux induces a force on the atom or ion, (radiation pressure), that is in all cases larger than the effects of gravity, by a factor of up to 77.2 [32] (these factors have been revised downwards by considerable amounts by Lagrange *et al.* (1998)[18]) for Ca II, and hence the cloud of ions is repelled away from the star, as is normally seen with an orbiting comet.

Collisions are essentially a force opposed to velocity, and being completely random it is assumed that any directional variations will have an average value of zero. It is also assumed here that the surrounding gas that the ions are moving in, is also produced by the infalling comet, and is falling with it. This is a necessary assumption for producing red-shifted features, since any motion in a gas that was not infalling (at low velocities) would only produce blue-shifted features.

By taking typical values from Comet Halley of parameters such as particle size and ejection velocity, simulations have been carried out, that enable a far greater understanding of the physical conditions needed to reproduce the observed effects within β Pic. By altering parameters such as gas production rates, orbital inclinations and perihelions, synthetic

spectra have been produced in good agreement with the observed spectra.

The only simulations that produced results similar to those observed were within an orbital angle, (the angle between the axis of orbit and the line of sight), of $\phi = -150 \pm 10°$, and between perihelion values of q = 5-30 R_*. Variations within the limits of these values were able to produce the various different absorptions present in the spectra.

All synthetic spectra shown in the following sections have been reproduced from Beust *et al.* (1990)[32].

4.2 Low-velocity features

The LVFs are hypothesised to be the result of comet-like bodies passing into the line of sight at distances of the order of 20-30 R_*.

Simulations such as those in Fig. 4.2 well model the actual spectra. From these it is found that the gas production rate of Ca II ions must be $\sim 15 \times 10^{33}$ atoms/s, and a total mass production rate of $\sim 0.010 \times 10^{10}$kg/s. Assuming this to be the case, kilometre-sized comet-like bodies are needed to produce this amount of gas.

Fig. 4.2 shows a simulation of the temporal evolution of the line variation caused by a kilometre-sized body, at 23.5 R_*, passing into our line of sight. The first appearance of an absorption occurs at 19H30min and by 24H0min the absorption is finished. This gives a typical time for a LVF to cross our line of sight of ~4 hours. However many of the observed LVFs can last days or even weeks. For this reason the idea of a stream of infalling comets, Fig. 4.3 [33], was proposed. Under this scenario a successive comet, not necessarily at the same perihelion, also enters our line of sight before the remnant tail of the previous comet has been dispersed. This also explains the multiple structure that can be seen in some of the absorption features.

4.3 High-velocity features

The HVFs are hypothesised to be the result of comet-like bodies passing into the line of sight at distances of the order of ~3-10 stellar radii. At distances less than ~10 R_* the radiation pressure from the star on the Ca II ions increases rapidly, 12.5 times stronger at 7 R_* than at 25 R_*, which in turn prevents the Ca II cloud around the nucleus from reaching a size large enough to produce any readily noticeable variations. However since the evaporation rate of the nucleus will increase the closer it gets to the star, this leads to a greater number of collisions with H atoms and therefore a larger cloud of ions. Fig. 4.4 shows a simulation of this scenario with the gas production rate 4 times that of the LVFs, with the other parameters remaining unchanged. This produces a synthetic spectrum which well models the observed variations.

This higher radiation pressure is also responsible for a higher ejection velocity of matter off the comet, and a higher dispersion velocity of the ions, leading to much broader profiles than those seen in the LVFs.

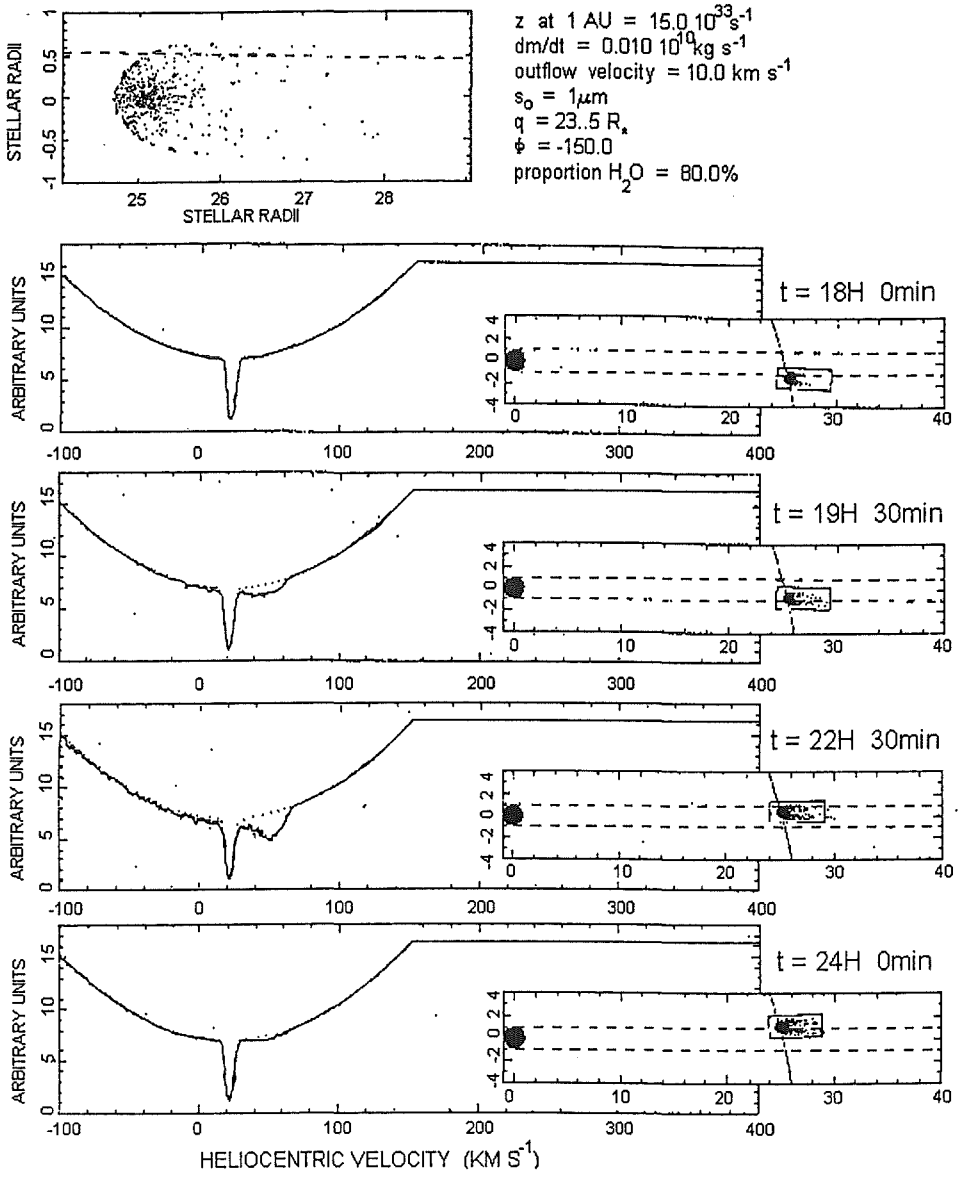

Figure 4.2: Simulations of the LVF line variations caused by a comet-like body entering and leaving our line of sight, at a distance from the star of 23.5 R_*.

The evolution time of the HVF absorptions is much shorted than that of the LVFs since they are produced closer to the star. This gives a far greater orbital velocity to the body and as such it crosses the line of sight more rapidly. The higher the red-shift of a variable feature the smaller its variation time scale is expected to be. It is therefore unlikely that another body will enter the line of sight during the crossing-time of the first body. The infalling shower of comets as proposed for the LVFs, is therefore not as likely to result in the continuous presence of HVFs.

Within a distance of $\sim 10\, R_*$ blue-shifted features should also be able to be observed. These are the result of a larger inclination angle between the axis of orbit and the line

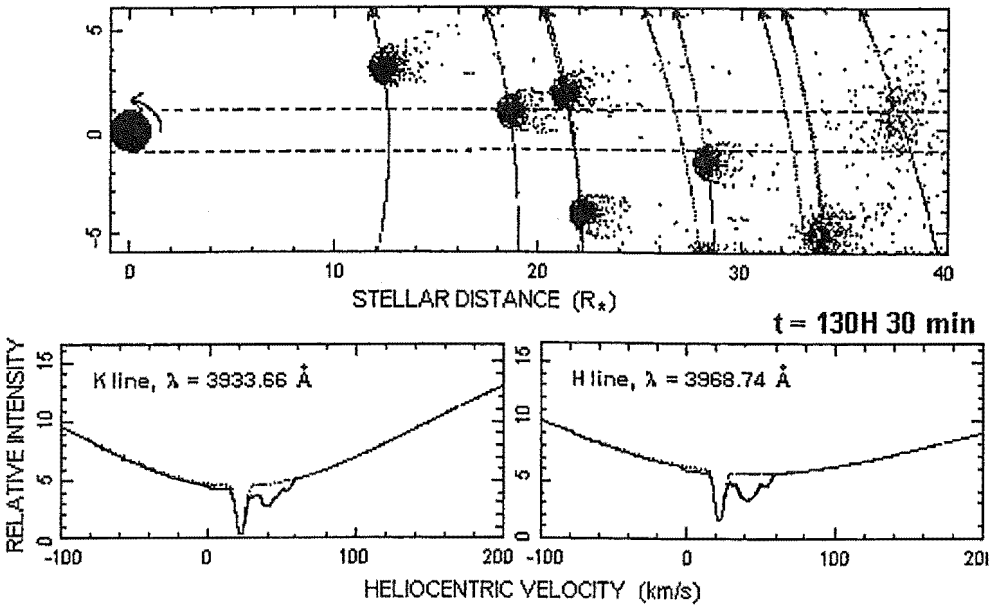

Figure 4.3: Simulation of a stream of infalling comet-like bodies. The resulting multicomponent red-shifted features are similar to those observed, and are due to the the effect of several FEBs crossing our line of sight.

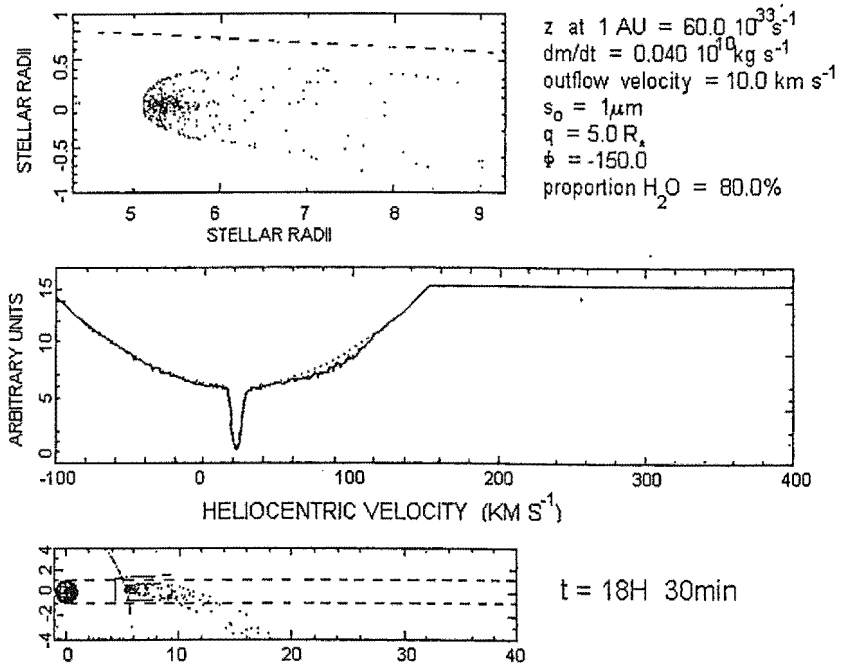

Figure 4.4: Simulations of the HVF line variations caused by a comet-like body entering and leaving our line of sight, at a distance from the star of $5\,R_*$. The comet-like body is plotted to the same scale as the one in Fig. 4.2 and is seen to be narrower, longer and more centrally condensed.

of sight (~180°)[34]. The difficulty with the blue-shifted features is that they are also produced by the ionic tail of a comet, in the case where the tail is moving towards us in the line of sight, while the head of the comet is moving away from us. The head of

the comet creates a deeper, sharper red-shifted component, with the tail broadening the absorption, and if the ejection and dispersion velocities of the Ca II off the comet are great enough, also producing "noisy" blue-shifted features.

4.4 Filling Factors

Even though a line is saturated, it does not reach zero intensity because the ionic cloud responsible for the absorption does not cover the entire stellar disk. Measurements of the Ca II H and K doublet can be used to determine the size of the ionic cloud relative to the stellar disk. This is done from simultaneous measurements of the depth of the Ca II H and K lines. For saturated lines, α, the fraction of the stellar disk being occulted, or filling factor, can be easily and well determined, but for weak and unsaturated lines only a lower limit on the size of the obscuration can be given.

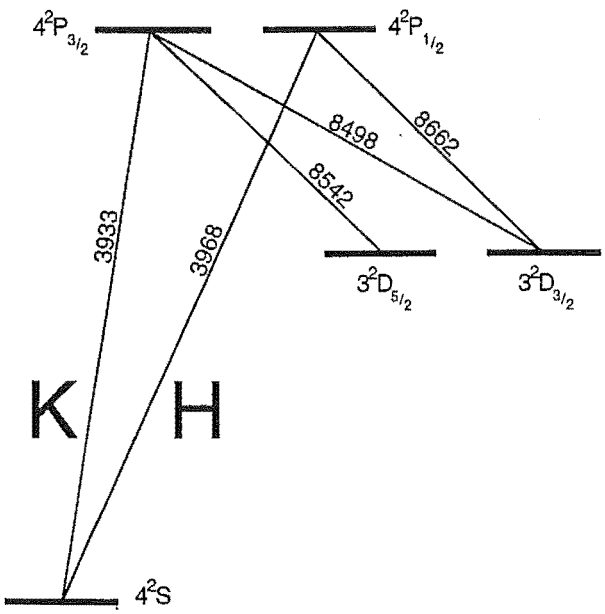

Figure 4.5: Energy levels of the Ca II H and K line. The transition wavelengths in Å are indicated.

This can be achieved because of the differing oscillator strengths of the H and K lines. The oscillator strength, also called the f value, is different for each atomic transition and is related to the atomic transition probability, which is the probability that an electron will leave one energy level and go to another [35].

Fig.4.5 shows an energy level diagram for Ca II. Ca II is particularly interesting in that the ^{2}D term is metastable, and atoms typically get there by transitions to the ^{2}P level, via either an H or K excitation, followed by an infrared cascade down to the ^{2}D level [36]. The oscillator strength for the K line (0.69), is twice that of the H line (0.344), meaning the K transition is twice as likely as the H transition, and that the strength of any K line absorption should be twice that of any H line absorption, in the case of optically thin lines.

By comparison of the H and K line variable features, information can be obtained on the possible saturation of the Ca II lines and therefore also information on the size of the absorbing clouds occulting the star. Since the flux decreases exponentially through the ionic cloud, and p_H and p_K are measurements of how much flux has been absorbed at 3968.470Å and 3933.664Å [37] respectively, we can obtain relations for p_H and p_K as functions of their optical depths τ_H and τ_K. Since the K line has twice the oscillator strength of the H line, it will also have twice the optical depth of the H line, $\tau_K = 2\tau_H$. If α is the ratio of the size of the cloud of ions to the size of the stellar disk (the so called filling factor), then the depths of the H and K line can be calculated. Assuming the stellar disk to be uniform, the flux from the whole star is F_λ, and with a cloud of ions occulting the

disk, the total transmitted flux F_t is:

$$F_t = F_\lambda(1-\alpha) + F_\lambda.\alpha.\mathrm{e}^{-\tau} \tag{4.1}$$

$$F_t = F_\lambda[1-\alpha+\alpha\mathrm{e}^{-\tau}]. \tag{4.2}$$

Therefore the depths of the H and K lines relative to the continuum can be given by:

$$p = \frac{F_\lambda - F_t}{F_\lambda} = 1-[1-\alpha+\alpha\mathrm{e}^{-\tau}] \tag{4.3}$$

$$p = \alpha \times (1-\mathrm{e}^{-\tau}). \tag{4.4}$$

In terms of the H and K lines this becomes:

$$p_\mathrm{H} = \alpha \times (1-\mathrm{e}^{-\tau}) \text{ and } p_\mathrm{K} = \alpha \times (1-\mathrm{e}^{-2\tau}) \tag{4.5}$$

where τ is the optical depth of the H line (weaker line).

Eliminating $\mathrm{e}^{-\tau}$ between these two expressions results in an expression for the filling factor α:

$$\alpha = \frac{p_\mathrm{H}^2}{2p_\mathrm{H} - p_\mathrm{K}}. \tag{4.6}$$

Theoretically, this enables α to be measured in any case. However a more illuminating approach is a graphical solution to α, as in Fig.4.6, found by plotting iso-α curves in the $(p_\mathrm{H}, p_\mathrm{K})$ plane, for differing values of the optical depth τ from optically thin lines to saturated ones. Each point between the optically thin and thick lines, is therefore a function of the optical depth and the filling factor, with each position corresponding to a unique value of the optical depth, τ, and the filling factor, α. The plots are limited by

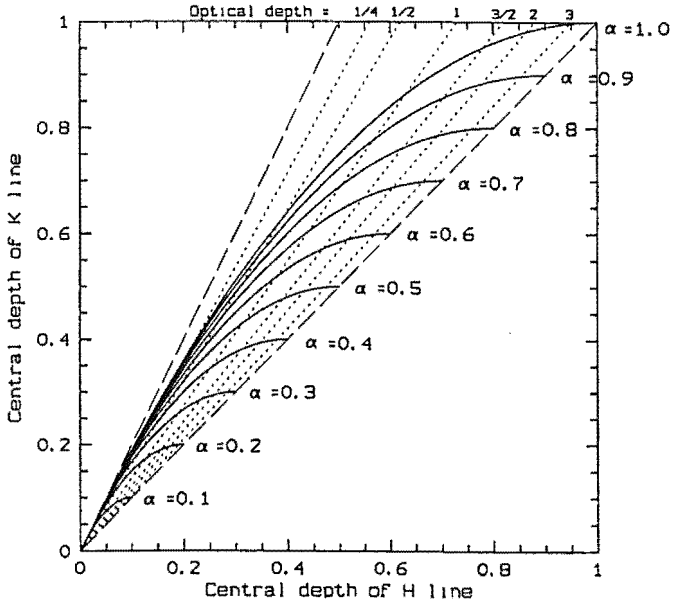

Figure 4.6: Theoretical diagram of the depths of the H and K lines, for the different values of the filling factor α. Also plotted are various values of the optical depth τ, for the region between the optically thin and optically thick lines.

the two lines corresponding to $p_K \simeq p_H$ for strong, saturated lines, and $p_K \simeq 2 \times p_H$ for weak unsaturated lines.

As Fig. 4.6 shows, α can be easily determined for saturated lines, but not so easily for unsaturated lines, because at low optical depths the iso-α lines are close together. In practice this means there is no way to be able to distinguish between weak, optically deep lines from a cloud covering a small part of the stellar surface, from optically deeper, but still weak lines from a cloud covering a smaller part of the star. Therefore when the lines are not saturated it is only possible to get a lower limit on the size of the absorbing cloud.

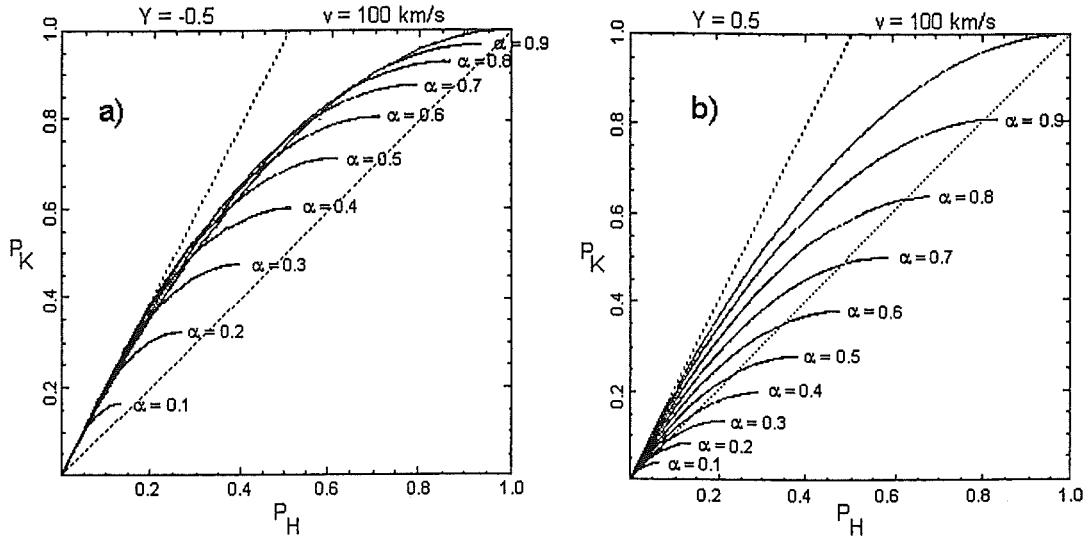

Figure 4.7: Theoretical diagram of the depths of the H and K lines, for the different values of the filling factor α, when stellar rotation is considered. Plots (a) and (b) correspond respectively to Y=-0.5 (cloud masking portion of disk rotating towards us) and Y=0.5 (cloud masking portion of disk rotating away from us).

Fig. 4.6 shows iso-α curves for the case of a non-rotating star. When consideration is made to the rotation of the star a number of differences occur as shown in Fig.4.7. Depending on which side of the star the cloud of ions is occulting, results in differences in the Doppler shifting of the H and K line wavelengths. When the cloud occults the portion of the star rotating towards us, the wavelengths are shortened, having the effect of moving the iso-α curves more towards the optically thin $p_K \simeq 2 \times p_H$ region of the graph. In the case of the cloud occulting the portion of the star rotating away from us, Doppler shifting results in longer wavelengths moving the iso-α curves more towards the saturated $p_K \simeq p_H$ region of the graph. This is of particular interest since, as can be seen in Fig. 4.7, the curves extend beyond the limit of $p_H = p_K$ therefore implying that p_H can exceed p_K despite the H line oscillator strength being only half that of the K line.

This is also shown in Fig. 4.8, which shows the evolution of the equivalent widths of the H and K line as an FEB crosses the stellar surface [38]. The two lines obviously behave differently, once again showing the peculiar situation where the strength of the H line exceeds that of the K line. No unequivocal cases of this have been observed, mainly due

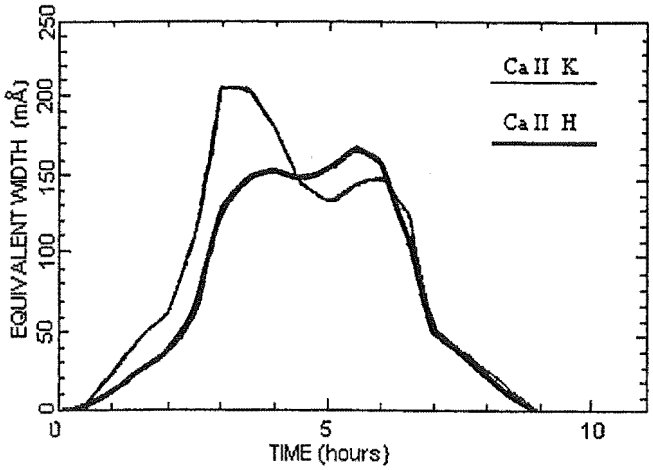

Figure 4.8: Comparison between the evolution of the H and K lines for a FEB crossing the stellar disk.

to the non-simultaneity of observations of the H and K lines. With the installation of the focal reducer and larger Series 200 CCD system to the MJUO échelle spectroscope, simultaneous observations of the H and K lines became possible allowing further testing of this scenario and confirmation, or otherwise, that the strength of the H line can, in some instances, exceed that of the K line.

Chapter 5

Previous Results

This thesis follows the same methods employed by the multi-site and multi-wavelength observing campaign performed in December 1992 [1]. This campaign coordinated high-resolution spectroscopy from ground-based observatories at differing locations, as well as with the IUE and HST, to further characterise the variable absorptions seen in the spectrum of β Pictoris. The MJUO was one of the observatories participating in this campaign. As a result of this a further 4 years of observations were made from MJUO, shown in Orlon Petterson's MSc thesis [2].

The results summarised below can be found in greater detail in Lagrange *et al.* (1996) [1], Petterson (1996) [2] and Petterson & Tobin (1998) [39].

5.1 Line variations

Observations confirmed the existence of the three types of features outlined in Chapter 4; circumstellar, low-velocity and high-velocity features.

Almost all the spectra obtained showed obvious Ca II absorption in addition to the stable photospheric and circumstellar lines.

The period from November 1994 - December 1996 was one of near-continuous absorption activity. Of the 313 spectra obtained, 690 variable absorptions were measured in 307 spectra with multiple absorptions present in most cases.

When considering features that last for several hours as a single event the 225 hours of absorptions observed can be summarised as:

- 15 blue-shifted events.
- 10 20-40 $\mathrm{km\,s^{-1}}$ red-shifted events $\Rightarrow$ $\sim$50 composite events per year.
- 35 40-100 $\mathrm{km\,s^{-1}}$ red-shifted events $\Rightarrow$ $\sim$500 composite events per year.
- 10 $\geq$100 $\mathrm{km\,s^{-1}}$ red-shifted events $\Rightarrow$ $\sim$400 events per year.

A large number of LVFs with red-shifts of $\sim$5-20 $\mathrm{km\,s^{-1}}$ were observed which are certainly suggestive of a year-long stream of infalling bodies crossing the line of sight at a distance of a few tens of stellar radii. This is apparent by the generally-slow evolution of the absorption depths and equivalent widths of the features, which can be explained from an averaging effect due to several bodies. It has been estimated that during this

time an average of 4-5 comet-like bodies were within the line of sight at any given time. If a crossing time through the line of sight of 12 hours in assumed, one obtains a rate of ~3300 individual objects per year traversing our line of sight.

Intermediate velocity features (~30-60 km s^{-1}) are also present lasting for as long as days, or in some cases appearing and disappearing within an hour. This can also be interpreted in terms of streams of infalling bodies although at these velocities the streams would be shorter lived.

HVFs (~70-90 km s^{-1}) are seen to persist for several hours, but their appearance and disappearance is rapid and they are not seen on successive nights. Much higher-velocity features ($\geq$100 km s^{-1}) occur occasionally, sometimes only in a single spectrum. The absorptions are broad and shallow making them difficult to observe, especially in the H line.

One particularly interesting feature observed was that on the 9th June 1995 [2]. It is a narrow, high-velocity feature that is very short lived, having dispersed again in the space of half an hour (time between exposures). It is the only such feature observed, so the reality of this must be questioned, since it is possible that it may have resulted from dust within the spectrograph.

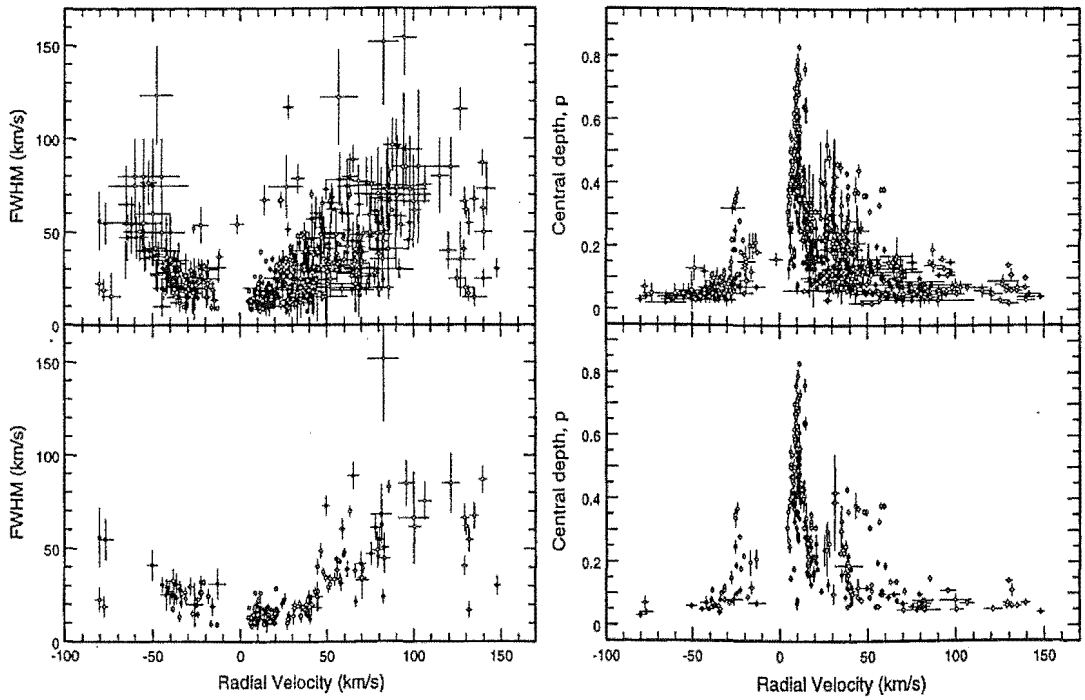

Figure 5.1: *Upper panels:* The (a) FWHM and (b) central depths of the 690 variable absorptions detected in 1994-1996 are plotted as functions of their radial velocity with respect to the circumstellar feature. The H line is plotted as a filled symbol and the K line as an open symbol. *Lower panels:* As above but restricted to only well-defined single absorptions.

Fig. 5.1(a) shows plots examining the correlation between the FWHM and the radial velocity with respect to the circumstellar feature. The general correlation is confirmed, and is also found to apply to the blue-shifted features. The upper panel shows all absorptions observed while the lower panel shows only the well-defined single absorptions. Significant spread is apparent in both plots; in particular the range of FWHMs is large for the highest-velocity features.

Fig. 5.1(b) shows plots examining the correlation between the central depth of the absorptions and the radial velocity with respect to the circumstellar feature. The deepest features can be seen to be present only at very low-velocities, and the highest-velocity absorptions are always shallow. At any velocity, especially lower velocities, a range of depths is possible.

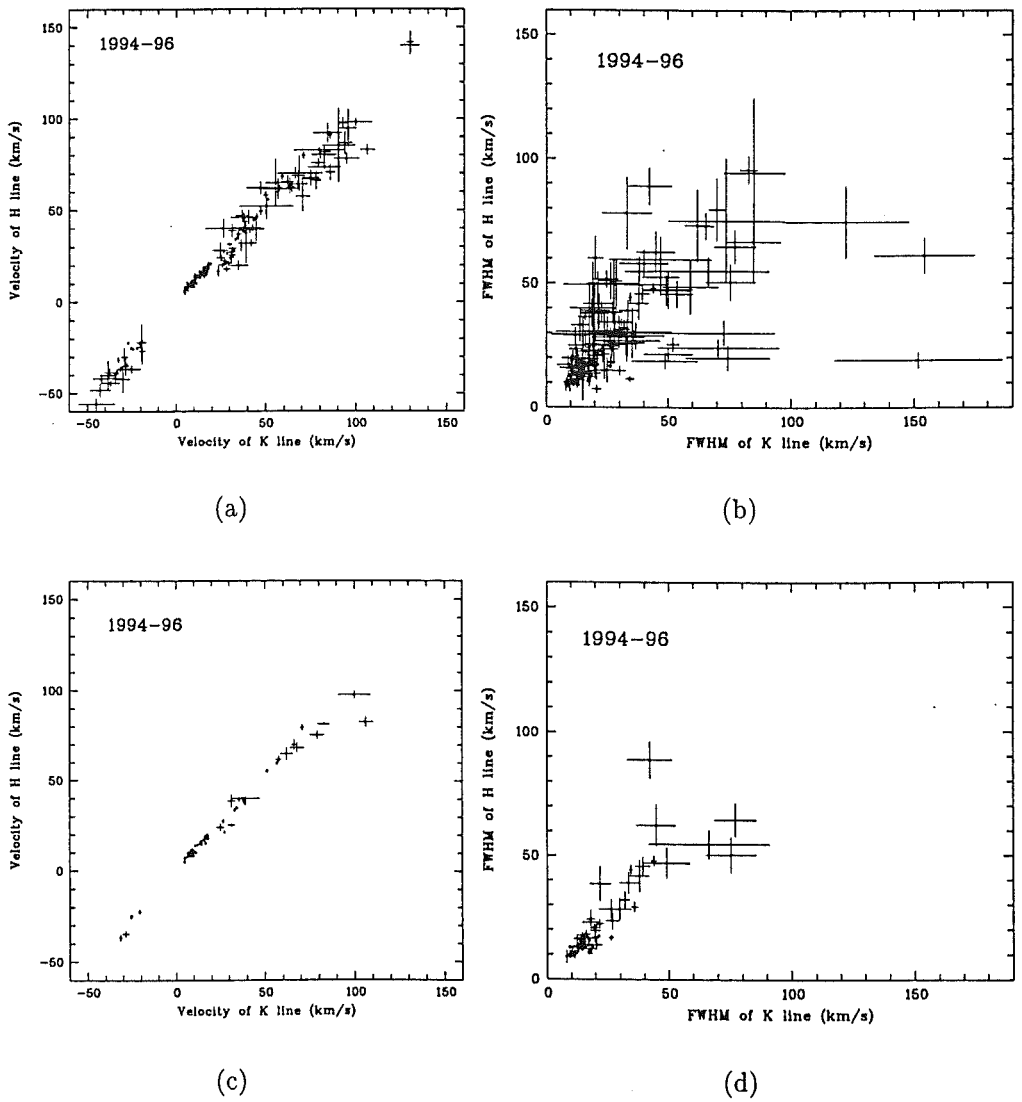

Figure 5.2: Plots (a) and (b) show the comparison between the velocity and FWHM respectively, for all sequential observations of the H and K lines. Plots (c) and (d) show the same comparisons limited to good absorptions for both the H and K lines.

Figs. 5.2(a) and (c) show the correlation found between the H and K line absorption velocities, for the 1994-1996 observations. A strong correlation is observed, especially for (c) containing only those absorptions classified as good singles or blends, despite the H and K line observations being sequential and differing by at least half an hour (time between exposures). It does however confirm that an absorption feature observed at a particular velocity in either the H or K line should also be observable at the same velocity in the other.

Figs. 5.2(b) and (d) show the correlation found between the FWHM of the H and K line absorptions, for the 1994-1996 observations. A stronger correlation is observed in case (d) where only the absorptions classified as either good singles or blends are shown. This suggests that in addition to the velocities of features being the same in the H and K lines, and FWHM may also be the same in each line.

5.2 Filling Factors

One of the interesting results of the 1992 campaign was the discovery, in *sequential* observations, that the Ca II H line (which has the lower oscillator strength) was in fact sometimes stronger than the K line.

Fig. 5.3 shows a plot of the central depth of the H line (p_H) versus the central depth of the temporally-closest K line (p_K) for the 1994-1996 observations. In only one case

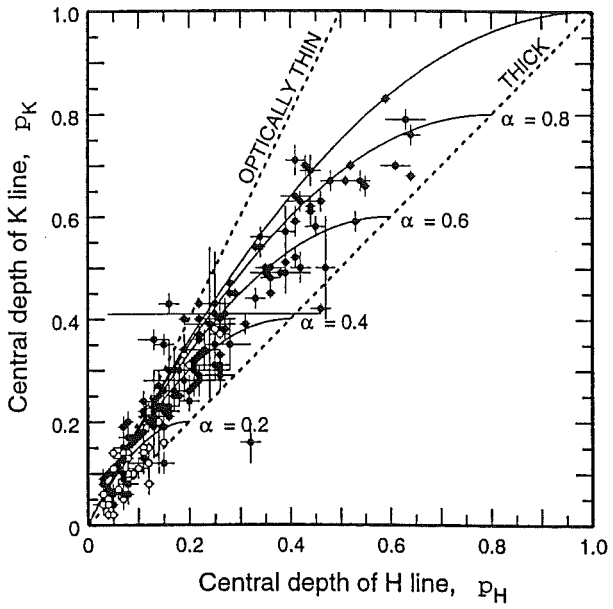

Figure 5.3: Plot of the central depth of the H line versus the central depth of the temporally-closest K line, for the 1994-1996 observations. The dashed lines correspond to slopes of 1 and 2 for optically thick and thin absorptions respectively. LVFs ($<40\,\mathrm{km\,s^{-1}}$) are plotted as filled circles, and HVFs ($>40\,\mathrm{km\,s^{-1}}$) as open circles. The full lines represent various values of the covering factors α.

is p_H formally greater than p_K, and this corresponds to a blue-shifted feature. For the

next ranked cases where $p_H > p_K$ they correspond to fast-evolving HVFs, where the non-simultaneity of the observations produces a large part in the differences between the H and K lines. From the observations made during these campaigns, no unequivocal cases of H absorptions deeper than K have been found.

By comparing the points on Fig. 5.3 with the iso-α lines for the differing fractions of the stellar disk being occulted (refer Section 4.4), it becomes apparent that the LVFs covering factors can be significant, often larger than 50% and in some cases approaching unity (100%), implying the cloud of ions is covering a significant fraction of the entire stellar disk. In the case of the HVFs however the filling factors are only occasionally as big as 0.4, and usually less, implying that typically, only a small portion of the stellar disk is covered.

5.3 Summary

- Variable absorptions fall into two velocity regimes: *low-velocity features* (LVFs) with red-shifts less than a few tens of kilometres per second, and *high-velocity features* (HVFs) with red-shifts up to $\sim 100\,\mathrm{km\,s^{-1}}$.
- LVFs tend to be narrower, deeper, frequent long-lived absorptions covering large proportions of the stellar disk.
- HVFs tend to be broader, shallower, rarer, short-lived absorptions covering less than 40% of the stellar disk.
- FWHMs and velocities are often the same for the H and K lines.
- No features have been definitively detected for which the H line is stronger than the K line.

Chapter 6

Observations

For the requirements of this thesis observations were primarily carried out of β Pictoris. However at times during the year β Pic became too low in the sky to be observable, even though it is a circumpolar star from MJUO. During these times observations were made of 51 Ophuchius, taking advantage of the 12 hour difference in the right ascension.

It was also decided that several observations should be made of the standard star Canopus, separated by $\simeq 26'$ from β Pic, so as to monitor and correct for any changes in the β Pic profile that could be caused by instrumental fluctuations. This is further outlined in Section 7.2.

6.1 Telescope and Échelle Spectrograph

Observations were made using the Mount John University Observatory (MJUO) McLellan 1-metre telescope. The telescope is a Dall-Kirkham type optical system with interchangeable secondary mirrors enabling the telescope to be used in either a f/8 or f/13.5 cassegrain configuration. For use with the MJUO échelle spectrograph the telescope was used with the f/13.5 secondary. In addition, a correcting lens at the front of the spectrograph case brings the telescope beam to f/10 in order to match with the focal ratio of the spectrograph's collimator mirror. This is necessary to ensure optimal light usage is obtained. The échelle spectrograph is located at the cassegrain focus of the telescope.

The échelle spectrograph is a high resolution spectrograph designed to give a high dispersion, that is a few nanometres per millimetre on the échellogram. This is obtained by working in high orders ($n = 23 - 75$), but is limited to fairly bright stars since there needs to be enough radiation to be spread out so broadly and thinly; however, the high dispersion does mean that a wealth of detail appears in the spectrum, and finer features can be seen that would not be visible at lower dispersion [40]. The spectrograph is a copy of the Harvard College Observatory échelle spectrograph.

Detailed working of the MJUO échelle spectrograph is described by Hearnshaw (1977,1978) [41] [42]. Simply, however, light passing through the spectrograph slit falls on a collimator mirror which provides a parallel beam of light onto the échelle grating, which disperses the light into the high orders required. The dispersed spectra are then fanned into a two-dimensional stack by an order-separating cross grating. The camera mirror then takes the fanned spectra and brings them into focus on the focal plane to be recorded by the detector.

All user adjustments are carried out by a collection of micrometers on the exterior of

the spectrograph. Adjustment of the micrometers enables the spectrograph to be correctly focussed, and to locate the region of the spectrum required for the observations. Internally the spectrograph consists of a 79 groove mm^{-1} échelle grating with a blaze angle of $\theta_B = \tan^{-1} 2 = 63°26'$. The spectrograph has a typical resolving power of R = 5.4×10^4, giving a dispersion of $\sim$1.7Åmm^{-1} at 5000Å; and R = 2.9×10^4, corresponding to $\sim$2.0Åmm^{-1} in the ultra-violet, at the Ca II lines (Refer Section 7.1).

For the purpose of this thesis, a focal reducer was used in the spectrograph, located at the front of the CCD chip. With the focal reducer and new Series 200 CCD detector system, it was possible to observe the H and K lines simultaneously and oversampling was reduced. Fuller details of the focal reducer can be found in Section 6.3.

With the Ca II lines being in the blue/ultra-violet region of the spectrum, a blue cross-grating was installed to maximise the efficiency of transmission of blue light through the spectrograph.

The collimator focus is set so that the spectrograph entrance slit is at the focal point of the collimator mirror. This corresponded to a collimator micrometer setting of 635. This value remains constant for the year and does not need to be checked on a nightly basis.

The slit width was set to correspond to $\simeq$2.05 arc-sec irrespective of the seeing conditions. This corresponded to a slit width of $\simeq100\mu$m and a micrometer setting of 438. The slit length was set to a value of $\simeq$2.07mm, corresponding to a micrometer setting of 280. The slit position micrometer was set to 250, corresponding to a shift of the slit by $\simeq$2.55mm from the nominal position.

By using the thorium lines and the known wavelengths of the Ca II H and K lines, the remaining settings were used to position of H and K lines in the desired area of the chip. The only real consideration made here was in the positioning of the lines to avoid a corrupt column of pixels in the Series 200 CCD chip. The cross-grating micrometer is used to alter the angle at which the cross-grating is mounted and hence the orders that fall on the chip. Using the PM3000 CCD (see Section 6.2) this was set to 1.521, then adjusted to 1.517 with the Series 200 CCD.

The échelle tilt micrometer changes the angle of the camera mirror in such a way to adjust the position along the orders on the chip. When using the PM3000 CCD without the focal reducer the micrometer settings used were 477 and 386 for the H and K lines respectively. With the installation of the focal reducer these settings changed slightly to 465 and 362. When using the Series 200 CCD and focal reducer together both the H and K lines could be observed simultaneously at a micrometer setting of 375.

In order to obtain the correct focus of the spectrograph, light was passed from the thorium arc, through an entrance slit of $\simeq50\mu$m, corresponding to a micrometer setting of 458. By narrowing the slit (from 100μm), finer lines were observed making the focusing procedure easier. The spectrograph was adjusted to give the maximum sharpness, ie smallest FWHM, of the observed lines. This was achieved by moving the camera mirror by means

Internal Settings	Smooth-fielding filter	1mm BG39
	Cross-grating	Blue
	Collimator focus	635
External Settings	Slit width micrometer	438
	Slit position micrometer	250
	Slit height micrometer	280
PM3000 CCD	Cross-grating micrometer	1.521
	Echelle tilt - H line	477
	- K line	386
	Camera focus micrometer	975
PM3000 CCD + focal reducer	Cross-grating micrometer	1.521
	Echelle tilt - H line	465
	- K line	362
	Camera focus micrometer	960
Series 200 CCD + focal reducer	Cross-grating micrometer	1.517
	Echelle tilt	375
	Camera focus micrometer	787

Table 6.1: Typical initial settings of the MJUO échelle spectrograph.

of a micrometer. For use with the PM3000 CCD without the focal reducer the best focus was at a micrometer setting of 975. With the focal reducer installed this changed to 960. When using the Series 200 CCD and focal reducer together the sharpest focus was at a micrometer setting of 787.

Note: When adjusting the micrometers the settings were always approached from lower numbers. By rotating the dials in one direction only to a particular setting it was hoped that any backlash in the micrometers would be avoided.

Table 6.1 shows the typical initial settings of the échelle spectrograph.

For smooth fielding of the CCD a blue filter (BG39) was inserted behind the entrance slit to block out scattered light at longer wavelengths from the tungsten lamp. Since the tungsten lamp is much brighter at longer wavelengths, this is an important step which reduced the inter-order background by a factor of $\sim$1.6, and improves the contrast between the smooth field and scattered light by over 50%.

6.2 MJUO CCD systems

During the course of this thesis two CCD systems were used. The first system used was the Photometrics 3000 CCD camera purchased in December 1988 from Photometrics Ltd of Tucson, USA. The second system used was the Photometrics Series 200 CCD camera purchased in August 1996. Due to various initial problems with this camera and its vacuum however, it was not able to be used on the telescope until April 1997.

	PM3000	Series 200
Date Acquired	December 1988	April 1996
Operational software	FORTH command language	Digital Optics V for windows
Chip	TH7882CDA	SITe SI-003AB
Pixel Size	23μm	24μm
Number of Pixels	384 × 576	1024 × 1024
Chip size	0.9 × 1.3 cm	2.5 × 2.5 cm
Peak Quantum Efficiency	40%	73%
Metachrome II coating	Yes	Yes
Operational temperature	−110°C	−100°C

Table 6.2: Comparison of MJUO CCD systems.

Table 6.2 compares the two CCD systems.

6.3 Focal Reducer

The principal motivation for the installation of the focal reducer was so that together with the larger Series 200 CCD chip, simultaneous observations of the Ca II H and K lines would be possible. The scientific interest of this is outlined in Section 4.4. In addition to this, the focal reducer results in less pixel oversampling, which was experienced with the previous system, and which added extra read-out noise to the spectra with no gain in resolution.

The focal reducer is essentially a demagnifying collection of four lenses, designed to demagnify the image by a factor of ~1.5, allowing $1.5^2 = 2.3$ times greater spectral coverage. A schematic diagram of the focal reducer is shown in Fig 6.1, which also shows the location of the focal reducer within the spectrograph, just in front of the cryostat entrance window, in order to keep the size of the lenses to a minimum.

The focal reducer has a longitudinal demagnification half that of its lateral one. For this reason the angle at which the CCD was mounted at had to halved to ensure the focal plane of the spectrograph remained aligned with the chip over the 42mm diagonal dimension of the Series 200 CCD for which it was designed. The procedure for the alignment of the focal planes is detailed in Appendix A.

Further details on the focal reducer, its design and construction are outlined by Tobin *et al.* (1998)[43].

6.4 Observation Procedure

The set-up procedures followed for the MJUO échelle spectrograph started at least 1 hour prior to any observations being made. The liquid nitrogen cryostat is required to be filled

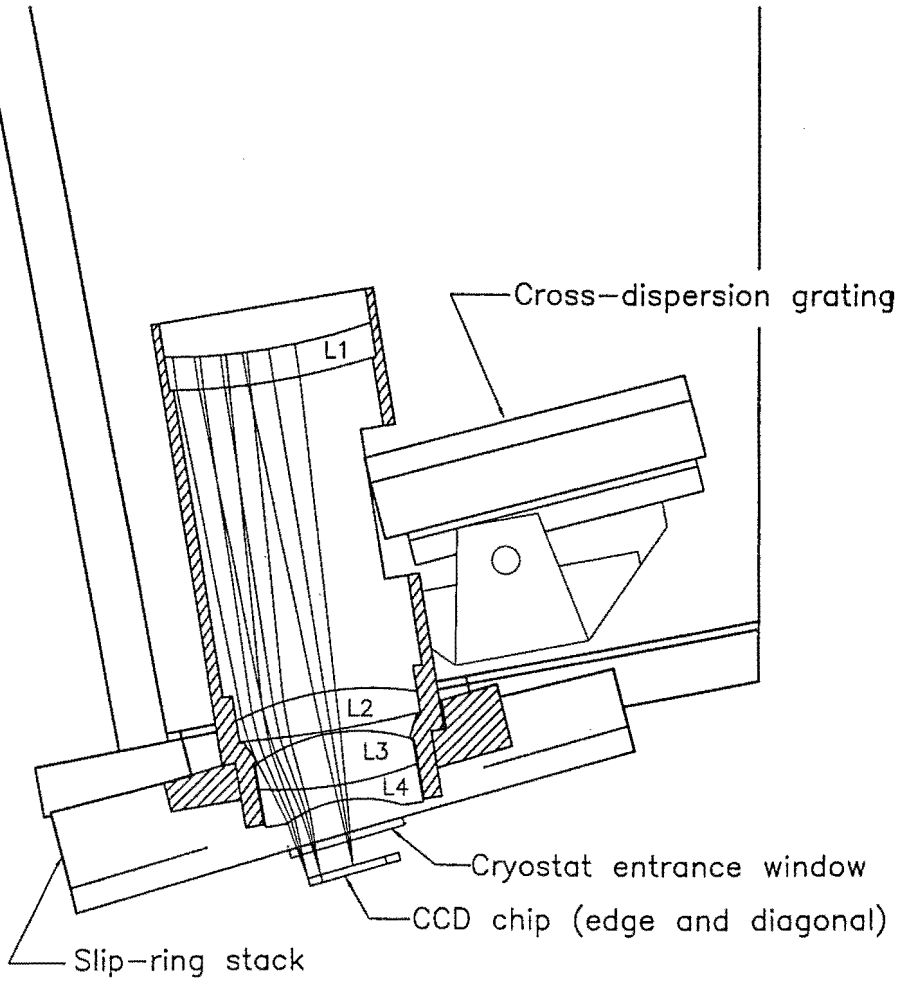

Figure 6.1: Schematic diagram of the focal reducer, and its location within the MJUO échelle spectrograph.

at the start and completion of the night. It was necessary to fill the cryostat at least one hour before making any observations to allow the CCD time to readjust and maintain a steady temperature. It was found that the bias readout can fluctuate by several ADUs immediately following the filling of the dewar, also making it necessary to wait an hour before taking any readings.

Once the chip temperature had re-stabilised and readings were able to be made, the échelle calibrations were made.

The first is to obtain a bias frame from the CCD. This is a readout of the chip with the shutter closed, immediately after the chip has been flushed. The purpose of this procedure is to check that the system is functioning correctly.

Three dark exposures, each of 10 seconds duration, were then obtained. By taking the median of these frames, an image was obtained for the dark current of the CCD for that night that was free of any cosmic rays. In fact, these images were not used for dark subtraction, but were a further test of the correct functioning of the Series 200 CCD system.

The final calibration procedure was to expose the spectrograph slit with a tungsten lamp to obtain the smooth fields (or flat fields) necessary for identifying the position of the orders in the reduction procedures, and for correcting pixel-to-pixel sensitivity variations in the chip. A 1mm BG39 filter was placed behind the slit to reduce the high amount of red scattered light that would otherwise be present. Exposures for the smooth fielding were typically 30 seconds. Three smooth fields were taken and the resulting images added together for the reduction process in order to reduce the magnitude of any cosmic rays. When the PM3000 CCD was being used, separate smooth fields were taken at the settings used for each the H and K lines.

The dome shutter was opened, and the telescope covers removed shortly after sunset each night to allow plenty of time for the dome and telescope to reach equilibrium with the outside air temperature. This reduces currents of rising hot air which otherwise degrade the seeing.

Focusing of the telescope was done using the star Canopus, also used as a standard star for profile corrections. Being a $V=-0.72$ star this meant exposure times could be kept to a minimum for the purposes of focusing. During the times of the year when Canopus was too low to be observed after sunset, λ Scorpii would be used instead, as this was the closest star to 51 Oph that was bright enough to be quickly and easily used for focusing.

The spectrograph was focussed by narrowing down the slit size and exposing it with the thorium-arc lamp. The camera micrometer could then be adjusted until the sharpest image of the slit was obtained. This setting remained the same for a given run so did not need to be checked and refocused nightly. Temperature variations during the year however did result in changes to the focusing of the spectrograph, making periodic checks during the year necessary to maintain the sharpest focus.

Particularly during the colder winter months, a number of spectra were spoilt, due to having condensation on the cryostat entrance window. This was recognisable as a circular distortion in the CCD image such as those shown in Fig. 6.2. This was removed by taking the CCD off the telescope, and soaking up the moisture on the entrance window with lens cleaning tissues. The effect this had on the stellar spectra can be seen in Fig. 8.72, where condensation appeared on the entrance window twice during the night. These spectra could not be reduced and further analysed.

During 1997 telescope allocations were made during the months from March to November for the collection of data for this thesis. Typically one week a month was allocated although some months were shorter to allow for a longer observing time the following month, in order to sample longer timescales. Table 6.3 contains a list of the dates that observations were made at MJUO during 1997 and the échelle spectra that were obtained.

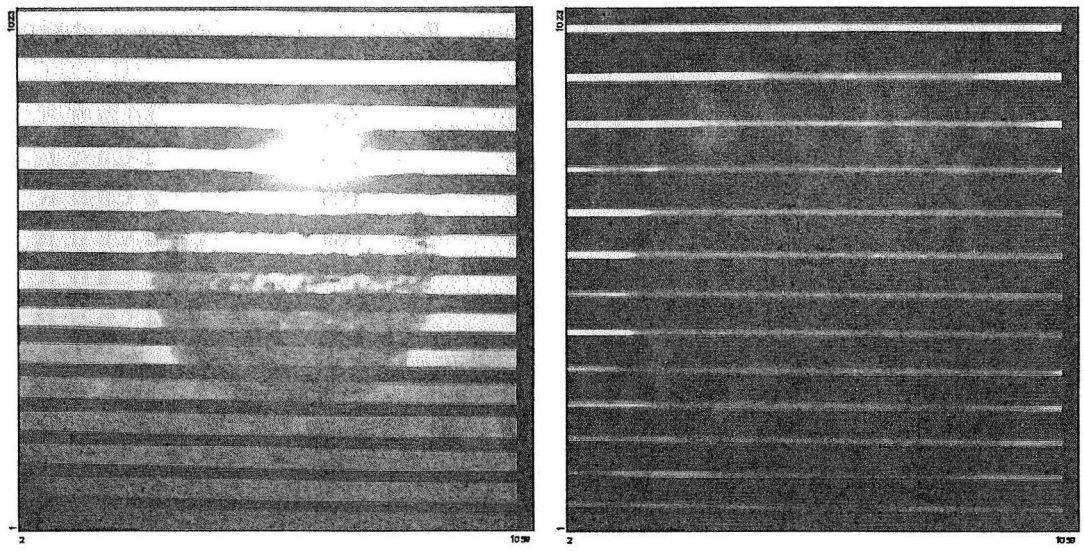

(a) (b)

Figure 6.2: Images (a) and (b) show the effect of condensation (false-colour enhanced) on the cryostat entrance window, for smooth-field and stellar CCD images respectively.

Table 6.3: Observations made at MJUO during 1997 and spectra obtained of Ca II lines.

Date of Observation	Star	CCD system	Focal Reducer	Spectra obtained
7 March	Canopus	PM3000	No	1 Ca II K
	β Pic	PM3000	No	2 Ca II K
8 March	Canopus	PM3000	No	2 Ca II K
	Canopus	PM3000	No	2 Ca II H
	β Pic	PM3000	No	4 Ca II K
	β Pic	PM3000	No	4 Ca II H
9 March	Canopus	PM3000	No	1 Ca II K
	Canopus	PM3000	No	1 Ca II H
	β Pic	PM3000	No	4 Ca II K
	β Pic	PM3000	No	2 Ca II H
27 March	Canopus	PM3000	Yes	3 Ca II K
	Canopus	PM3000	Yes	1 Ca II H
	β Pic	PM3000	Yes	1 Ca II K
	β Pic	PM3000	Yes	1 Ca II H

Table 6.3 continued on next page

Table 6.3 continued

Date of Observation	Star	CCD system	Focal Reducer	Spectra obtained
28 March	Canopus	PM3000	Yes	1 Ca II K
	Canopus	PM3000	Yes	2 Ca II H
	β Pic	PM3000	Yes	2 Ca II K
	β Pic	PM3000	Yes	2 Ca II H
	51 Oph	PM3000	Yes	2 Ca II K
	51 Oph	PM3000	Yes	2 Ca II H
29 March	Canopus	PM3000	Yes	1 Ca II K
	β Pic	PM3000	Yes	2 Ca II K
	51 Oph	PM3000	Yes	2 Ca II K
	51 Oph	PM3000	Yes	1 Ca II H
30 March	Canopus	PM3000	Yes	1 Ca II K
	Canopus	PM3000	Yes	1 Ca II H
	β Pic	PM3000	Yes	7 Ca II K
	β Pic	PM3000	Yes	1 Ca II H
	51 Oph	PM3000	Yes	2 Ca II K
	51 Oph	PM3000	Yes	2 Ca II H
31 March	Canopus	PM3000	Yes	1 Ca II K
	Canopus	PM3000	Yes	1 Ca II H
	β Pic	PM3000	Yes	3 Ca II K
	β Pic	PM3000	Yes	3 Ca II H
	51 Oph	PM3000	Yes	1 Ca II H
21 April	Canopus	S200	Yes	2 Ca II H&K
	β Pic	S200	Yes	5 Ca II H&K
	51 Oph	S200	Yes	5 Ca II H&K
23 April	Canopus	S200	Yes	5 Ca II H&K
	β Pic	S200	Yes	7 Ca II H&K
	51 Oph	S200	Yes	6 Ca II H&K
24 April	Canopus	S200	Yes	3 Ca II H&K
	β Pic	S200	Yes	6 Ca II H&K
	51 Oph	S200	Yes	3 Ca II H&K
25 April	Canopus	S200	Yes	3 Ca II H&K
	β Pic	S200	Yes	3 Ca II H&K
	51 Oph	S200	Yes	4 Ca II H&K

Table 6.3 continued on next page

Table 6.3 continued

Date of Observation	Star	CCD system	Focal Reducer	Spectra obtained
26 April	Canopus	S200	Yes	3 Ca II H&K
	β Pic	S200	Yes	10 Ca II H&K
	51 Oph	S200	Yes	4 Ca II H&K
27 April	Canopus	S200	Yes	3 Ca II H&K
	β Pic	S200	Yes	10 Ca II H&K
	51 Oph	S200	Yes	6 Ca II H&K
28 April	Canopus	S200	Yes	3 Ca II H&K
	β Pic	S200	Yes	4 Ca II H&K
	51 Oph	S200	Yes	6 Ca II H&K
28 May	Canopus	S200	Yes	3 Ca II H&K
	β Pic	S200	Yes	4 Ca II H&K
	51 Oph	S200	Yes	2 Ca II H&K
29 May	Canopus	S200	Yes	2 Ca II H&K
	β Pic	S200	Yes	6 Ca II H&K
	51 Oph	S200	Yes	5 Ca II H&K
12 June	51 Oph	S200	Yes	2 Ca II H&K
13 June	Canopus	S200	Yes	3 Ca II H&K
	β Pic	S200	Yes	7 Ca II H&K
	51 Oph	S200	Yes	6 Ca II H&K
14 June	Canopus	S200	Yes	3 Ca II H&K
	β Pic	S200	Yes	3 Ca II H&K
	51 Oph	S200	Yes	4 Ca II H&K
25 June	Canopus	S200	Yes	3 Ca II H&K
	β Pic	S200	Yes	4 Ca II H&K
	51 Oph	S200	Yes	5 Ca II H&K
26 June	Canopus	S200	Yes	3 Ca II H&K
	β Pic	S200	Yes	12 Ca II H&K
	51 Oph	S200	Yes	4 Ca II H&K
27 June	Canopus	S200	Yes	3 Ca II H&K
	β Pic	S200	Yes	11 Ca II H&K
	51 Oph	S200	Yes	3 Ca II H&K

Table 6.3 continued on next page

Table 6,3 continued

Date of Observation	Star	CCD system	Focal Reducer	Spectra obtained
28 June	Canopus	S200	Yes	3 Ca II H&K
	β Pic	S200	Yes	12 Ca II H&K
	51 Oph	S200	Yes	6 Ca II H&K
29 June	Canopus	S200	Yes	3 Ca II H&K
	β Pic	S200	Yes	4 Ca II H&K
	51 Oph	S200	Yes	4 Ca II H&K
28 July	Canopus	S200	Yes	3 Ca II H&K
	β Pic	S200	Yes	8 Ca II H&K
	51 Oph	S200	Yes	4 Ca II H&K
30 July	β Pic	S200	Yes	3 Ca II H&K
	51 Oph	S200	Yes	5 Ca II H&K
31 July	51 Oph	S200	Yes	2 Ca II H&K
28 August	β Pic	S200	Yes	3 Ca II H&K
	51 Oph	S200	Yes	4 Ca II H&K
15 September	Canopus	S200	Yes	3 Ca II H&K
	β Pic	S200	Yes	6 Ca II H&K
	51 Oph	S200	Yes	3 Ca II H&K
17 September	Canopus	S200	Yes	3 Ca II H&K
	β Pic	S200	Yes	7 Ca II H&K
18 September	Canopus	S200	Yes	3 Ca II H&K
	β Pic	S200	Yes	9 Ca II H&K
19 September	Canopus	S200	Yes	3 Ca II H&K
	β Pic	S200	Yes	10 Ca II H&K
	51 Oph	S200	Yes	2 Ca II H&K
16 October	β Pic	S200	Yes	6 Ca II H&K
18 October	Canopus	S200	Yes	2 Ca II H&K
	β Pic	S200	Yes	13 Ca II H&K
19 October	Canopus	S200	Yes	3 Ca II H&K
	β Pic	S200	Yes	6 Ca II H&K

Table 6.3 continued on next page

Table 6.3 continued

Date of Observation	Star	CCD system	Focal Reducer	Spectra obtained
21 October	Canopus	S200	Yes	3 Ca II H&K
	β Pic	S200	Yes	7 Ca II H&K
22 October	Canopus	S200	Yes	3 Ca II H&K
	β Pic	S200	Yes	3 Ca II H&K
20 November	Canopus	S200	Yes	3 Ca II H&K
	β Pic	S200	Yes	5 Ca II H&K
21 November	Canopus	S200	Yes	3 Ca II H&K
	β Pic	S200	Yes	12 Ca II H&K
22 November	Canopus	S200	Yes	3 Ca II H&K
	β Pic	S200	Yes	9 Ca II H&K

Chapter 7

Data Reduction and Analysis

All of the data obtained at MJUO for the purposes of this thesis were reduced and analysed using the European Southern Observatory - Munich Image Data Analysis System (ESO-MIDAS or simply MIDAS). MIDAS is essentially a collection of general purpose programmes which can be used for the reduction and analysis of data from various instruments and detectors. A command language allows the user to create customised procedures to perform sequences of the various elementary MIDAS procedures required for the reduction and analysis of the data.

Reductions were initially performed using MIDAS version 94NOV on the University of Canterbury's Computer Services Centre Sparc Centre 2000, also known as 'cantua'. MIDAS version 96NOV was later used on the Physics and Astronomy Department's Dual Pentium pro PC 'yukawa'. Reductions were typically some 2–3 times faster on yukawa than cantua[1].

7.1 MIDAS échelle reduction package

All raw CCD data obtained from MJUO are stored in FITS format. Since FITS files are not directly recognised by MIDAS, image files need to be changed to the idiosyncratic internal format (.BDF) used by MIDAS.

The échelle package in MIDAS also requires images to be oriented in such a way that orders increase from top to bottom, and wavelength increases from left to right. For images obtained with the PM3000 CCD system, images had to be rotated 270°, while no rotations were required for the Series 200 CCD system. Once the images were in the correct format and orientation the MIDAS échelle reduction package was enabled allowing the use of procedures specific for échelle spectrographs (Section 7 MIDAS manual [44]).

The reduction procedure is as follows (actual reduction commands can be found in Appendix B):

Note: All images shown here have been false-colour enhanced to produce a better visualisation of fainter features.

1. The orders are firstly located by means of the smooth-field image. By performing a Hough transformation, the location and orientation of all the orders are computed

[1]Note however that cantua has recently (February 1998) been upgraded to a Sun Enterprise 450 machine.

and stored in a table. This then tells MIDAS where the orders are on the échellogram when it reduces the stellar images. Fig. 7.1(a) shows a typical smooth-field image showing the orientation and position of the 13 orders located.

2. The next step is to find the offset between the centre of the individual stellar spectra and the smooth field (They are not necessarily coincident because the star may not have been positioned half-way along the spectrograph slit). A Gaussian is fitted across one of the orders to obtain the centre value. The difference between this value and that from the smooth field reduction is recorded. At this stage the full width of the Gaussian profile is also recorded and defined as the width of the software slit, which MIDAS will use to extract and average the intensities to give the final spectrum.

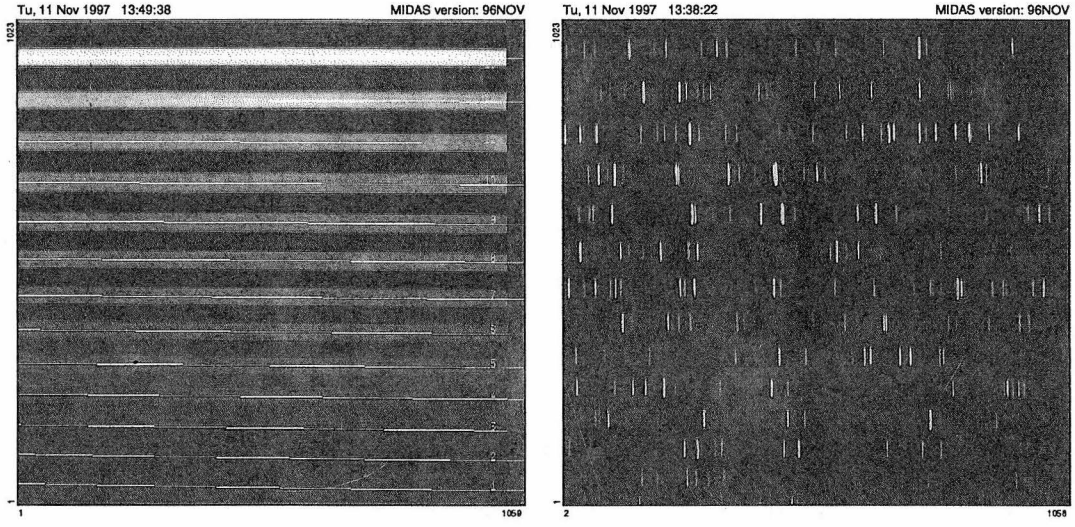

(a) (b)

Figure 7.1: Examples of (a) a smooth-field image and (b) a thorium-arc image used for calibrating the stellar spectra. In (a), the white lines indicate the central position of the orders found via a Hough transformation. The order numbers 1-13 are not the physical order numbers from the grating equation, but sequence numbers assigned by the software.

3. Next the spectrum needs to be calibrated for wavelength. This is done by means of a thorium-arc lamp for which the wavelength of many of the emission lines is well defined. Fig. 7.1(b) shows an example of a thorium-arc spectrum obtained for wavelength calibrations. MIDAS locates the emission lines in the spectrum and attempts to correspond them to the values found in a reference table created from the Atlas of the Thorium Spectrum [45]. A polynomial is fitted that best fits the wavelengths of the lines found in the reference table. The resulting polynomial is later applied to the extracted orders of the stellar spectrum to obtain a spectrum plotted on a wavelength scale.

4. The FWHM of each of the identified thorium lines is then found, and an average in each order is found so the resolution in each order can be calculated. Table 7.1

shows an example of typical values of the FWHM in angstroms for a thorium-arc spectrum. These values for the FWHM of the thorium lines in each order stayed constant throughout the year as would be expected. Therefore using these values the resolution in each of the thirteen orders were found, as shown in Table 7.1 [46]. Note: Ca II H line is order 58 and K line is in order 59.

Order	Central Wavelength	Resolution Pixels	Resolution $\Delta\lambda$ Å	Resolution Δv kms^{-1}	Resolving Power	Dispersion Åmm^{-1}
51	4529.9Å	2.391	0.133	8.80	34000	2.32
52	4442.5Å	2.681	0.149	10.05	29800	2.31
53	4359.5Å	2.443	0.132	9.08	33000	2.26
54	4279.4Å	2.511	0.135	9.46	31700	2.24
55	4202.0Å	2.684	0.142	10.13	29600	2.20
56	4126.9Å	2.468	0.125	9.08	33000	2.11
57	4054.8Å	2.406	0.121	8.95	33500	2.10
58	3985.2Å	2.731	0.134	10.08	29700	2.04
59	3918.1Å	2.765	0.134	10.25	29200	2.03
60	3852.9Å	2.635	0.125	9.73	30800	1.98
61	3790.2Å	2.537	0.119	9.41	31900	1.95
62	3729.5Å	2.543	0.116	9.32	32200	1.90
63	3670.3Å	2.536	0.113	9.23	32500	1.86

Table 7.1: Resolution and dispersion of the MJUO échelle spectrograph in each of the 13 orders.

5. The next step is the so-called filtering of the stellar image. This involves two processes: the removal of any background light, as well as filtering out cosmic rays both within the orders and between the orders. This will make the intensity level between the orders approximately zero, giving a more accurate indication of the intensity level within the orders. The background removal is done by a smoothing spline interpolation. A series of polynomials are fitted down the orders taking the inter-order intensities and interpolating across the orders. A merged image is created of each of these polynomials along the raw spectrum, which is the estimate of the background light present. Cosmic rays between the orders are removed by checking each pixel to those about it. If the intensity differs by more than a specified number of standard deviations, the pixel is replaced by the median of the surrounding pixels - hence the name median filtering. Within the spectra a point spread function is evaluated down each order. If a pixel differs from this function by more than a specified amount, it is assumed to be a cosmic ray and is replaced by a value corresponding to the point spread function for that pixel. The spectra were then examined by eye to ensure a satisfactory removal of the cosmic rays.

   Although no quantitative analysis was carried out to see if indeed the thinner Series 200 chip did result in fewer cosmic rays, a comparison of previous spectra obtained with the PM3000 chip did show a great deal fewer strikes. Fig. 7.2 shows an example of a filtered and unfiltered image.

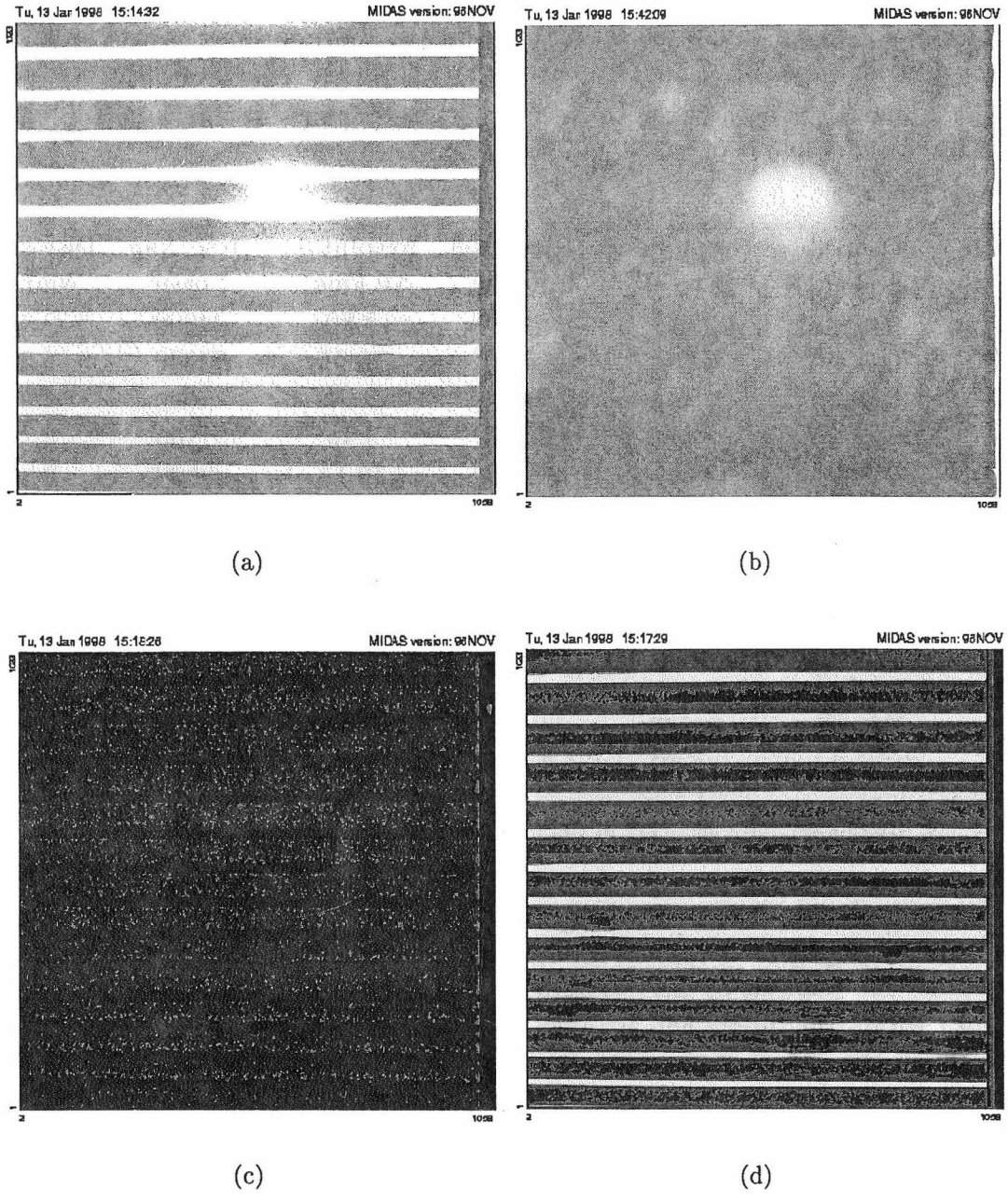

Figure 7.2: Examples of (a) an unfiltered image and (d) the final filtered image. Plots (b) and (c) show the background and cosmic rays respectively that are removed from (a) to produce (d).

6. A smooth-field correction is applied, which divides the raw spectrum by the normalised smooth-field image. This has the effect of taking out any pixel-to-pixel sensitivity variations. In addition, it removes the blaze response, but at the expense of dividing the stellar spectrum by the flux distribution of the tungsten smooth-field lamp.

7. A one-dimensional spectrum is then obtained by running a software slit along each order, collapsing the intensities vertically down the slit. (At the telescope, the rotation of the CCD cryostat was adjusted so that spectral lines fell parallel to

the pixel rows.) The 13 individual orders are then concatenated together into one reduced file. Fig. 7.3 shows a reduced spectrum containing all 13 orders present in the raw spectrum. The cosmic ray and thorium-arc images are also reduced to a one-dimensional file. Fig. 7.4 shows a plot of the 5th and 6th orders shown in Fig. 7.3, containing the Ca II H and K lines. This corresponds to orders 58 and 59 in the échellogram. Note that the H line has a more complex profile due to a blend with the strong photospheric H_ϵ line.

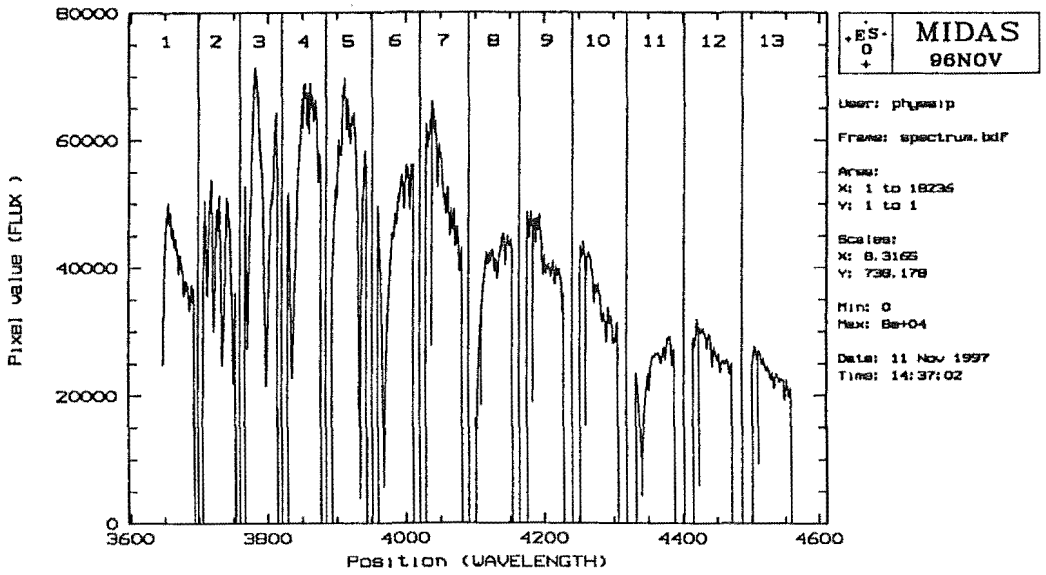

Figure 7.3: One-dimensional reduced spectrum for β Pic showing all 13 orders contained in the raw échellogram. The orders numbers are the same as in Fig. 7.1.

8. Barycentric corrections are then made to correct for the movement of the Earth in relation to the star, for the times of mid exposure recorded with each observation. The wavelength scale is altered accordingly to correct for the Doppler shifts in the wavelength of the light reaching us. This correction varies between -0.105Å and $+0.105$Å (-8 and $+8$ kms^{-1}) depending on the time of the year.

7.2 Normalising the Spectra

With the raw spectra reduced the next step was to normalise the data to a common intensity scale to allow for an easier comparison to be made between different spectra.

Each spectrum was firstly rebinned to the same starting wavelength value of 3600.0Å, and a step size of 0.050Å. This ensured that any slight differences in the échelle set-up from night to night did not change the position of the spectra in the normalised images. This meant that images then be could be overlayed for comparison.

Spectra were taken each night of the standard star Canopus in order to correct for any

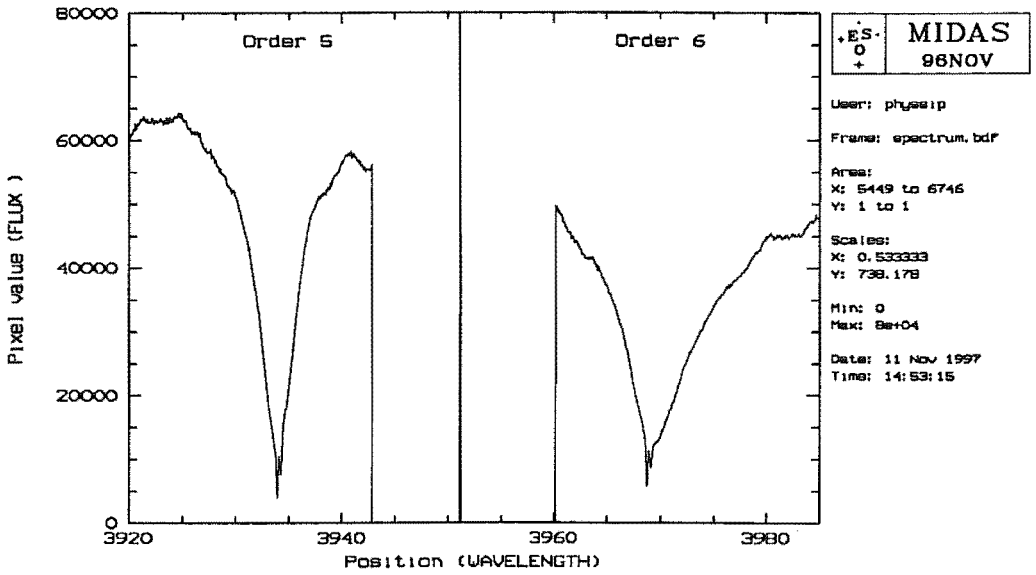

Figure 7.4: One-dimensional reduced spectra for β Pic plotted for the wavelength region containing the Ca II K and H lines. Software orders 5 and 6 correspond to physical orders 59 and 58 respectively.

instrumentational variations over the course of each run, and from run to run. The correction was achieved by adding together the Canopus spectra from each night and comparing to a Canopus reference spectrum to see if any differences were present. Being a standard star it would be expected that there should be no differences in the spectra. This was generally the case but in a few instances differences did occur. Each spectrum taken for the night was then corrected by the ratio of the Canopus spectra to compensate for this difference, to attempt to make each spectrum taken during the year as free as possible of any instrumental changes or set-up differences.

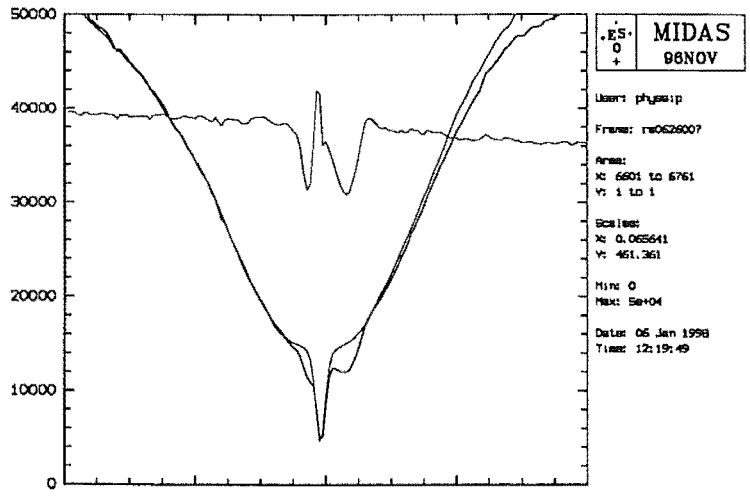

Figure 7.5: Typical β Pic K line spectrum overlayed with the reference spectrum (red) and the normalised spectrum (blue), clearly showing both a red-shifted and blue-shifted absorption.

The spectra were next divided by the reference spectrum.

The reference spectrum is a spectrum that is free of any variable absorptions that can be compared to the spectra of interest in order to highlight any variable absorptions in them. The reference spectrum was made by taking the average of different spectra from two different times of the year (25th June and 18th September). The images were chosen to be as

free as possible of any absorptions, and also with a strong signal level and hence high signal-to-noise ratio. Once the spectra had been averaged a few minor alterations were made by hand to obtain the cleanest possible spectrum. The reference spectrum can be seen in Fig. 7.5, it is also plotted in each of the nightly stack plots in Figs. 8.1 to 8.32.

Once the stellar spectrum has been divided by the reference spectrum the presence of any absorptions should become apparent as any departure from the horizontal line, or 'pseudo-continuum', as can be seen in Fig. 7.5. Because the circumstellar line at the centre of the profiles has a low central intensity (it may well be saturated), the intensity is much lower and hence the quality of the background subtraction during the reductions can affect the depth of the line. This in turn results in an uncertain division close to the circumstellar line. Fig. 7.5 shows such a case. For this reason the central region of the divided spectra is not included in the later analysis procedures.

The divided spectrum is then normalised to the ratio of the signal levels between the reference and raw spectra. To normalise this to unity the average intensity was found outside the region of absorptions, and this value divided into the normalised spectrum to make it normalised to unity. This means all spectra obtained during the year should be on the same wavelength scale, have any instrumental fluctuations accounted for, and be normalised to unity.

In order to change the spectra from wavelength space to velocity space the normalised spectra first had the central wavelength of the circumstellar feature subtracted leaving the spectra with the circumstellar feature at 0Å. (Note it was at this point that the heliocentric radial velocity correction of each star was made. By subtracting an additional 0.3Å off the wavelength scale of the H and K lines of β Pic, a correction of $\sim$20 kms^{-1} was made to account for the radial velocity. An additional 0.24Å was added on for 51 Oph to give a radial velocity correction of ~ -20kms^{-1}). This altered wavelength scale could then be converted to a velocity scale by the multiplication of a conversion factor found by:

$$\frac{\Delta\lambda}{\lambda} = \frac{v}{\mathrm{c}} \tag{7.1}$$

Where $\lambda = 3968.470$ Å for H line and 3933.664 Å for K line [37], and c is the speed of light.

This then gives a conversion factor of 1 Å being 75.59kms^{-1} and 76.26kms^{-1} for the H and K lines respectively. Because both H and K lines are on the one composite spectrum, an average conversion factor of 75.93kms^{-1} was used.

The spectra are now ready to have the absorptions defined and classified.

7.3 Fitting the absorption features

With the spectra now normalised to unity and in velocity space, the existence of any absorptions can next be fitted with Gaussian that best approximate the absorption. Gaussians have been used by earlier workers (eg, Lagrange-Henri *et al.* (1992)[34]) and have been found to fit the variable absorption features adequately. Gaussians are fitted to both the H and K lines simultaneously.

The first step in fitting the absorption features is to fit either a straight line or a quadratic to the pseudo-continuum; whichever fits best. Despite the precautions taken, the pseudo-continuum is not always horizontal.

The absorption profiles are fitted using the MIDAS non-linear Gaussian fitting routines. A MIDAS procedure was written that used the cursor to give the approximate position of the central depth and FWHM of each of the absorptions. These initial values were fed to the MIDAS fitting routine which uses the following equation to fit the best Gaussian to each identified absorption profile:

$$GAUSS(x; a, b, c) = a \exp\left[-\ln 2 \left(\frac{2(x-b)}{c}\right)^2\right]. \tag{7.2}$$

The Gaussian parameters a, b and c refer to the relative depth, central velocity and FWHM respectively, of the absorption profiles.

From the initial input from the cursor, the values of a, b and c were iterated many times until the optimum Gaussian was found to fit the absorption. The initial values entered via the cursor are done so on the K line. Having twice the oscillator strength of the H line it was generally true that the K line absorptions were more prominent and hence easier to identify. (If this was not the case a separate procedure was used so the profiles could be firstly identified on the H line.) With the absorption fitted on the K line, the MIDAS procedure simultaneously attempted to find a profile on the H line with the same Gaussian parameters of a, b and c as initial parameters. It then once again steps through many iterations until the best values of a, b and c were found for the H line. This method usually resulted in a successful modelling of profiles in both the H and K lines, the exception being when a profile was only in one of the H or K lines. The simultaneity of the H and K observations allow for a much greater confidence in the derived fit parameters, if they are consistent between the H and K lines.

This same method for modelling the profiles was repeated for each absorption. Once all the profiles had been fitted for a given normalised spectrum, the fitted Gaussians were overlayed onto the spectrum to enable a visual evaluation as to whether the fit was satisfactory. The values of a, b and c and their associated errors were also printed from which information can be derived about the cometary absorptions. Fig. 7.6 shows an example.

As explained earlier in Section 7.2, the central component of the circumstellar feature does not normally divide out as well as the rest of the spectrum so a region 3 pixels to the violet and 5 pixels to the red of the central position was excluded from the Gaussian fitting procedure. (These values correspond to the width of the circumstellar feature in the reference profile). This ensures that any absorption profiles close to or extending over the circumstellar feature are not corrupted by a poor division with the reference spectrum.

How the profiles are initially defined with the cursor is a very user-sensitive process. Whether the MIDAS procedure is instructed to find, say, one broad profile or a collection of narrower profiles is up to the user. This became especially prevalent with profiles extending across the circumstellar feature. Since the central region is not included in fitting

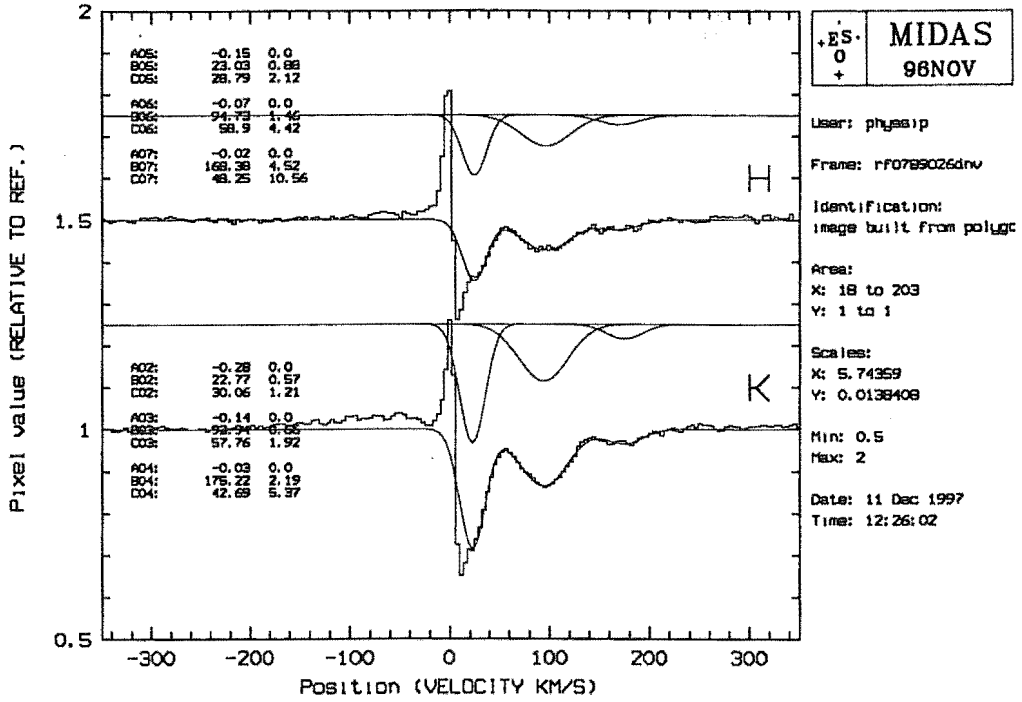

Figure 7.6: Fitted Gaussians to the H(red) and K(blue) lines of a β Pic normalised spectrum and the Gaussian parameters a, b and c and their formal errors for each profile (An error shown as 0.0 is smaller than 0.005 and is reported as 0.01 in Appendix D). The spectrum being fitted is shown in black.

the Gaussians, MIDAS was in some cases able to find either a red and blue shifted feature on either side of the circumstellar feature, or one broad feature crossing the circumstellar feature, depending on what was identified with the cursor. In these cases spectra taken before and after were checked to see if they showed which scenario was more likely, and if this did not favour one particular option, then the most basic profile was chosen, ie, one broad profile rather than a collection of smaller ones.

7.4 Characterising the absorptions

The absorptions were then quality classified according to how well the MIDAS Gaussian fits modelled the observed absorptions. The classifications used are shown in Table 7.2, and Figs. 7.7 to 7.12 show examples of these different classifications.

With the absorptions all identified and modelled, the next step was to calculate the equivalent width (EW), an indicator of the strength, of each absorption. The EW is defined as the area of the Gaussian when the height of the Gaussian is measured with respect to the local pseudo-continuum. Given the general formulation of a Gaussian, where σ is its standard deviation, the area can be found as follows:

$$\text{Area Gaussian} = a\sigma\sqrt{2\pi}. \tag{7.3}$$

$$\text{Now } \sigma = \frac{\text{FWHM}}{2\sqrt{2\ln 2}}, \tag{7.4}$$

Abbreviation	Description
gS	'Good Single': an absorption that (possibly) no more than slightly overlaps with another and is well-fitted by a Gaussian profile.
pS	'Poorer Single': an absorption that (possibly) no more than slightly overlaps with another and is a poorer fit to a Gaussian profile, either because the spectrum is noisy or because the profile is obviously non-Gaussian.
gB	'Good Blend': an absorption that clearly overlaps with one-or-more others and is well-fitted by a Gaussian profile.
pB	'Poorer Blend': an absorption that clearly overlaps with one-or-more others and is a poorer fit to a Gaussian profile, either because the spectrum is noisy or because the profile is obviously non-Gaussian.
C	'Circumstellar': the feature blends with the circumstellar absorption, which has probably significantly affected the Gaussian parameters of the fitted profile, particularly if the division by the reference circumstellar profile has been imperfect.
UD	'Uncertain Decomposition': the feature has been fitted by a single Gaussian, but the signal-to-noise is insufficient to determine whether multiple Gaussians would provide a better fit.

Table 7.2: Quality classifications of the fitted absorption profiles.

therefore using the formulation of Equation 7.2 the area, or EW, is defined as:

$$\mathrm{EW} = \frac{ac}{2}\sqrt{\frac{\pi}{\ln 2}}. \tag{7.5}$$

The numerical factor here is $1.0645\,ac$. Since a is a fraction and hence unitless, the EW is in the same units as c, kms^{-1}.

In order to have the EW in mÅ, which is the preferred unit, a further numerical factor must be incorporated using Equation 7.1 as follows:

$$\mathrm{EW} = 1.0645 \left(\frac{\lambda}{\mathrm{c}}\right) ac. \tag{7.6}$$

Taking $\lambda = 3968750\,\mathrm{m\AA}$ for the H line and $3933850\,\mathrm{m\AA}$ for the K line yields factors of 14.082 (H line) and 13.959 (K line). It is then sufficient to take a mean of these to give a numerical factor of 14.02.

Therefore the EW in mÅ of a given absorption can be found by (with c in kms^{-1}):

$$\mathrm{EW} = 14.02\,ac. \tag{7.7}$$

The full table showing the final results of the absorptions and their corresponding parameters; such as position, depth, FWHM and EW, as well as the corresponding formal errors can be found in Appendix D. The equivalent width errors have been obtained from assuming the errors on a and c are independent, and adding them quadratically.

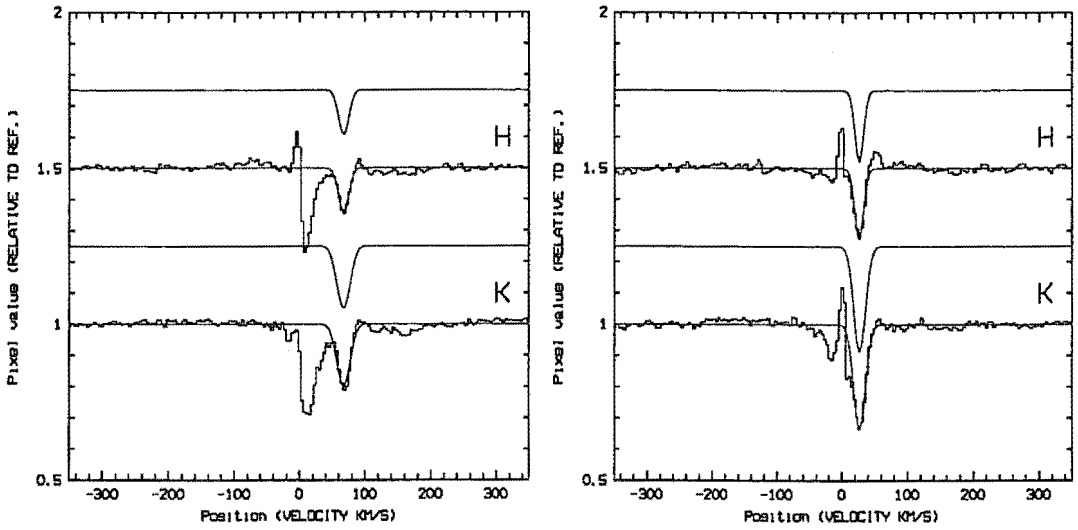

(a) (b)

Figure 7.7: Examples of 'Good Single' absorptions. Although (a) is slightly blended with other absorptions, and (b) with the circumstellar position, both are nonetheless prominent enough alone to be classified as a single profile.

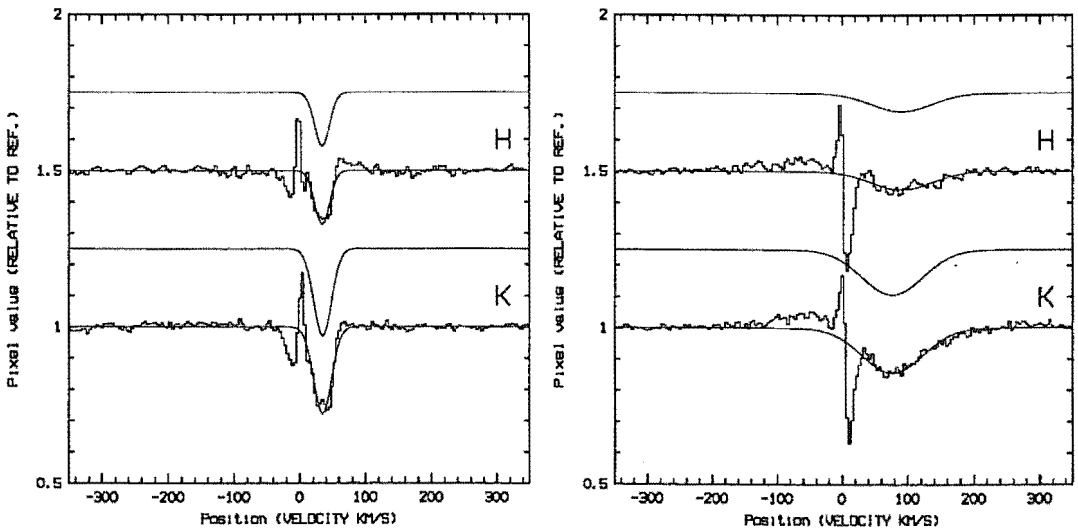

(a) (b)

Figure 7.8: Examples of 'Poorer Single' absorptions. In (a) the single profile fitted is not a good fit to the original spectra, and in (b) the profile is too noisy to classify as a good single.

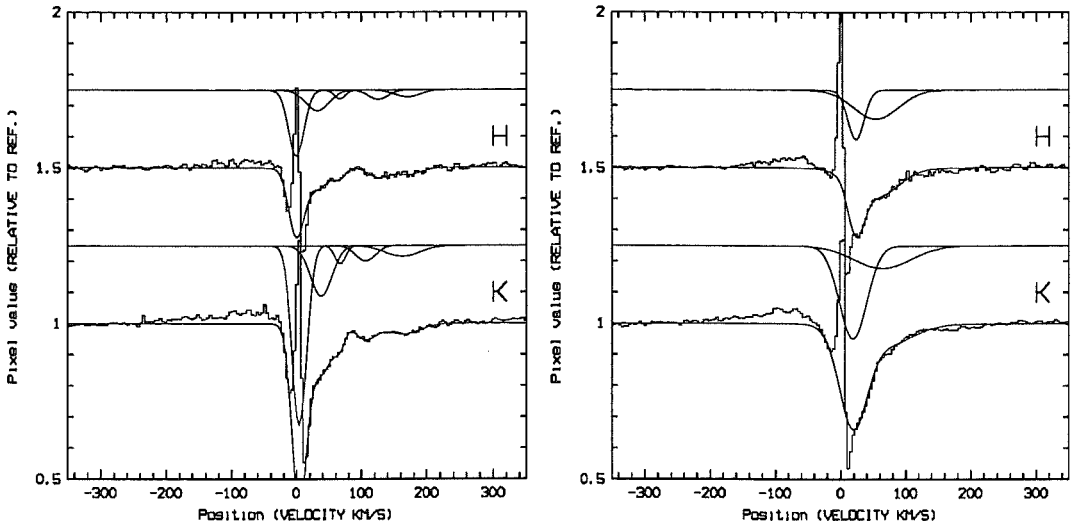

(a) (b)

Figure 7.9: Examples of 'Good Blend' absorptions. Case (a) shows 5 single profiles that together make a good model of the raw spectra, or in case (b) the circumstellar profile is well blended with another profile.

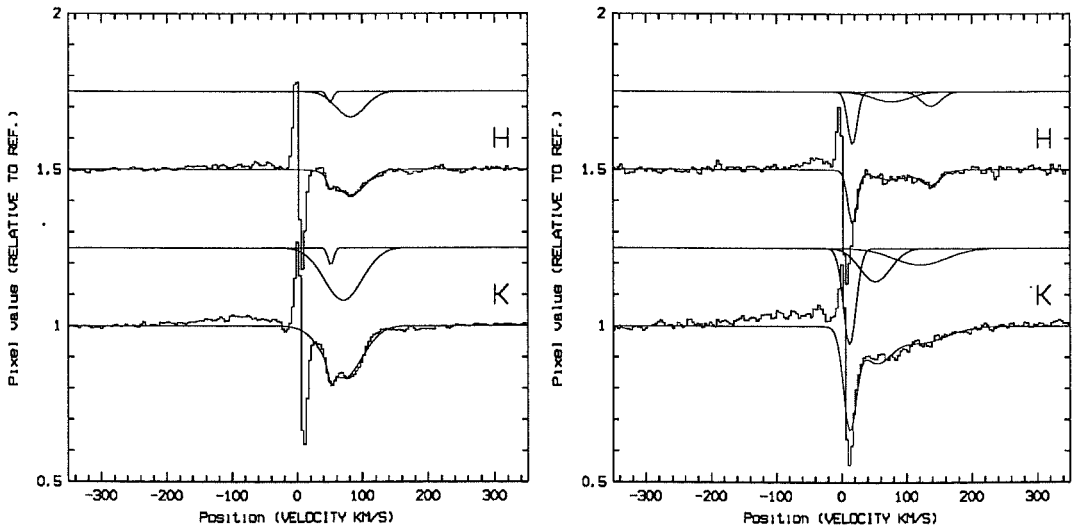

(a) (b)

Figure 7.10: Examples of 'Poorer Blend' absorptions. Case (a) shows what is obviously 2 blended profiles, however the MIDAS procedure was unable to well approximate them. Case (b) also contains more blended absorptions but the profile is too noisy to be able to well identify them.

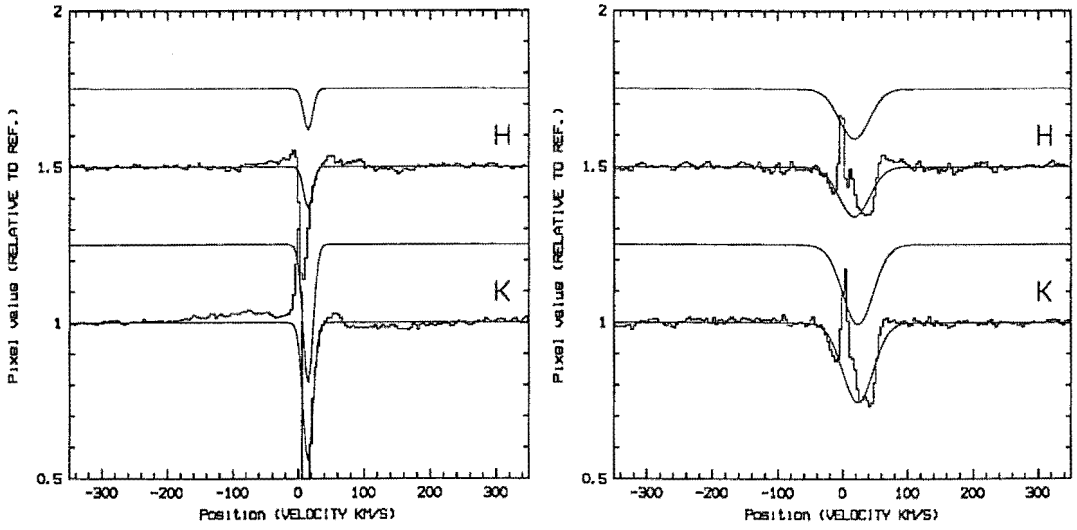

(a) (b)

Figure 7.11: Examples of 'Circumstellar' absorptions. Case (a) shows an example of a profile that is very close to the circumstellar feature so as such is difficult to model well. Case (b) shows what MIDAS identifies as the blue-shifted absorption. Because only a small part is not affected by the imperfect circumstellar division the modelled absorption is obviously only an approximation to what is actually present.

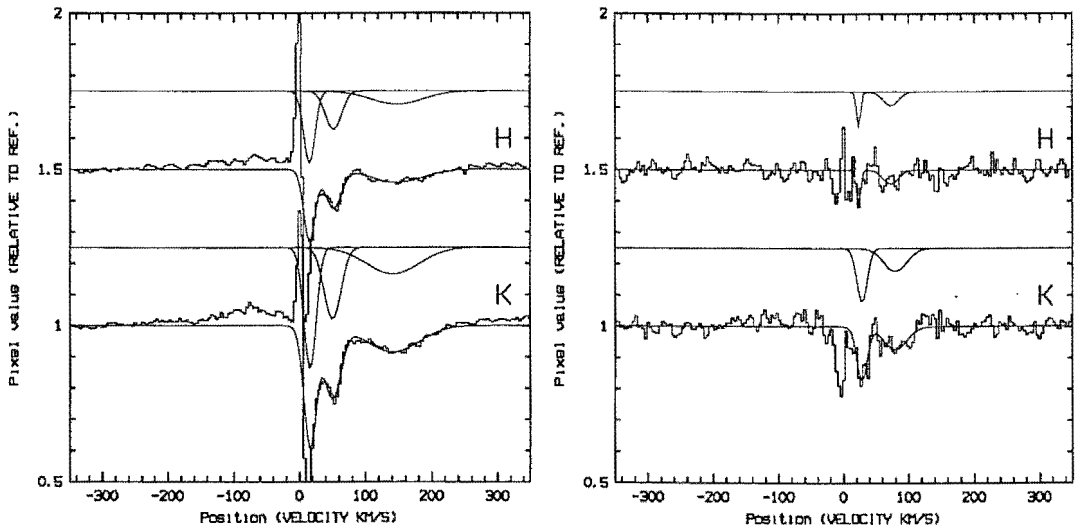

(a) (b)

Figure 7.12: Examples of 'Uncertain Decomposition' absorptions. In case (a), the large broad absorption is classified 'UD'. It can not be certain whether this one absorption or whether a number of smaller absorptions would better represent the actual profile. Case (b) shows an example of a noisy profile where it is not certain whether one or more absorptions are present in the profile.

Chapter 8

Presentation of Spectra

In this chapter the Ca II H and K spectra are presented graphically, in which the spectra are stacked on top of one another in time order (the complexity of the H line is the result of an additional blend with the photospheric H_ϵ line). Any additional variable absorptions in the line profiles are readily apparent by comparison to the reference profiles also shown in each plot. For completeness only spectra obtained containing both the H and K lines simultaneously have been analysised. Images taken with the PM3000 CCD system are not analysised.

Analysis of the features observed occurs in Chapter 9.

8.1 β Pictoris H and K lines

Fig. 8.1 to 8.32 present the H and K line profiles of the 219 β Pic spectra obtained over 32 nights from the 21st of April to the 22nd of November 1997. Fig. 8.33 to 8.64 show the same profiles normalised showing the presence of any absorption features as deviations from the horizontal pseudo-continuum.

Observation times (UTC) are shown by the horizontal lines which cut the y-axis and intersect with the corresponding K spectrum. The same time applies for the H spectrum since the H and K lines are both observed simultaneously. The times shown are those at the beginning of an exposure. Typical exposures for β Pic were 30 minutes, meaning an additional 15 minutes needs to be added on to give the times of mid-exposure as shown in Appendix D.

8.2 51 Ophiuchi H and K lines

Fig. 8.65 to 8.88 present the H and K line profiles of the 94 51 Oph spectra obtained over 24 nights from the 21st of April to the 19th of September 1997. Fig. 8.89 to 8.112 show the same profiles normalised showing the presence of any absorption features as deviations from the horizontal pseudo-continuum.

Observation times (UTC) are shown by the horizontal lines which cut the y-axis and intersect with the corresponding K spectrum. The same time applies for the H spectrum since the H and K lines are both observed simultaneously. The times shown are those at the beginning of an exposure. Typical exposures for 51 Oph were 60 minutes, meaning an additional 30 minutes needs to be added on to give the times of mid-exposure as shown in Appendix D.

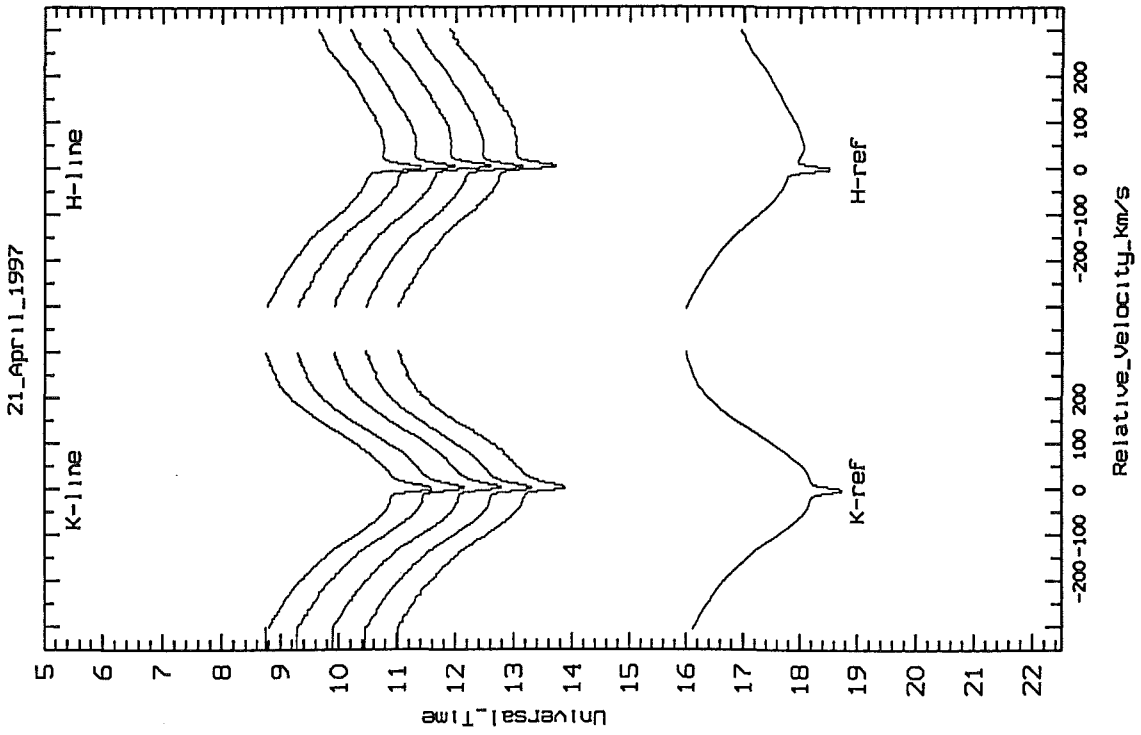

Figure 8.1: β Pic spectra taken on 21st April 1997.

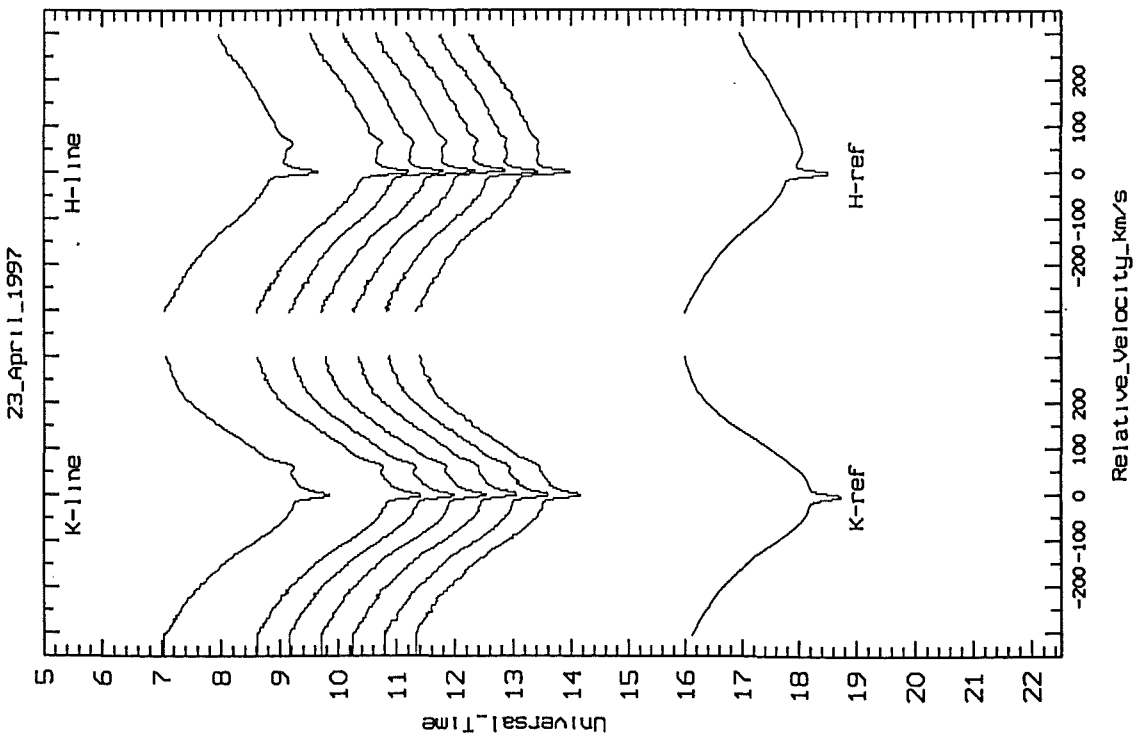

Figure 8.2: β Pic spectra taken on 23rd April 1997.

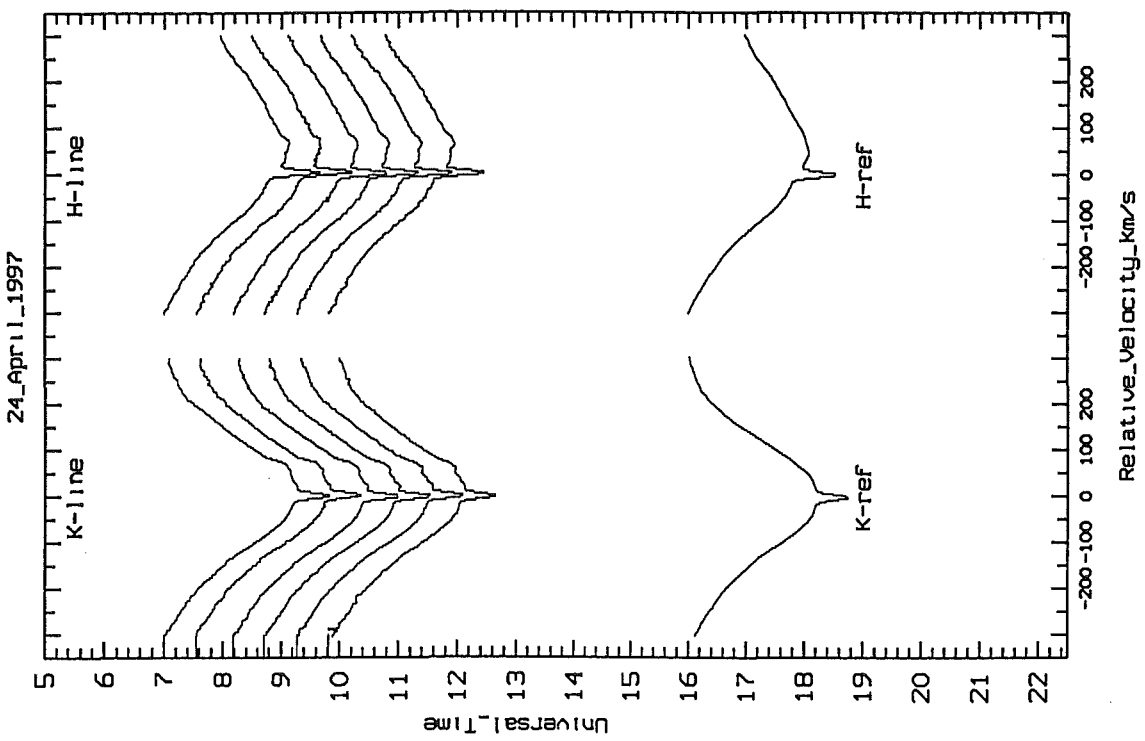

Figure 8.3: β Pic spectra taken on 24th April 1997.

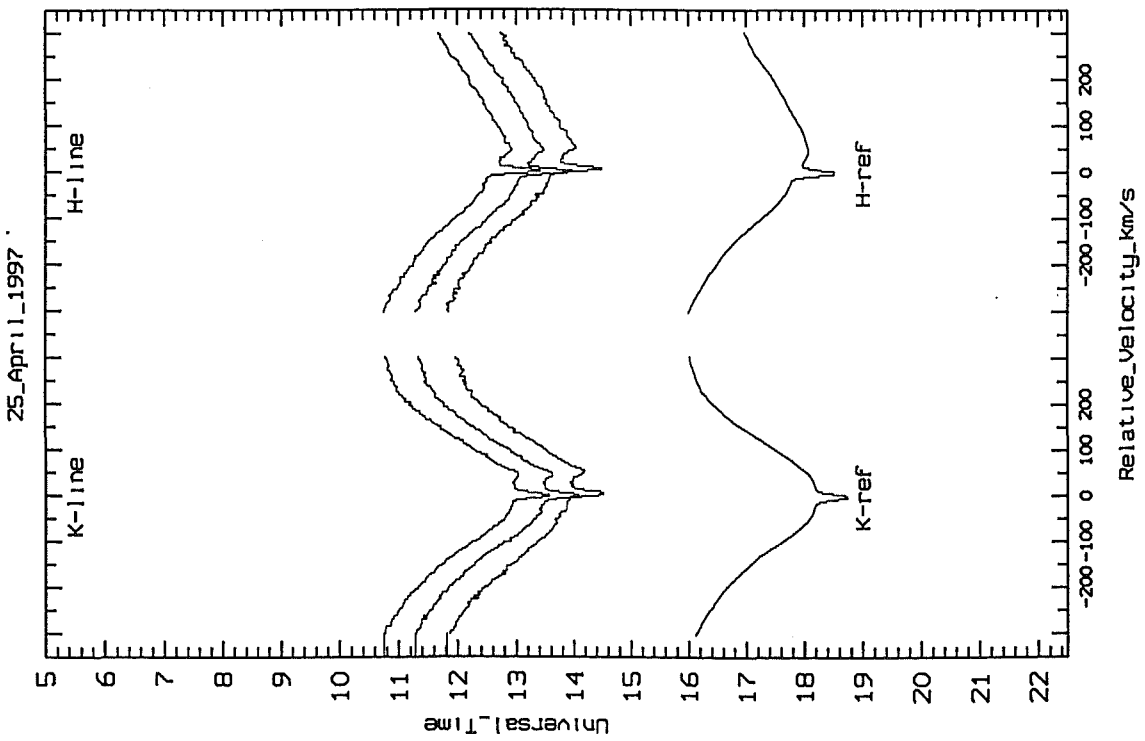

Figure 8.4: β Pic spectra taken on 25th April 1997.

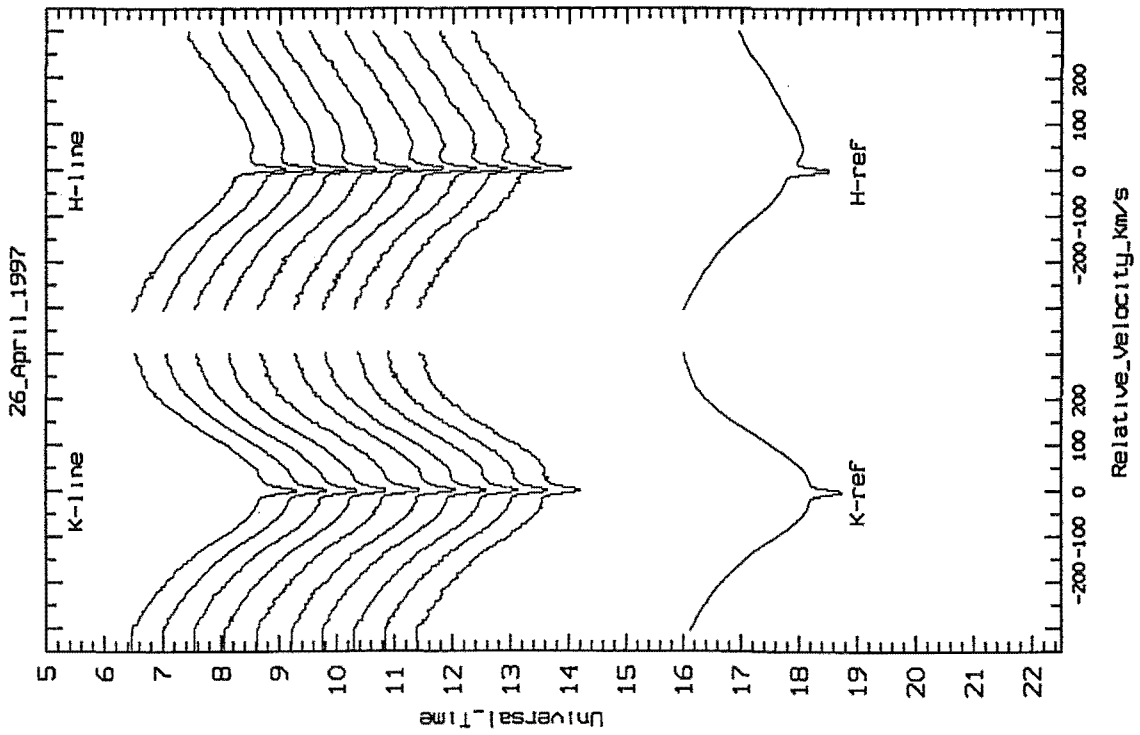

Figure 8.5: β Pic spectra taken on 26th April 1997.

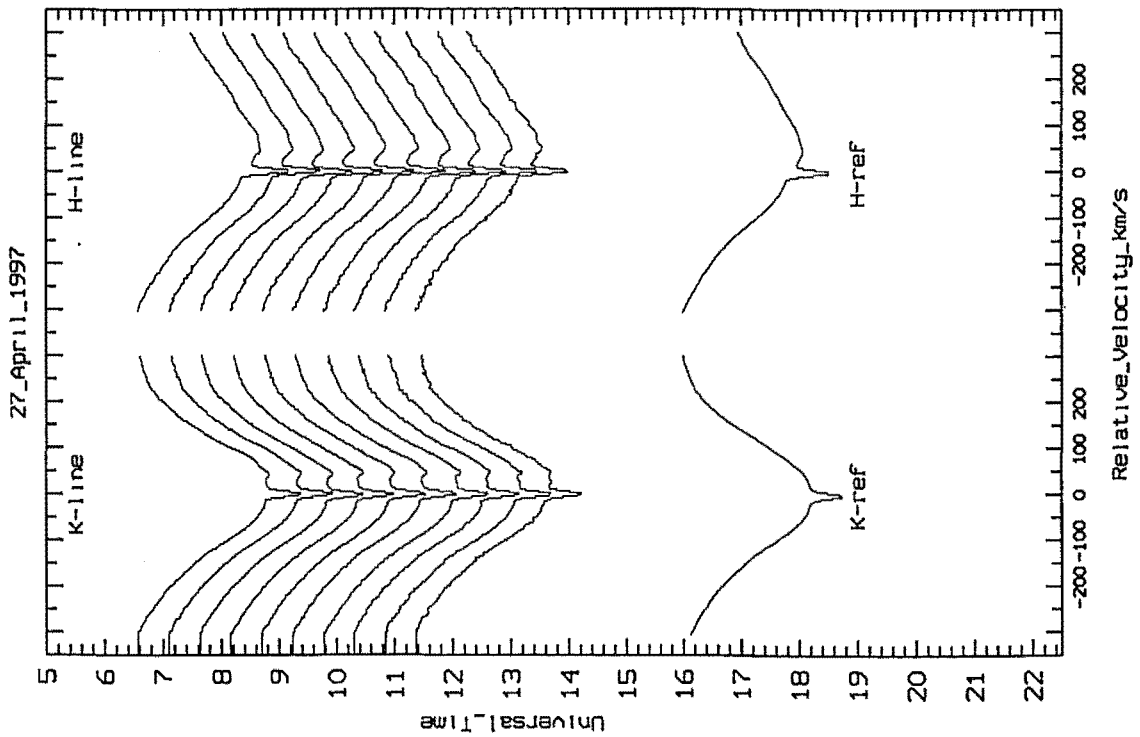

Figure 8.6: β Pic spectra taken on 27th April 1997.

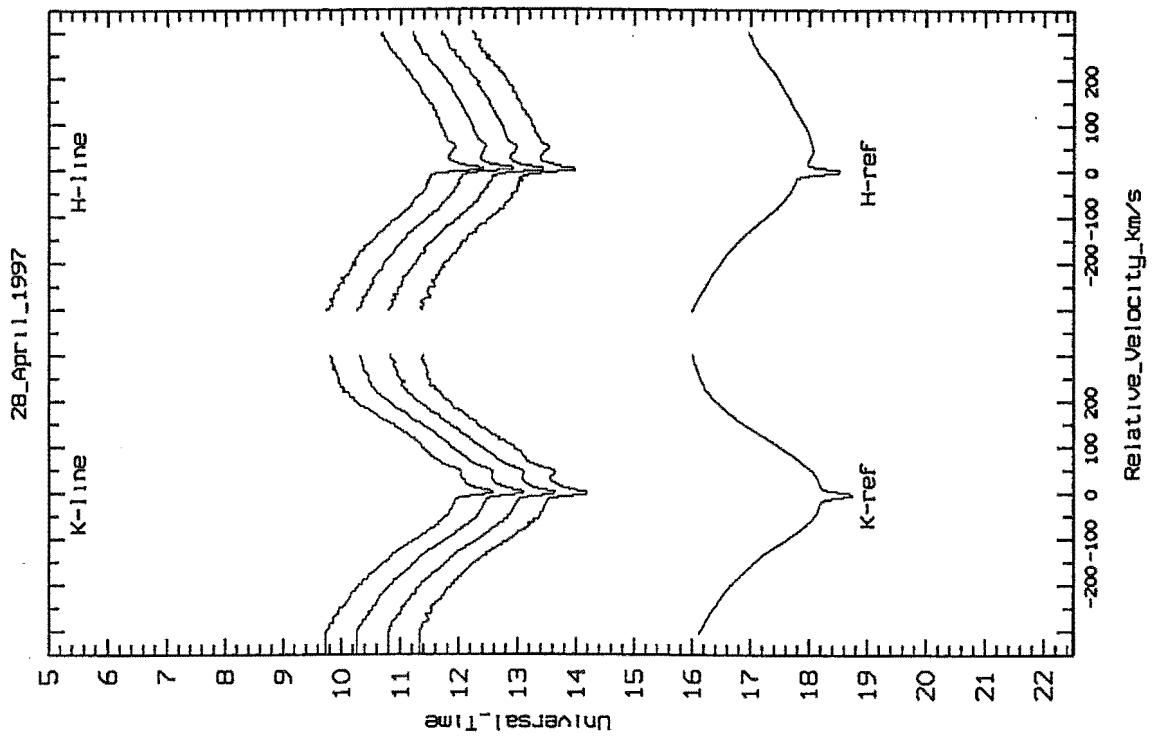

Figure 8.7: β Pic spectra taken on 28th April 1997.

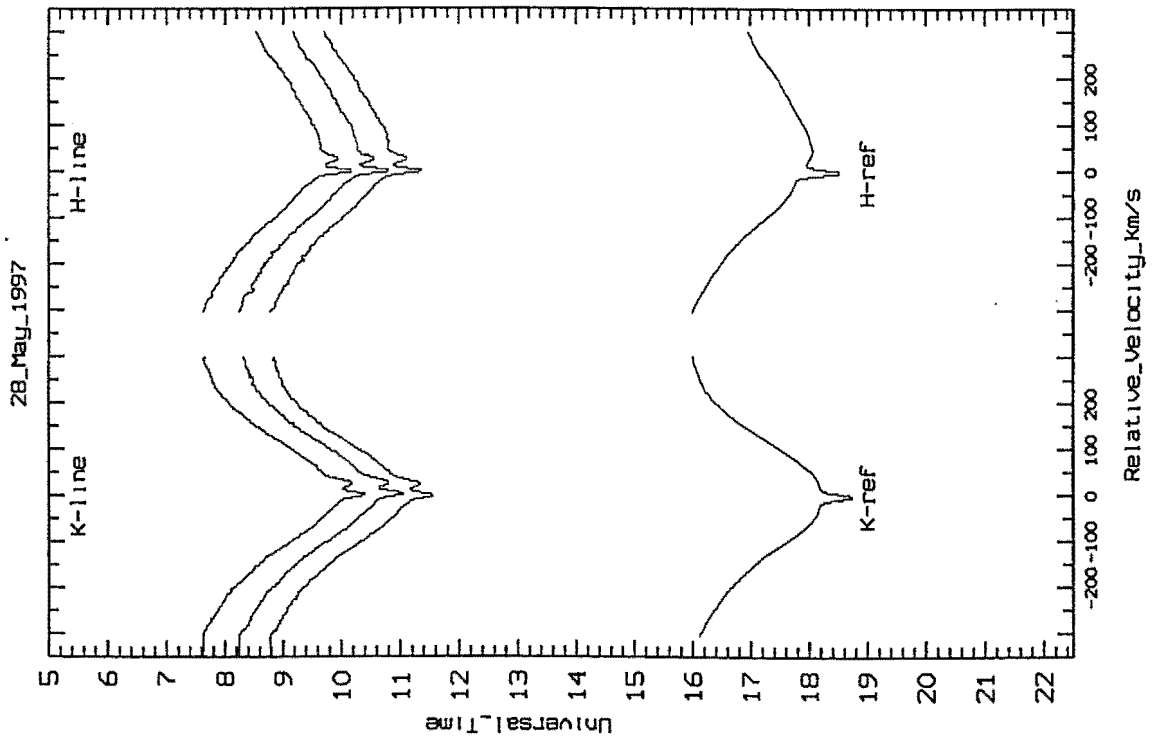

Figure 8.8: β Pic spectra taken on 28th May 1997.

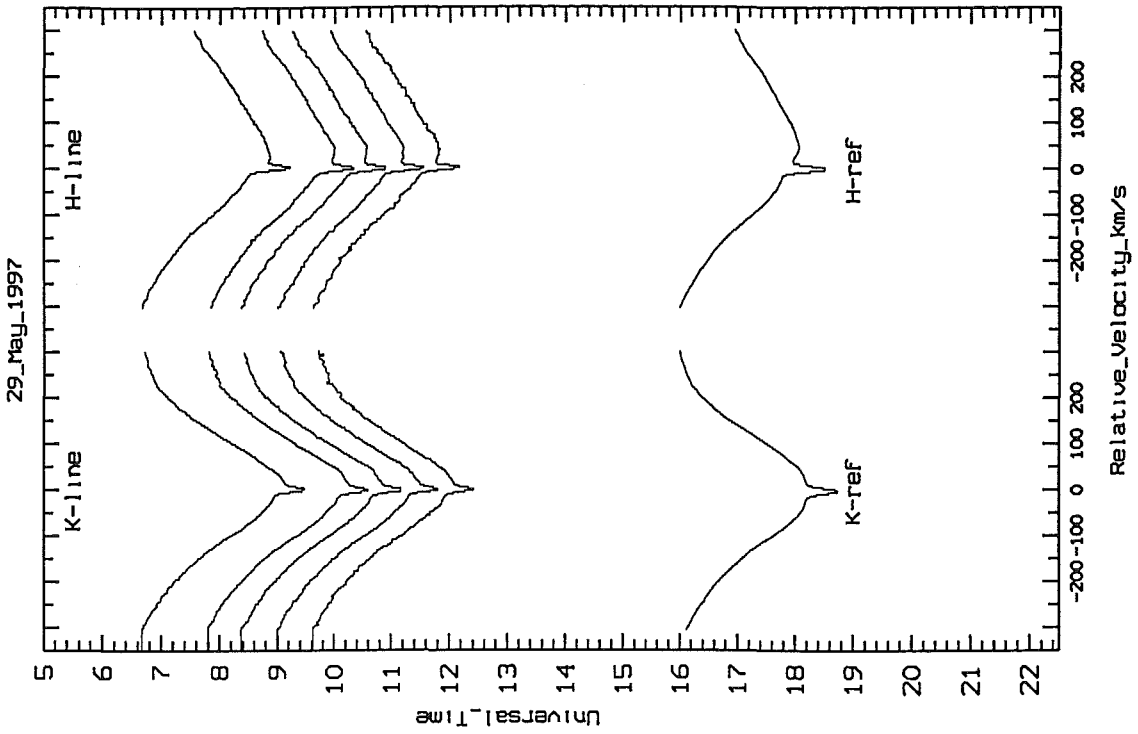

Figure 8.9: β Pic spectra taken on 29th May 1997.

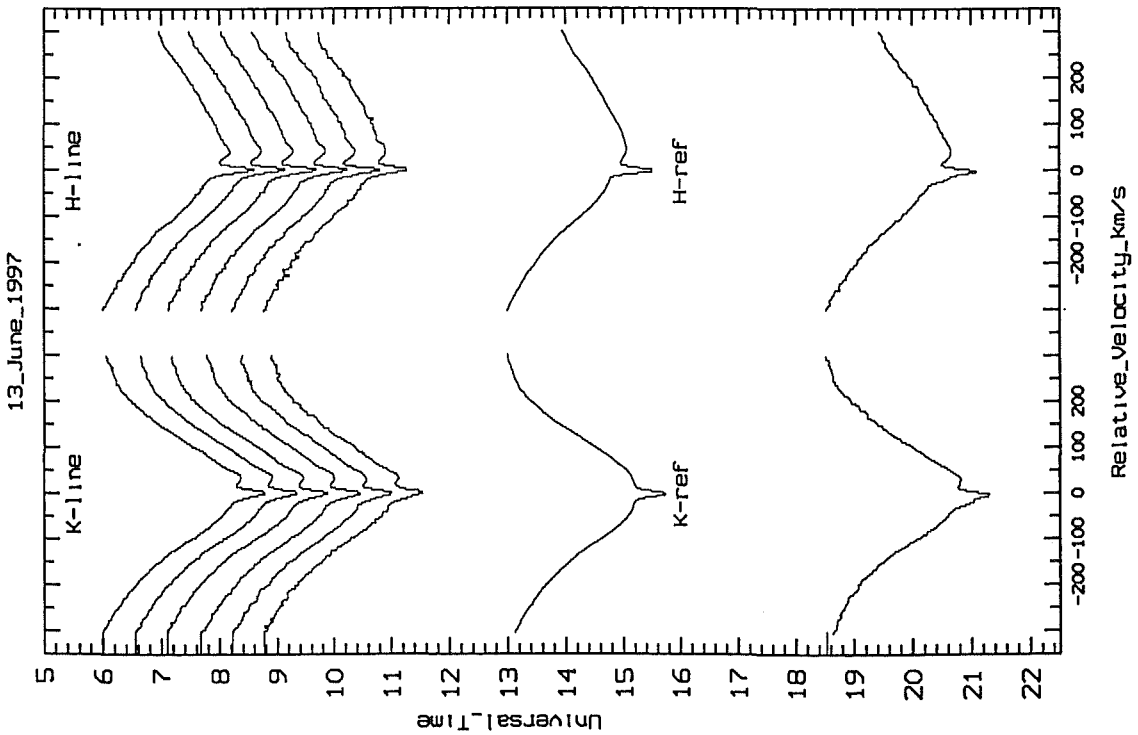

Figure 8.10: β Pic spectra taken on 13th June 1997.

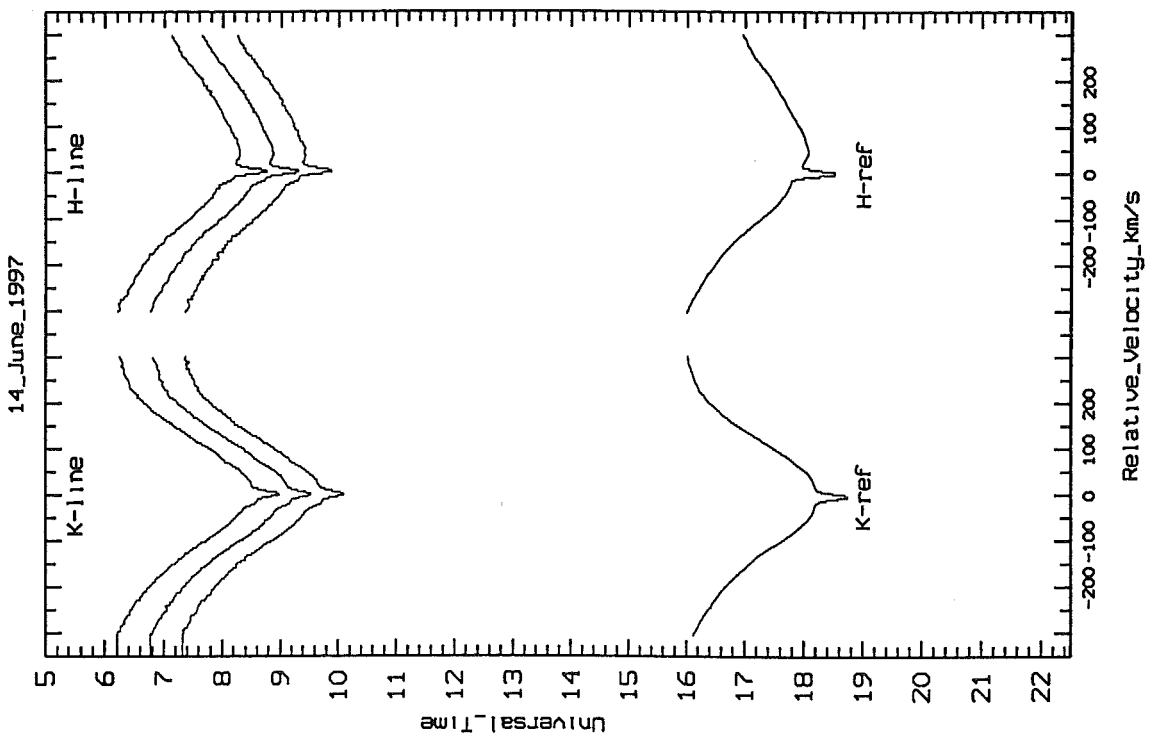

Figure 8.11: β Pic spectra taken on 14th June 1997.

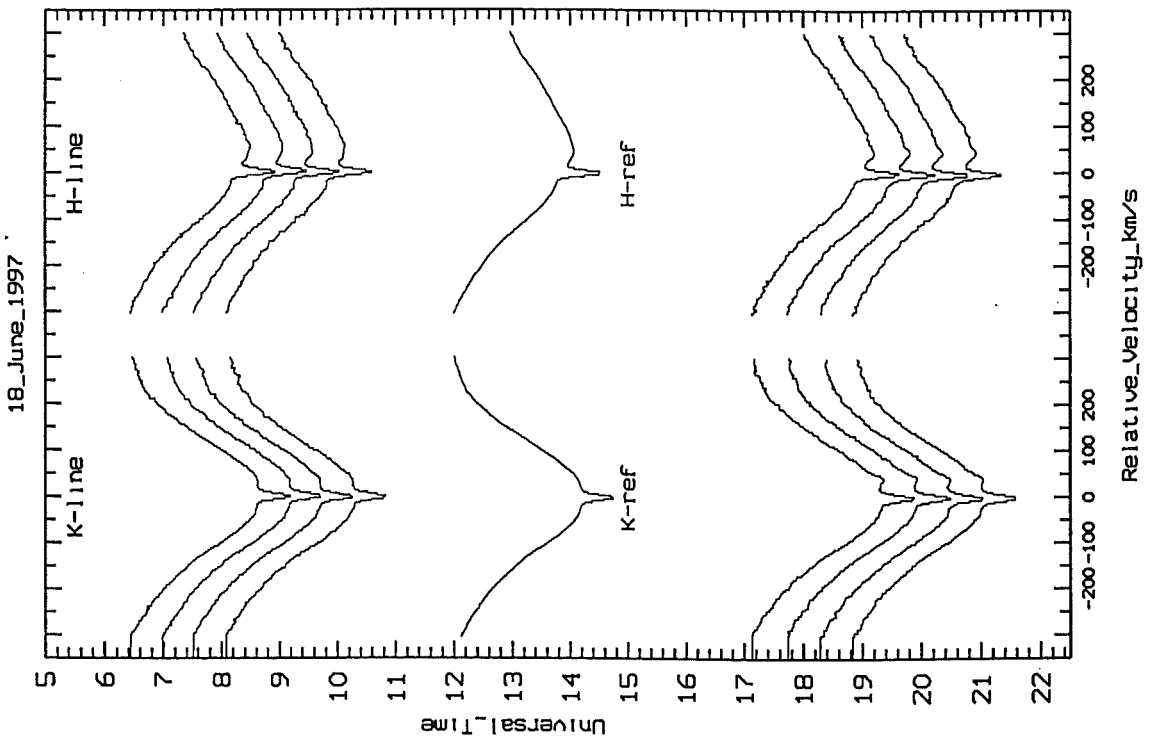

Figure 8.12: β Pic spectra taken on 18th June 1997.

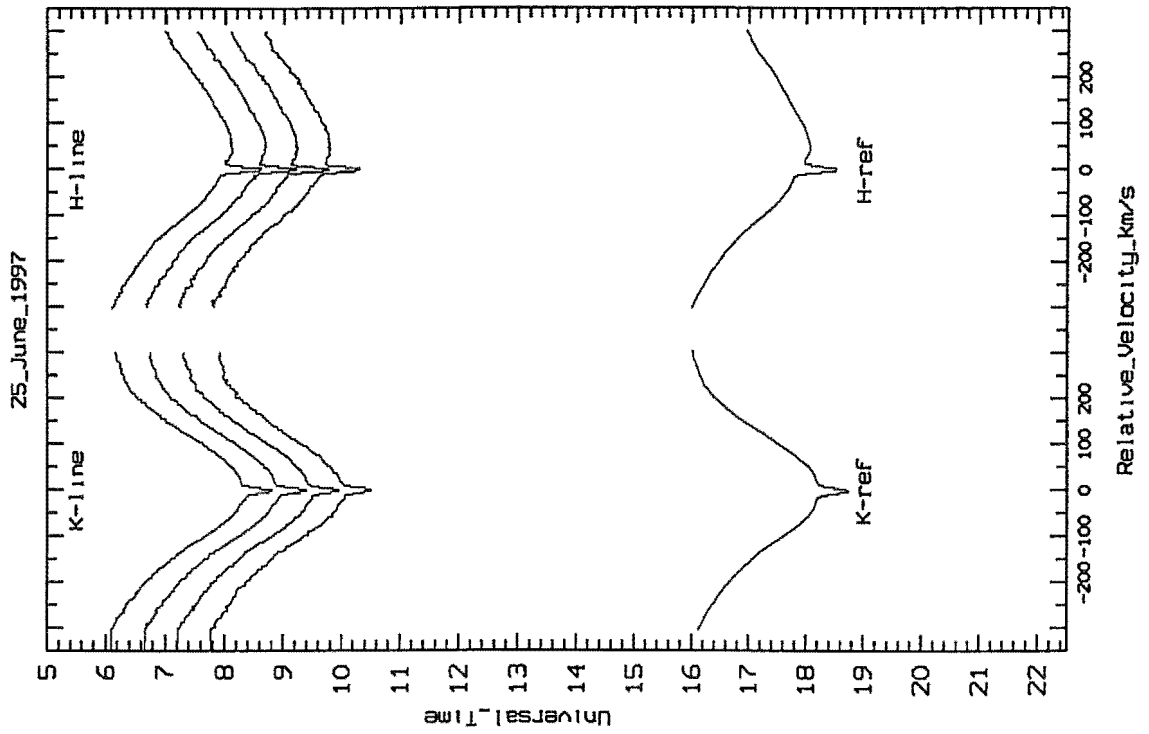

Figure 8.13: β Pic spectra taken on 25th June 1997.

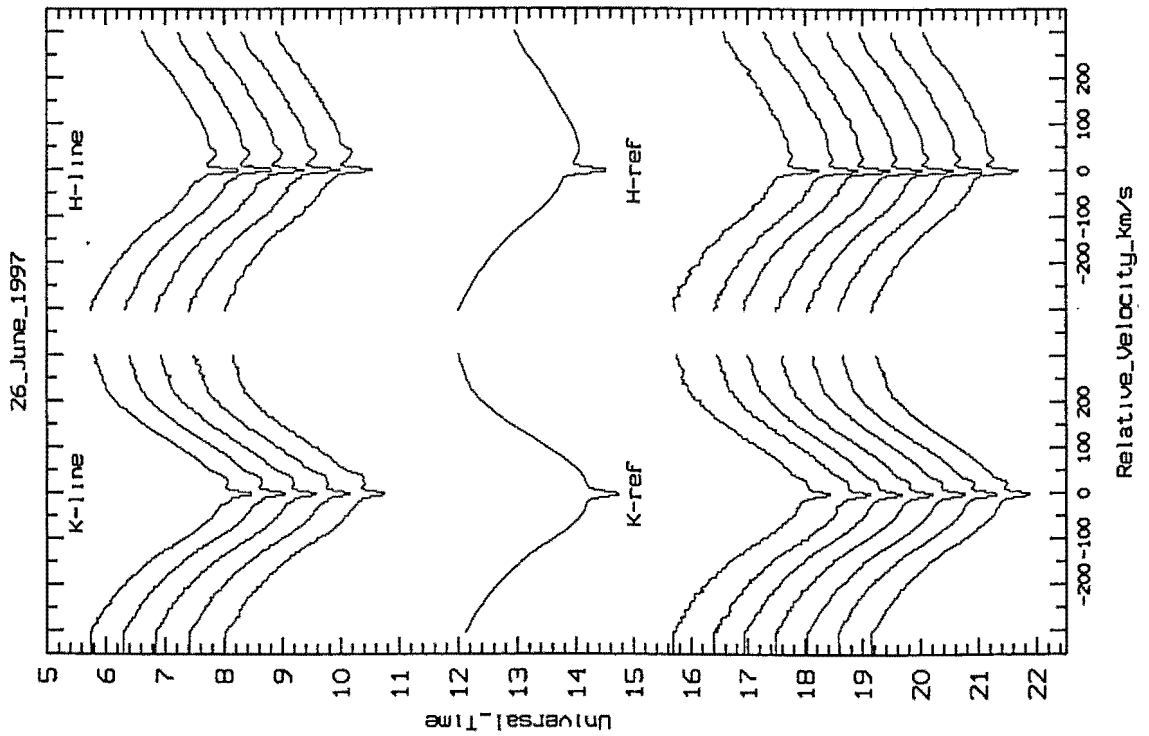

Figure 8.14: β Pic spectra taken on 26th June 1997.

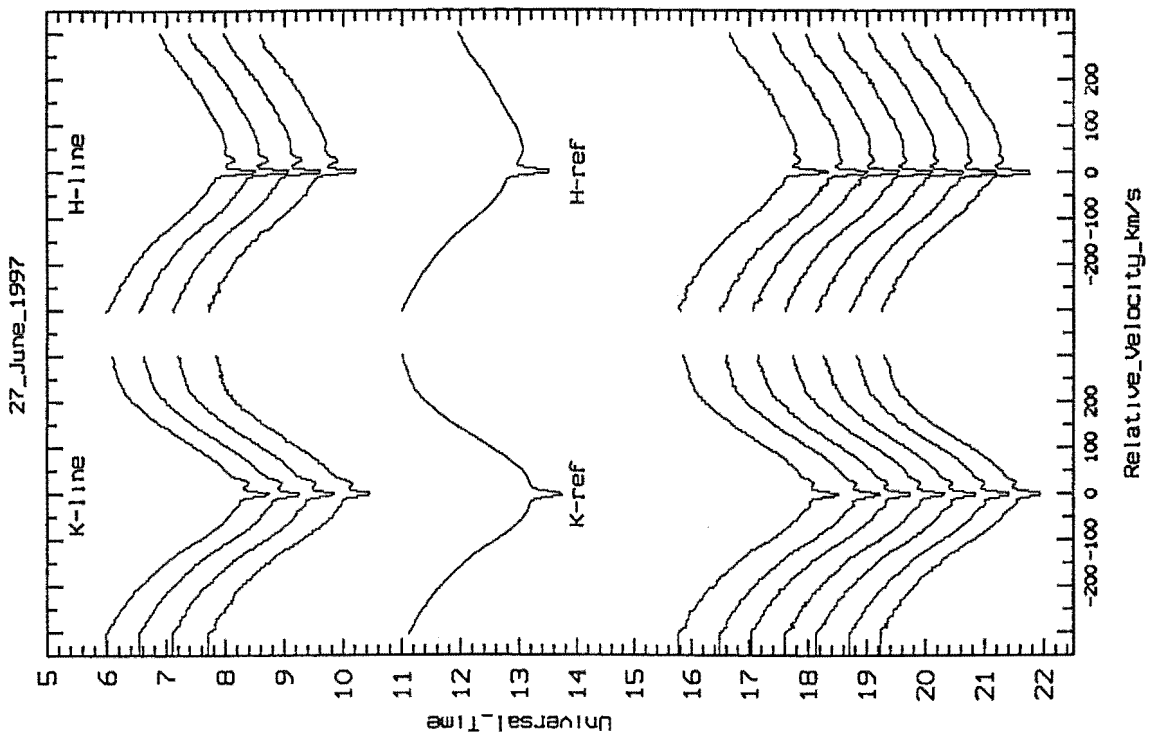

Figure 8.15: β Pic spectra taken on 27th June 1997.

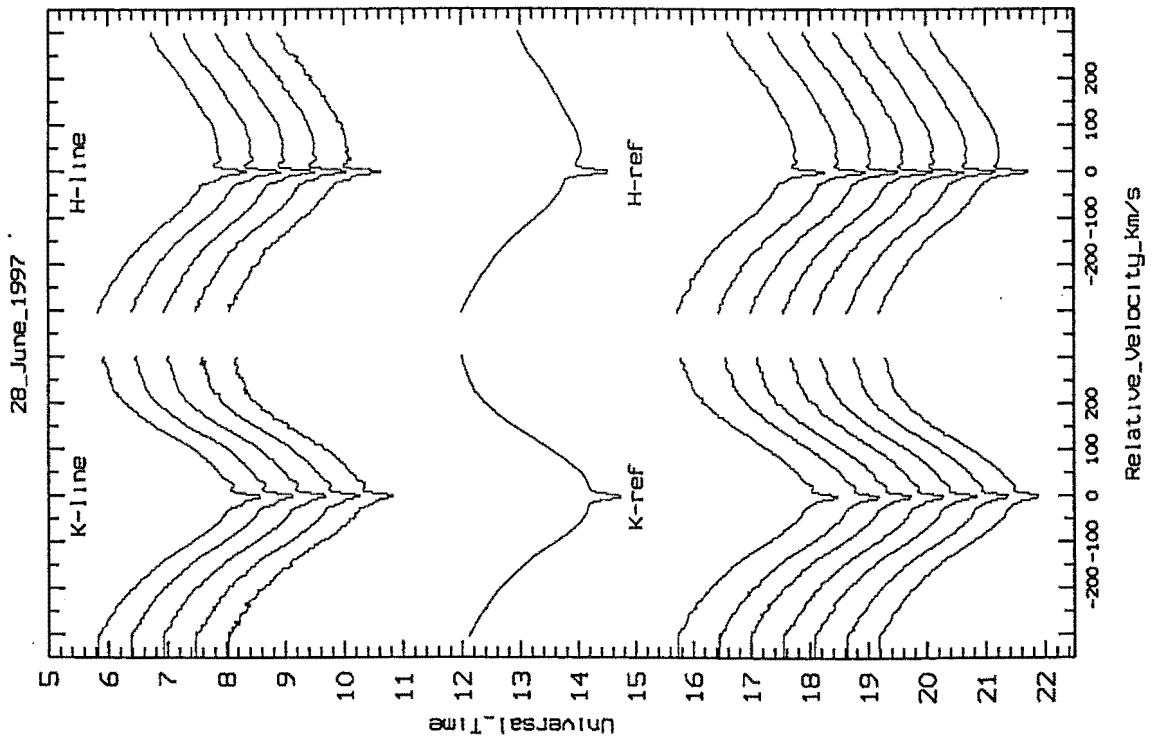

Figure 8.16: β Pic spectra taken on 28th June 1997.

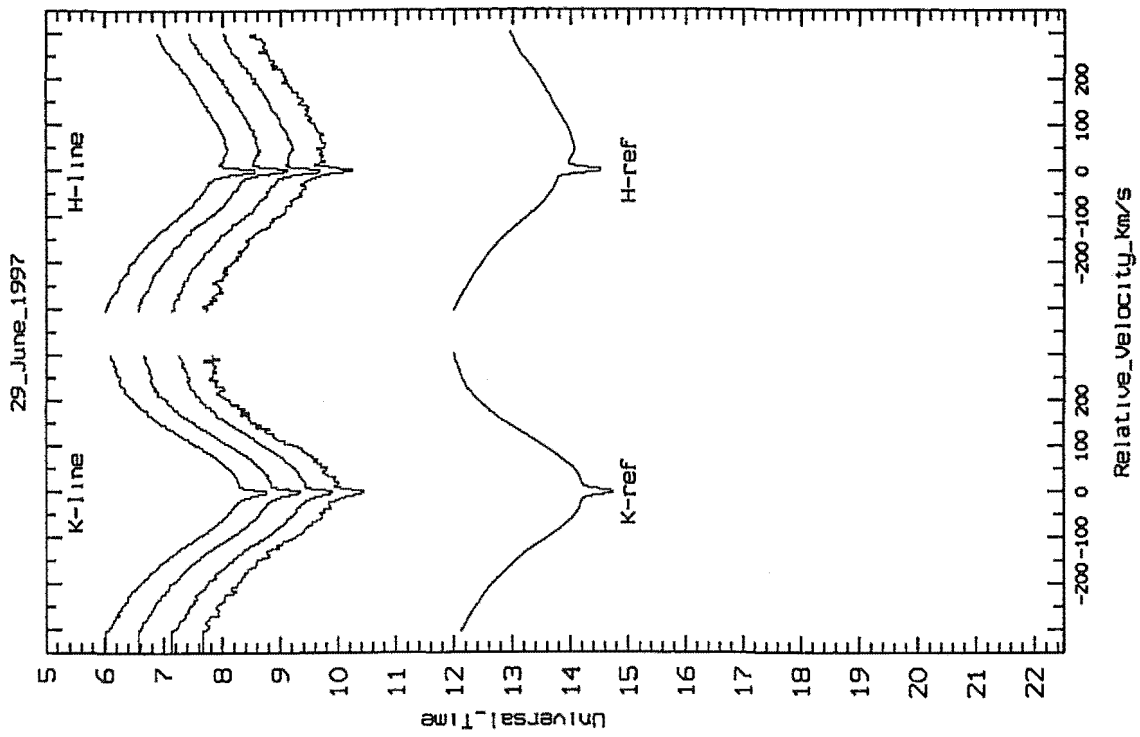

Figure 8.17: β Pic spectra taken on 29th June 1997.

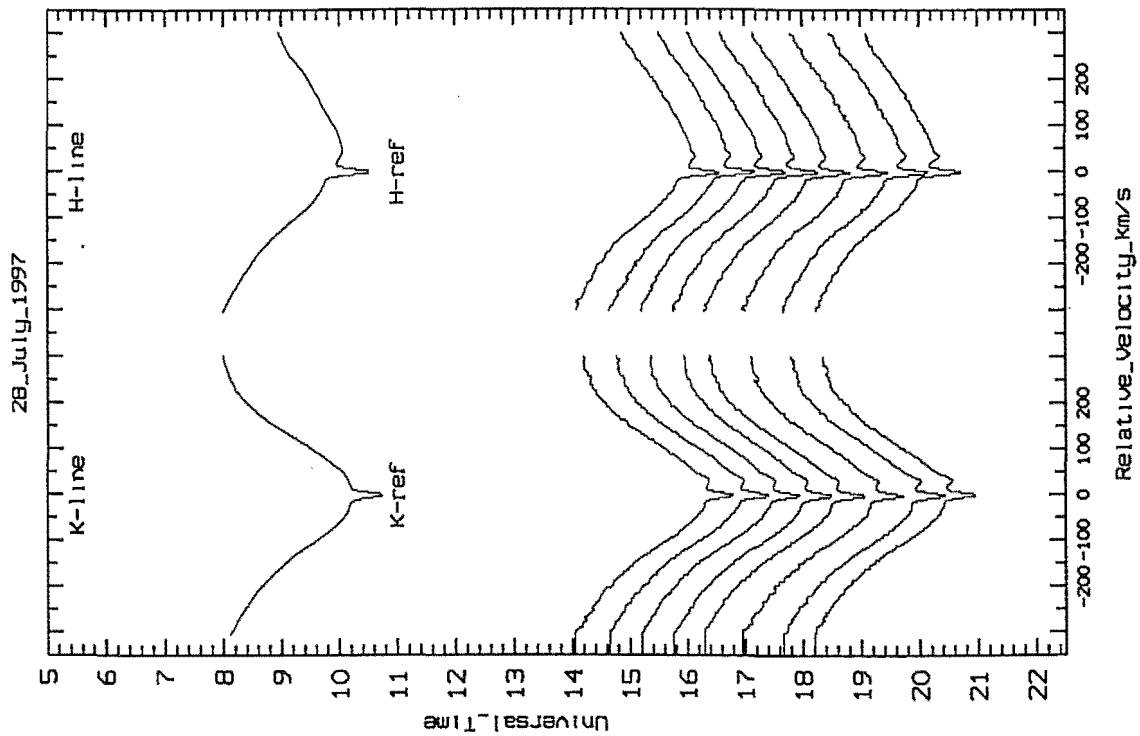

Figure 8.18: β Pic spectra taken on 28th July 1997.

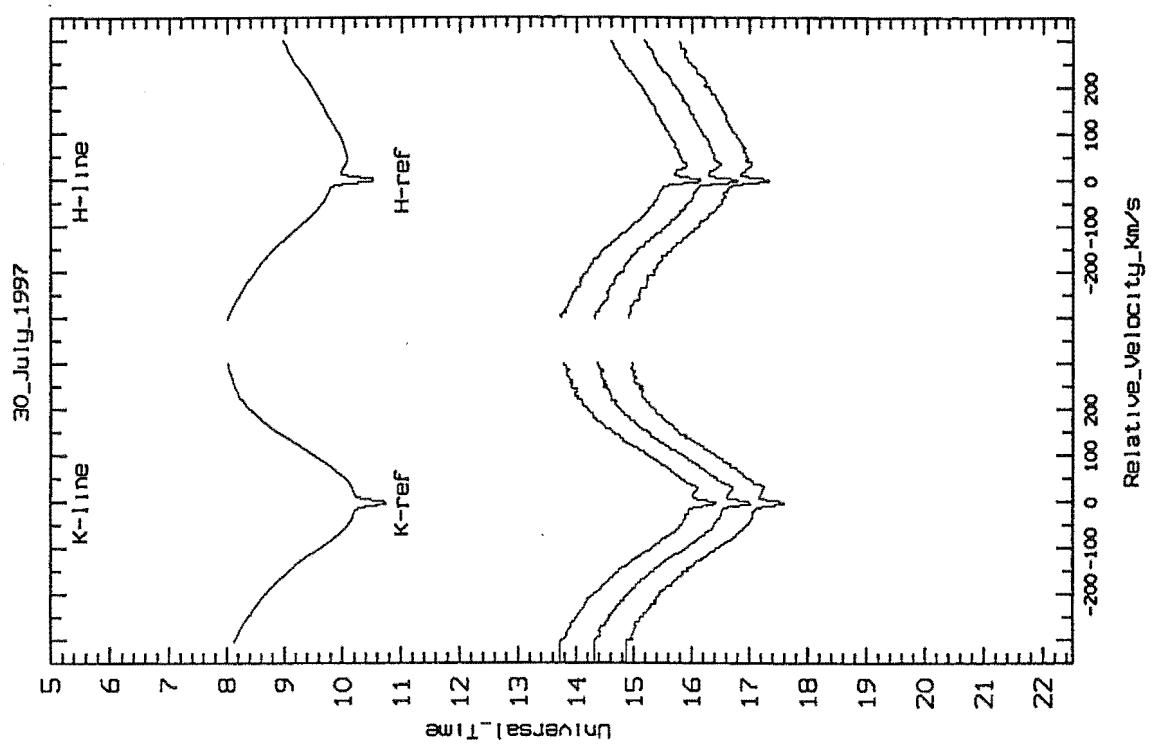

Figure 8.19: β Pic spectra taken on 30th July 1997.

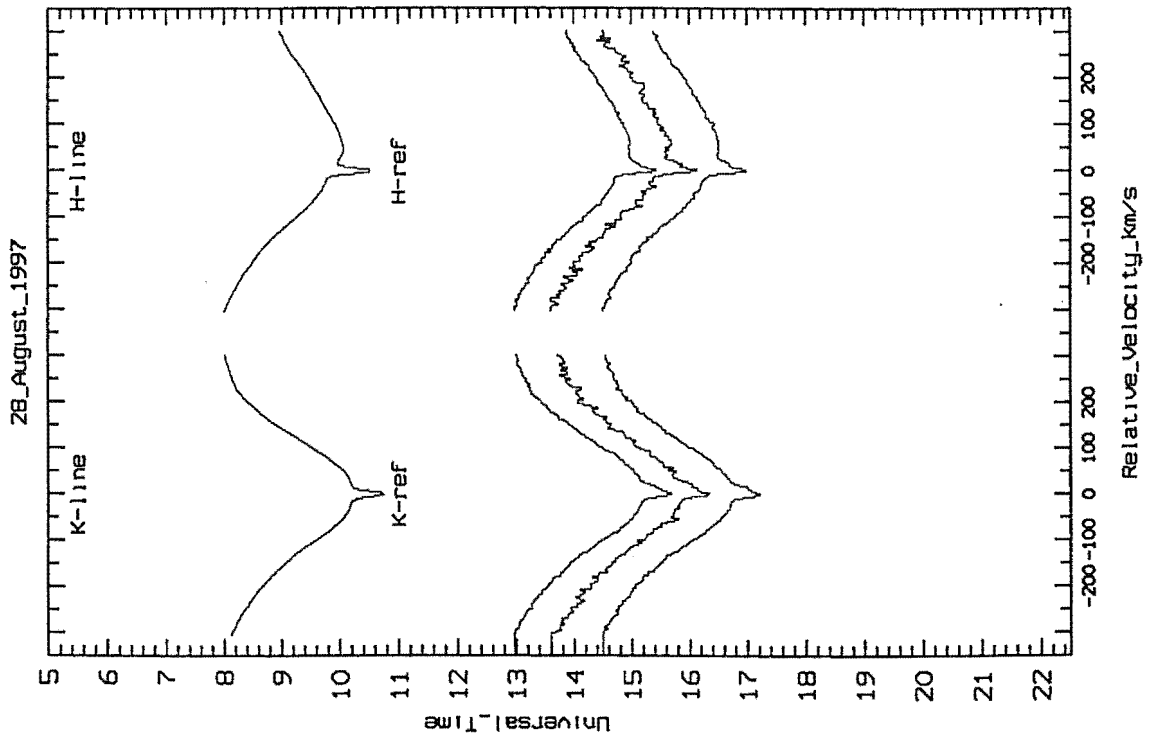

Figure 8.20: β Pic spectra taken on 28th August 1997.

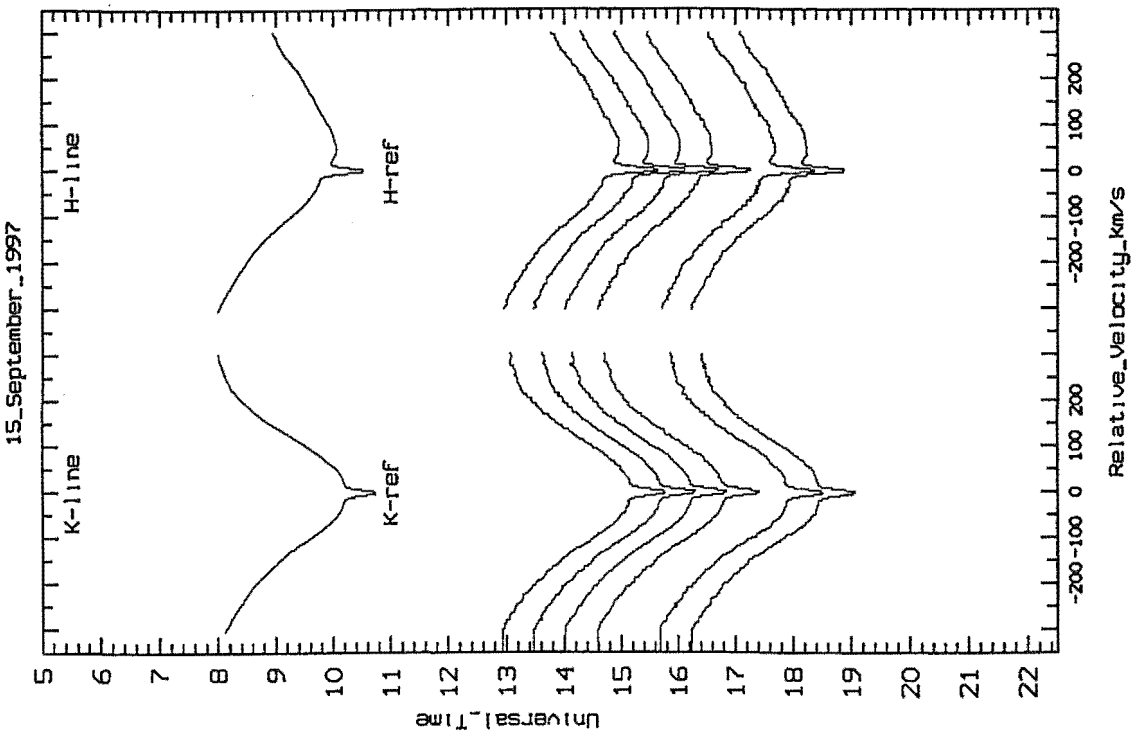

Figure 8.21: β Pic spectra taken on 15th September 1997.

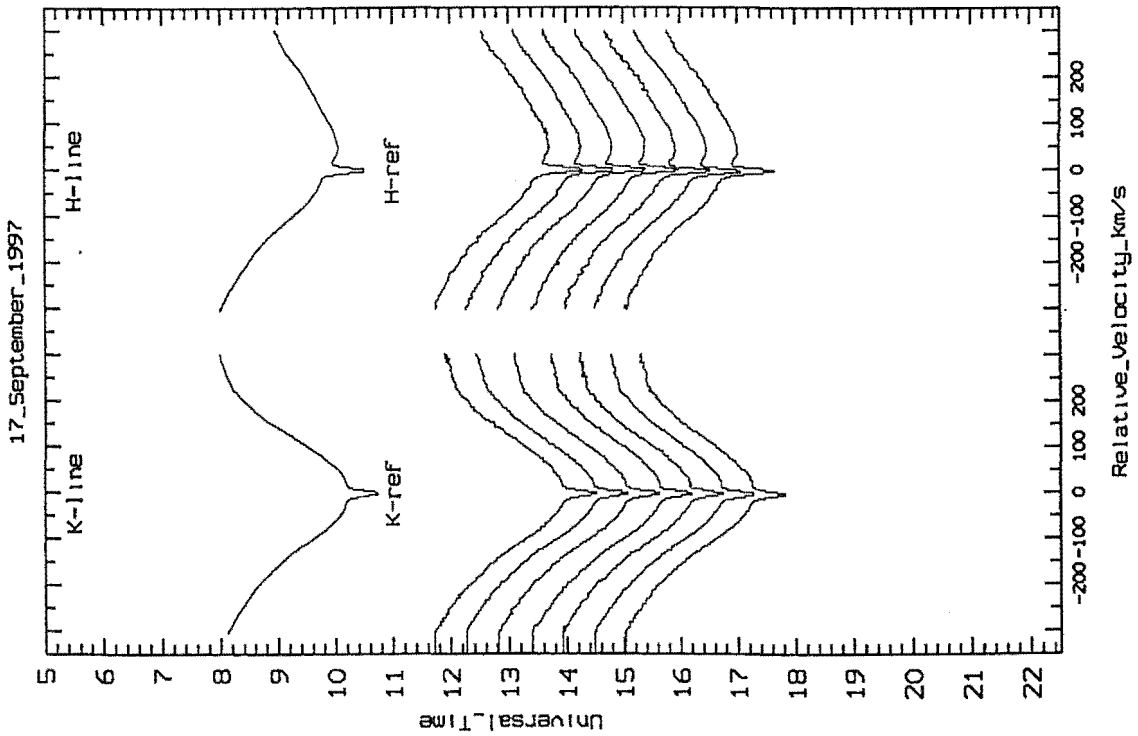

Figure 8.22: β Pic spectra taken on 17th September 1997.

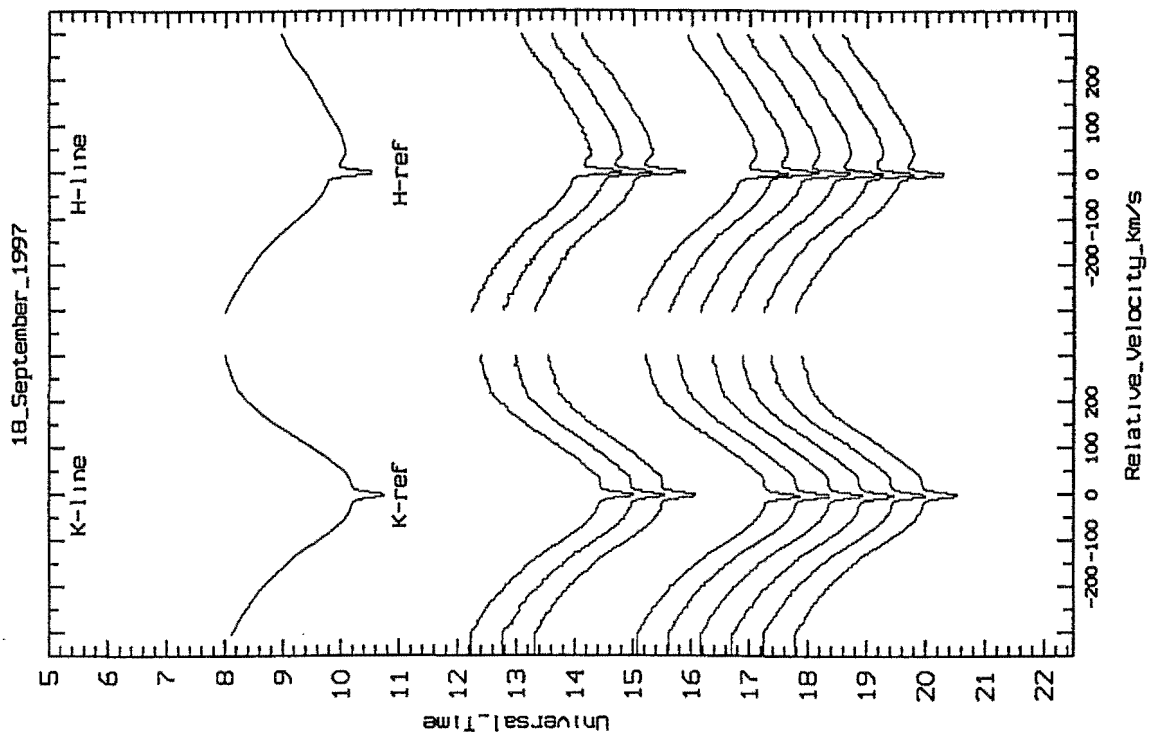

Figure 8.23: β Pic spectra taken on 18th September 1997.

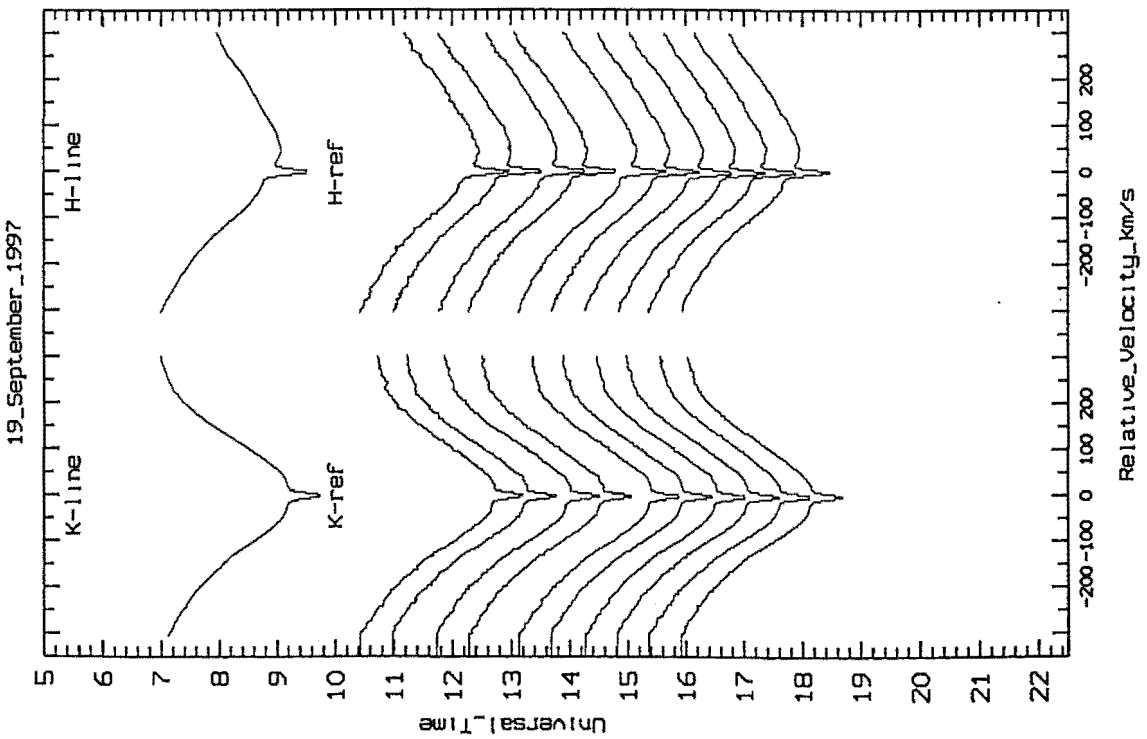

Figure 8.24: β Pic spectra taken on 19th September 1997.

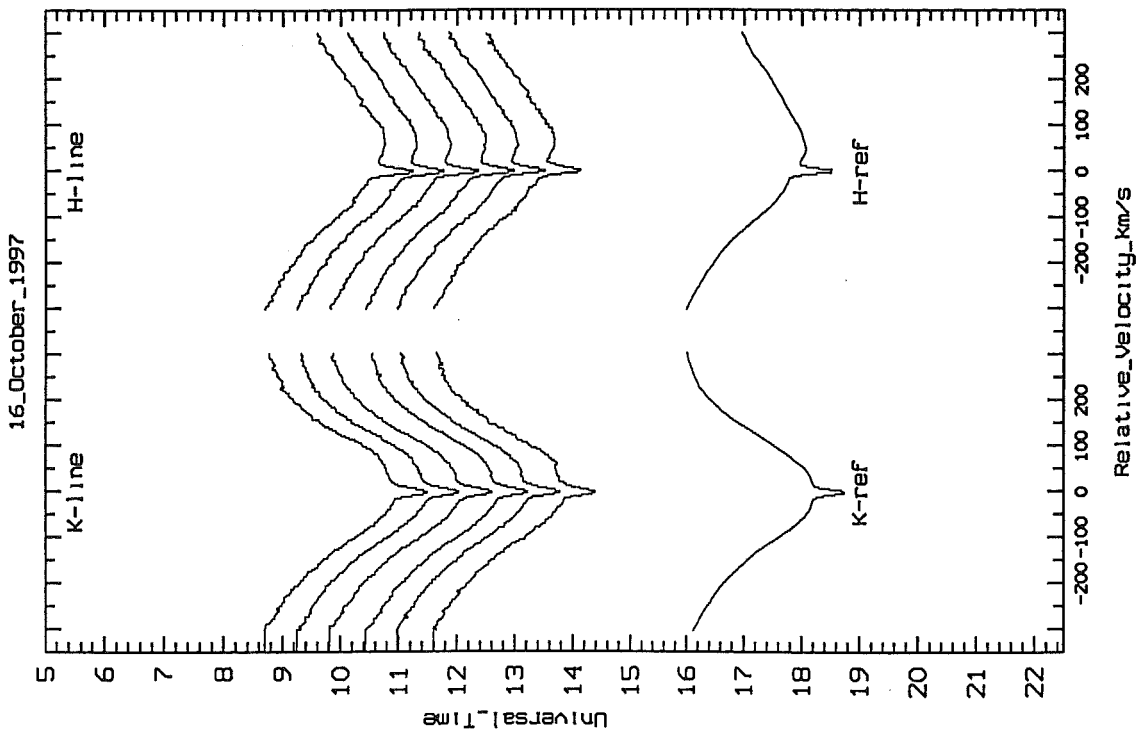

Figure 8.25: β Pic spectra taken on 16th October 1997.

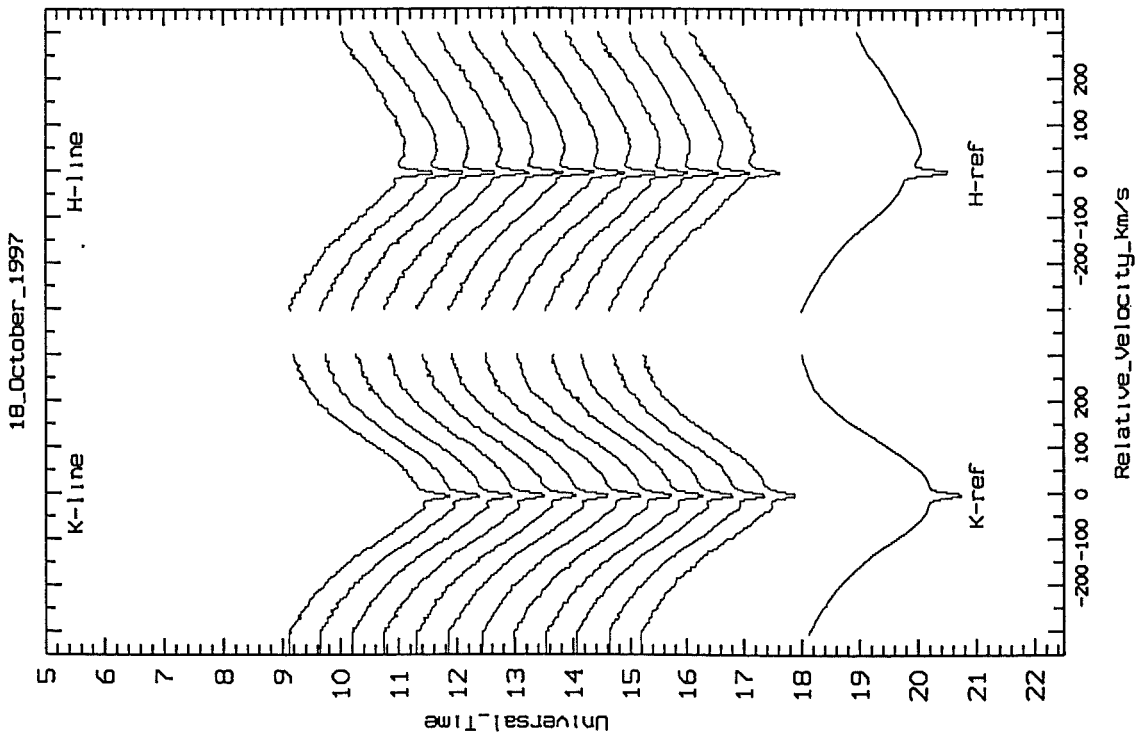

Figure 8.26: β Pic spectra taken on 18th October 1997.

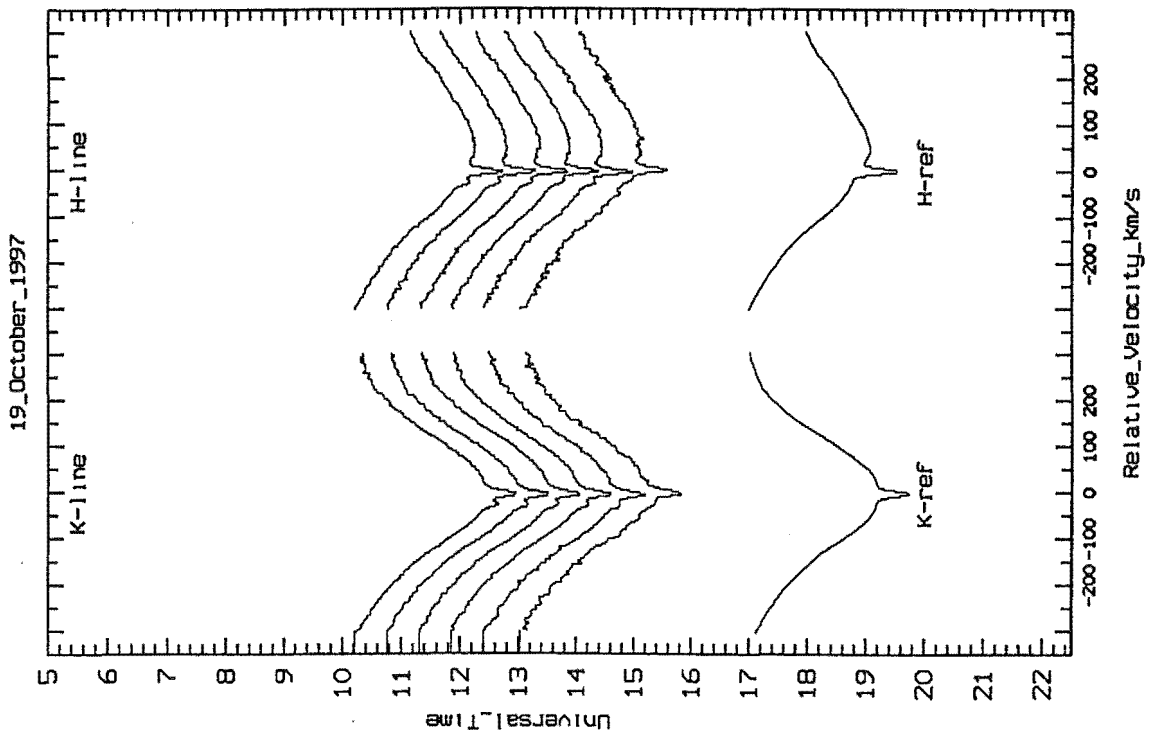

Figure 8.27: β Pic spectra taken on 19th October 1997.

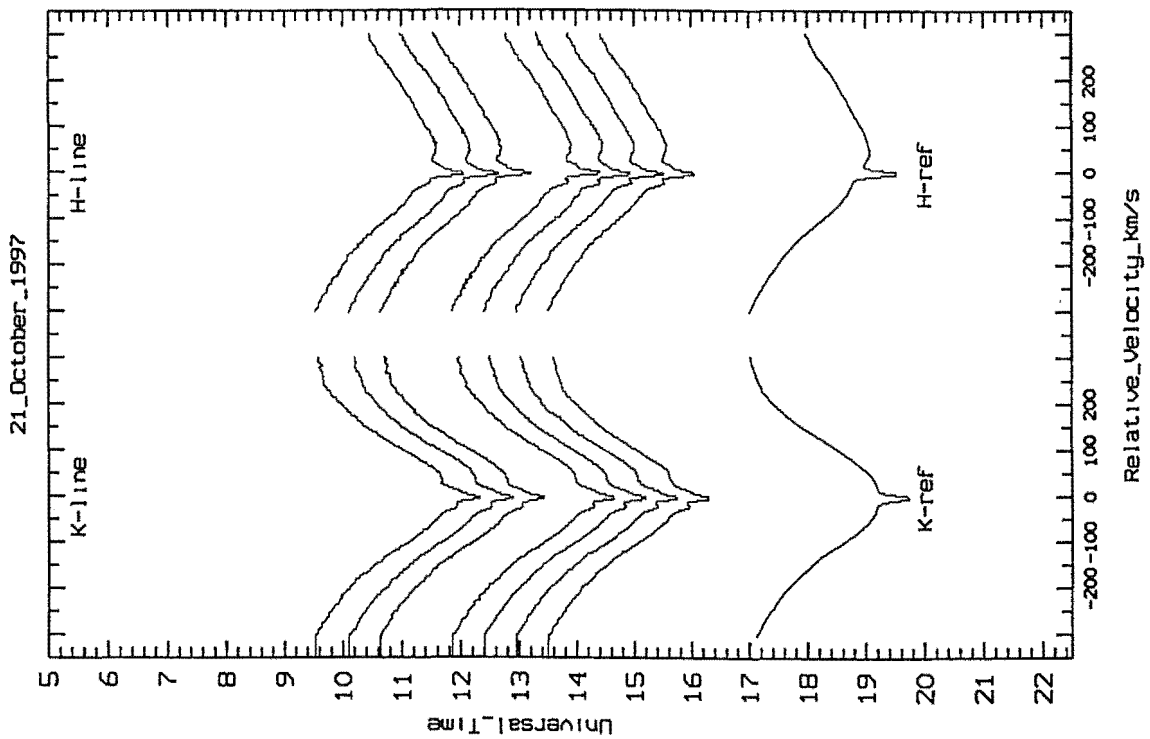

Figure 8.28: β Pic spectra taken on 21st October 1997.

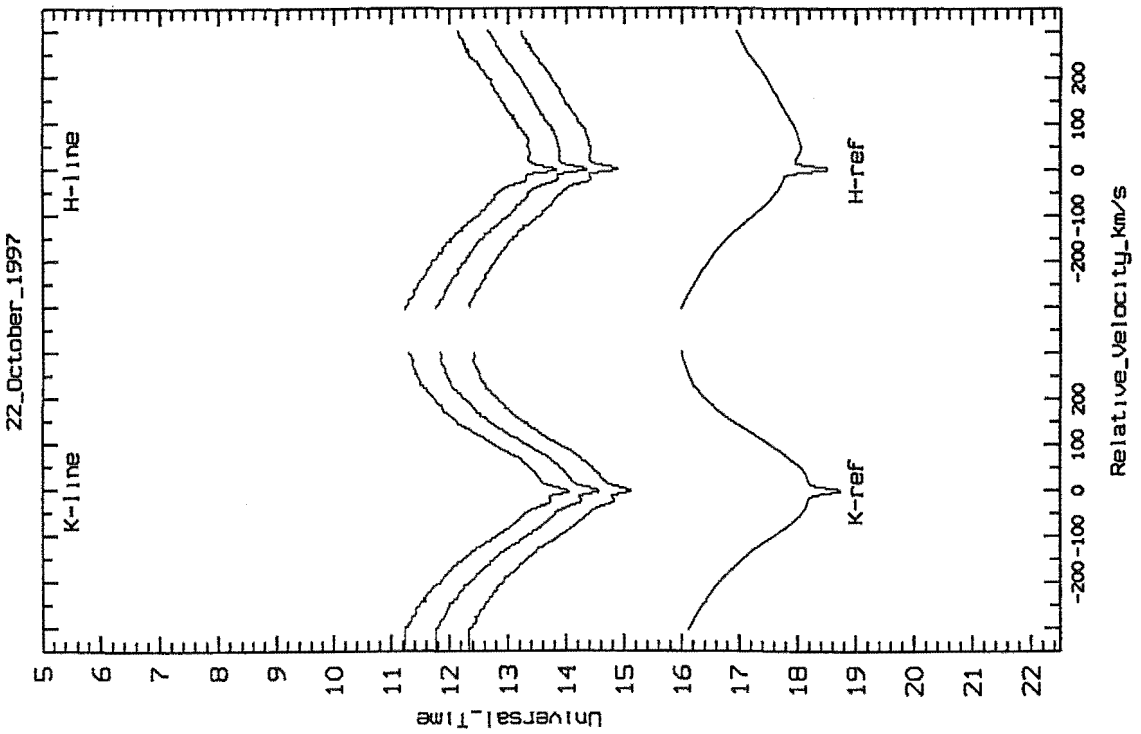

Figure 8.29: β Pic spectra taken on 22nd October 1997.

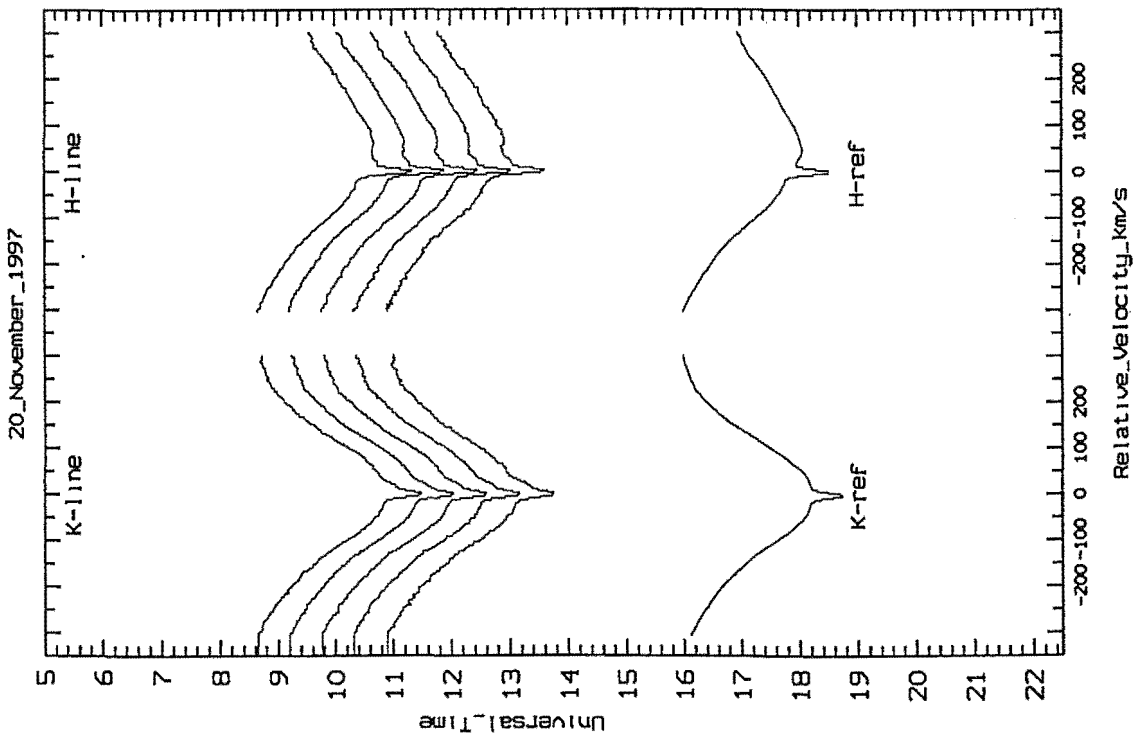

Figure 8.30: β Pic spectra taken on 20th November 1997.

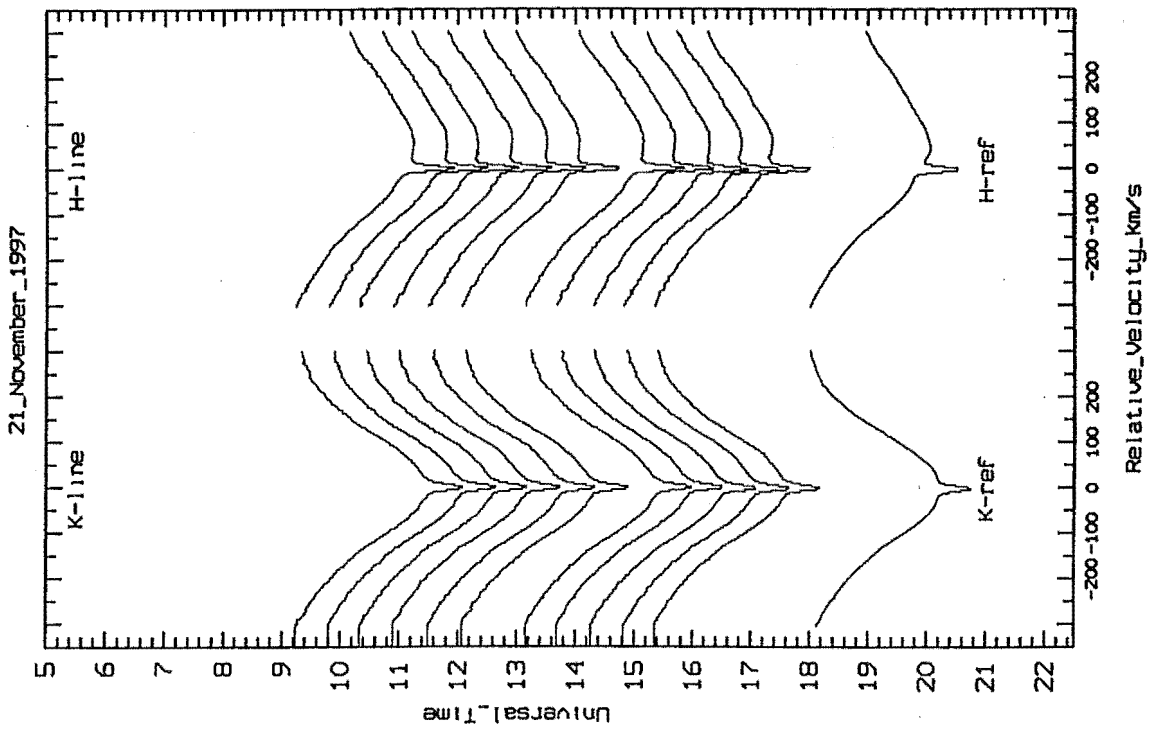

Figure 8.31: β Pic spectra taken on 21st November 1997.

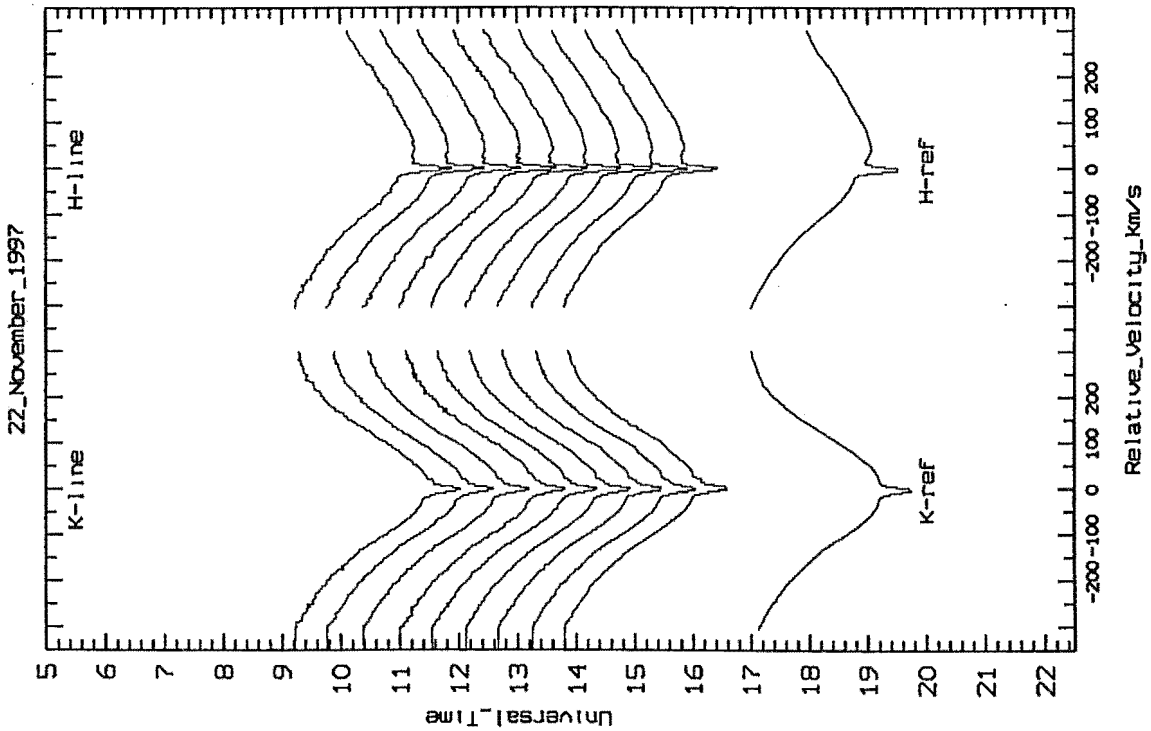

Figure 8.32: β Pic spectra taken on 22nd November 1997.

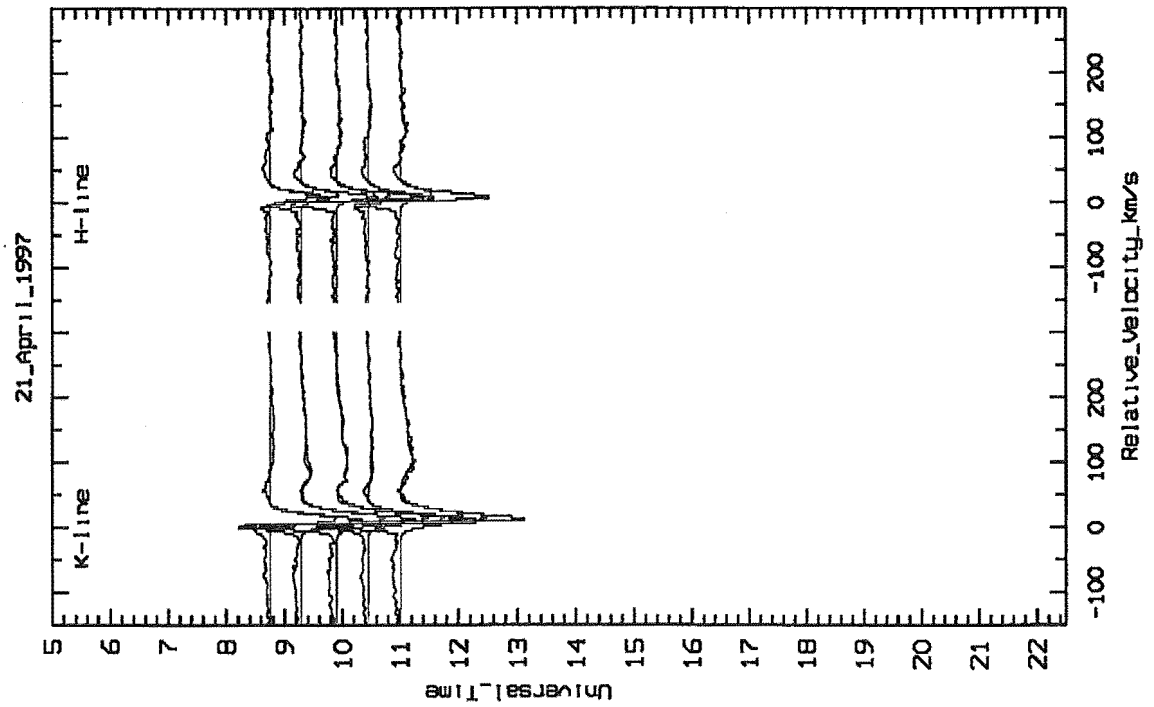

Figure 8.33: Normalised β Pic spectra taken on 21st April 1997.

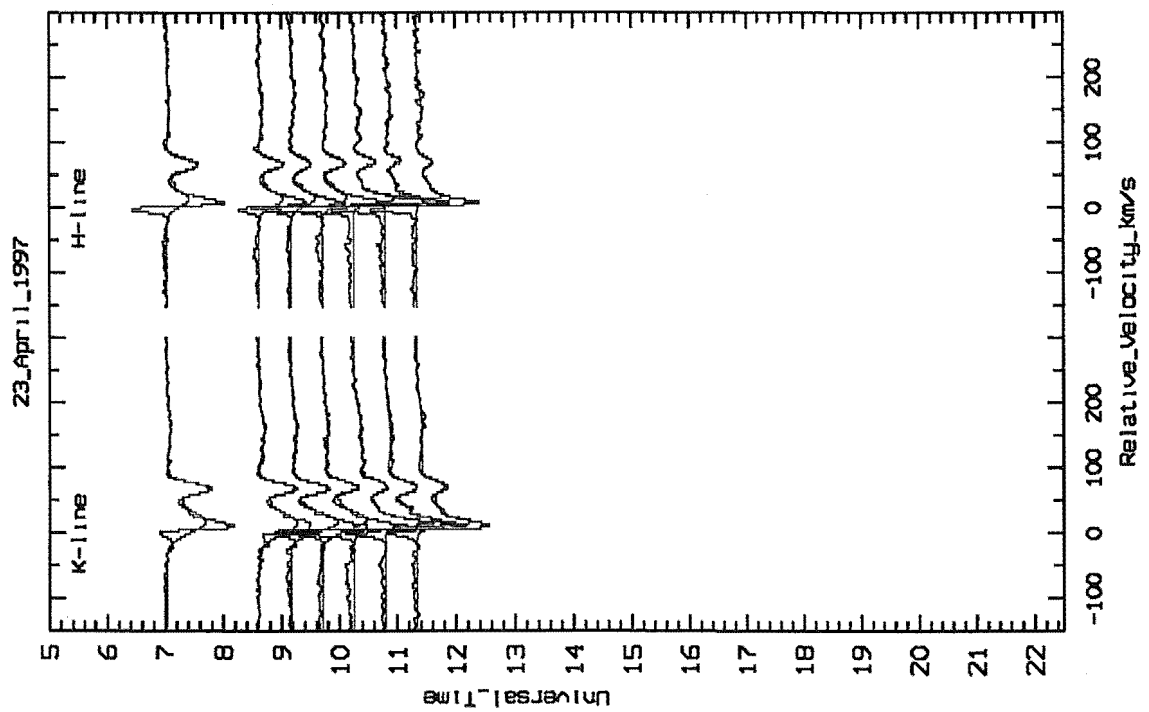

Figure 8.34: Normalised β Pic spectra taken on 23rd April 1997.

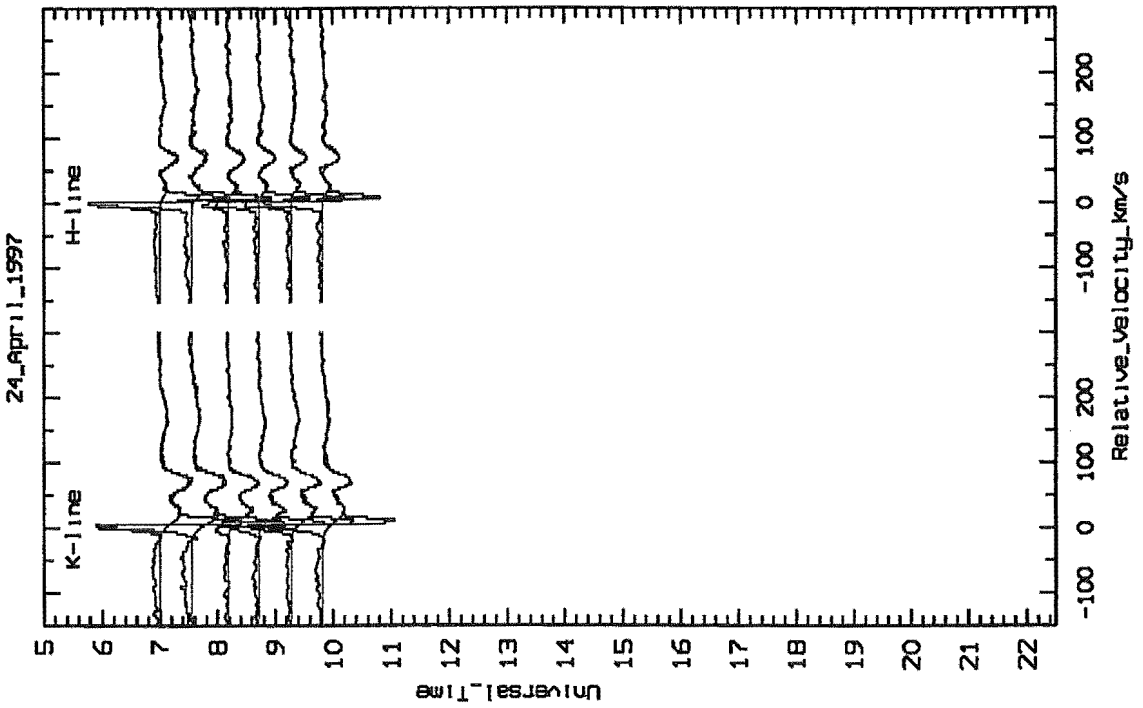

Figure 8.35: Normalised β Pic spectra taken on 24th April 1997.

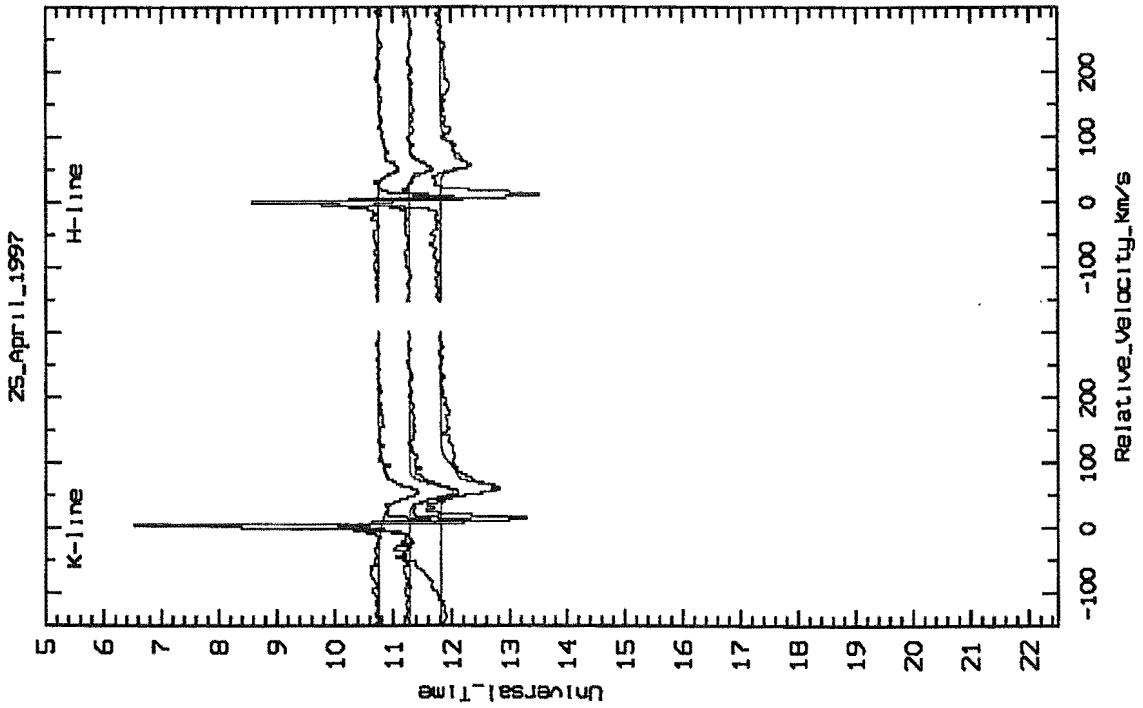

Figure 8.36: Normalised β Pic spectra taken on 25th April 1997.

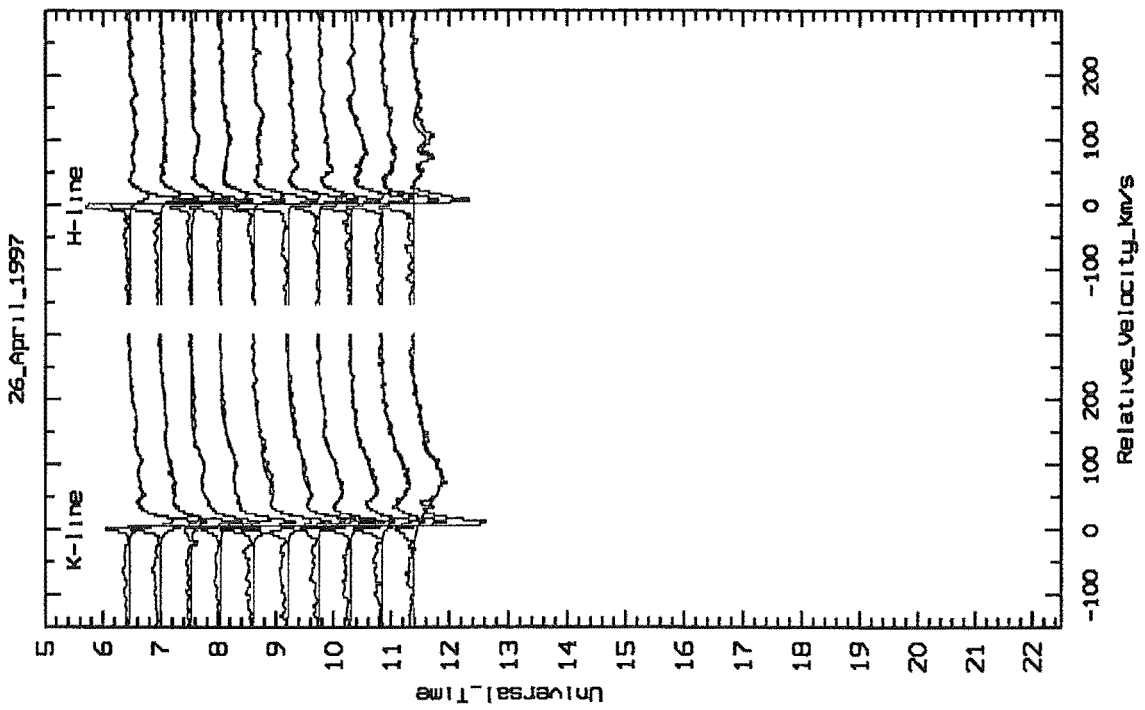

Figure 8.37: Normalised β Pic spectra taken on 26th April 1997.

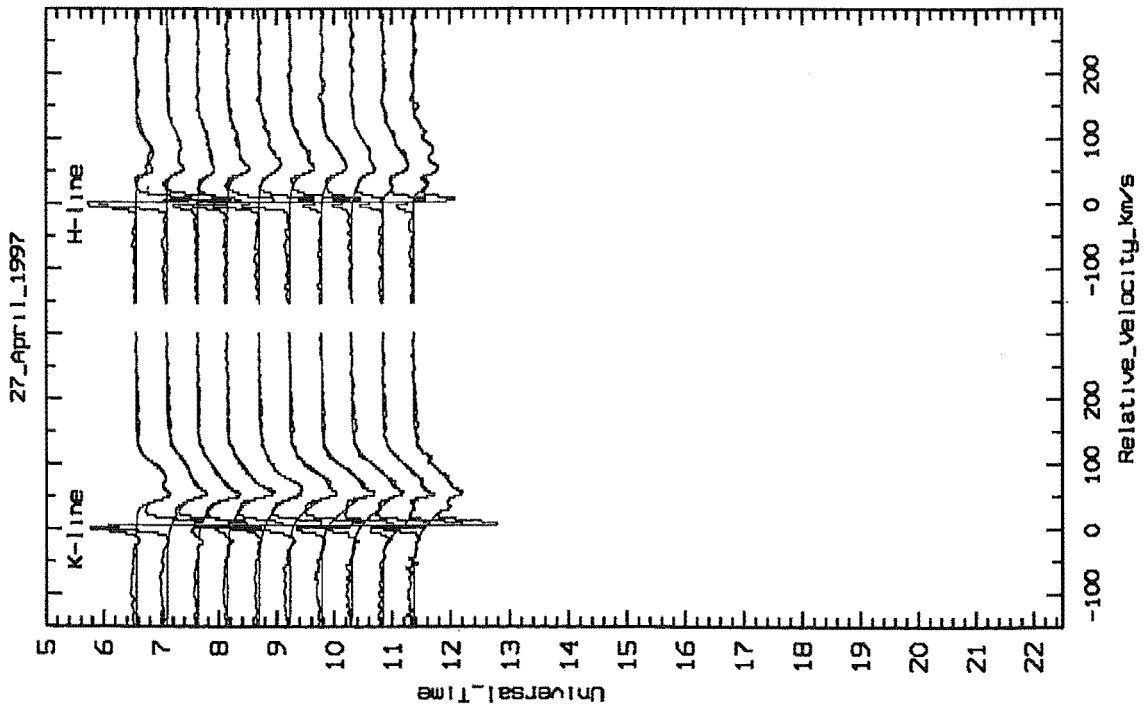

Figure 8.38: Normalised β Pic spectra taken on 27th April 1997.

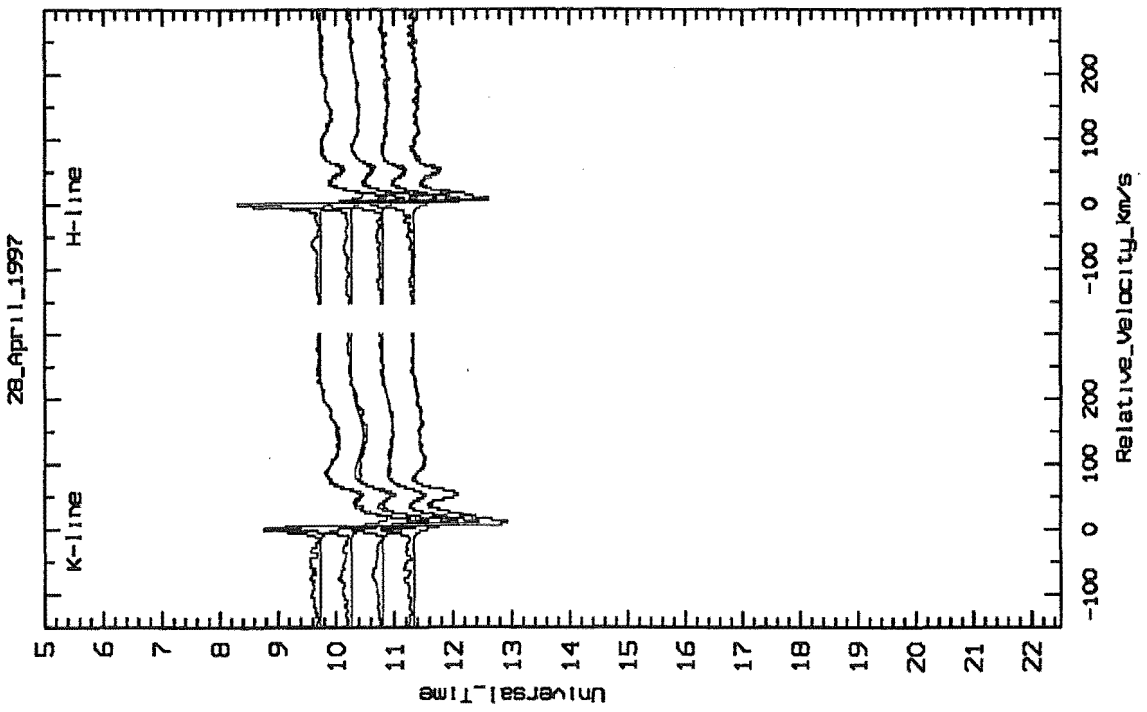

Figure 8.39: Normalised β Pic spectra taken on 28th April 1997.

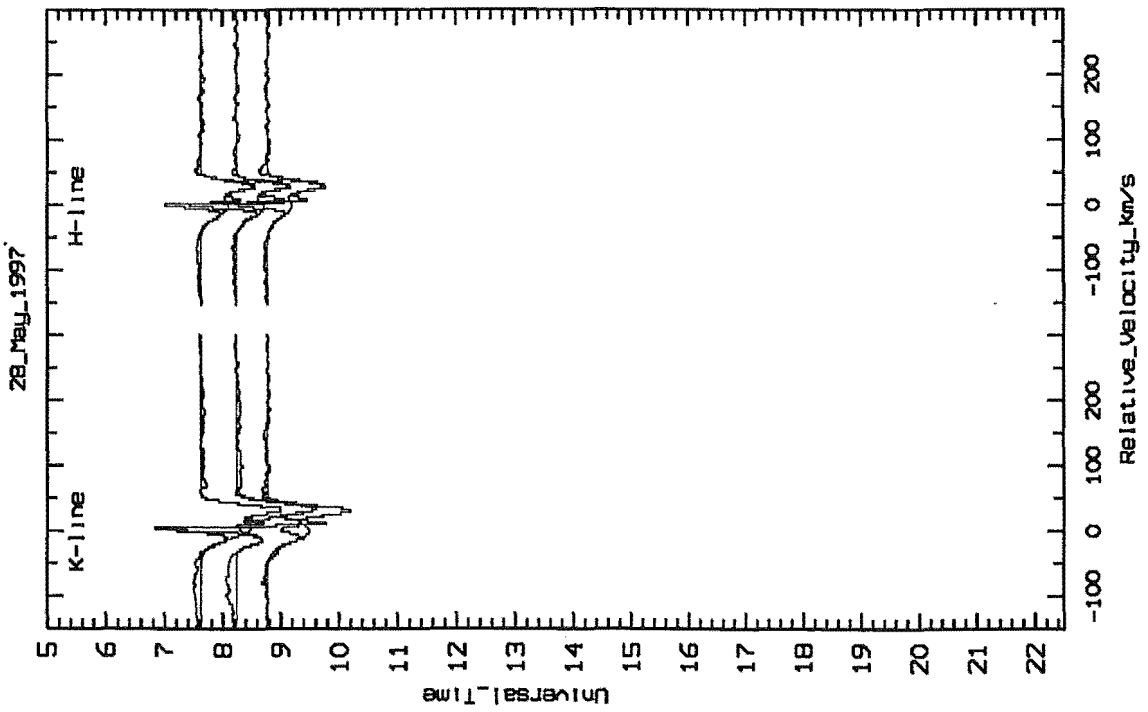

Figure 8.40: Normalised β Pic spectra taken on 28th May 1997.

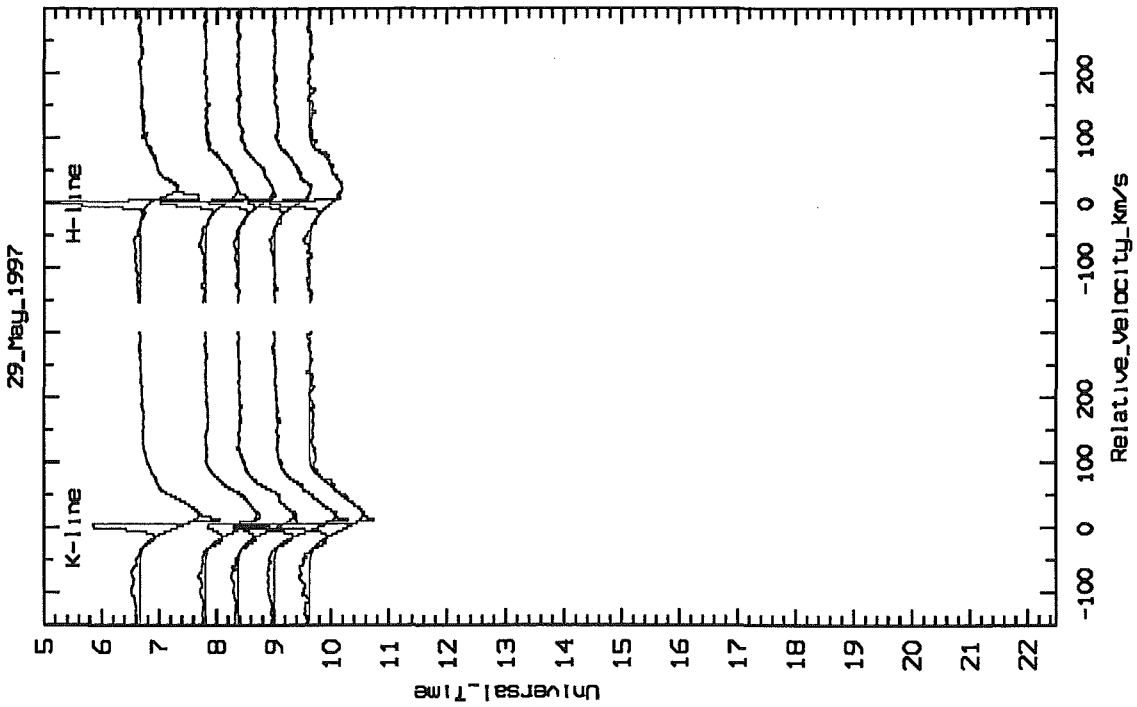

Figure 8.41: Normalised β Pic spectra taken on 29th May 1997.

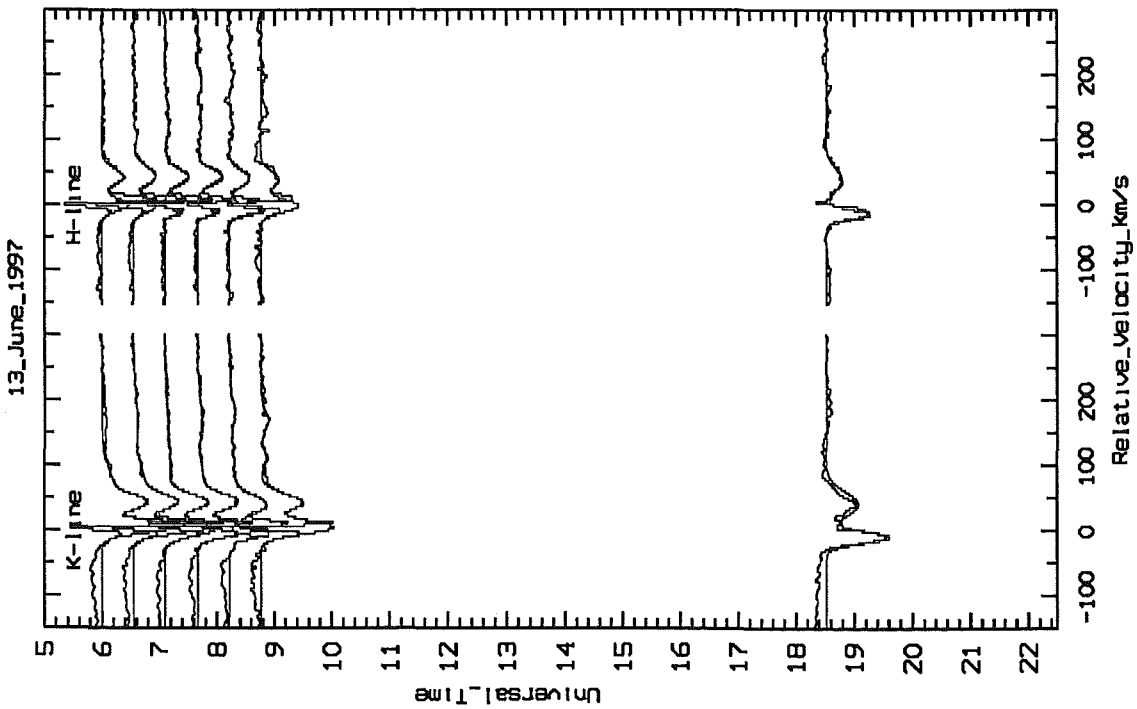

Figure 8.42: Normalised β Pic spectra taken on 13th June 1997.

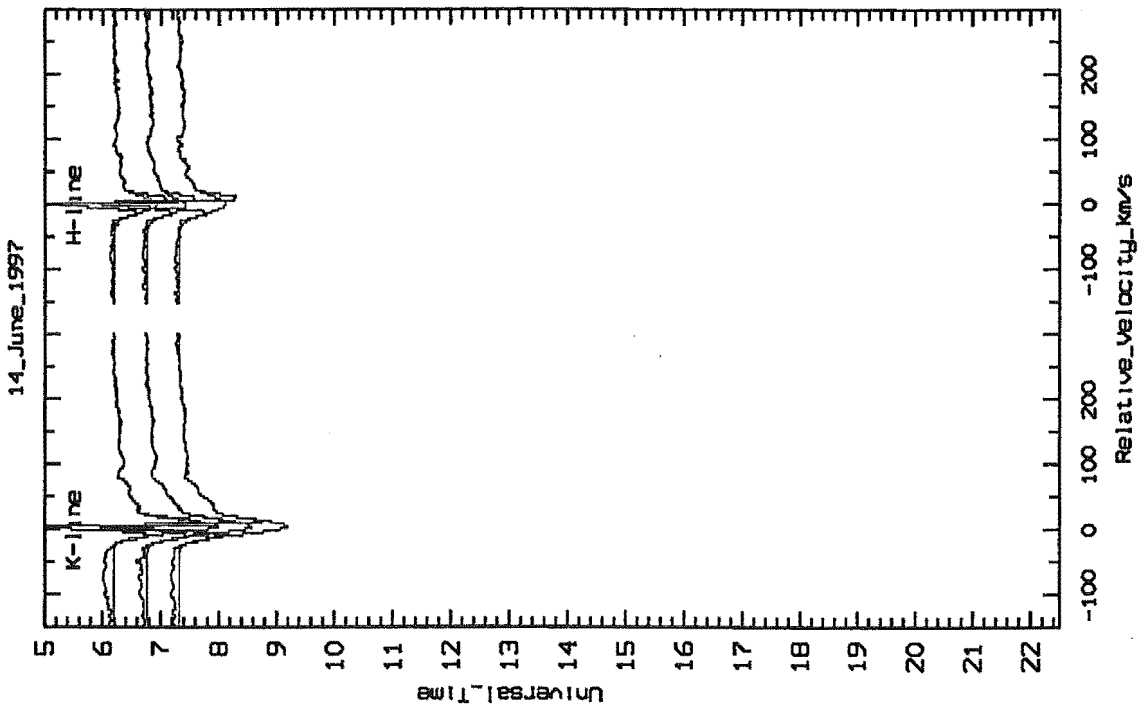

Figure 8.43: Normalised β Pic spectra taken on 14th June 1997.

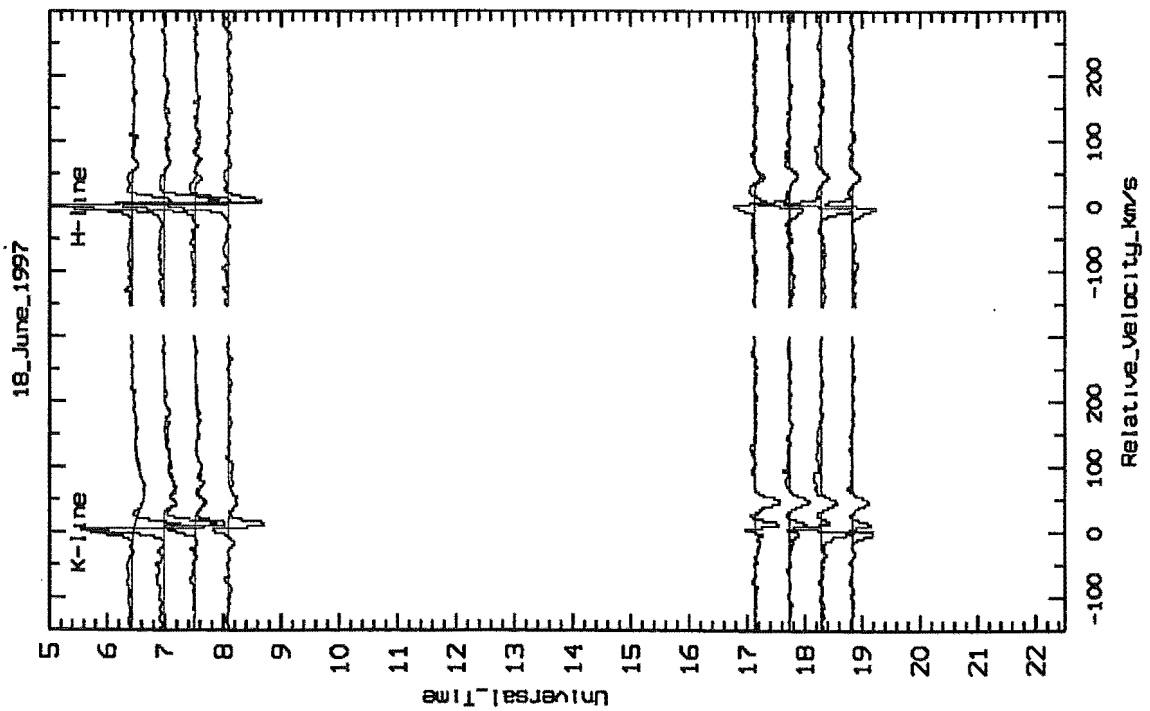

Figure 8.44: Normalised β Pic spectra taken on 18th June 1997.

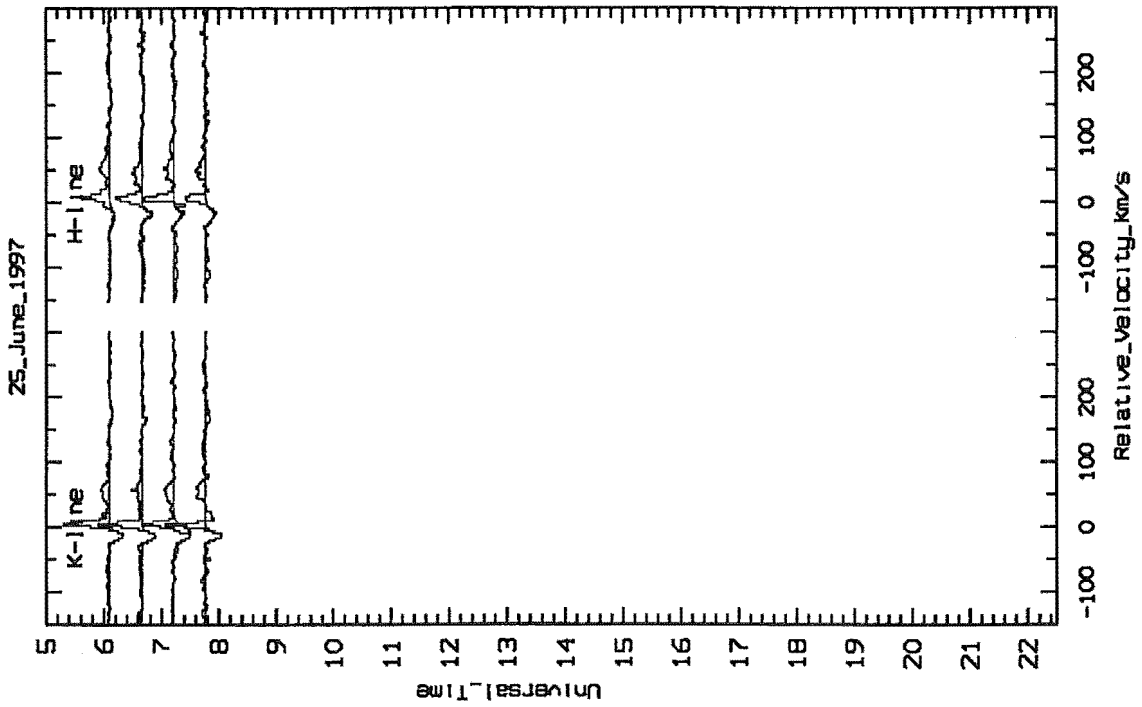

Figure 8.45: Normalised β Pic spectra taken on 25th June 1997.

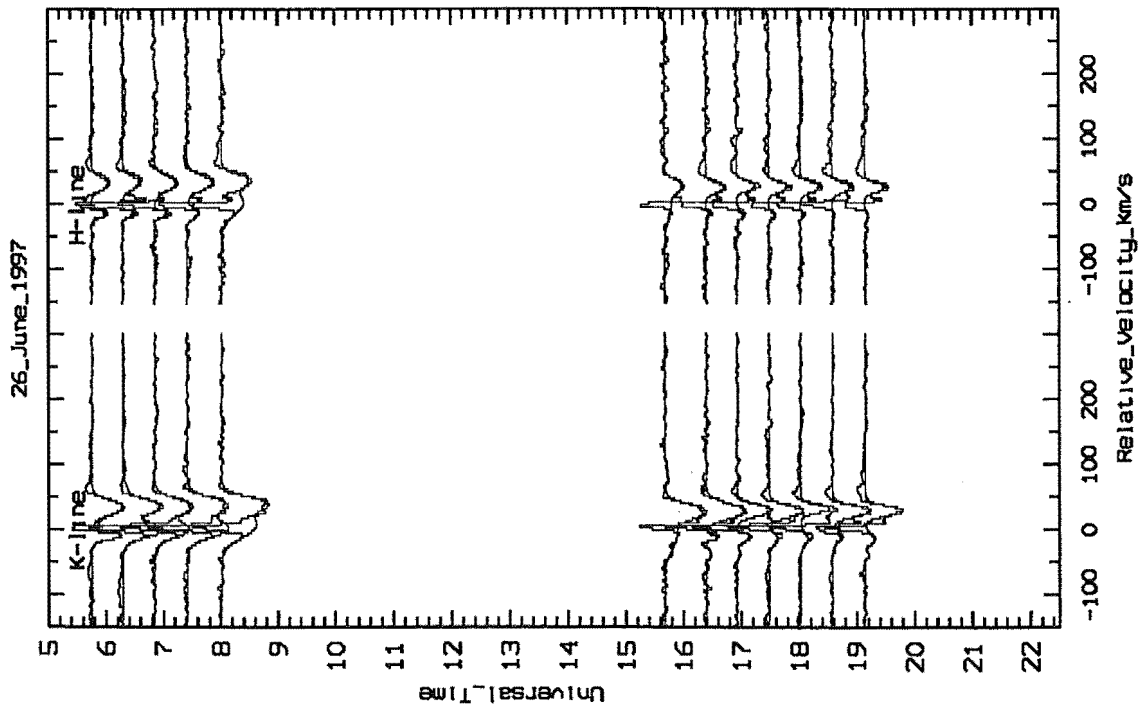

Figure 8.46: Normalised β Pic spectra taken on 26th June 1997.

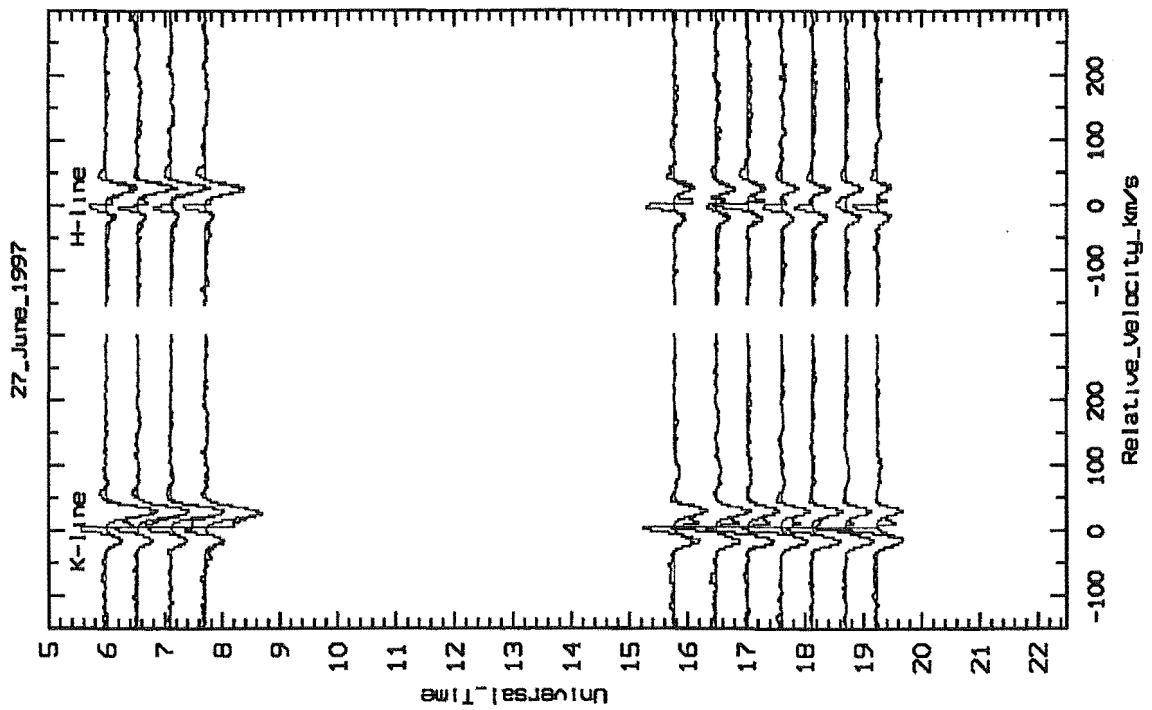

Figure 8.47: Normalised β Pic spectra taken on 27th June 1997.

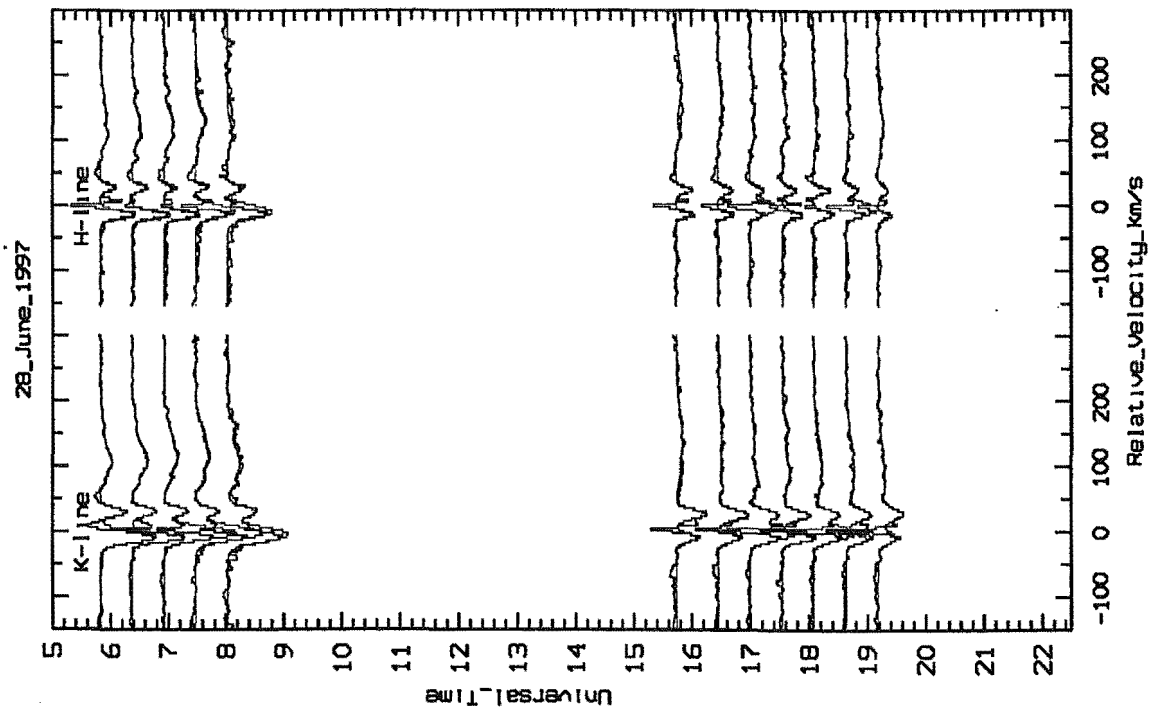

Figure 8.48: Normalised β Pic spectra taken on 28th June 1997.

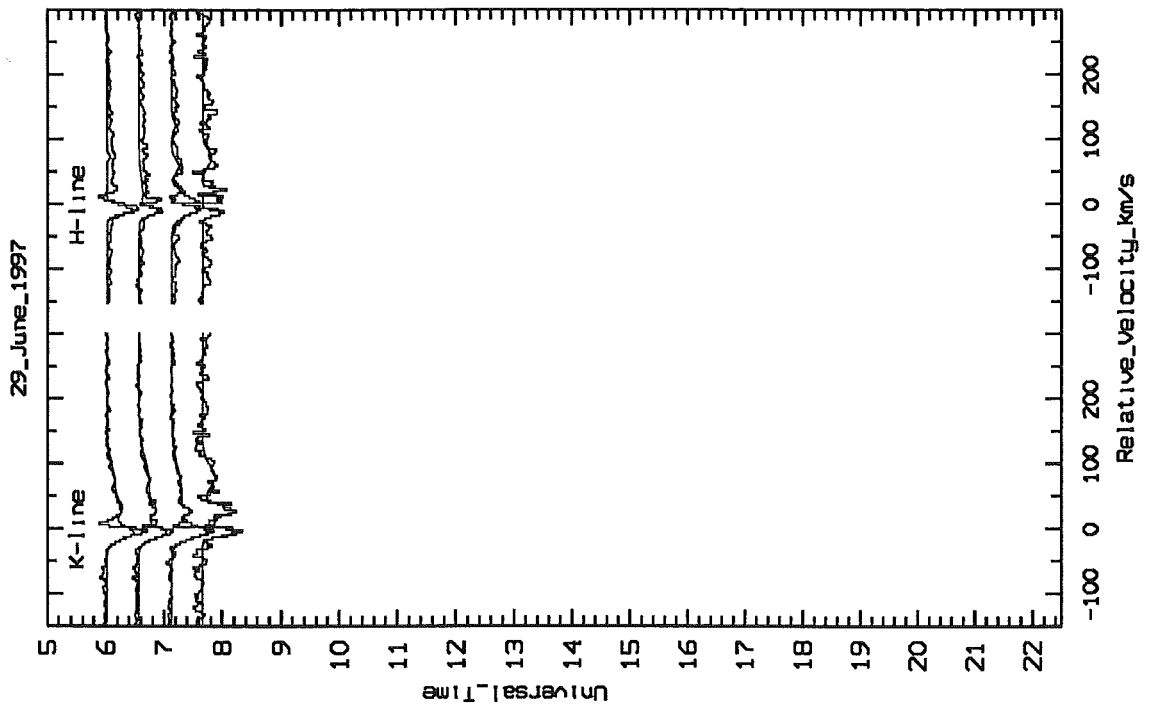

Figure 8.49: Normalised β Pic spectra taken on 29th June 1997.

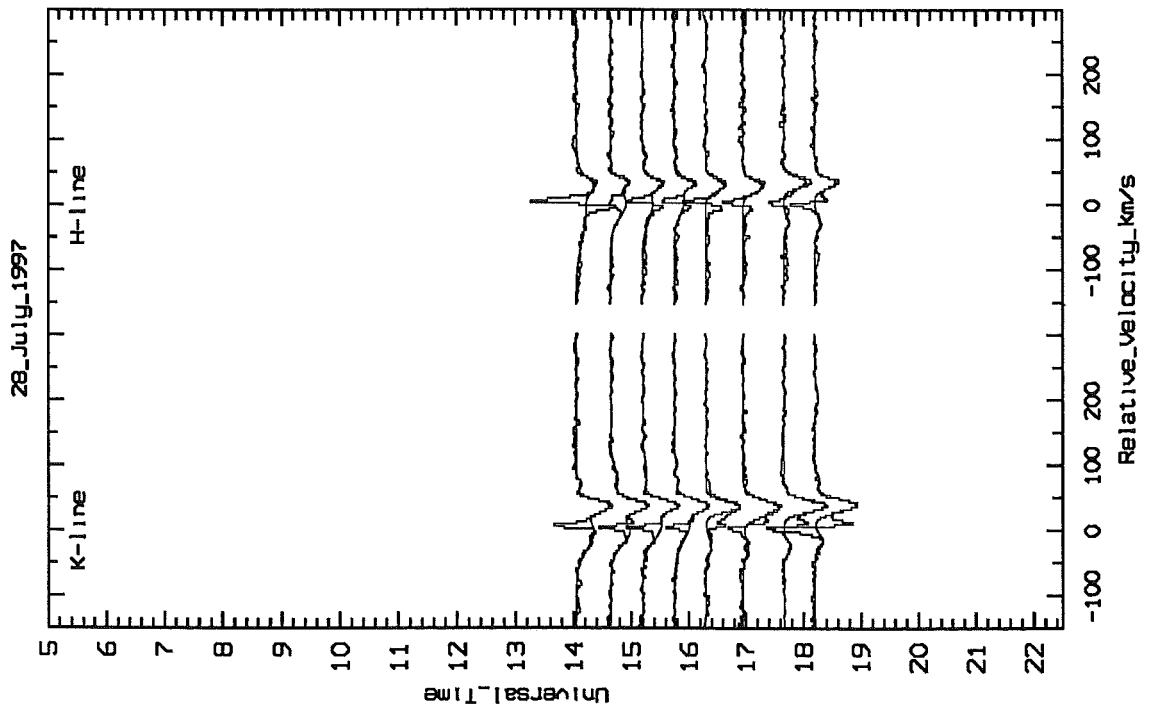

Figure 8.50: Normalised β Pic spectra taken on 28th July 1997.

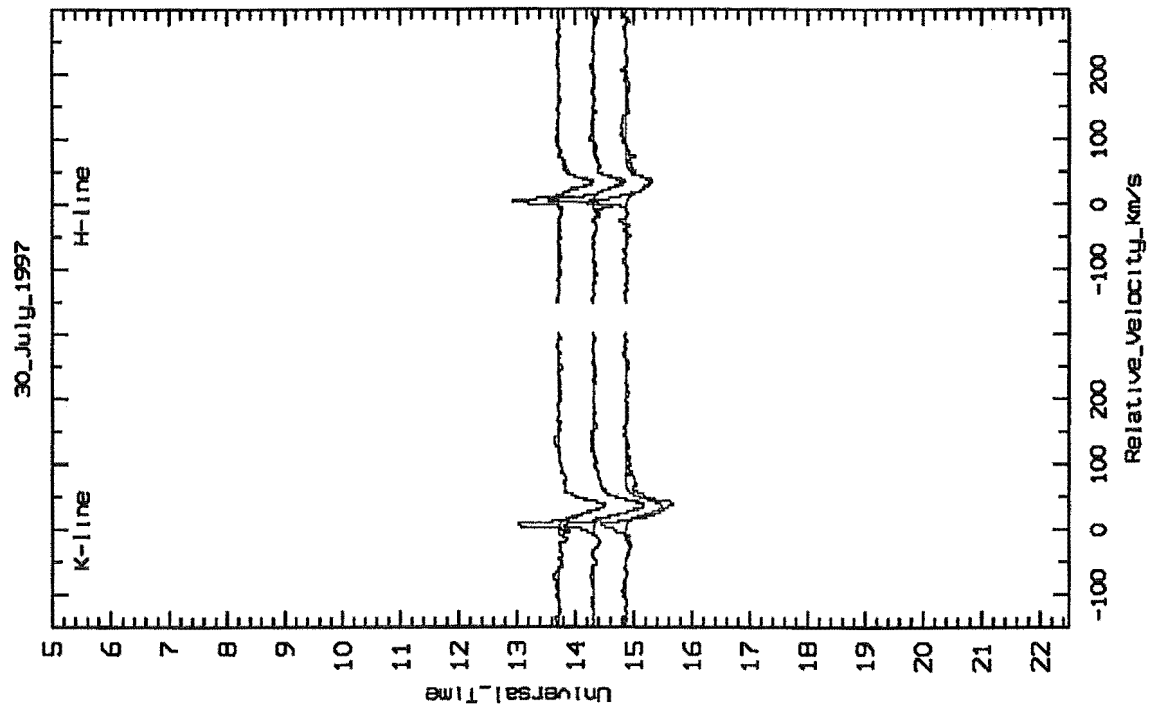

Figure 8.51: Normalised β Pic spectra taken on 30th July 1997.

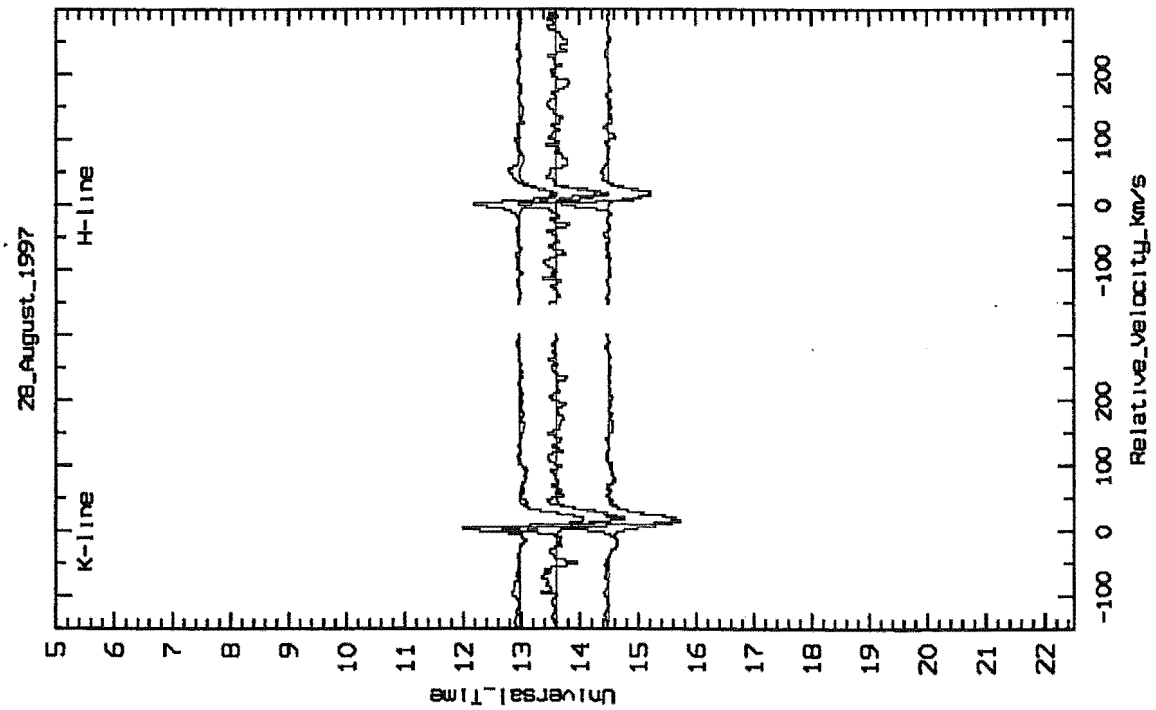

Figure 8.52: Normalised β Pic spectra taken on 28th August 1997.

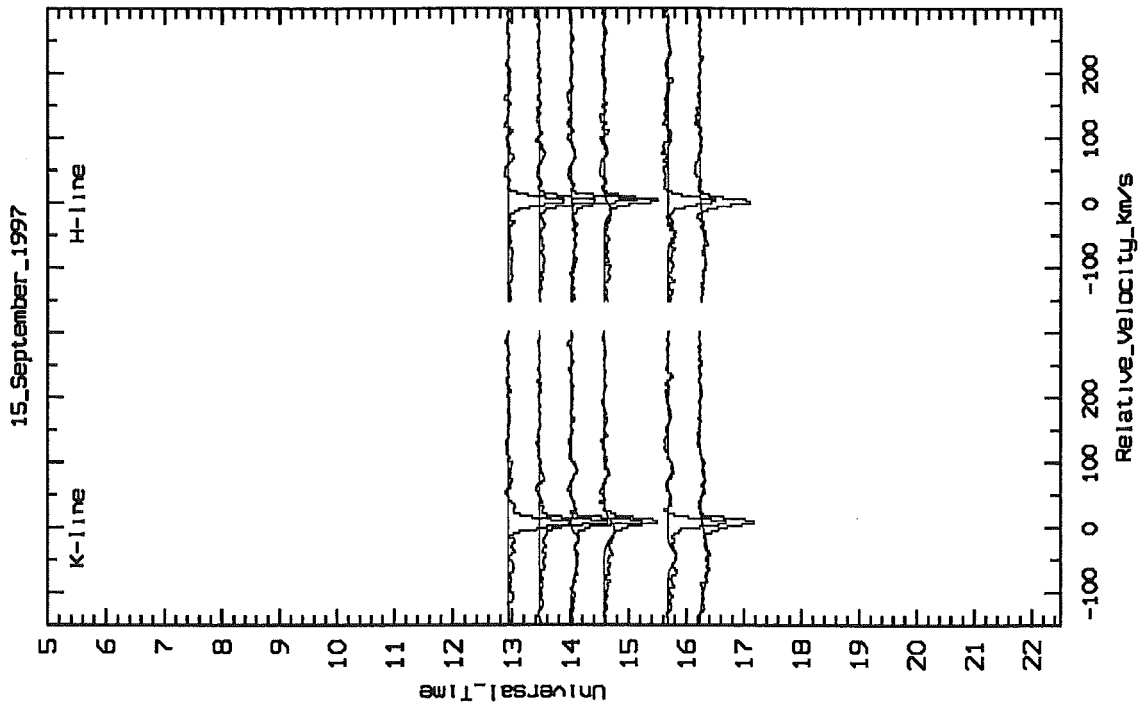

Figure 8.53: Normalised β Pic spectra taken on 15th September 1997.

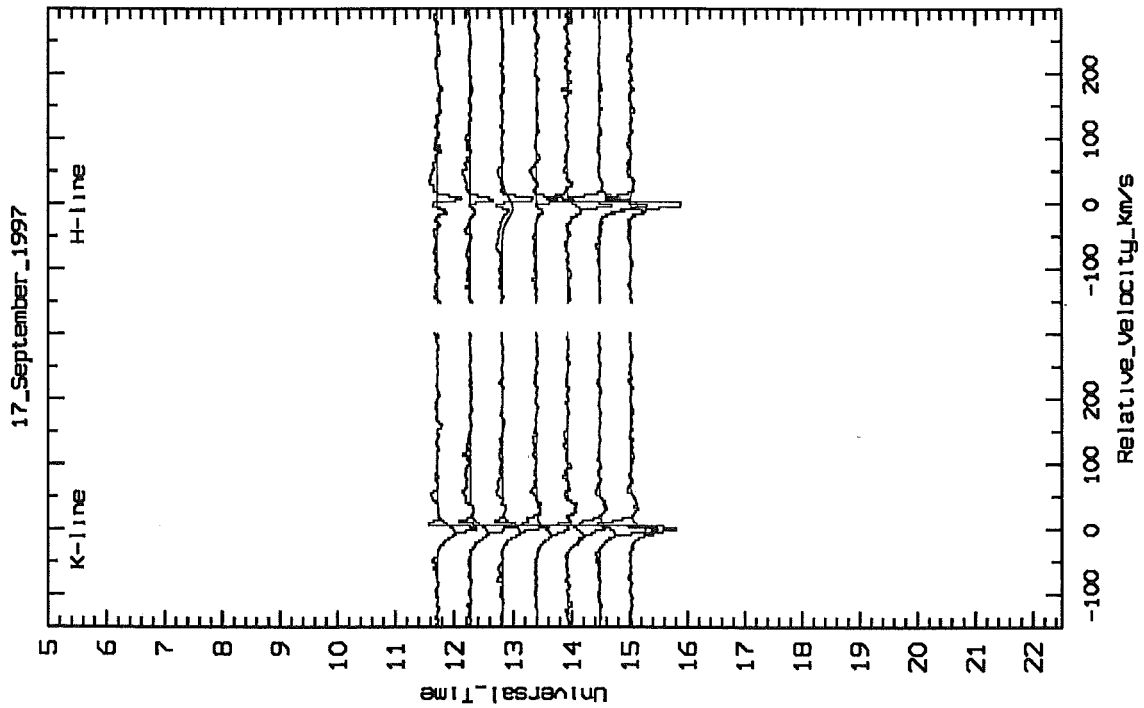

Figure 8.54: Normalised β Pic spectra taken on 17th September 1997.

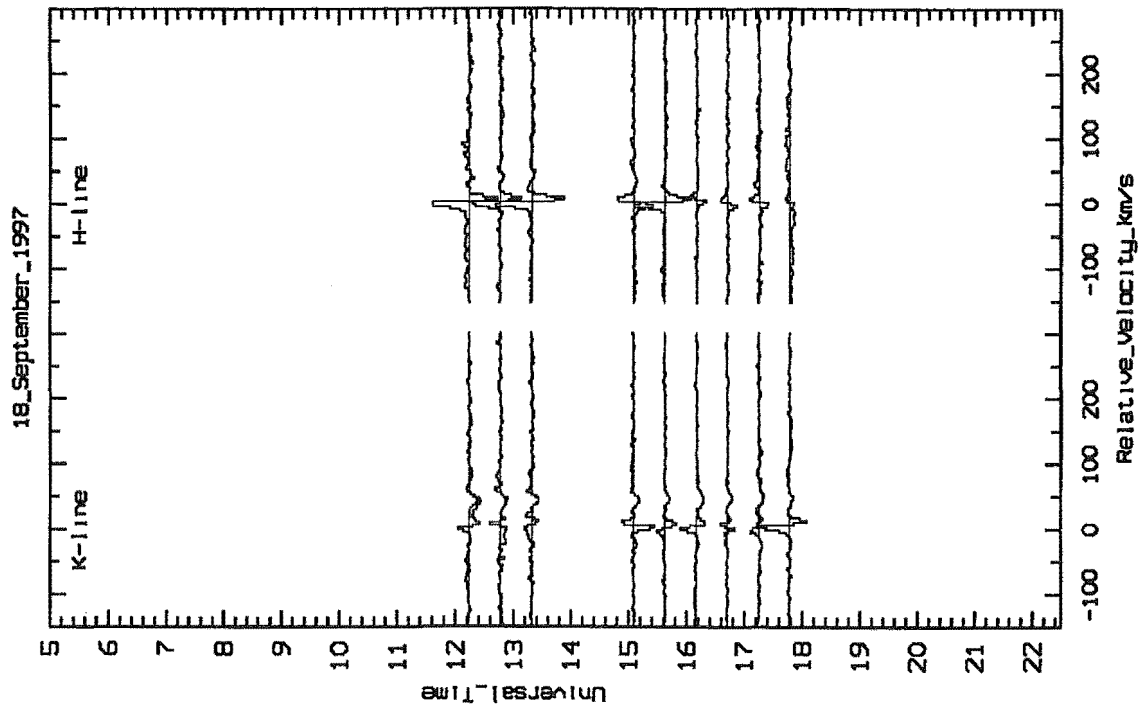

Figure 8.55: Normalised β Pic spectra taken on 18th September 1997.

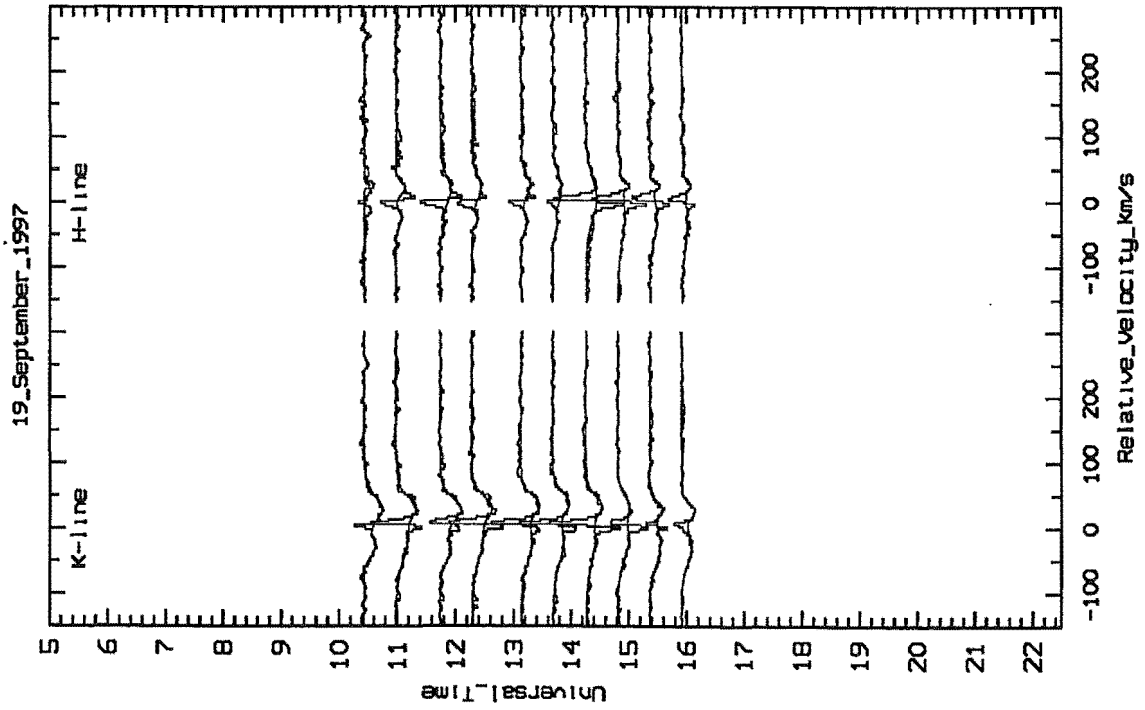

Figure 8.56: Normalised β Pic spectra taken on 19th September 1997.

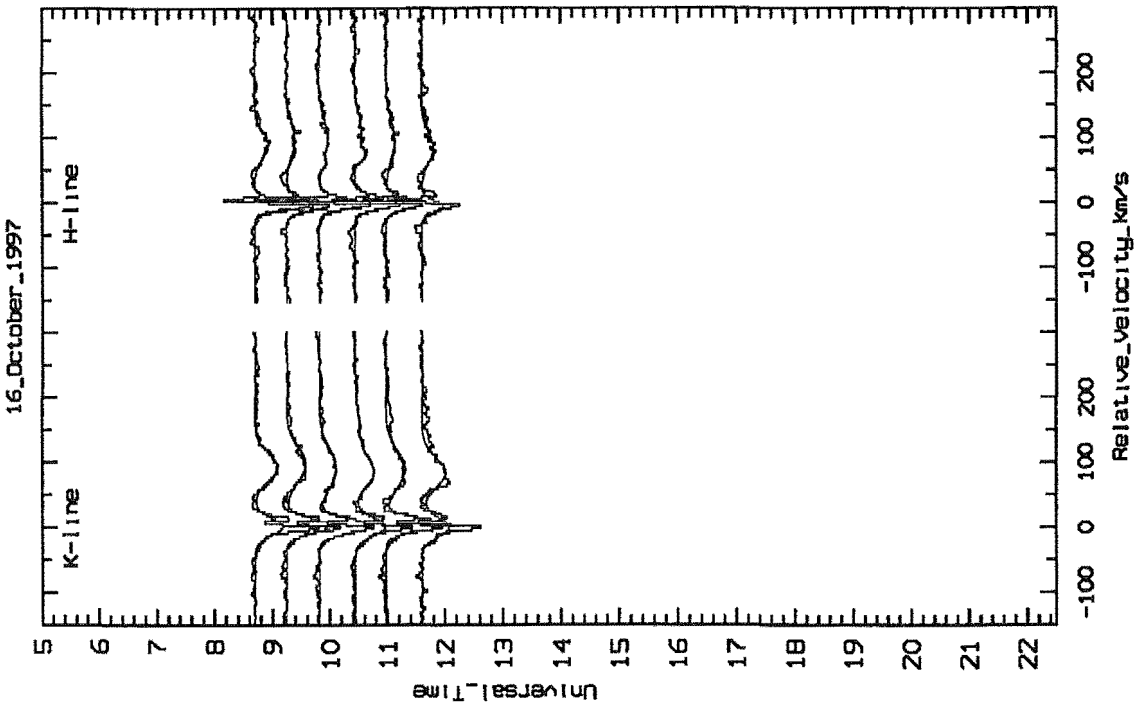

Figure 8.57: Normalised β Pic spectra taken on 16th October 1997.

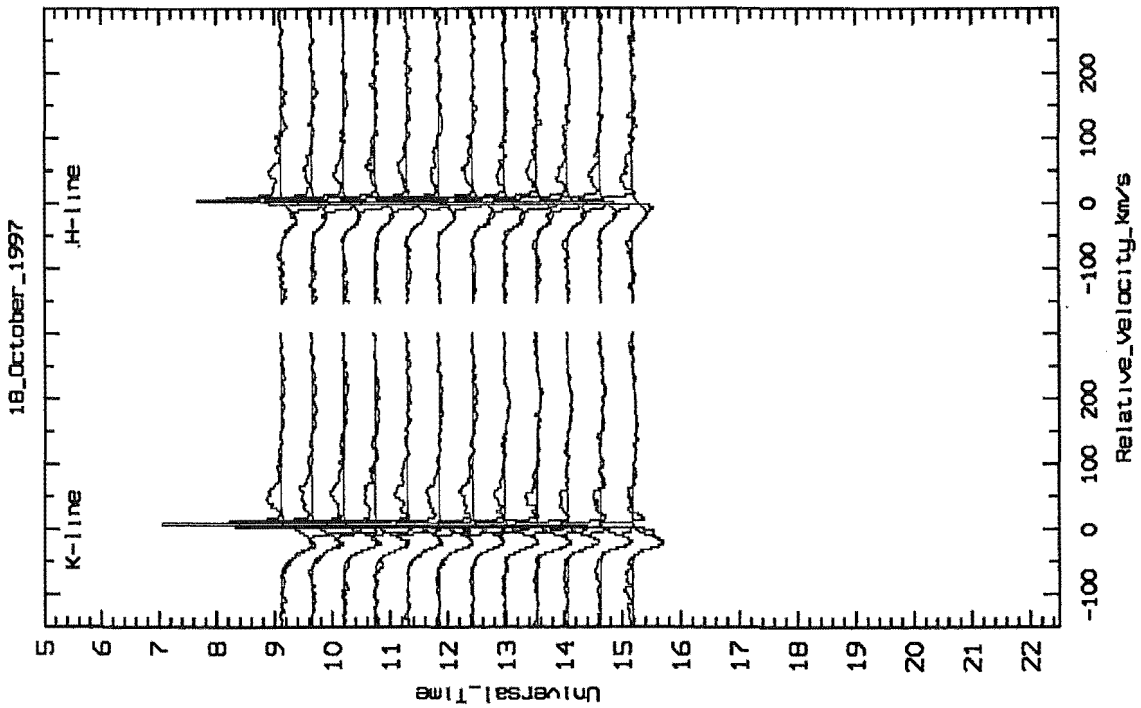

Figure 8.58: Normalised β Pic spectra taken on 18th October 1997.

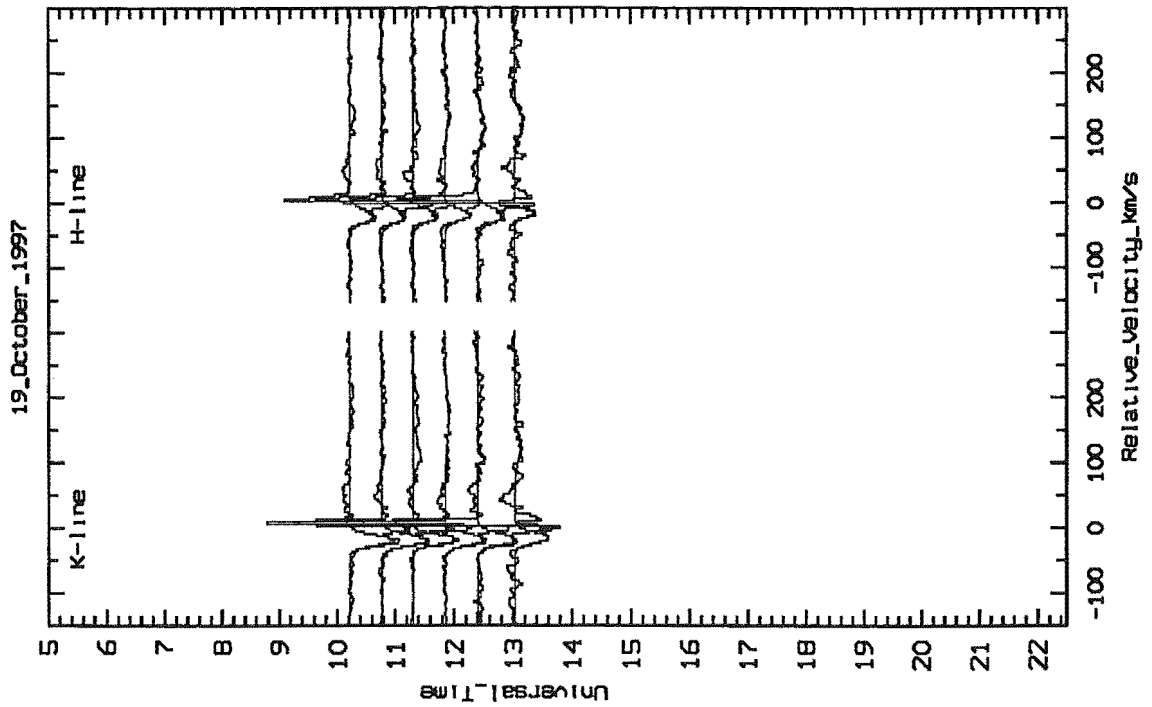

Figure 8.59: Normalised β Pic spectra taken on 19th October 1997.

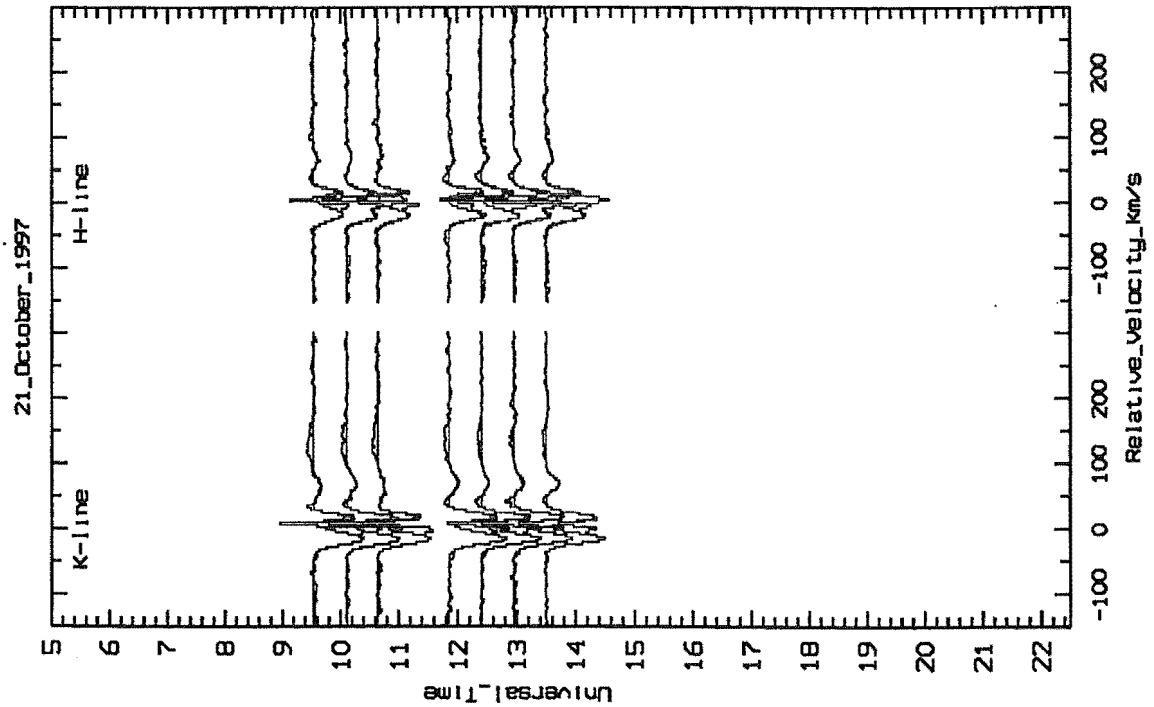

Figure 8.60: Normalised β Pic spectra taken on 21st October 1997.

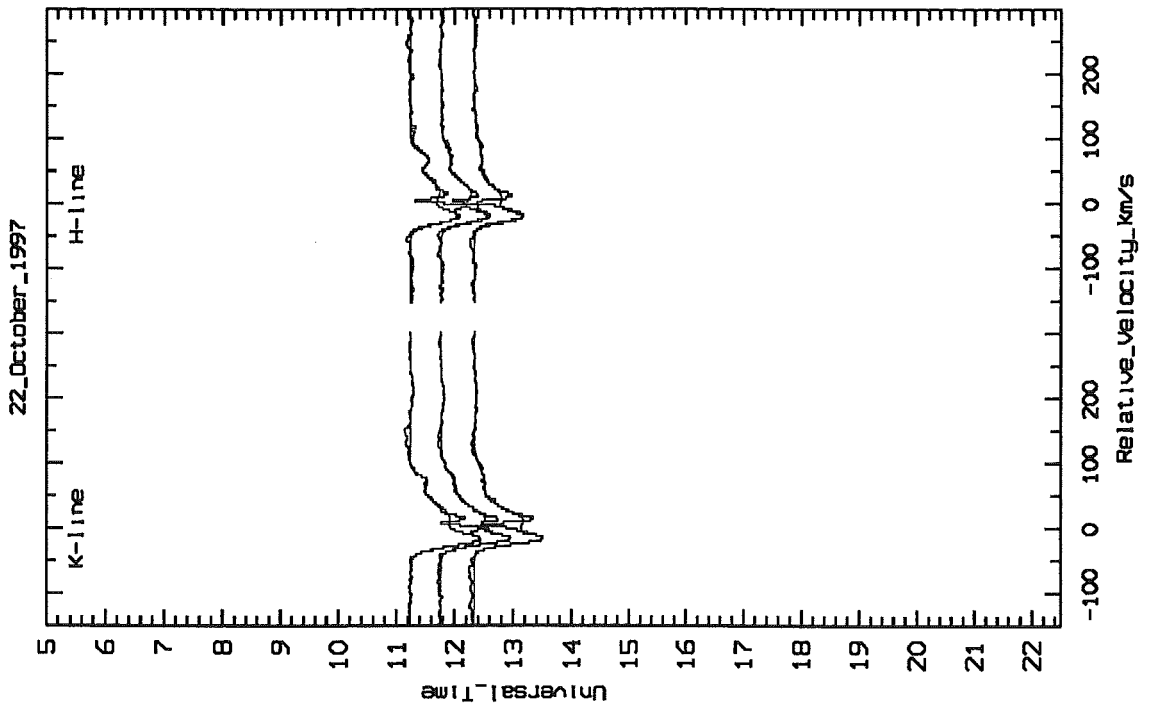

Figure 8.61: Normalised β Pic spectra taken on 22nd October 1997.

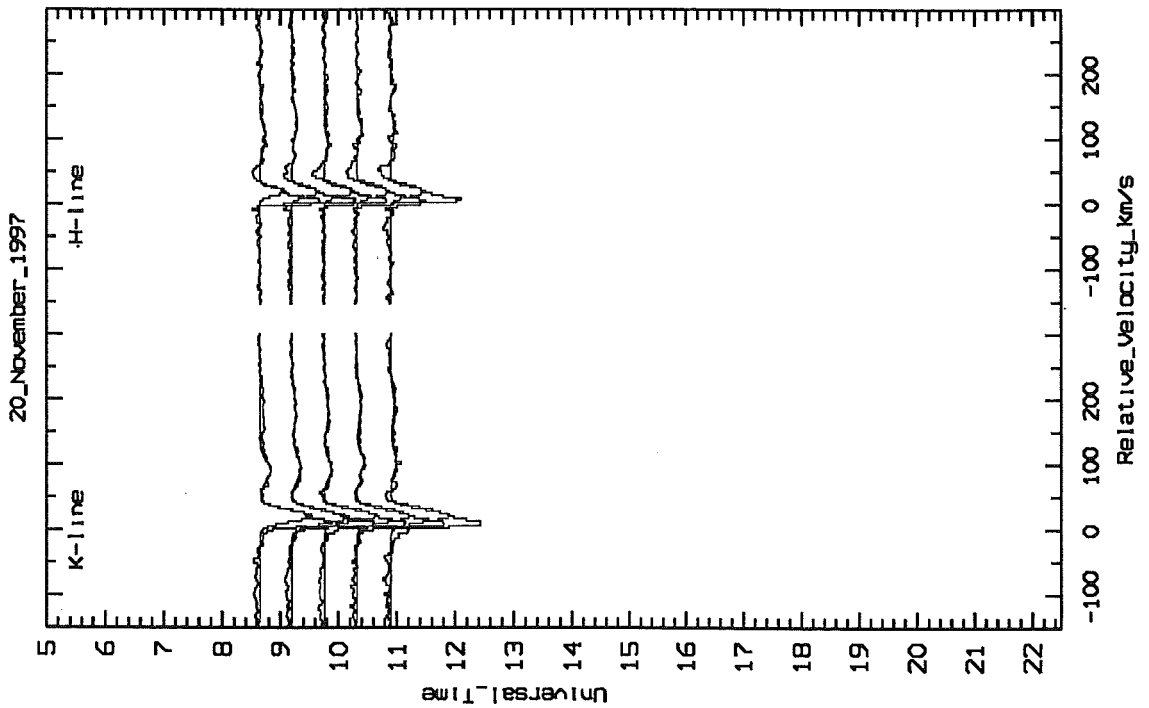

Figure 8.62: Normalised β Pic spectra taken on 20th November 1997.

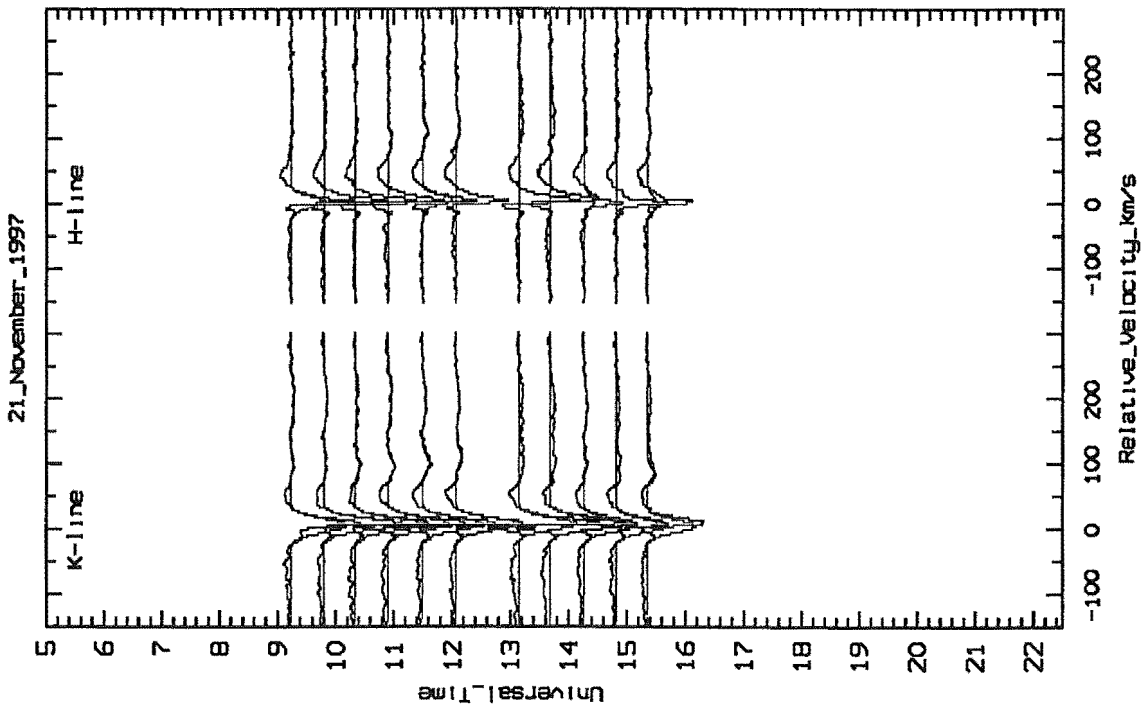

Figure 8.63: Normalised β Pic spectra taken on 21st November 1997.

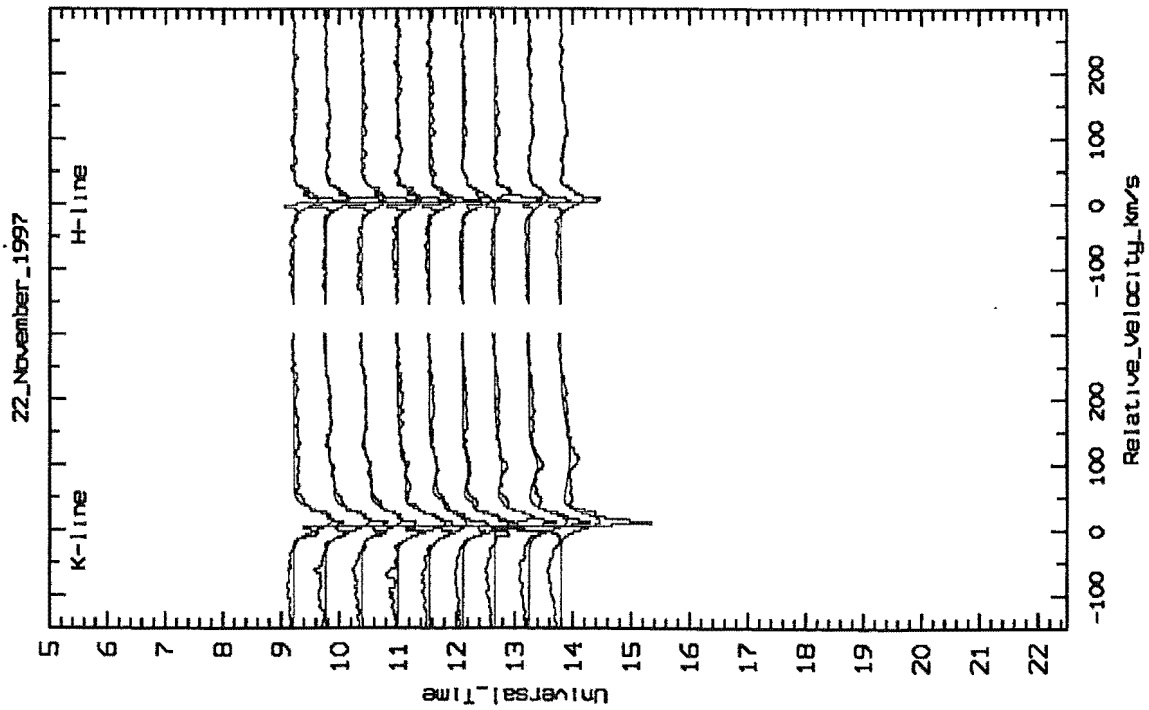

Figure 8.64: Normalised β Pic spectra taken on 22nd November 1997.

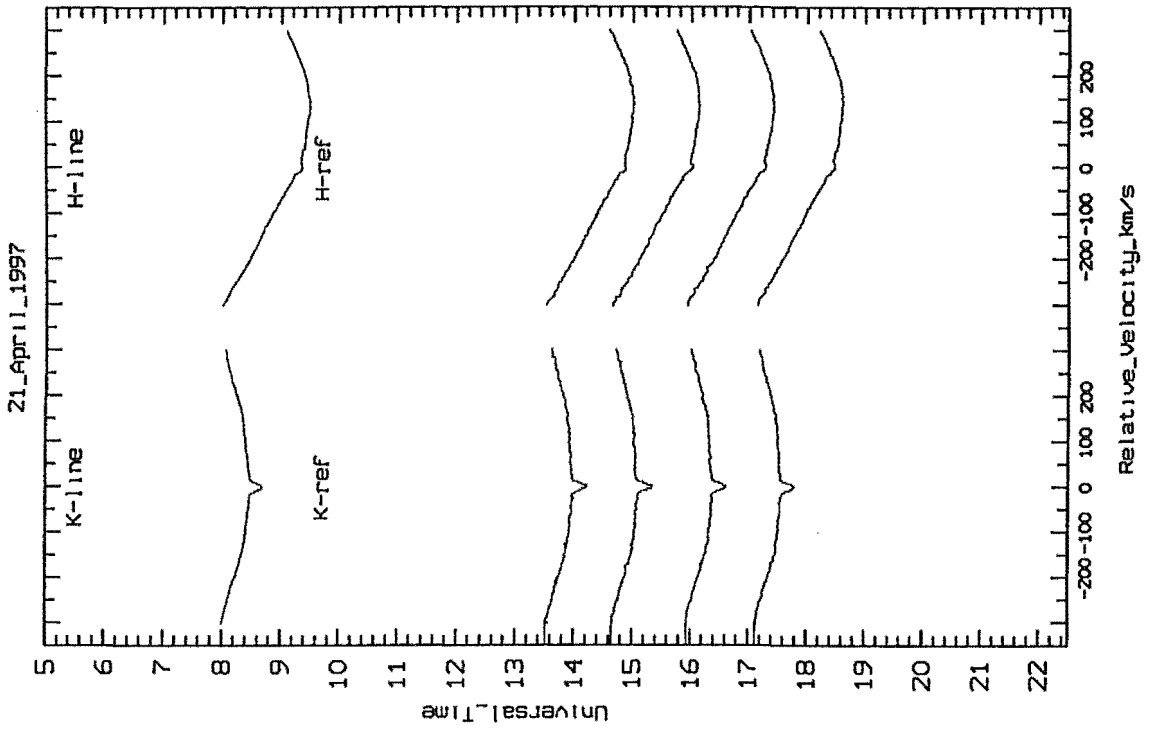

Figure 8.65: 51 Oph spectra taken on 21st April 1997.

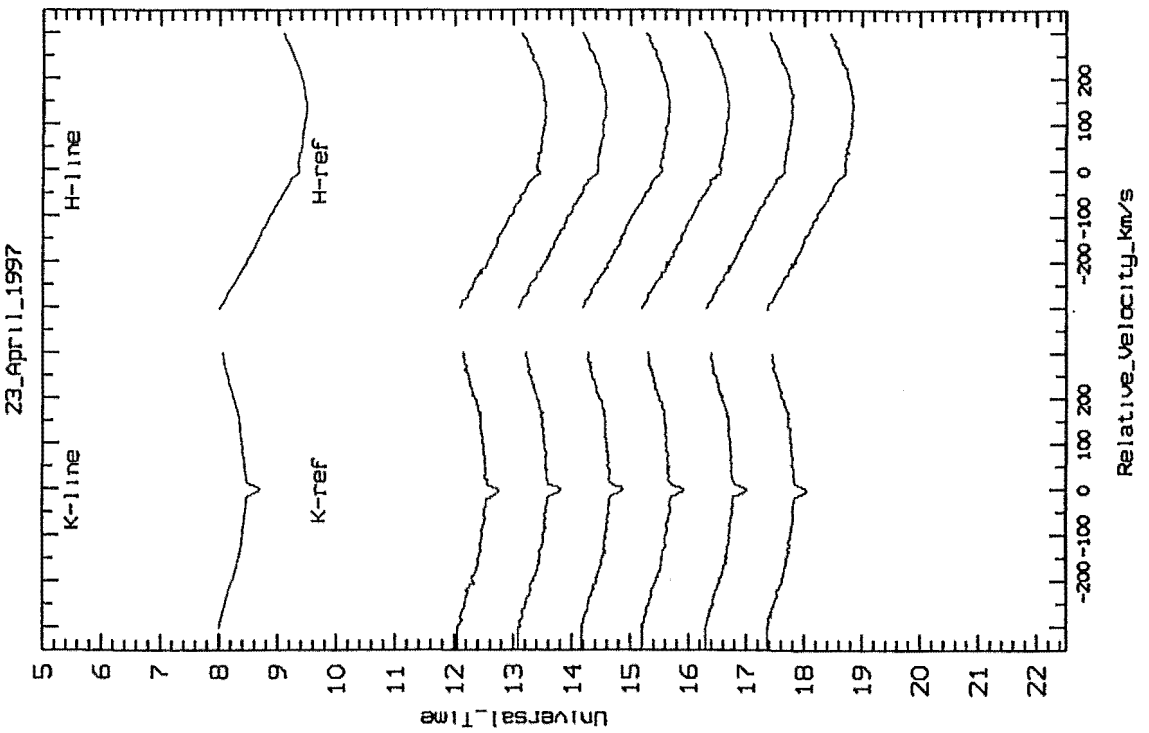

Figure 8.66: 51 Oph spectra taken on 23rd April 1997.

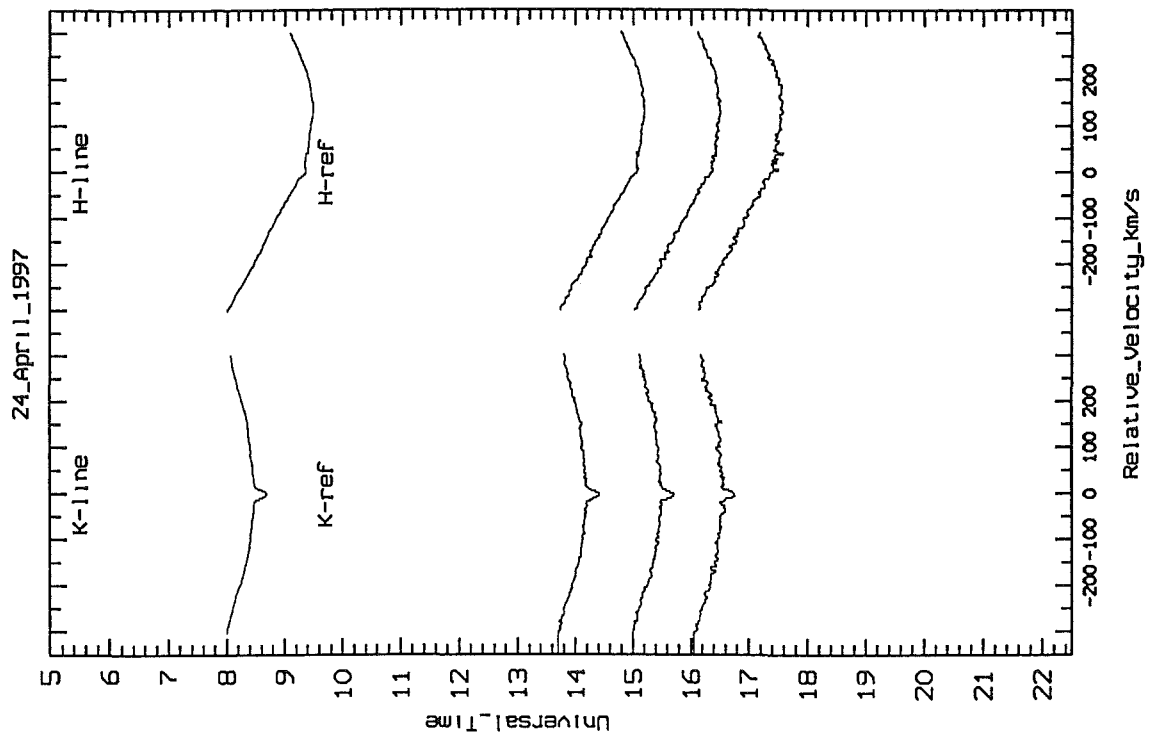

Figure 8.67: 51 Oph spectra taken on 24th April 1997.

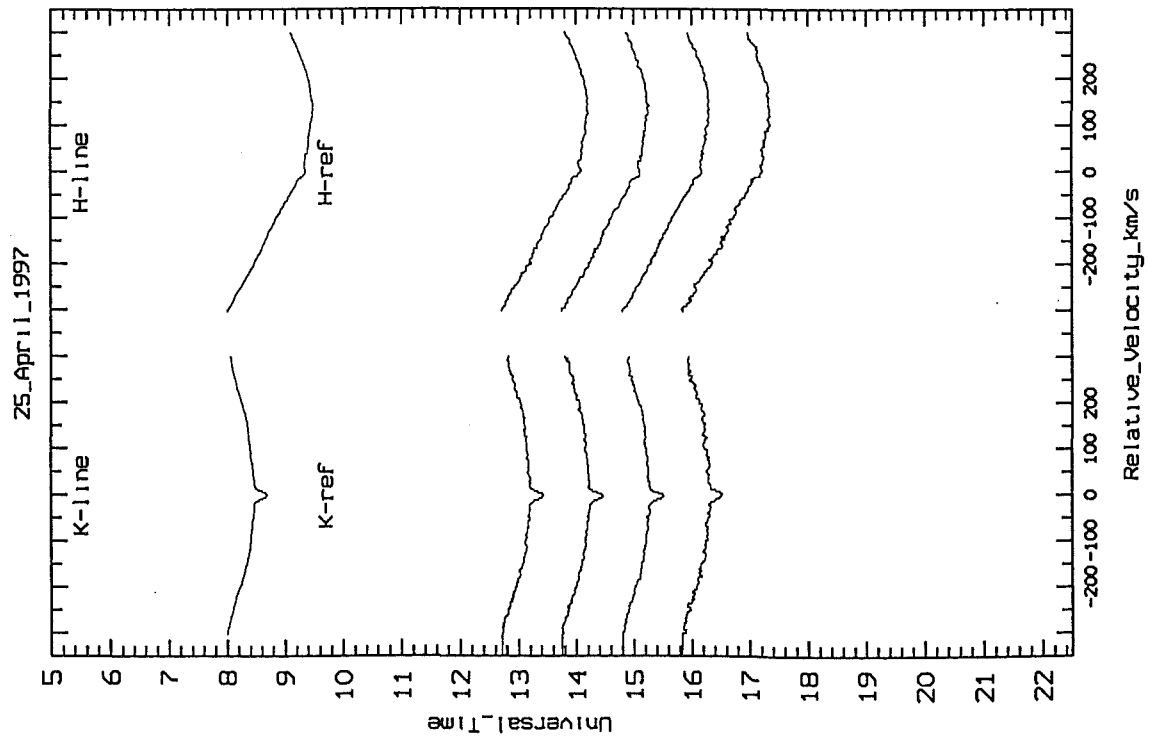

Figure 8.68: 51 Oph spectra taken on 25th April 1997.

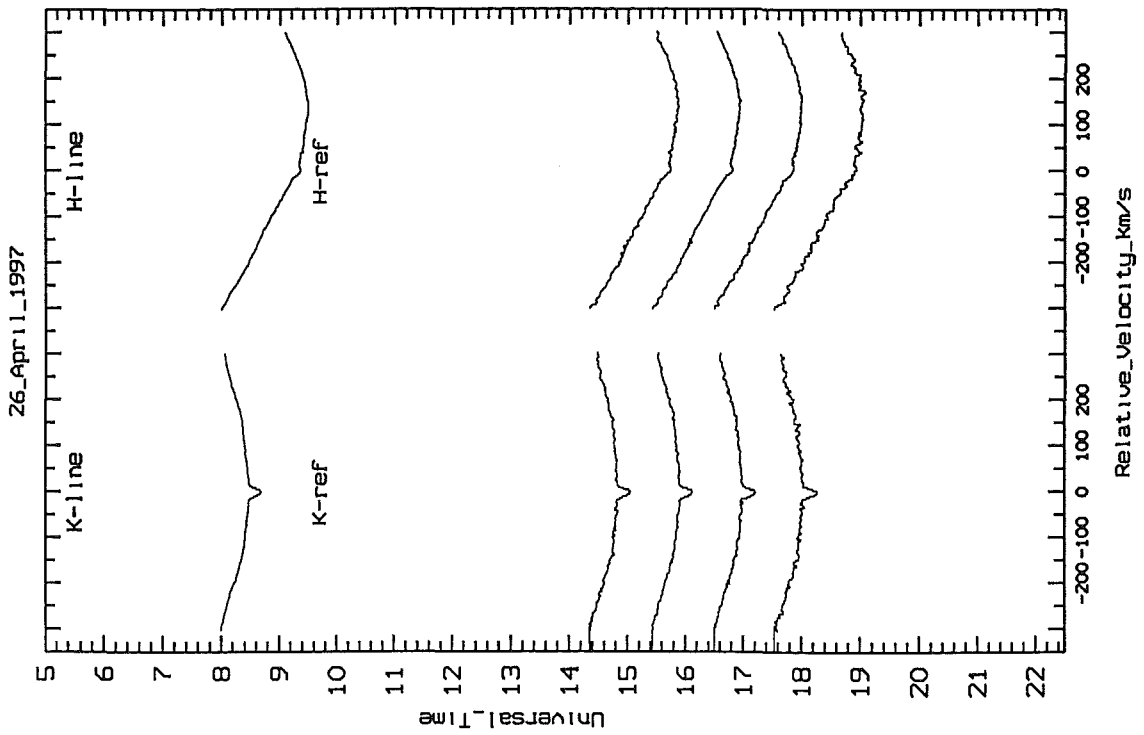

Figure 8.69: 51 Oph spectra taken on 26th April 1997.

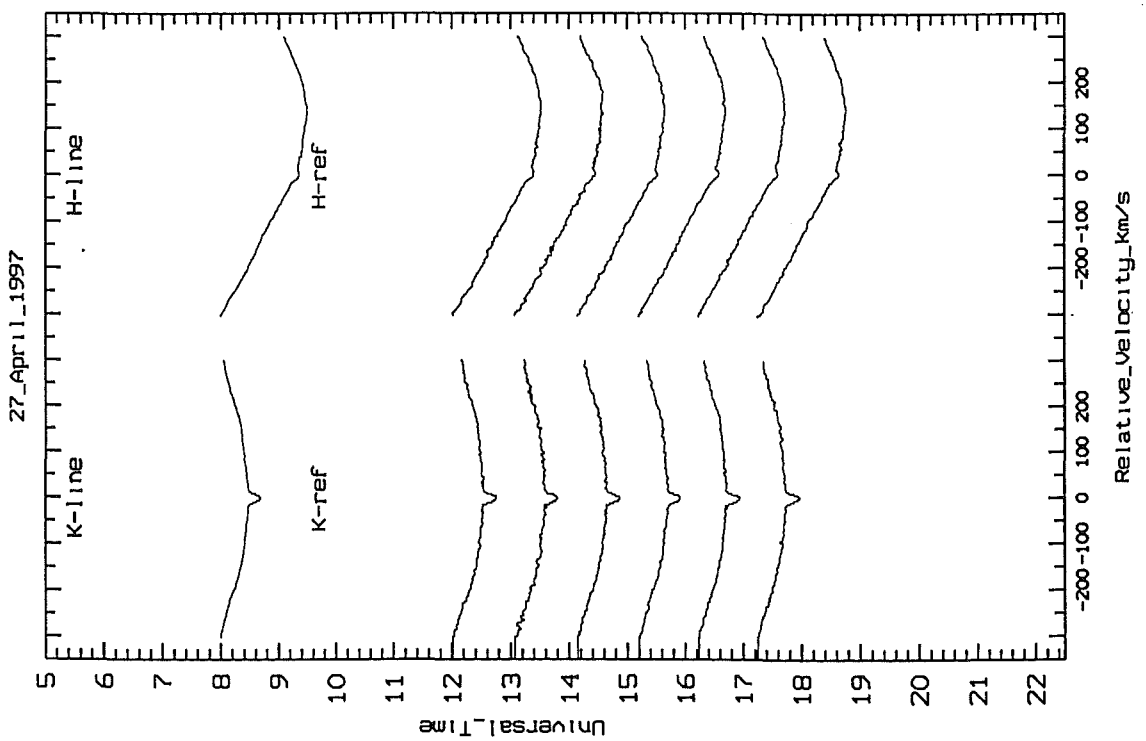

Figure 8.70: 51 Oph spectra taken on 27th April 1997.

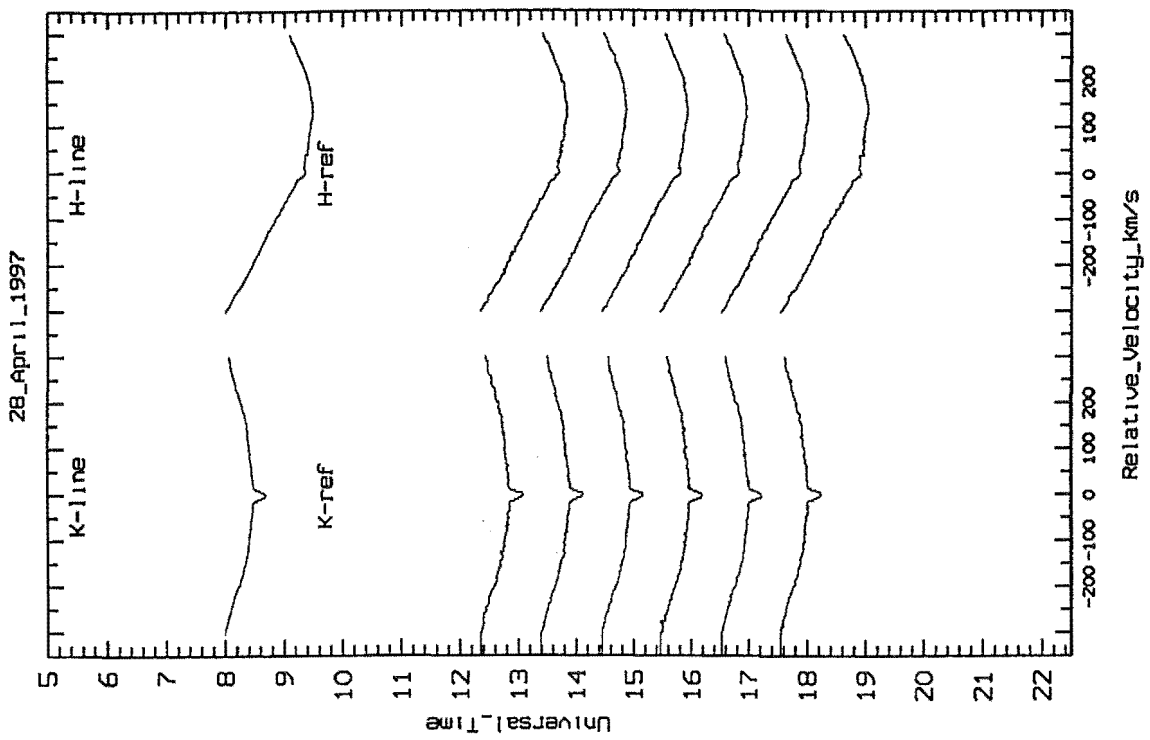

Figure 8.71: 51 Oph spectra taken on 28th April 1997.

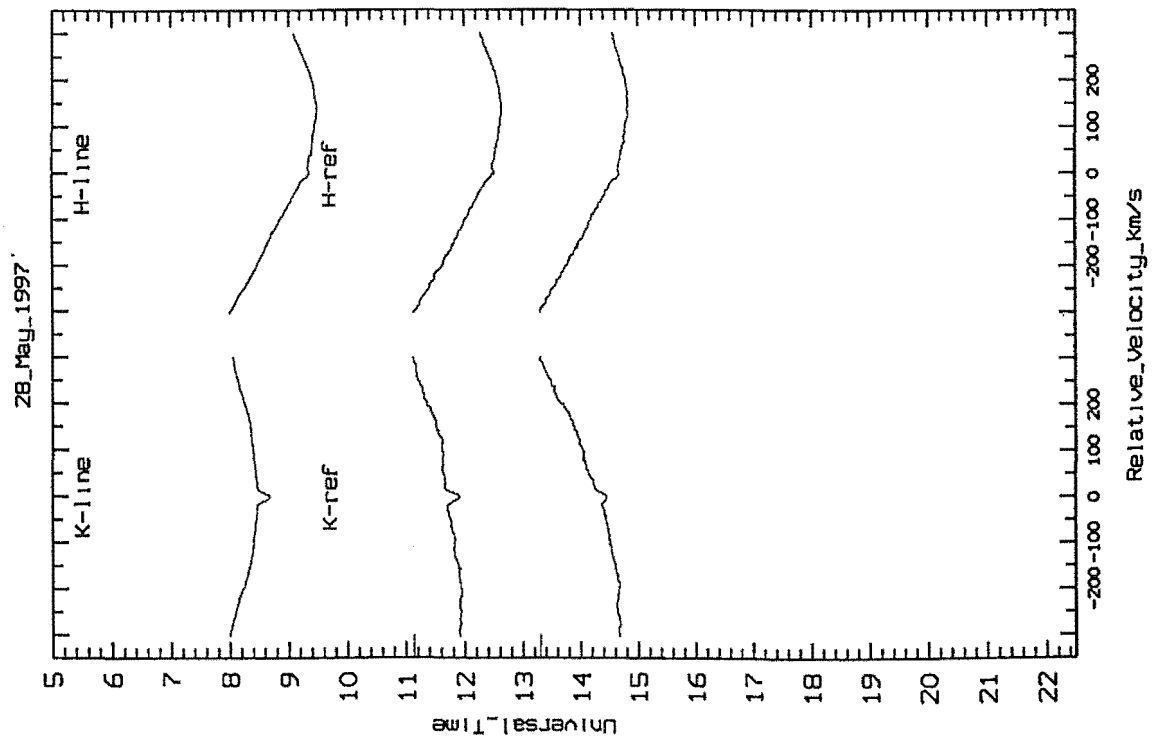

Figure 8.72: 51 Oph spectra taken on 28th May 1997. The difference in the K line spectra was due to condensation on the cryostat entrance window.

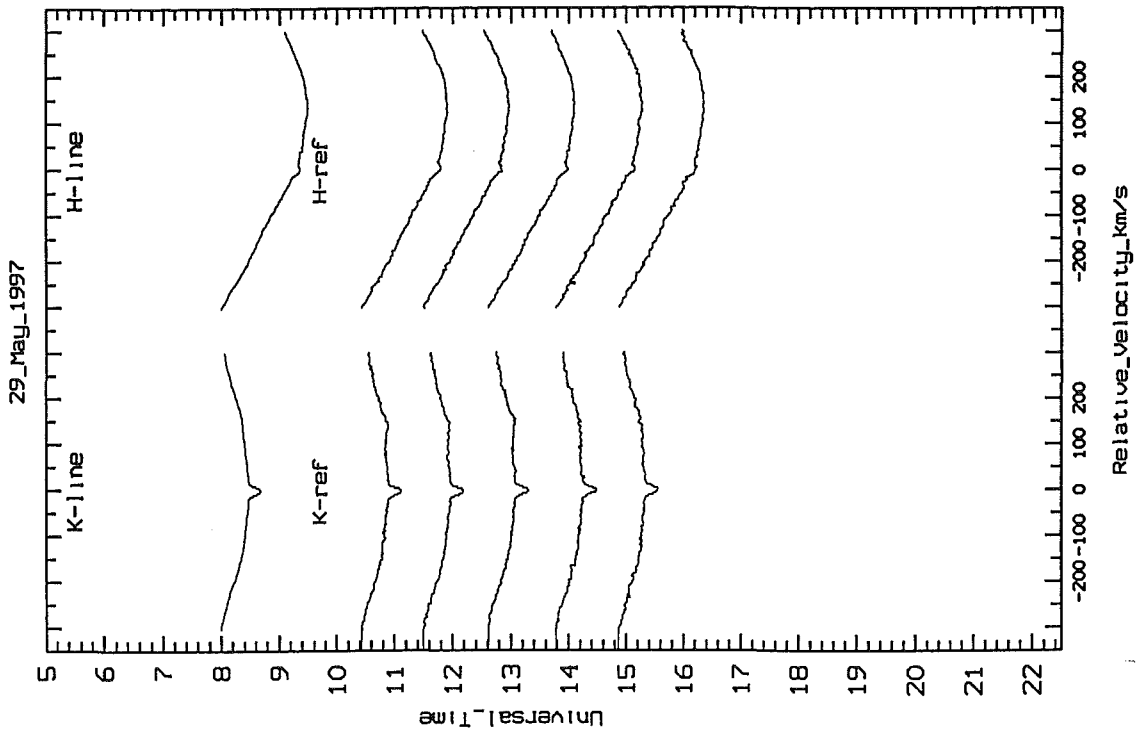

Figure 8.73: 51 Oph spectra taken on 29th May 1997.

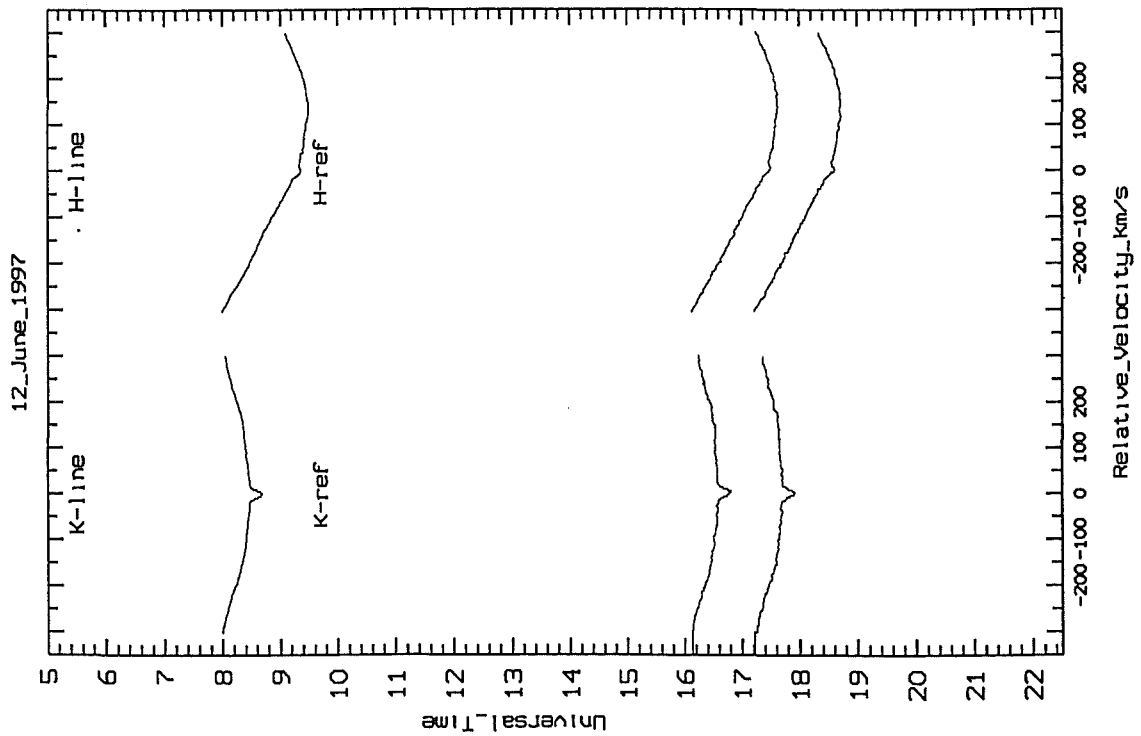

Figure 8.74: 51 Oph spectra taken on 12th June 1997.

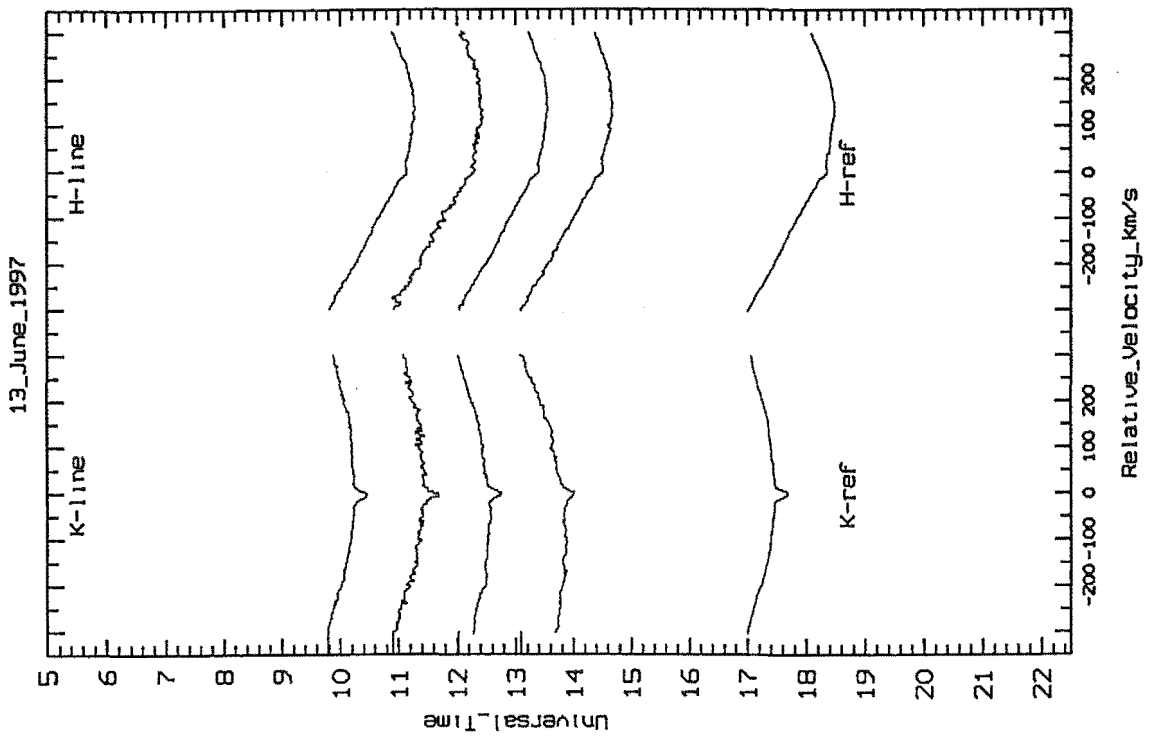

Figure 8.75: 51 Oph spectra taken on 13th June 1997.

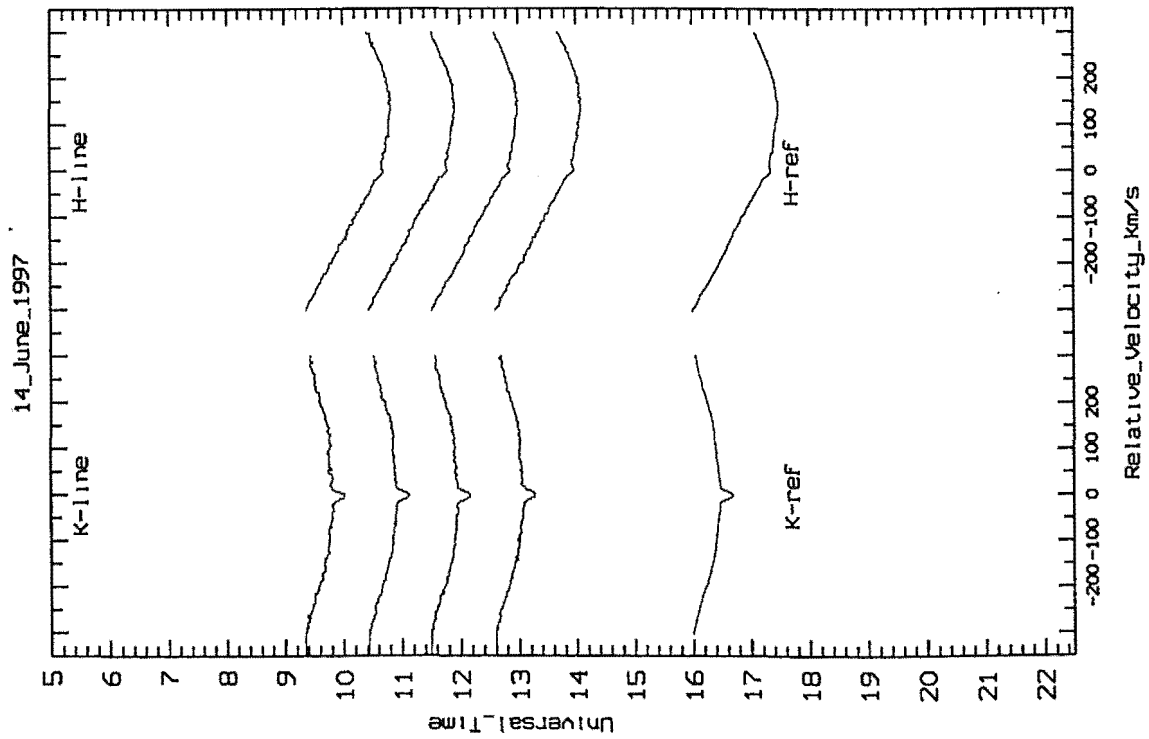

Figure 8.76: 51 Oph spectra taken on 14th June 1997.

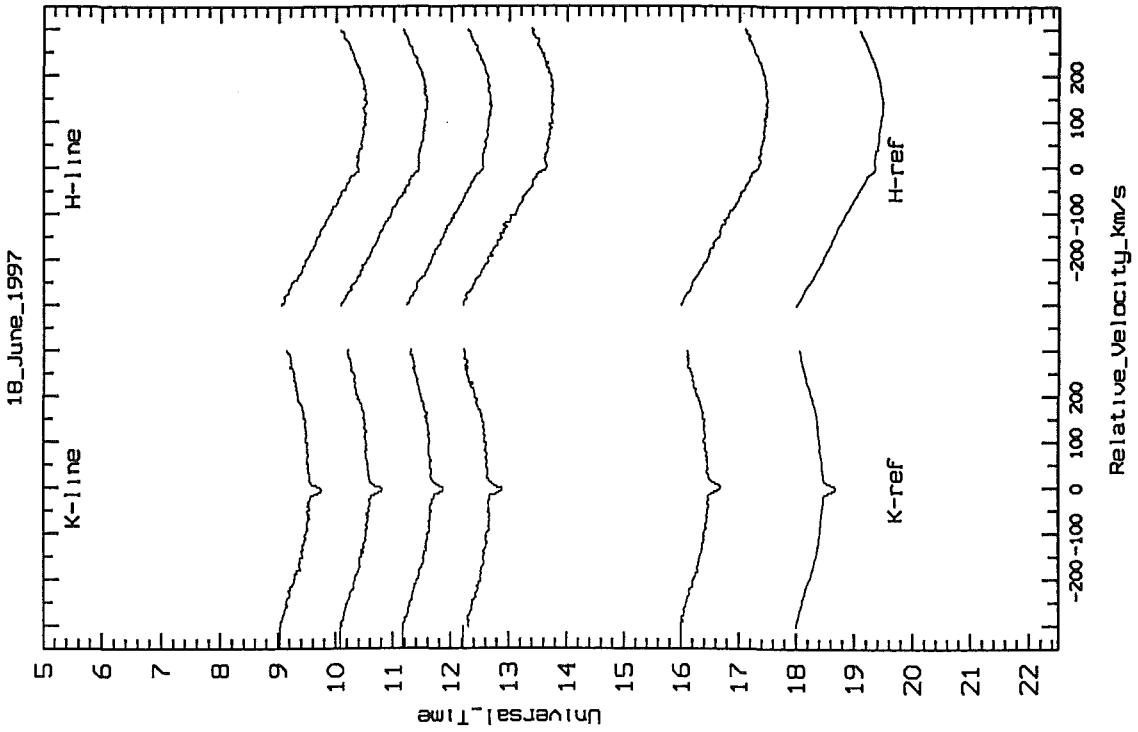

Figure 8.77: 51 Oph spectra taken on 18th June 1997.

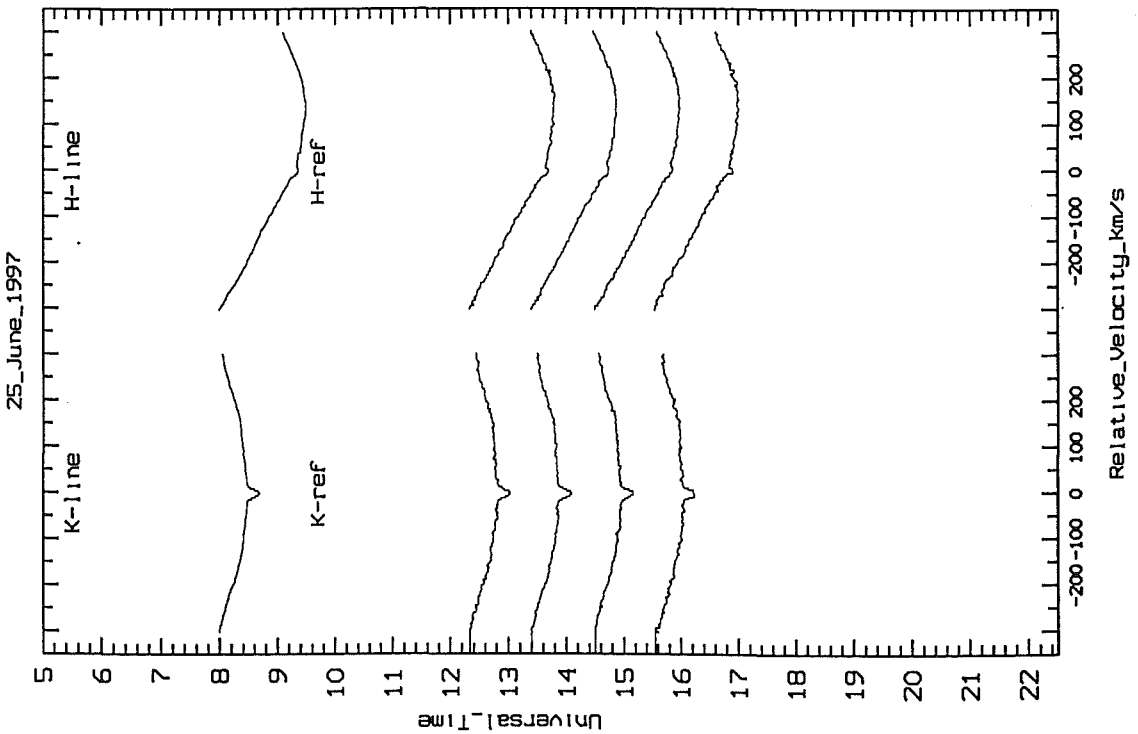

Figure 8.78: 51 Oph spectra taken on 25th June 1997.

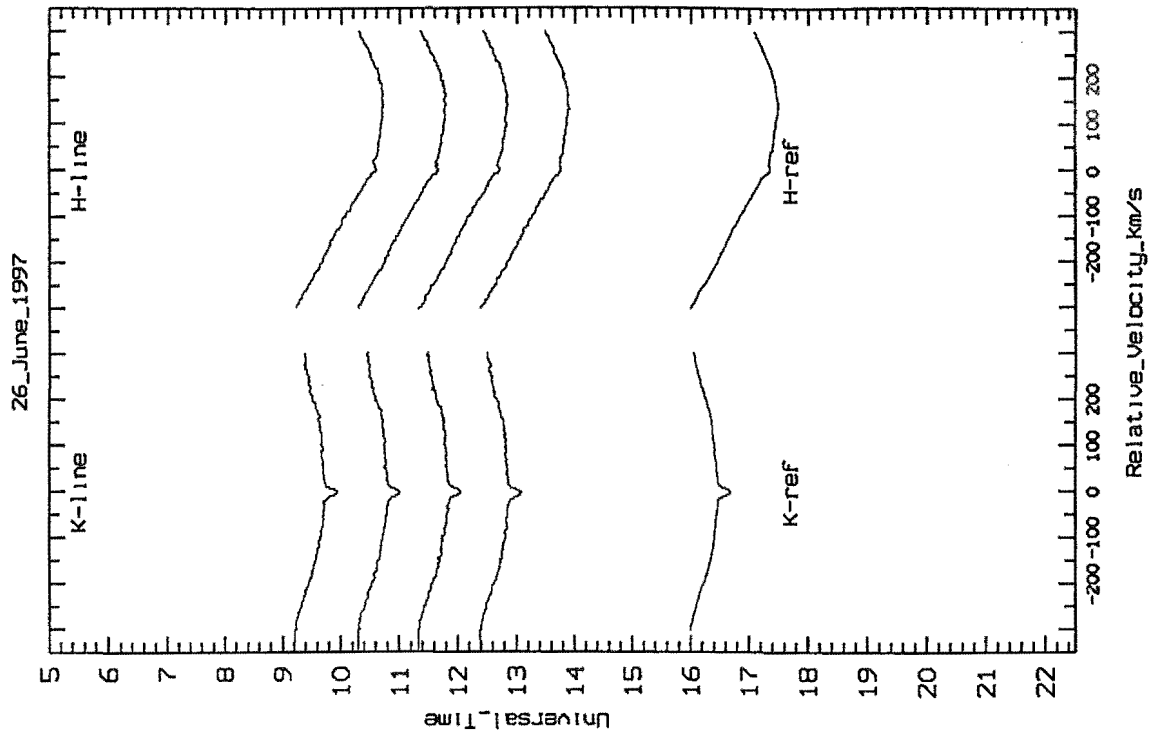

Figure 8.79: 51 Oph spectra taken on 26th June 1997.

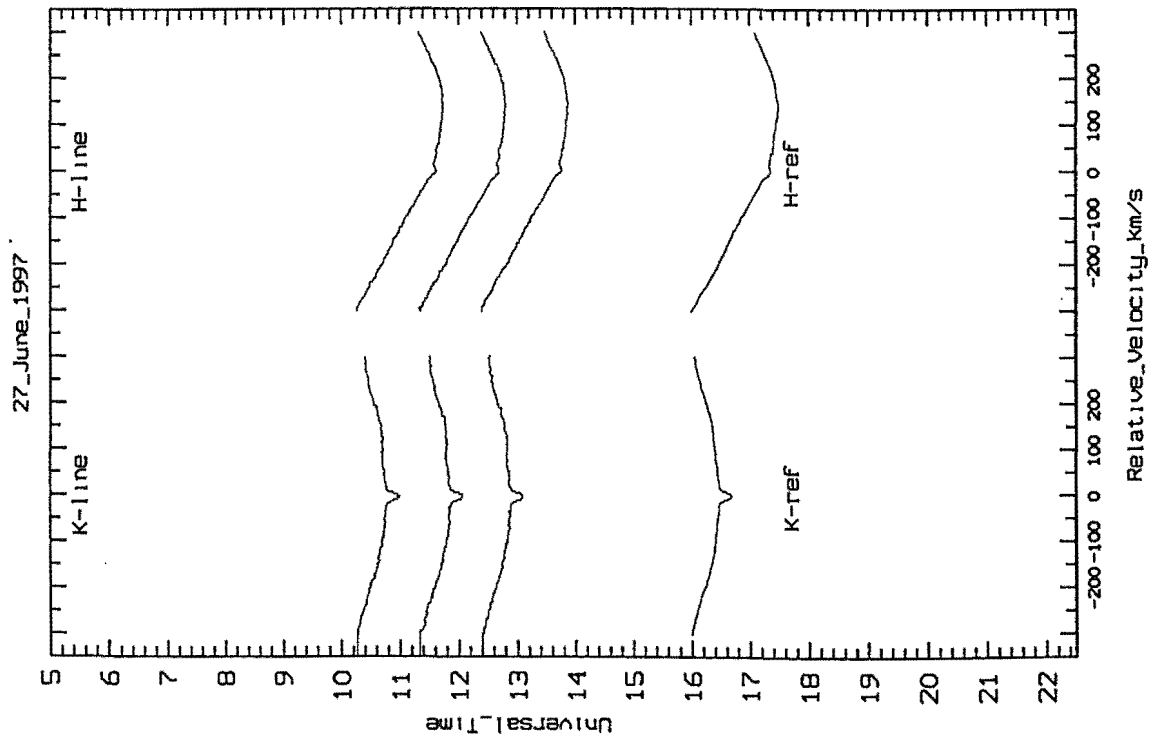

Figure 8.80: 51 Oph spectra taken on 27th June 1997.

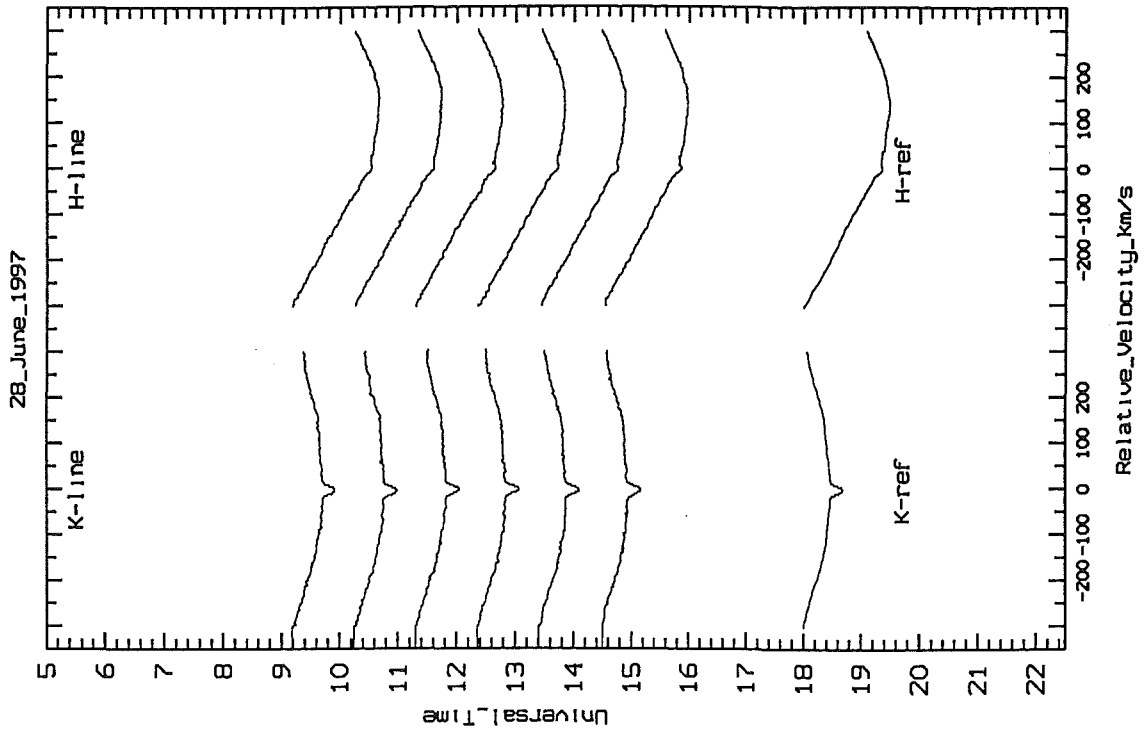

Figure 8.81: 51 Oph spectra taken on 28th June 1997.

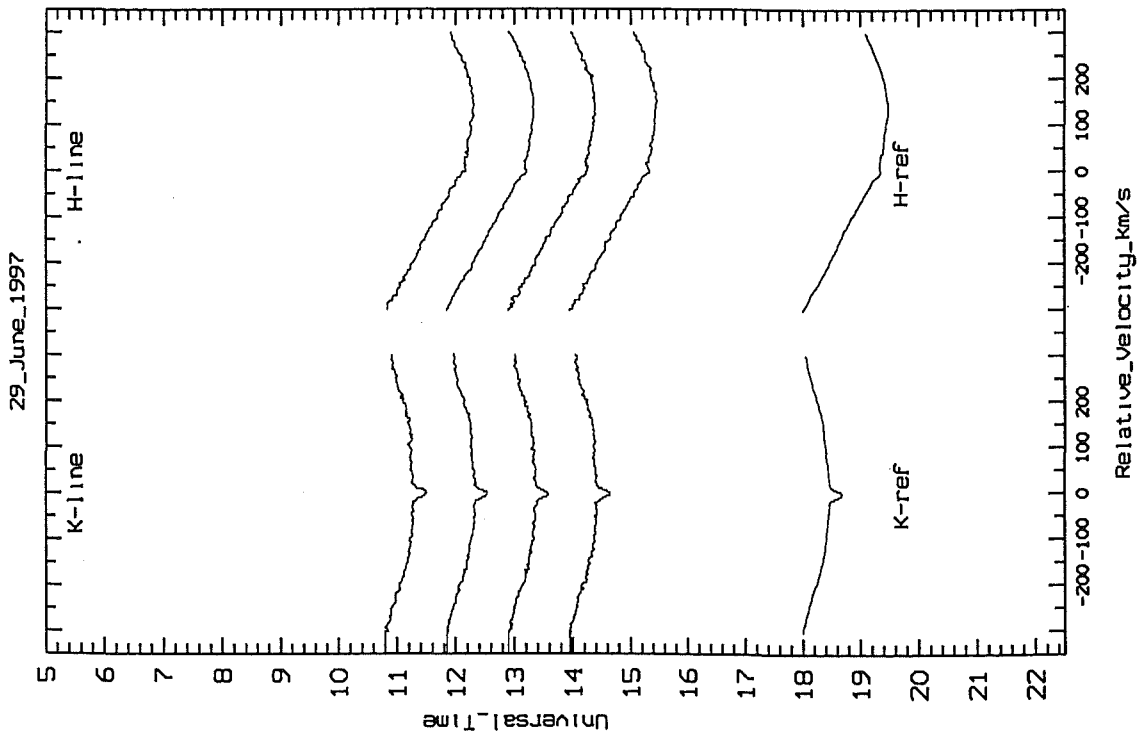

Figure 8.82: 51 Oph spectra taken on 29th June 1997.

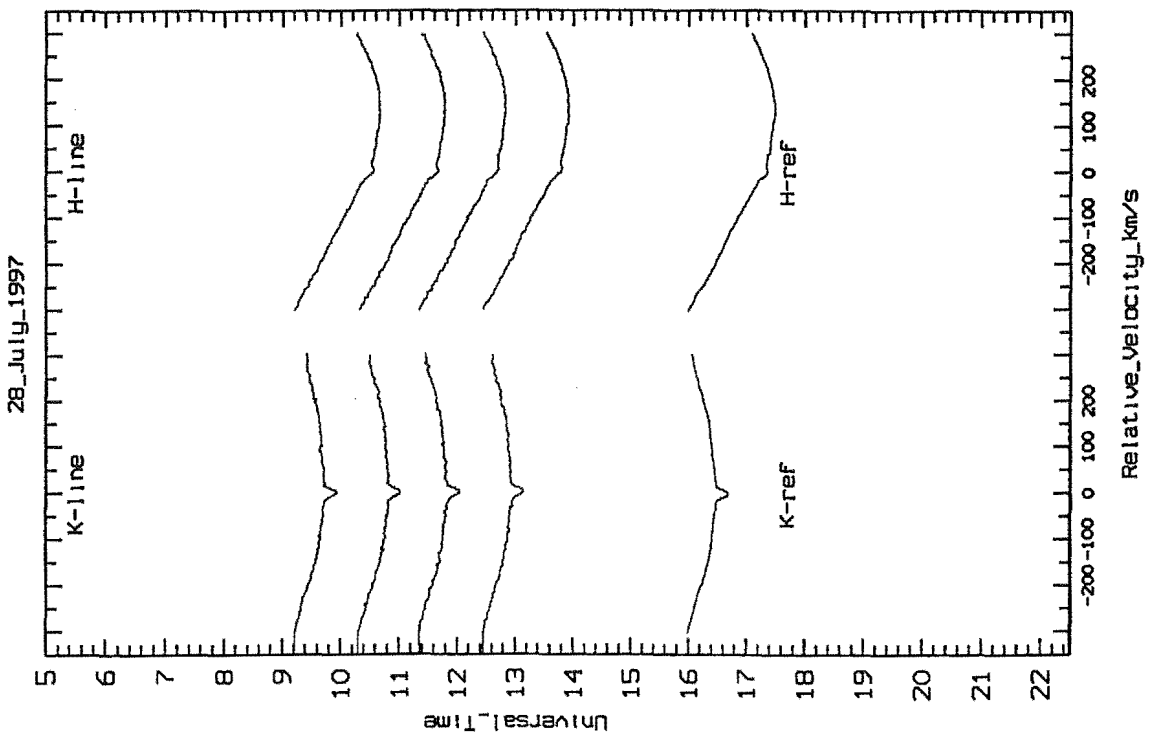

Figure 8.83: 51 Oph spectra taken on 28th July 1997.

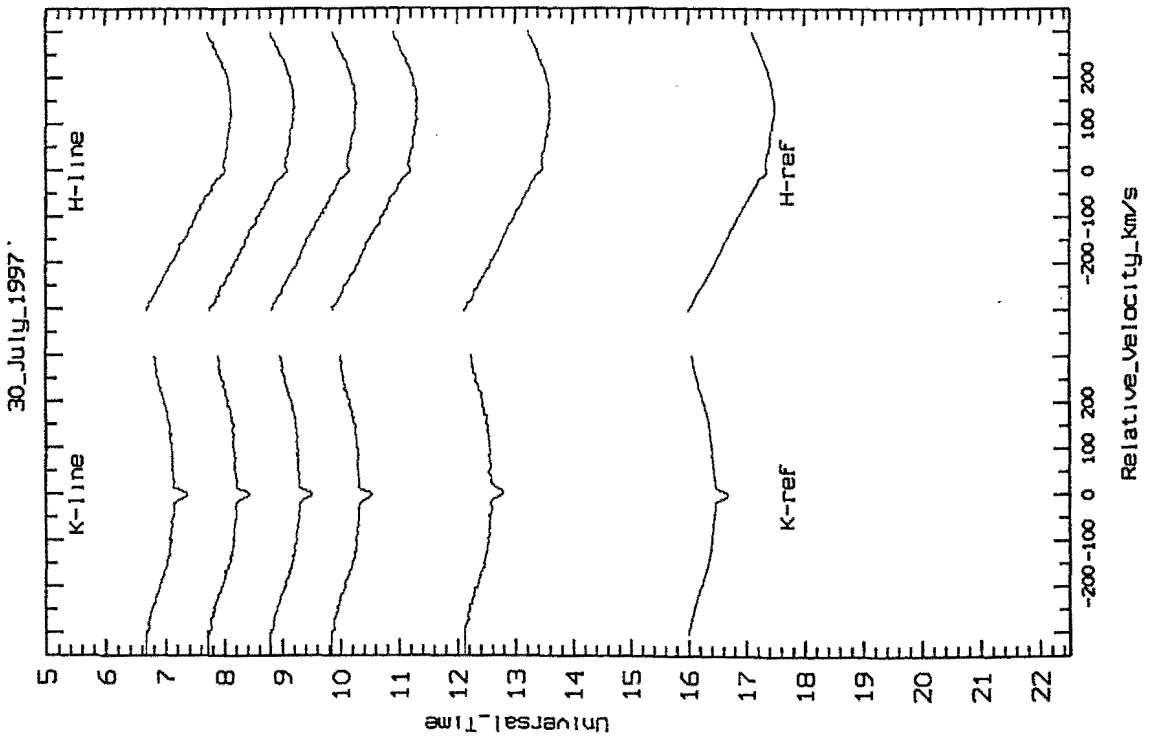

Figure 8.84: 51 Oph spectra taken on 30th July 1997.

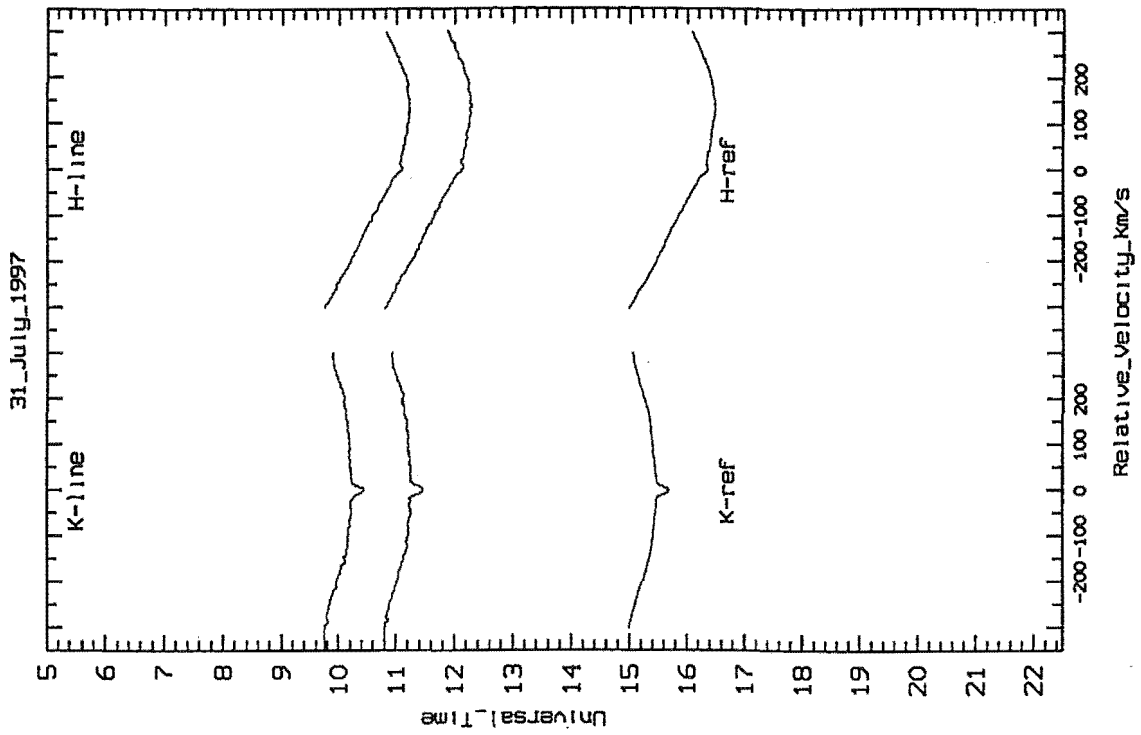

Figure 8.85: 51 Oph spectra taken on 31th July 1997.

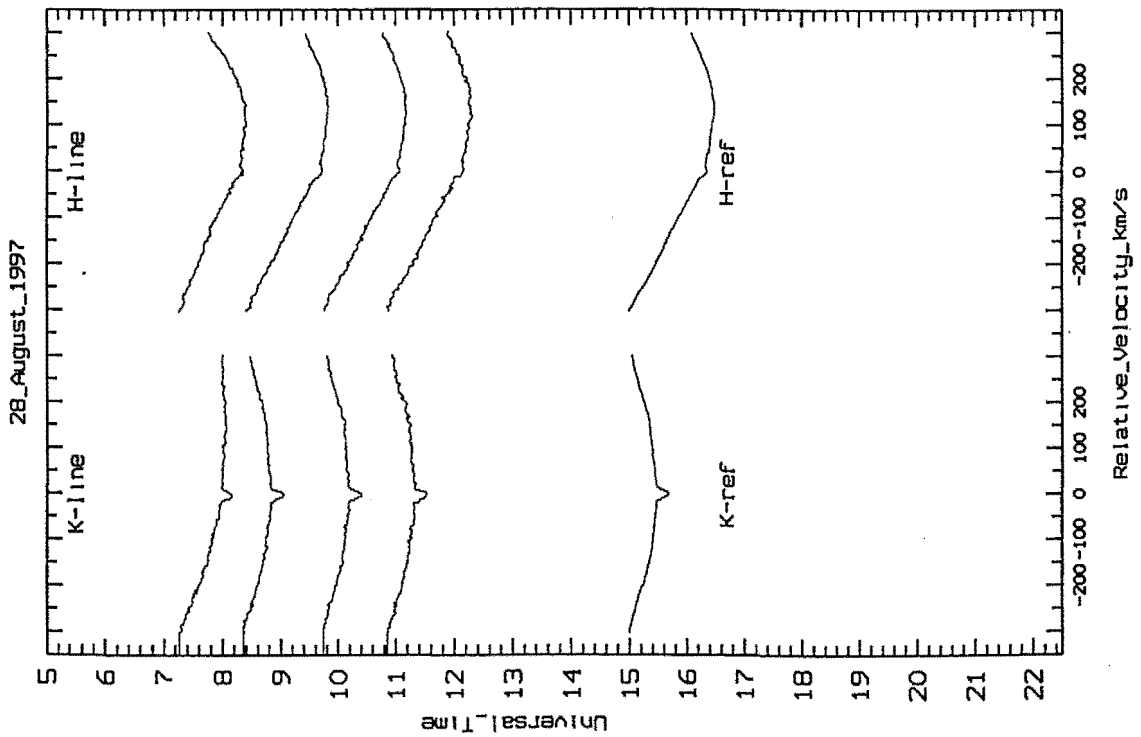

Figure 8.86: 51 Oph spectra taken on 28th August 1997. The difference in the first spectrum was due to condensation on the cryostat entrance window.

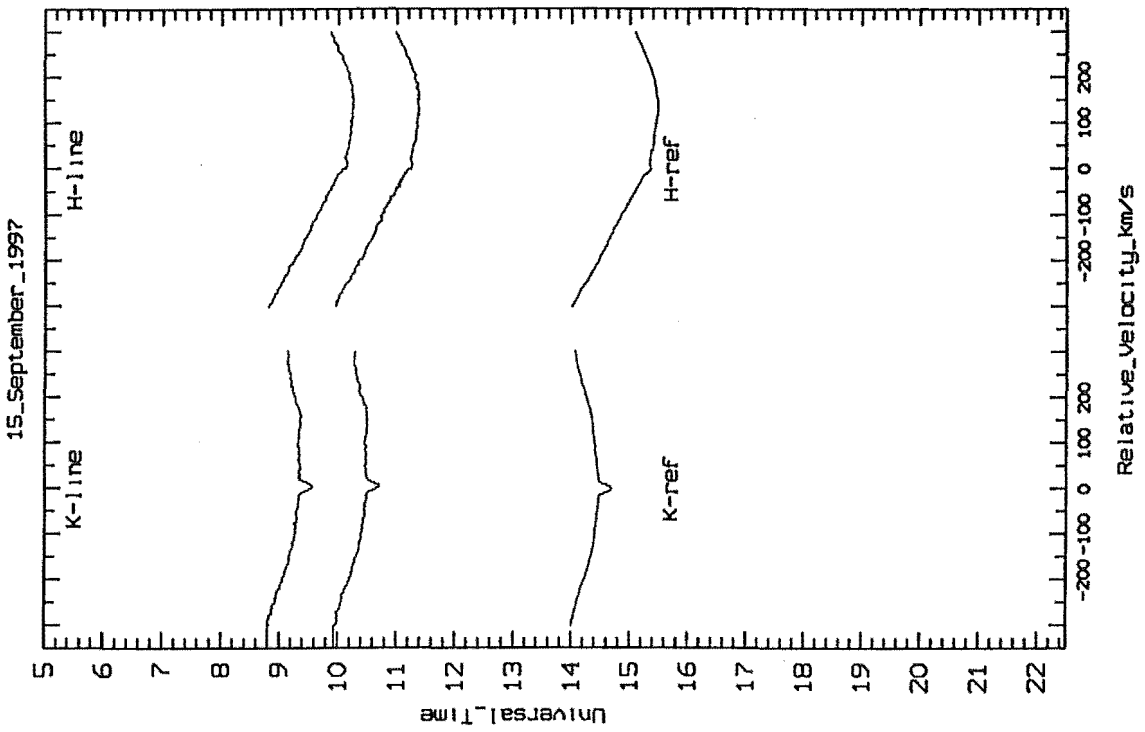

Figure 8.87: 51 Oph spectra taken on 15th September 1997.

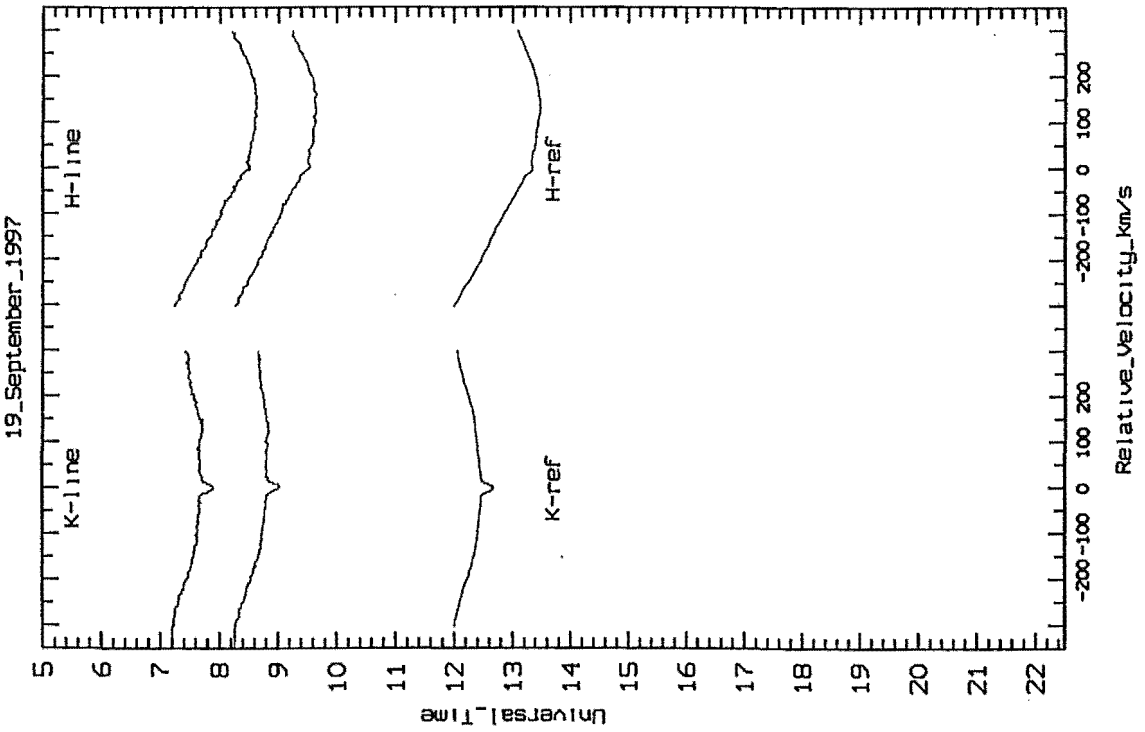

Figure 8.88: 51 Oph spectra taken on 19th September 1997.

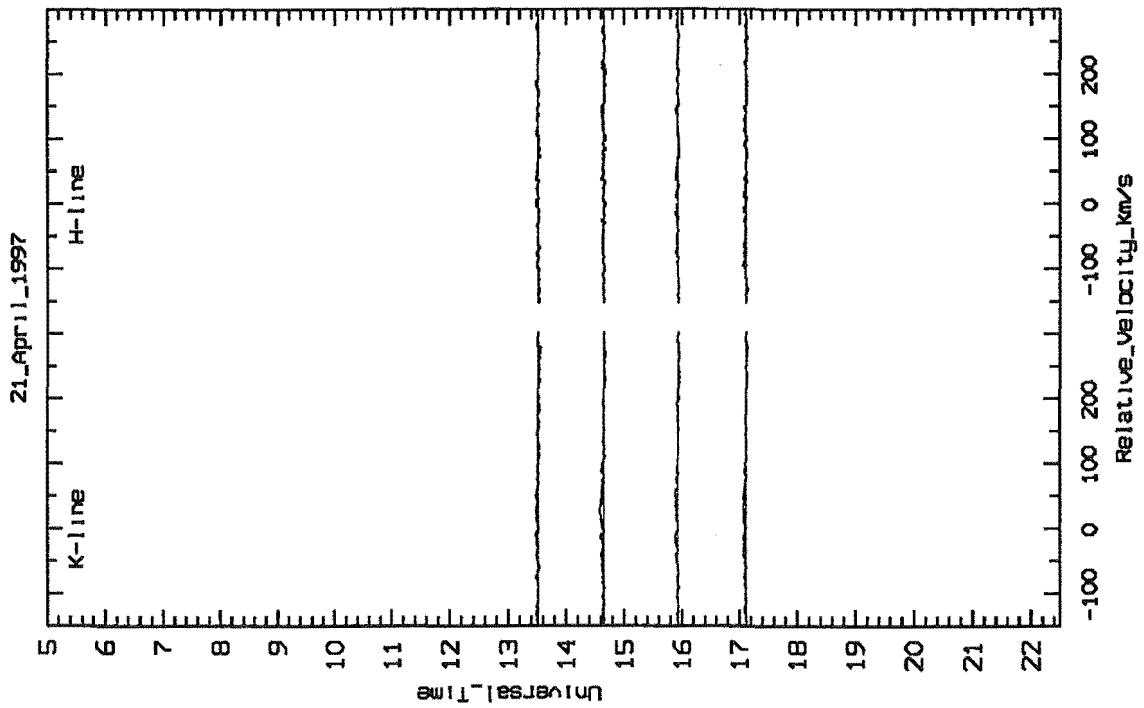

Figure 8.89: Normalised 51 Oph spectra taken on 21st April 1997.

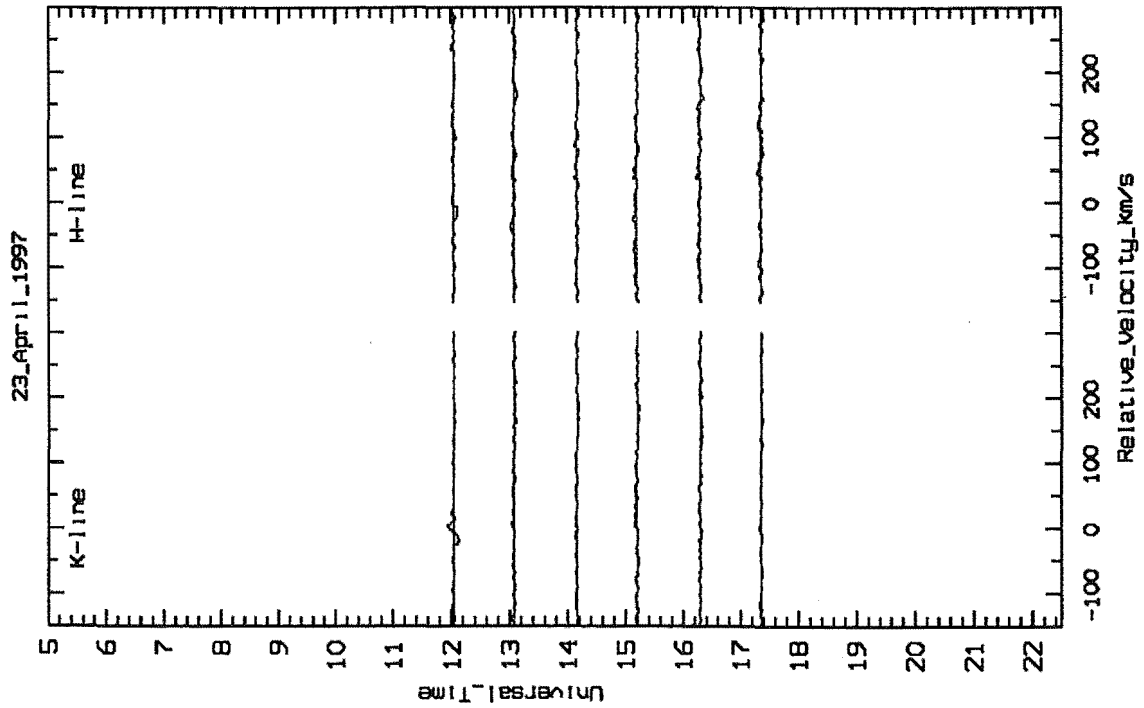

Figure 8.90: Normalised 51 Oph spectra taken on 23rd April 1997.

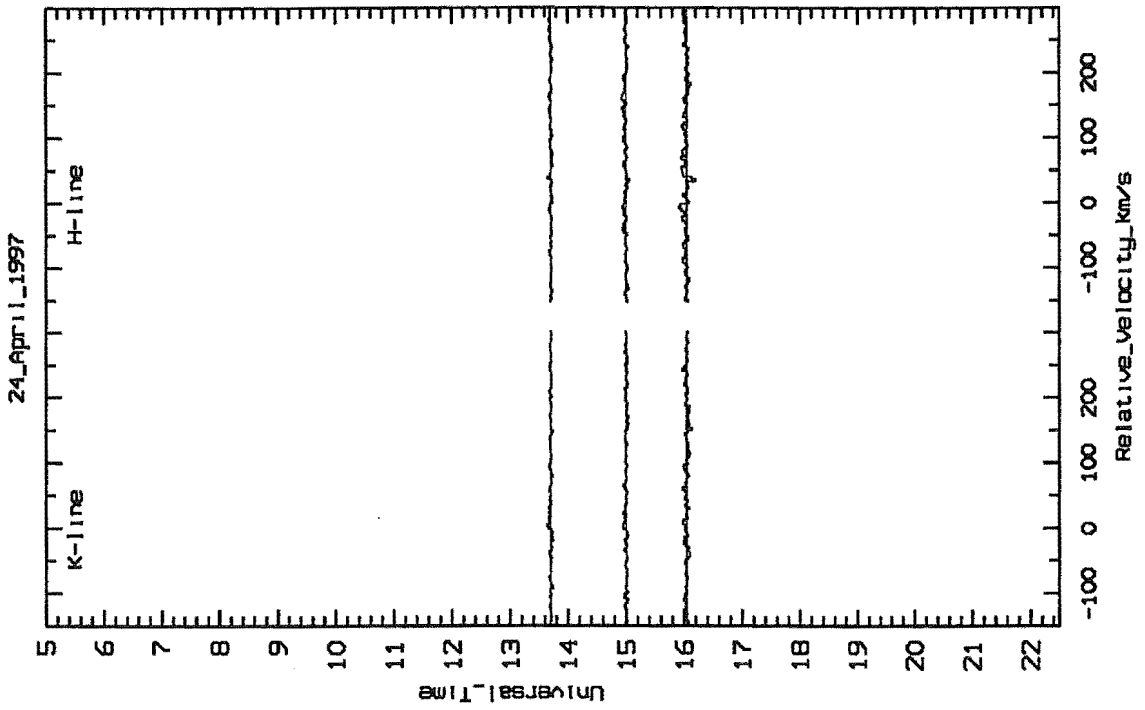

Figure 8.91: Normalised 51 Oph spectra taken on 24th April 1997.

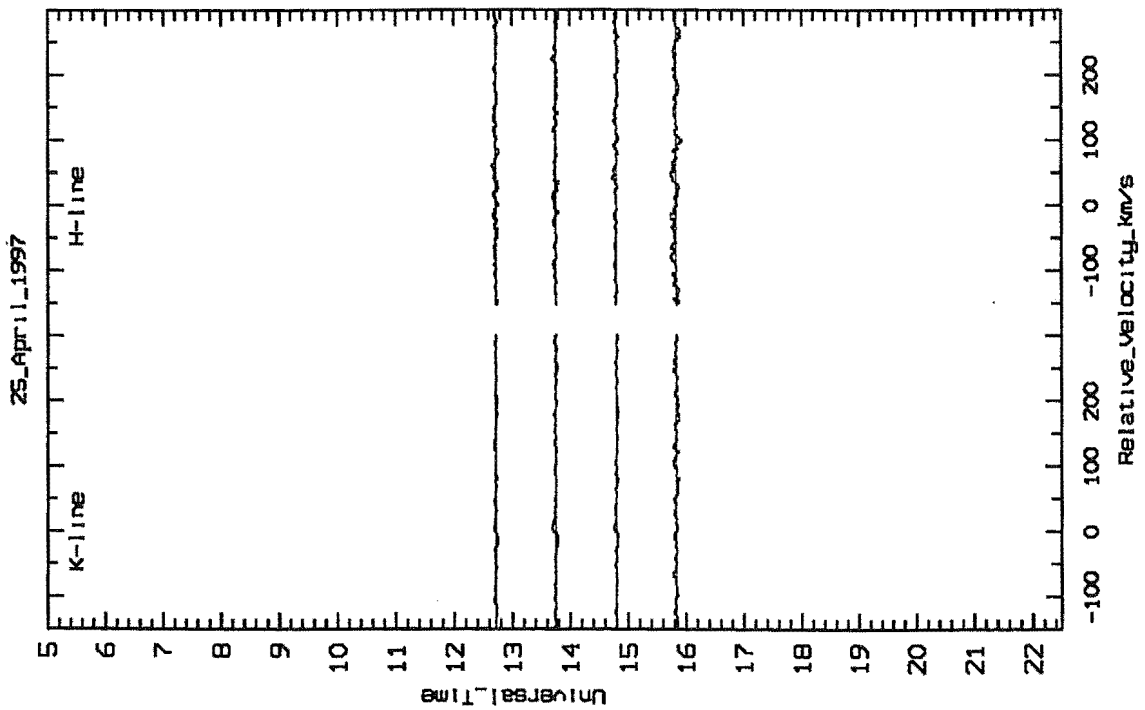

Figure 8.92: Normalised 51 Oph spectra taken on 25th April 1997.

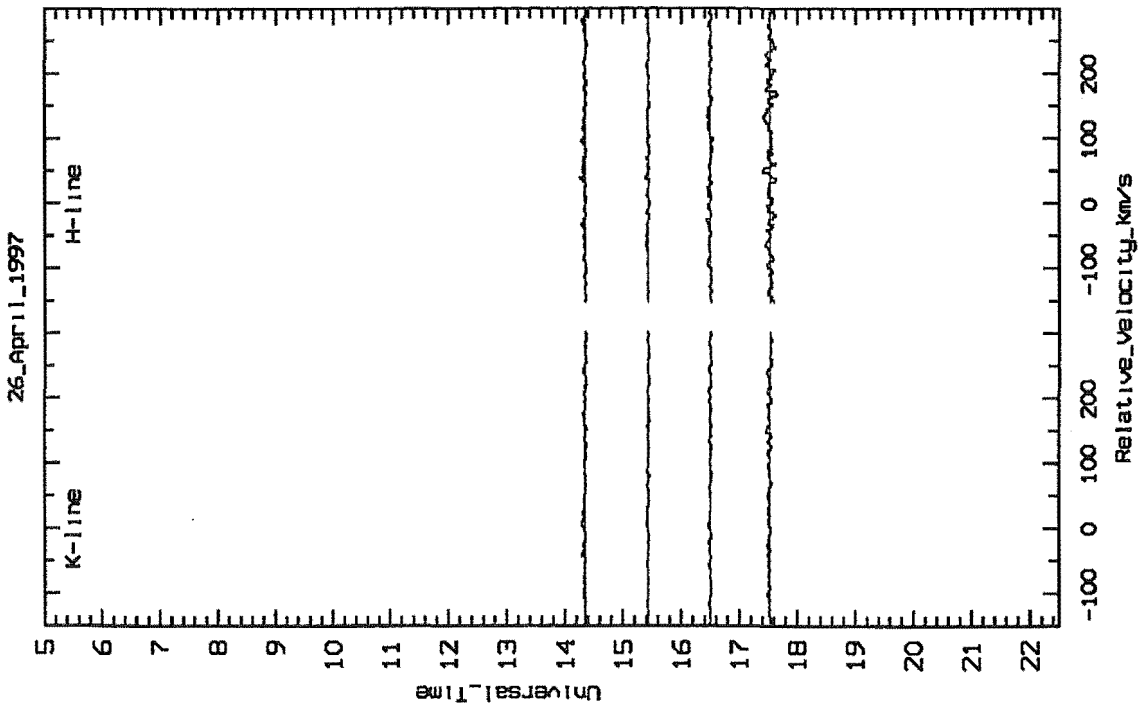

Figure 8.93: Normalised 51 Oph spectra taken on 26th April 1997.

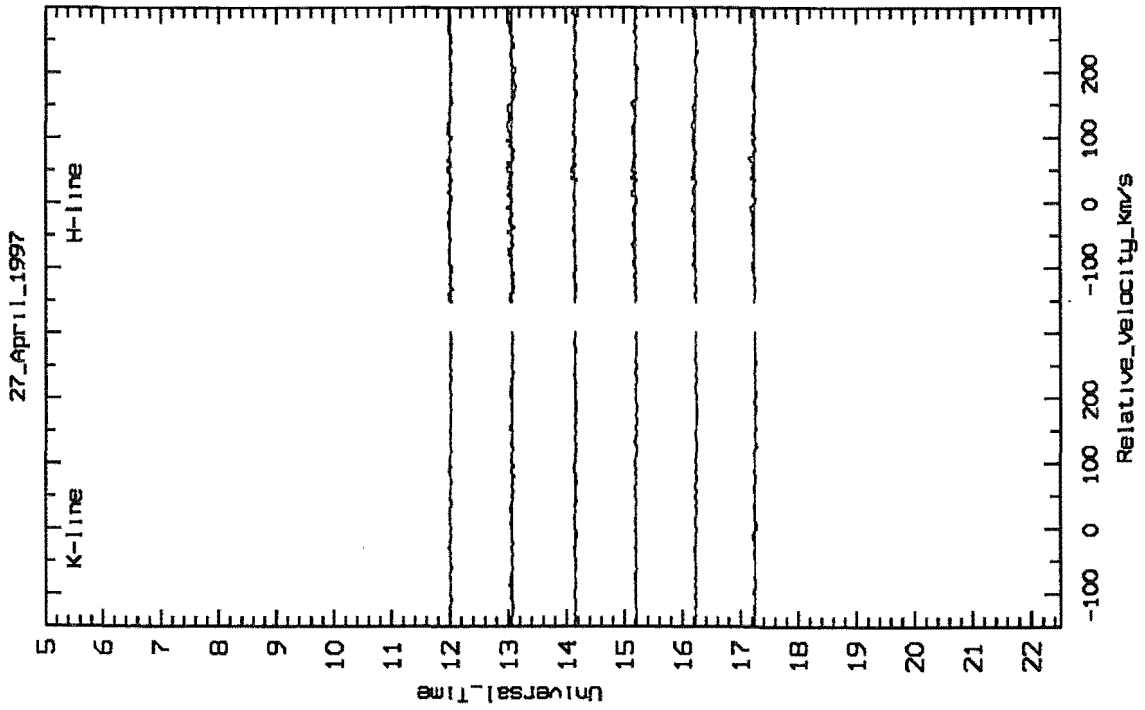

Figure 8.94: Normalised 51 Oph spectra taken on 27th April 1997.

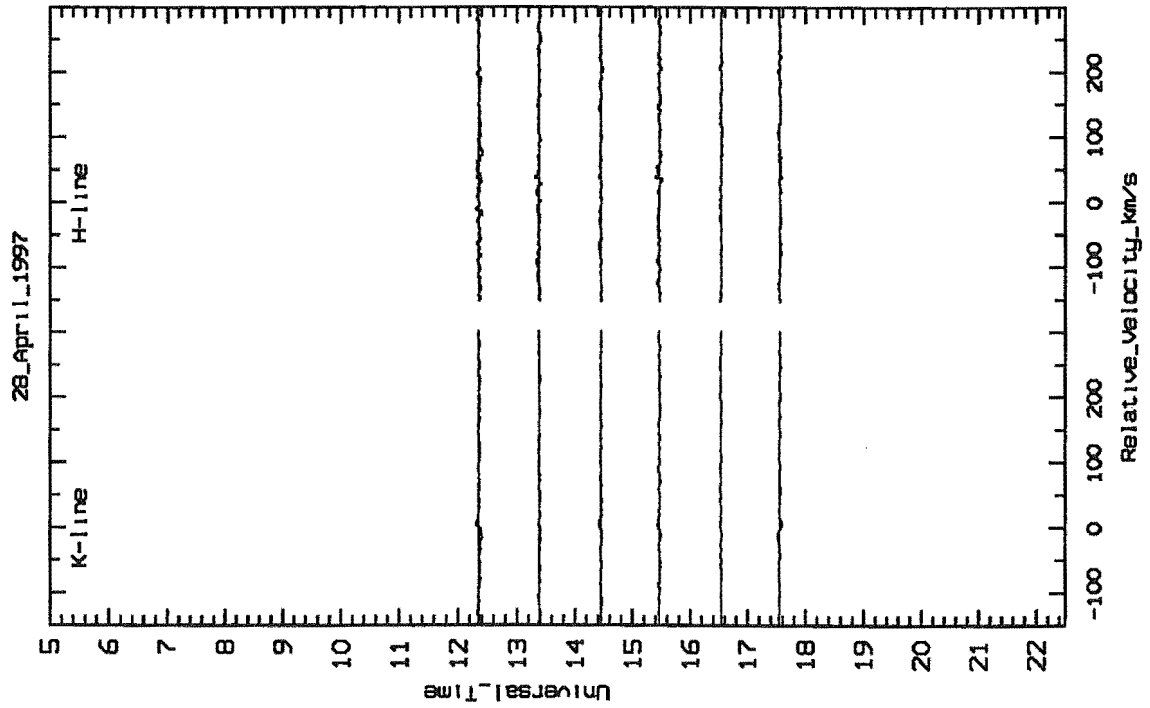

Figure 8.95: Normalised 51 Oph spectra taken on 28th April 1997.

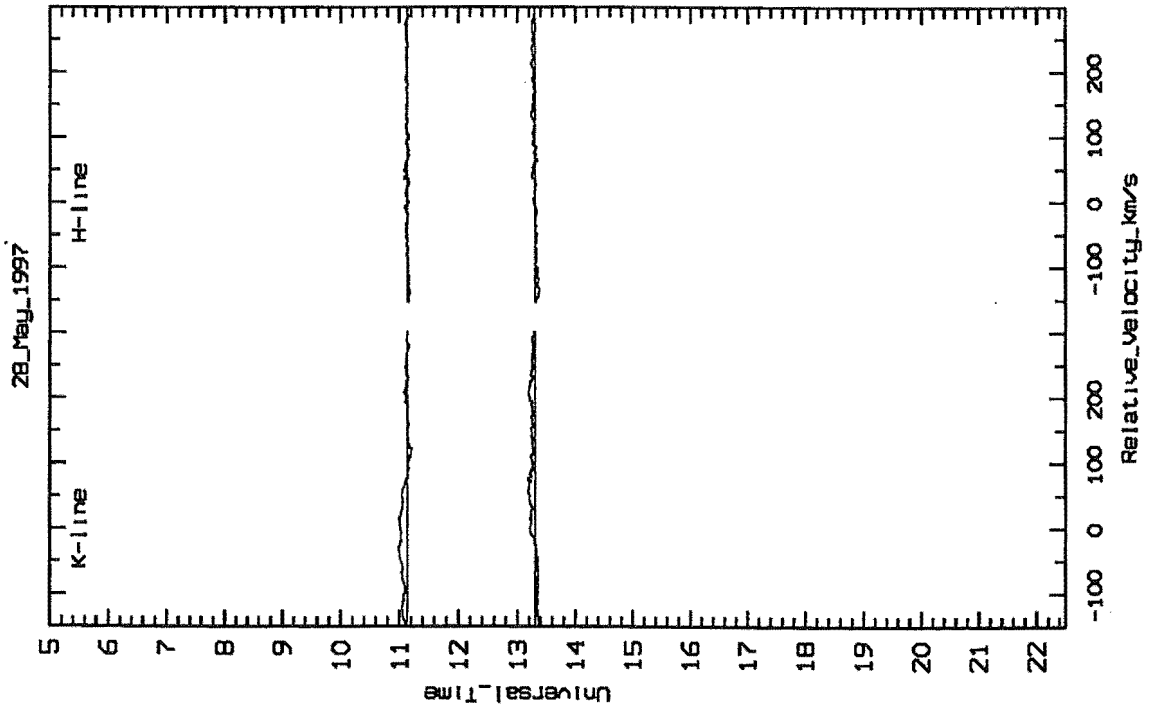

Figure 8.96: Normalised 51 Oph spectra taken on 28th May 1997.

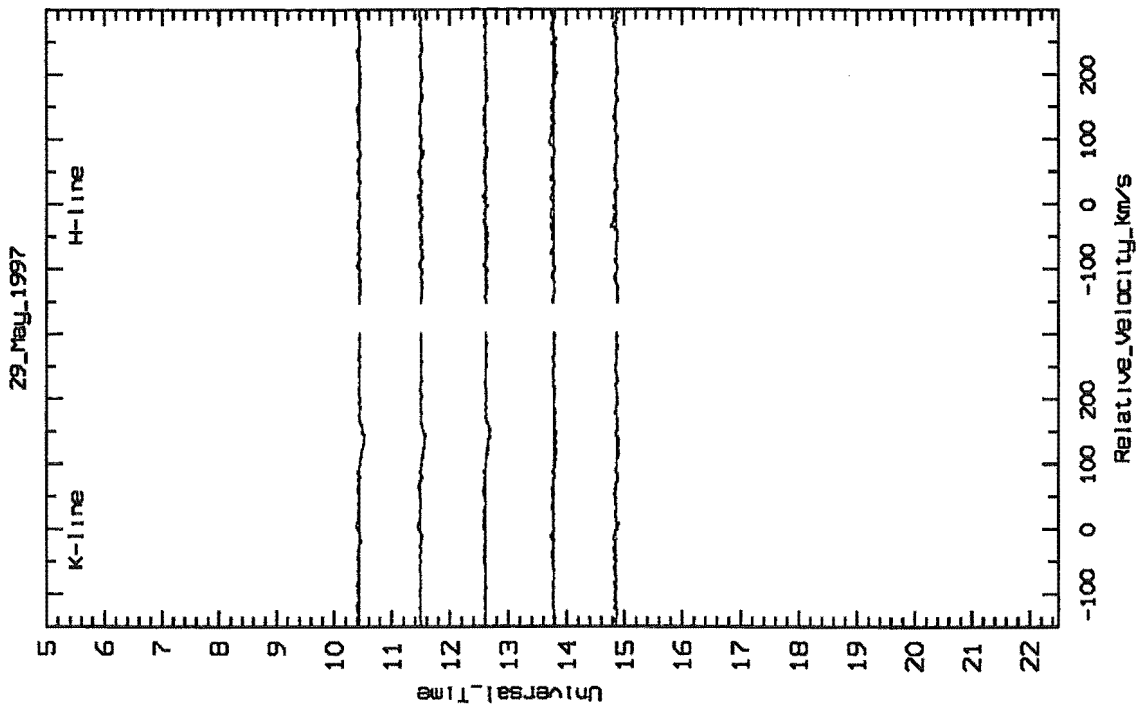

Figure 8.97: Normalised 51 Oph spectra taken on 29th May 1997.

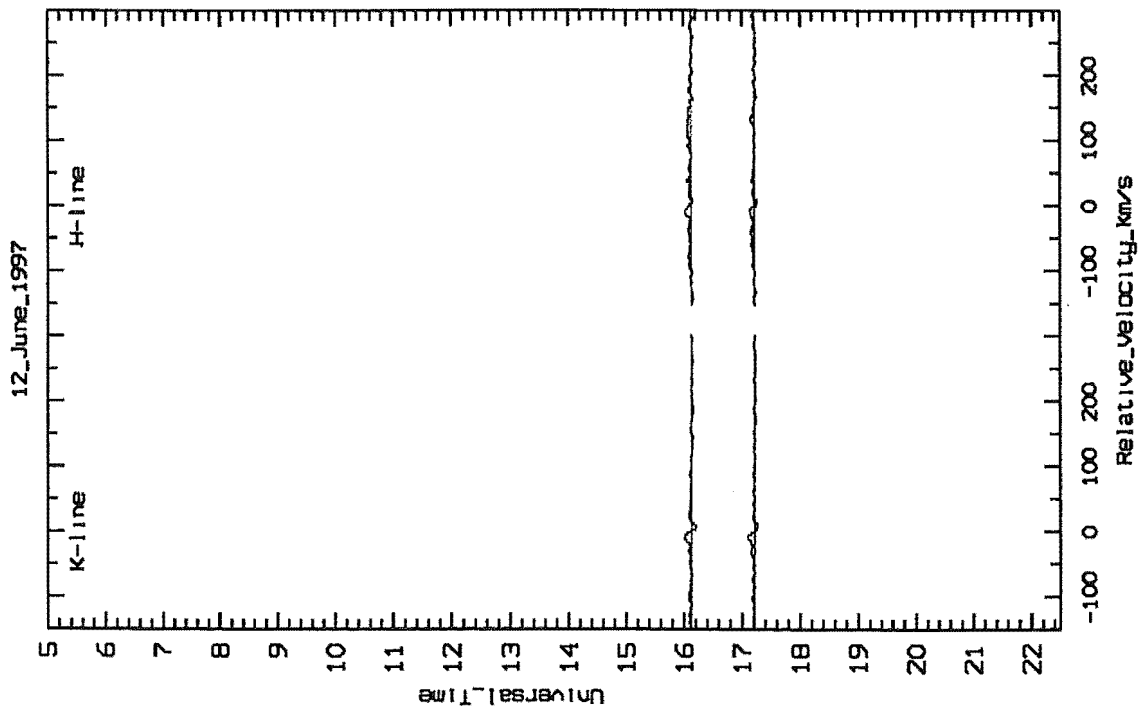

Figure 8.98: Normalised 51 Oph spectra taken on 12th June 1997.

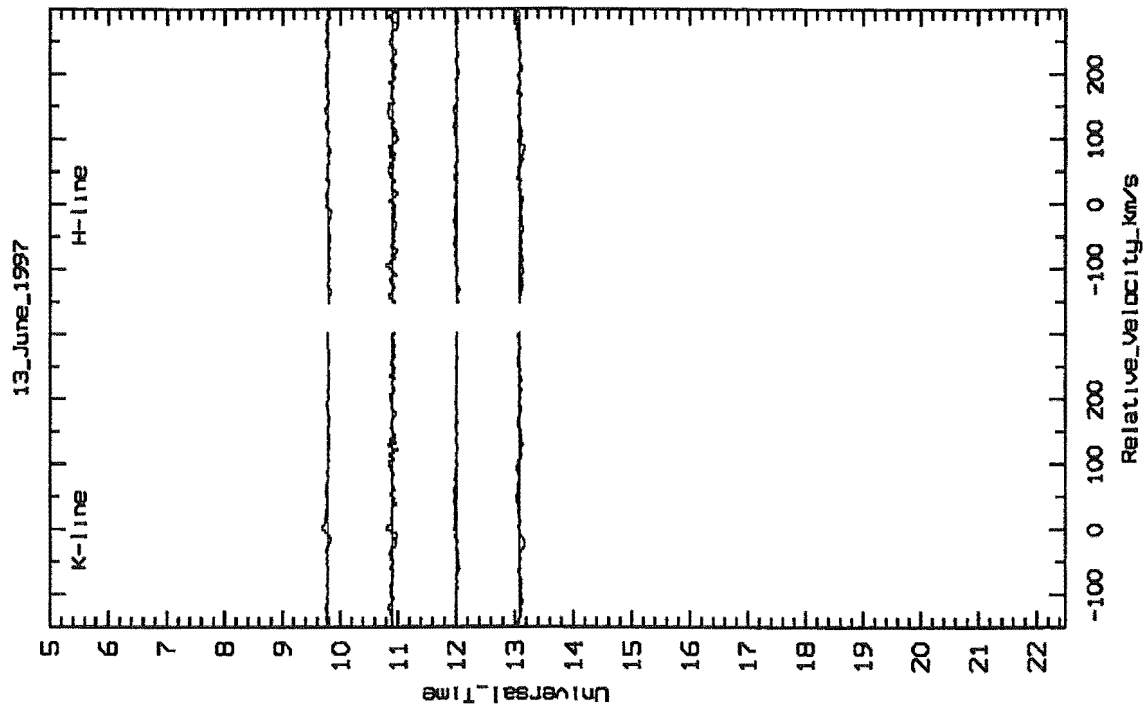

Figure 8.99: Normalised 51 Oph spectra taken on 13th June 1997.

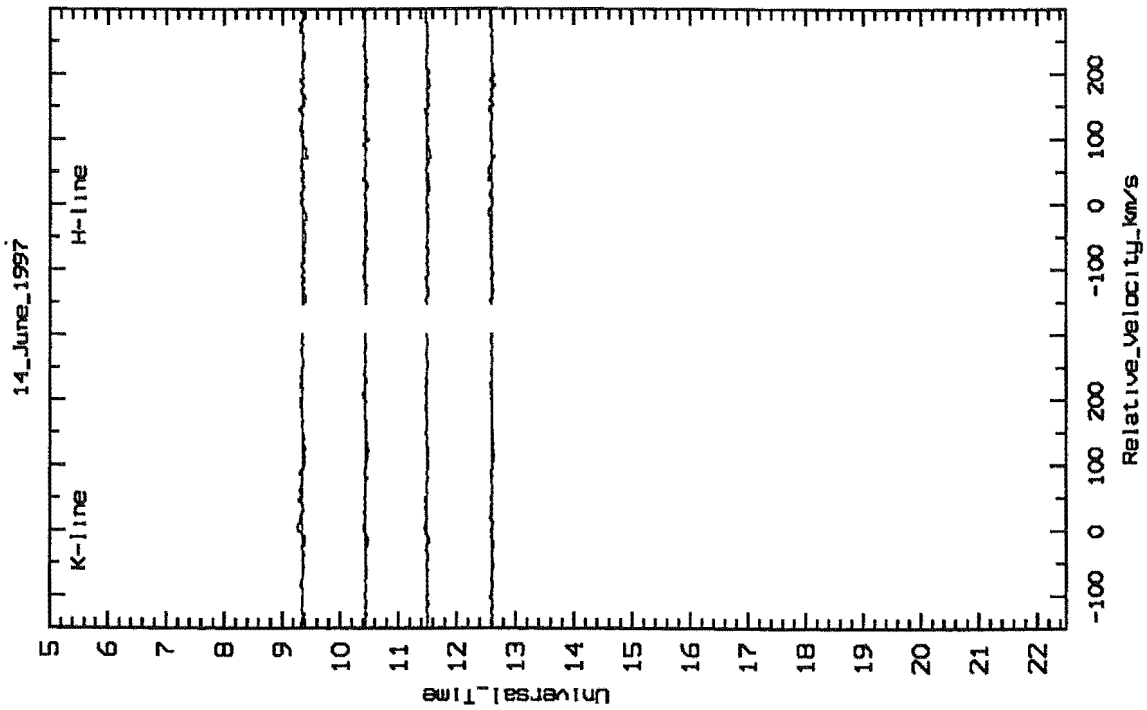

Figure 8.100: Normalised 51 Oph spectra taken on 14th June 1997.

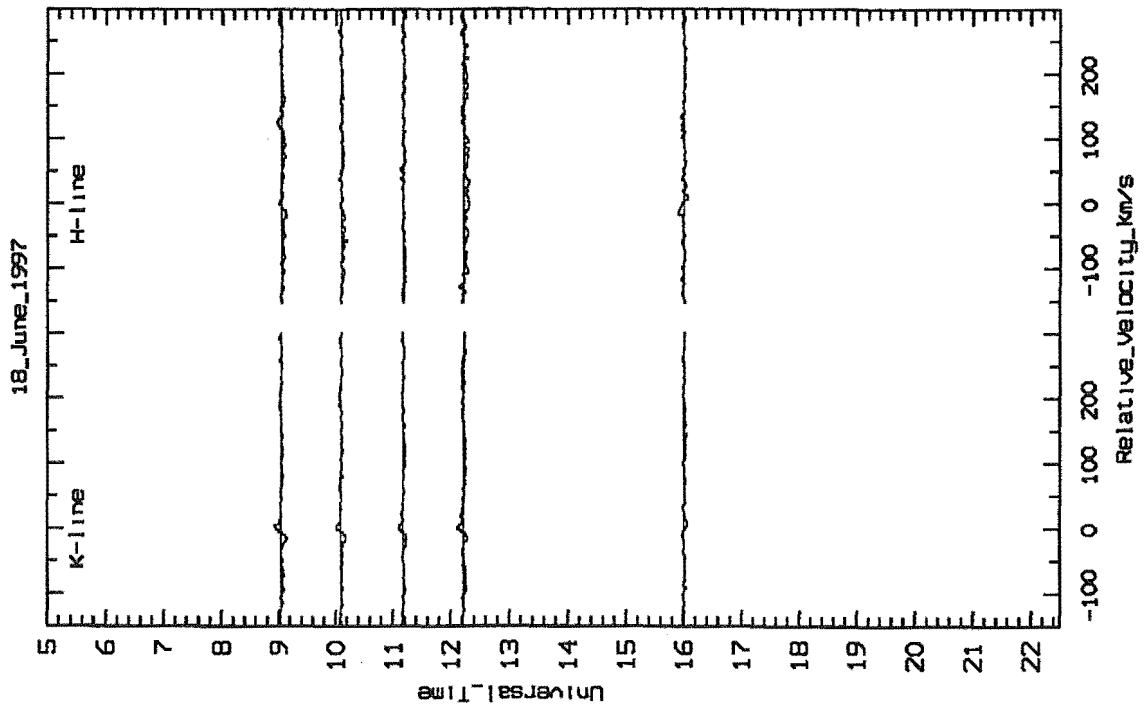

Figure 8.101: Normalised 51 Oph spectra taken on 18th June 1997.

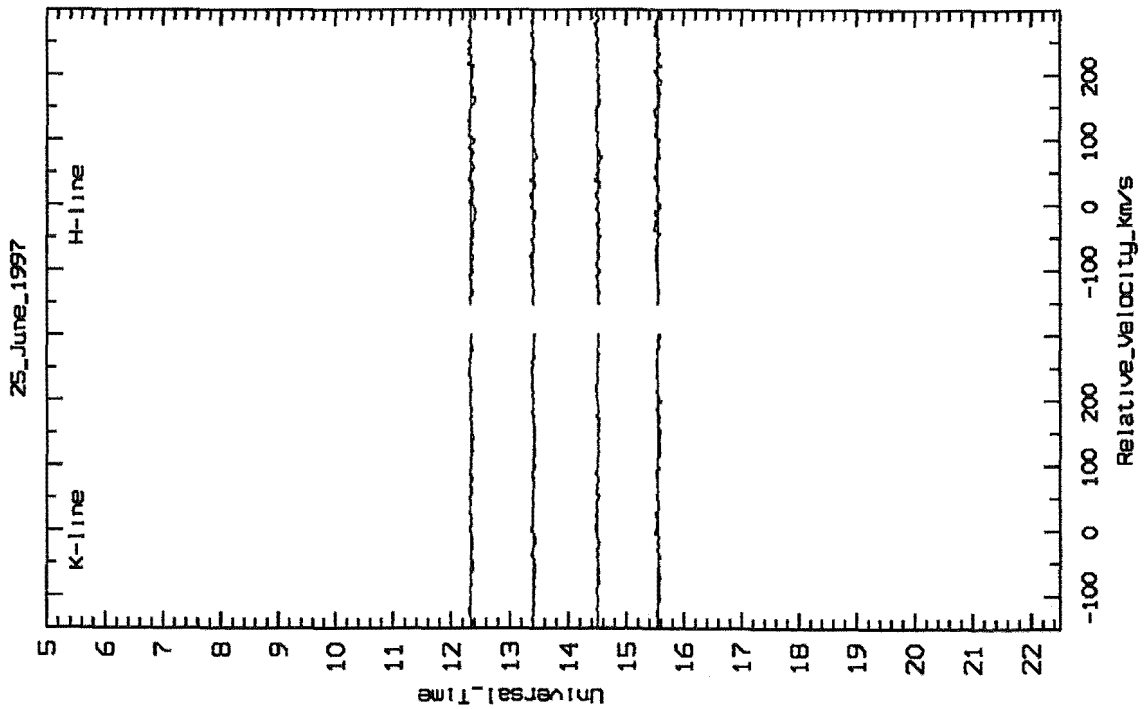

Figure 8.102: Normalised 51 Oph spectra taken on 25th June 1997.

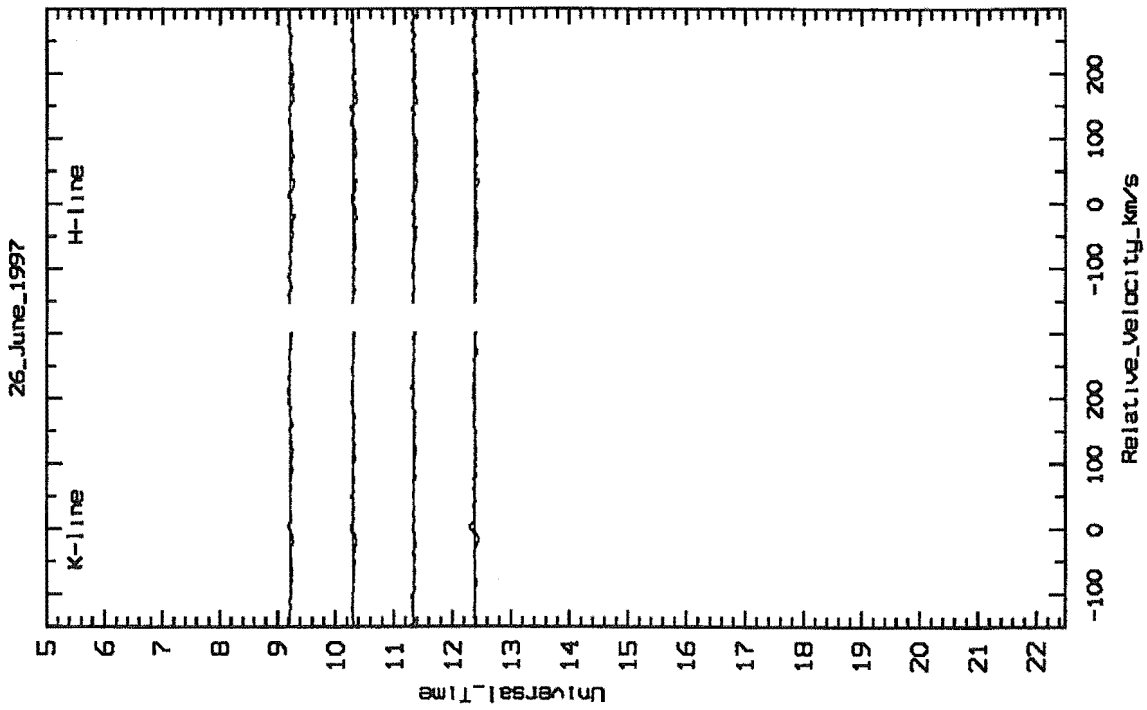

Figure 8.103: Normalised 51 Oph spectra taken on 26th June 1997.

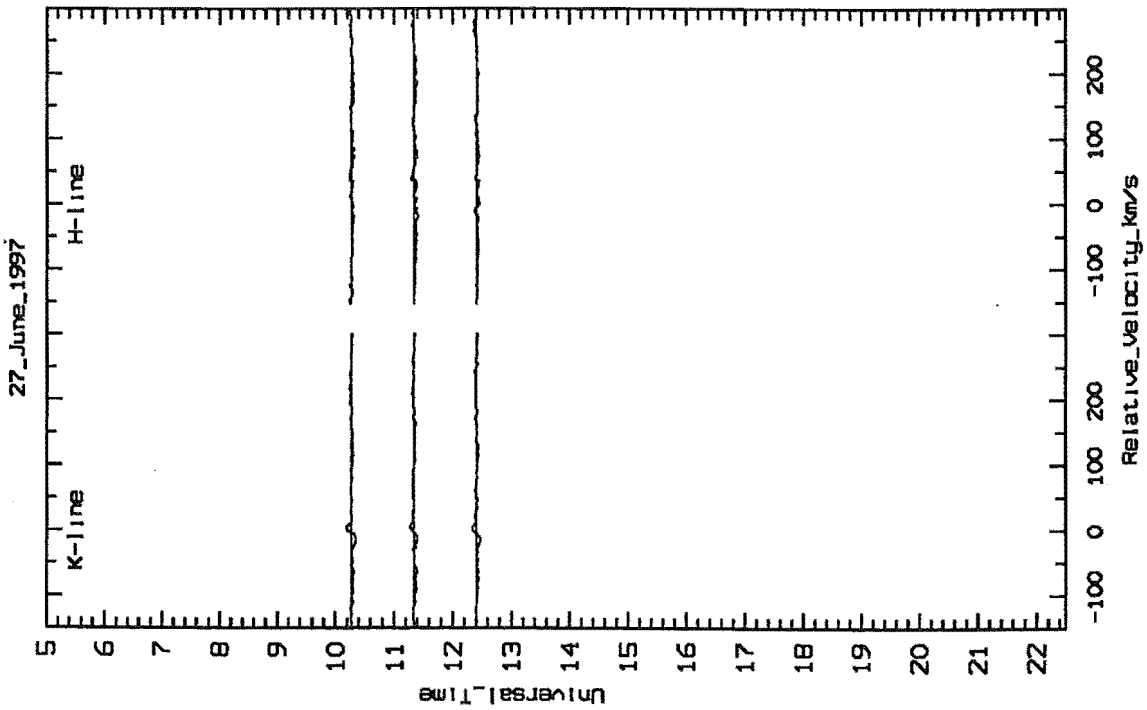

Figure 8.104: Normalised 51 Oph spectra taken on 27th June 1997.

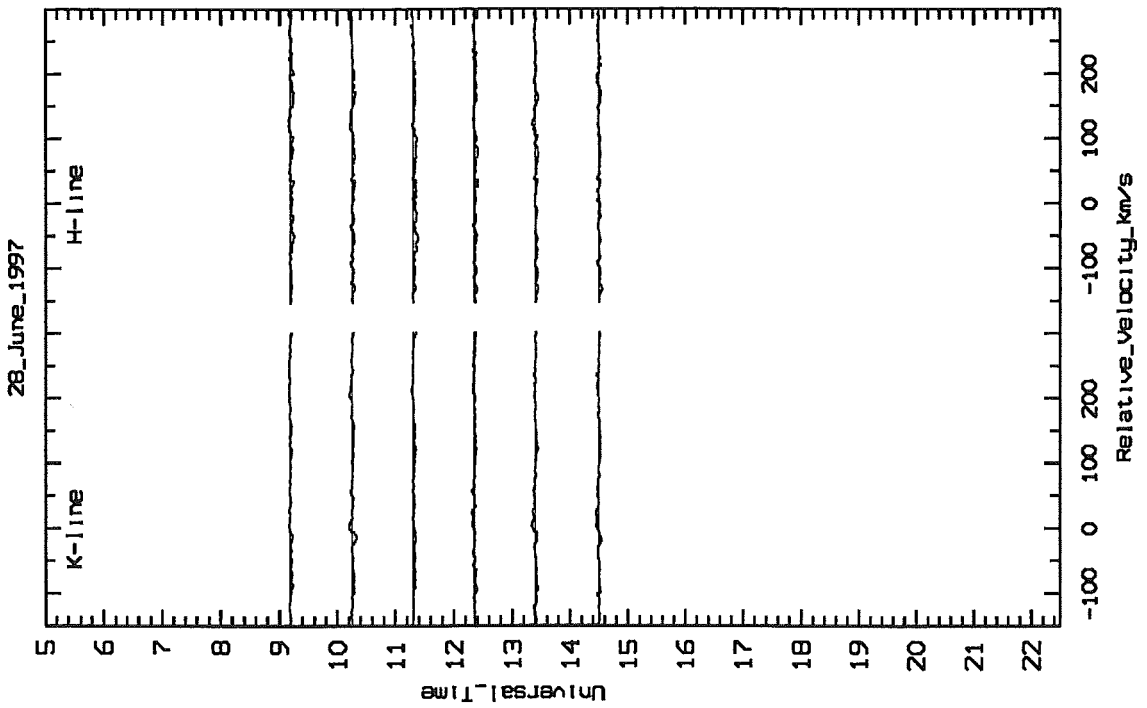

Figure 8.105: Normalised 51 Oph spectra taken on 28th June 1997.

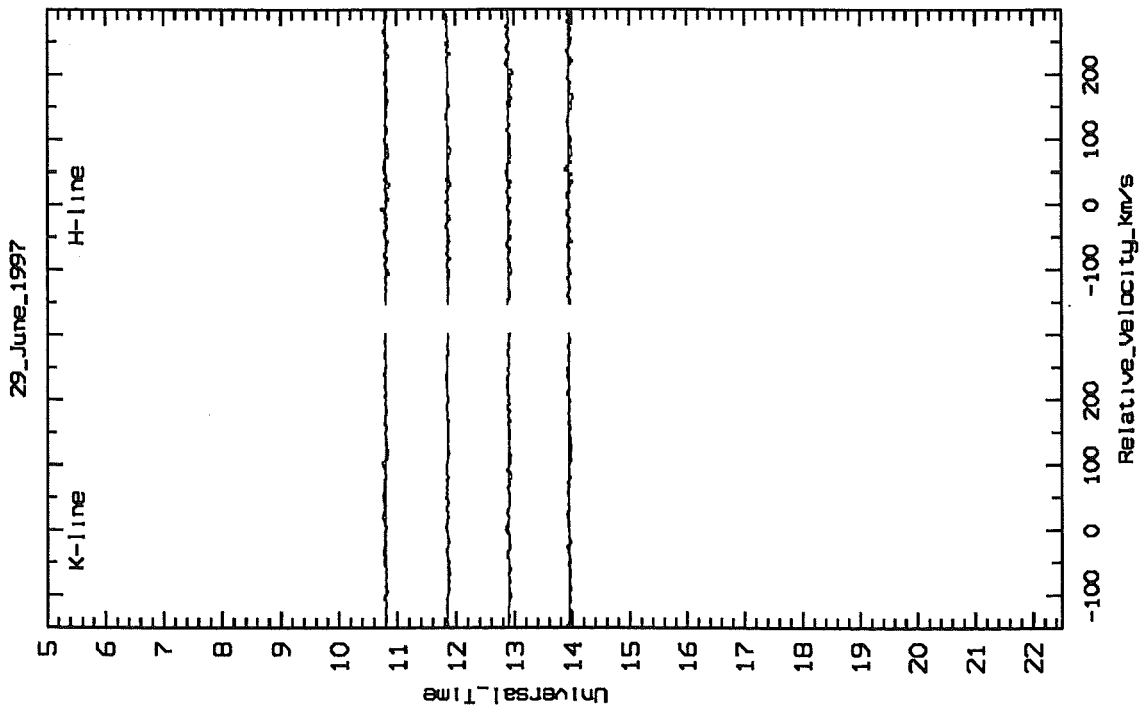

Figure 8.106: Normalised 51 Oph spectra taken on 29th June 1997.

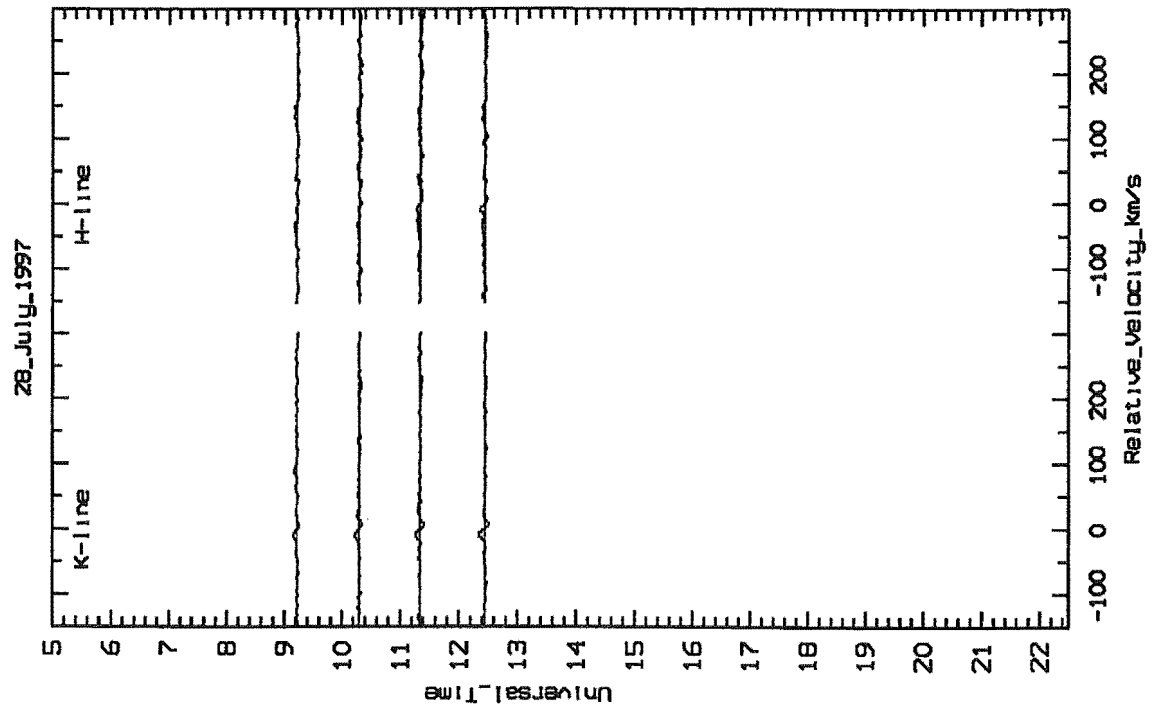

Figure 8.107: Normalised 51 Oph spectra taken on 28th July 1997.

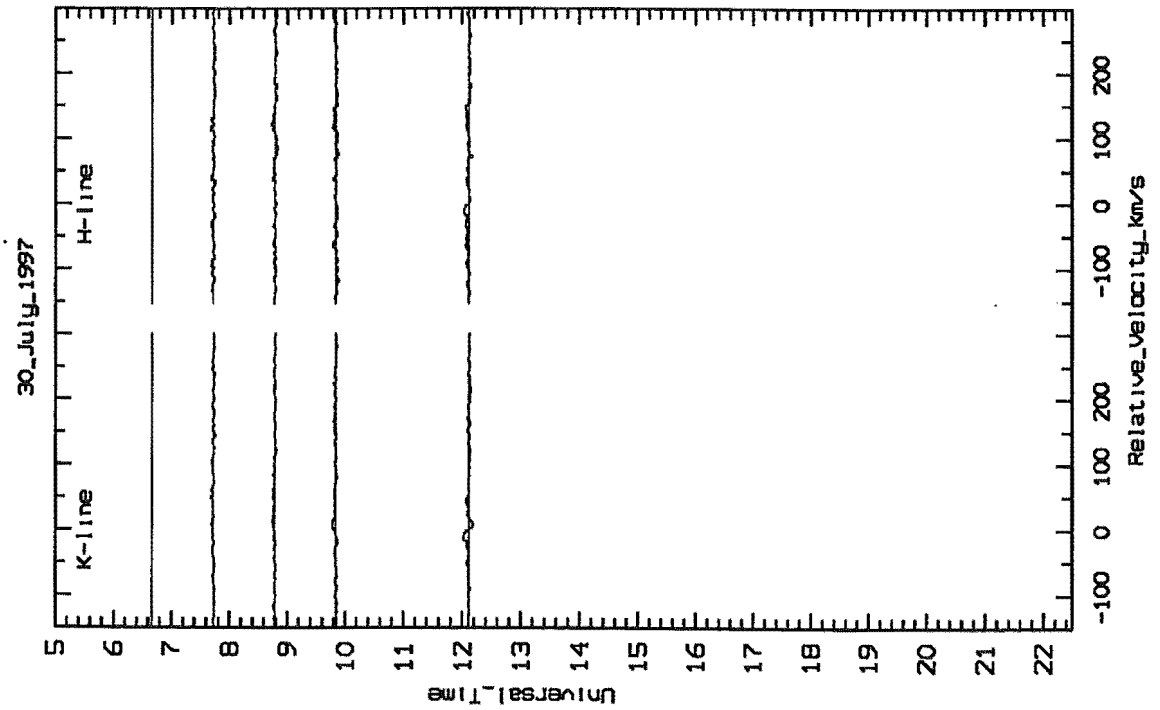

Figure 8.108: Normalised 51 Oph spectra taken on 30th July 1997.

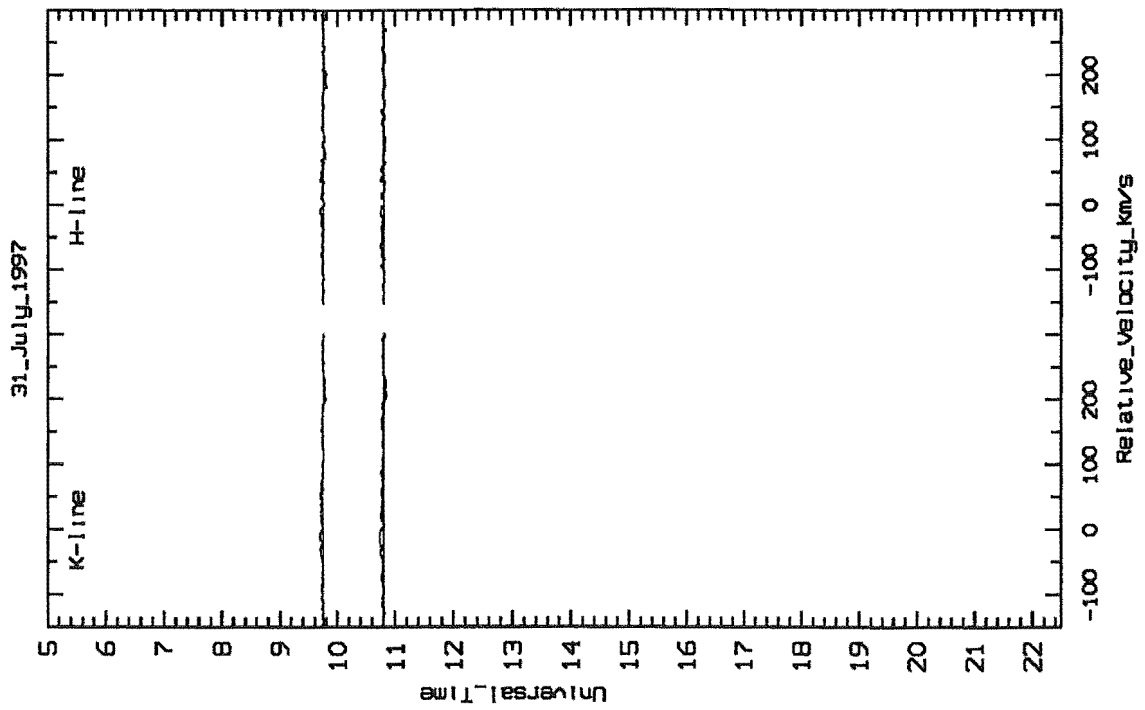

Figure 8.109: Normalised 51 Oph spectra taken on 31th July 1997.

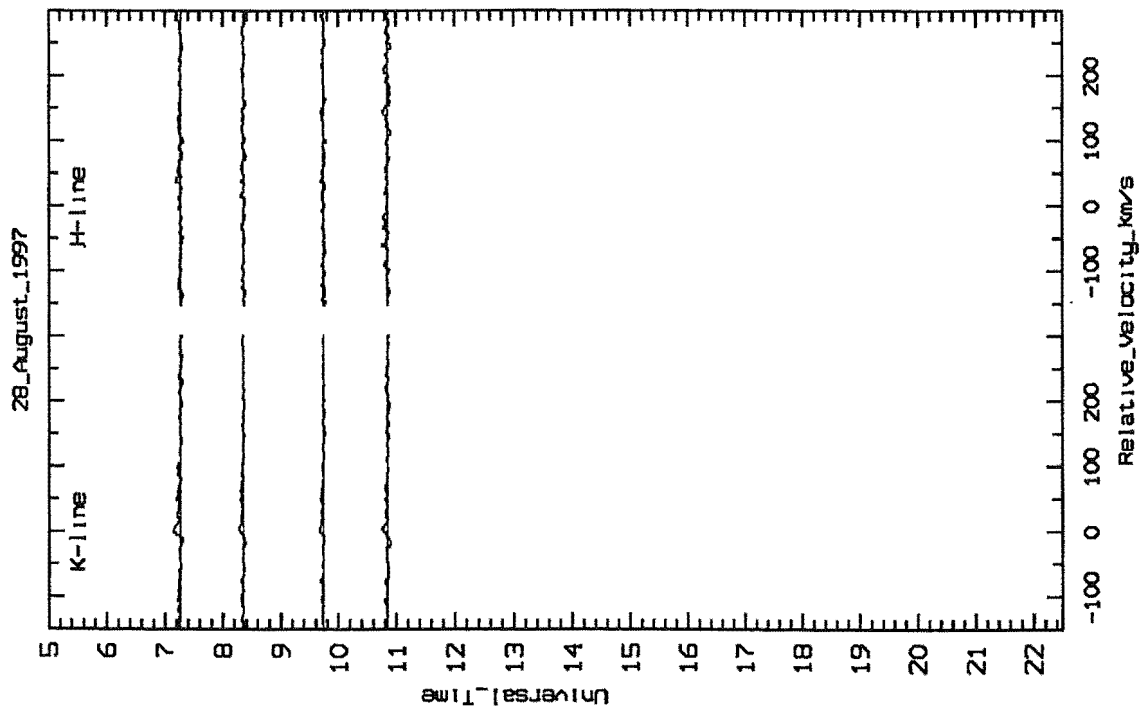

Figure 8.110: Normalised 51 Oph spectra taken on 28th August 1997.

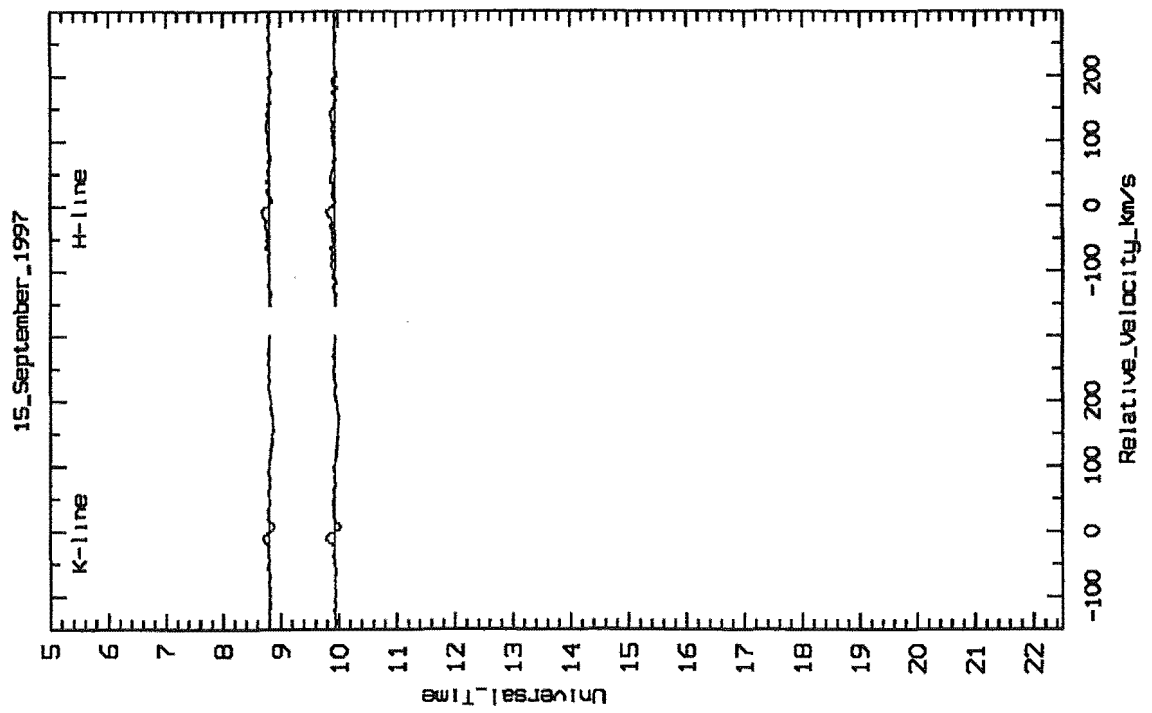

Figure 8.111: Normalised 51 Oph spectra taken on 15th September 1997.

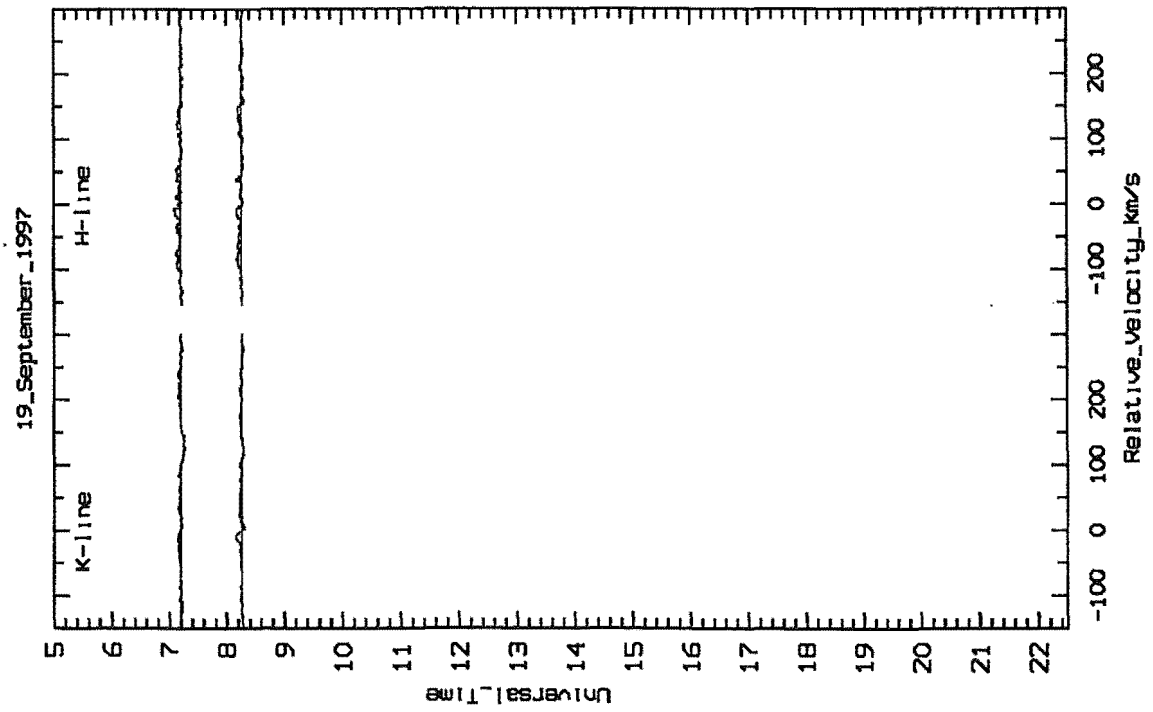

Figure 8.112: Normalised 51 Oph spectra taken on 19th September 1997.

Chapter 9

Analysis

Presented here are the results of the observations made during 1997 at MJUO taken of β Pictoris and 51 Ophiuchi. Only the simultaneous H and K observations are presented.

The data on the variable absorption features seen can be found in Appendix D, in Tables 1 and 2 for 51 Oph and β Pic respectively.

9.1 51 Ophiuchi

In all 94 spectra were taken over 24 nights of the star 51 Ophiuchi. Of these spectra only 7 possible absorptions were observed, all in the K line. The sizes of these variable absorptions were small which raises some doubts about their reality, but the fact that they are seen in at least two successive spectra gives support to their reality.

Since no absorptions are present in these spectra, the divided spectra would be expected to be a straight line. As Figs. 8.89 to 8.112 show the straightness of the plots gives confidence that the Canopus profile correction is useful and does work.

Note that the unusual profiles of 51 Oph in some spectra, such as that on 28th May 1997, are the result of condensation on the CCD cryostat window, and are not variable absorptions of any kind.

9.2 β Pictoris

In all 219 spectra were obtained over 32 nights of β Pic. Within these spectra 1108 variable absorptions were identified and Gaussian fitted.

The data is presented in Fig. 9.1 showing the velocity, FWHM, depth and equivalent width of all the identified variable absorptions. The data in this plot should be considered conjointly with the spectra presented in Figs. 8.1 to 8.64.

The 1108 absorptions can be summarised as follows:

- 599 K line absorptions
- 509 H line absorptions
- 306 absorptions classified as being "good singles"
- 85 absorptions classified as being "poor singles"
- 194 absorptions classified as being "good blends"

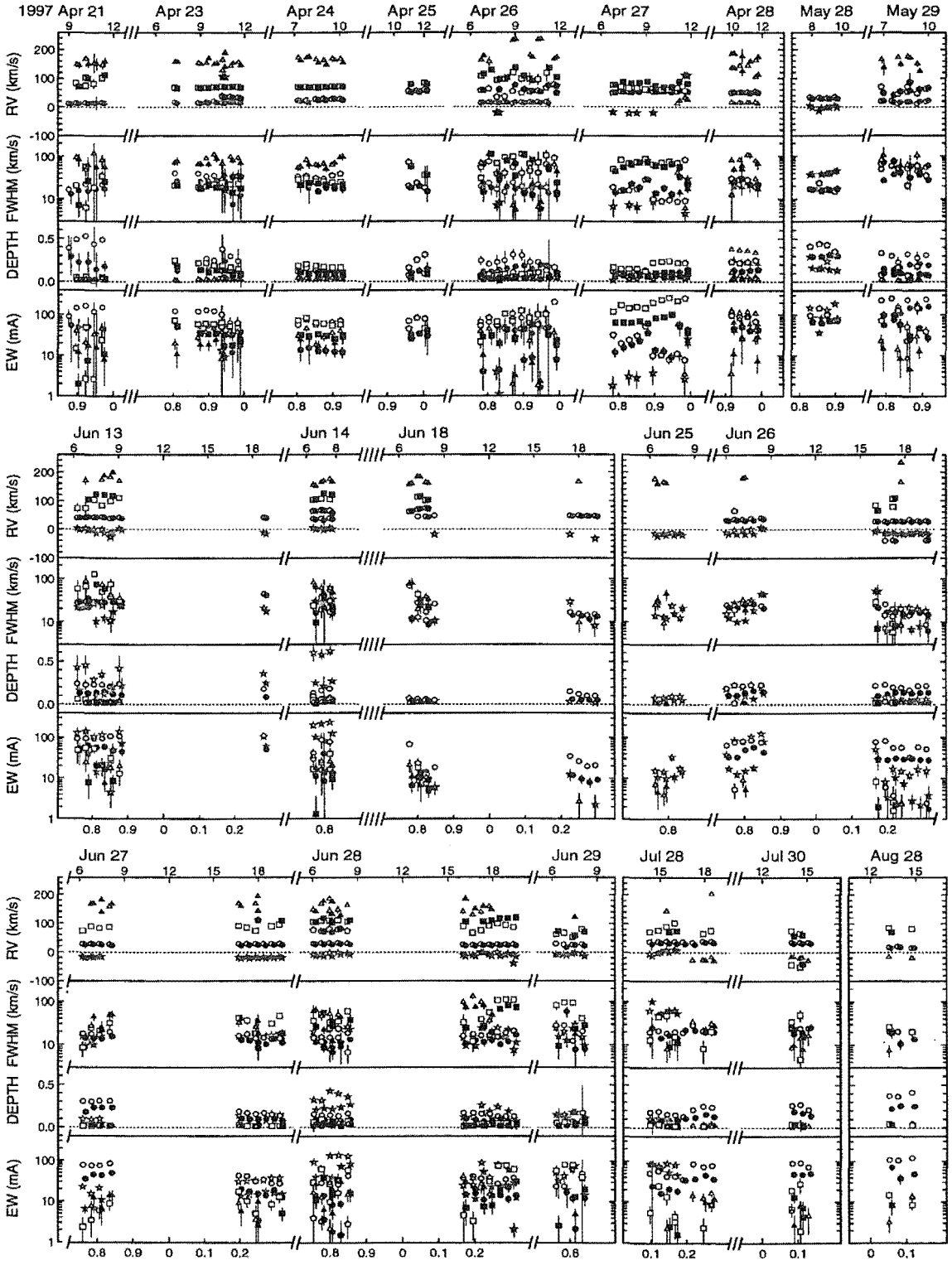

Figure 9.1: Graphical summary of the Ca II variable absorptions observed in β Pic during 1997. Full symbols refer to the H line, open ones refer to the K line. For legibility, the H symbols are displaced by 10 minutes with respect to the K symbols. Each individual absorption has been represented by the same symbol within each night and/or observing run as it evolves. The colours refer to the classifications used: black for good absorptions, magenta for poor absorptions, blue for uncertain decompositions, and green for circumstellar affected absorptions. Formal error bars from the Gaussian fits are plotted, but do not always exceed the symbol size.

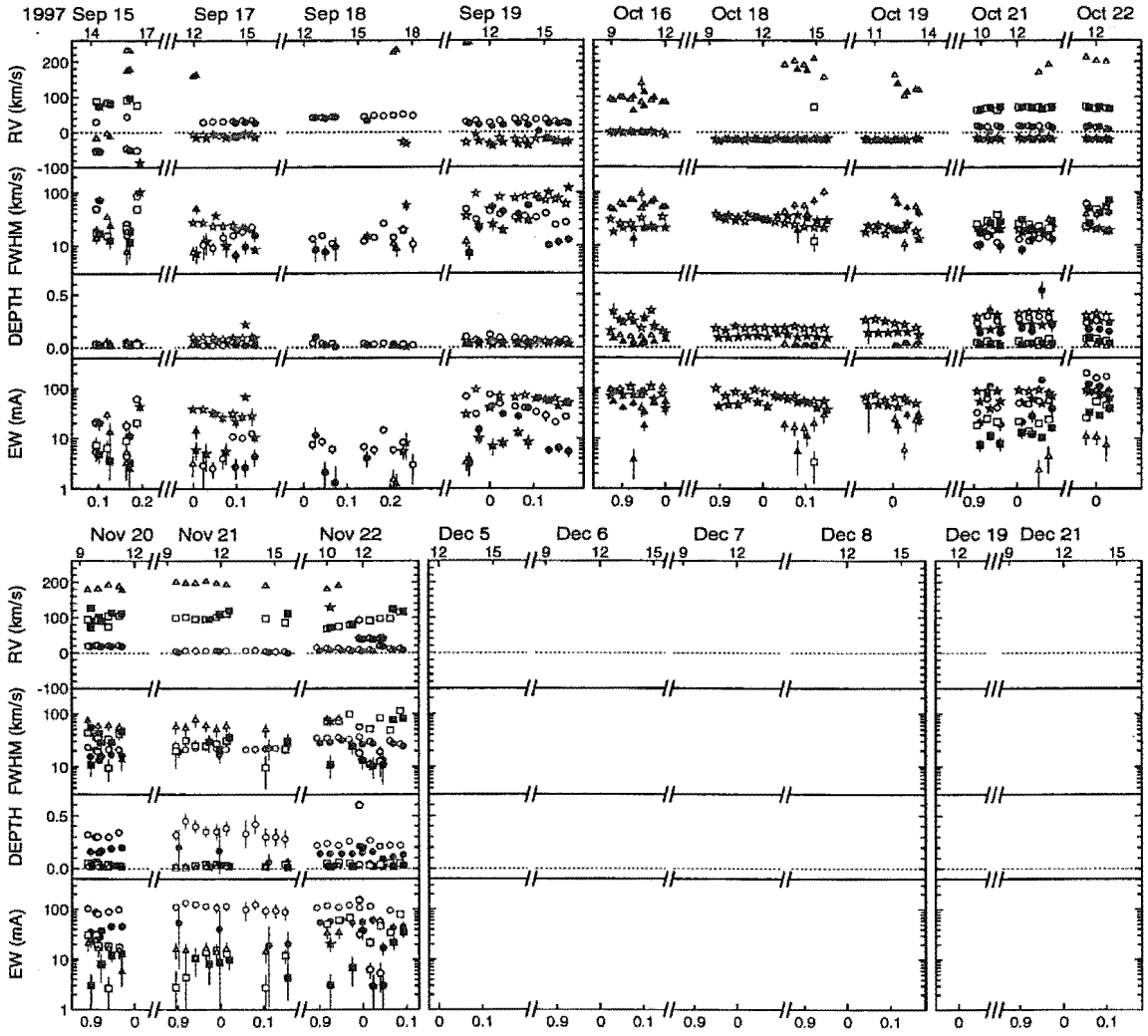

Figure 9.1: (continued). Note: Observations have been obtained in December and will form part of Stuart Barnes's MSc thesis.

- 80 absorptions classified as being "poor blends"
- 264 absorptions classified as being affected by the circumstellar feature
- 179 absorptions classified as being "uncertain decompositions"
- 241 blue-shifted events
- 329 0-40 $\mathrm{km\,s^{-1}}$ red-shifted events
- 298 40-100 $\mathrm{km\,s^{-1}}$ red-shifted events
- 240 $\geq$100 $\mathrm{km\,s^{-1}}$ red-shifted events.

9.2.1 Velocity Features

As shown previously, the variable absorptions can be summarised into the following velocity regimes:

- 241 blue-shifted events
- 329 0-40 km s^{-1} red-shifted events
- 298 40-100 km s^{-1} red-shifted events
- 240 $\geq$100 km s^{-1} red-shifted events.

Due to the increased instrumental stability, a large number of features were able to be detected at low velocities appearing as a broadening of the circumstellar feature. A number of these were strong red-shifted features such as can be seen on August 28th and November 20th (Figs. 8.20 and 8.30 respectively), and a large number were very clear strong blue-shifted features such as those seen on the days of June 13th, 14th and 28th, (Figs. 8.10, 8.11, 8.16 respectively). In addition to these a number of other blue-shifted features are clearly visible between October 18th-22nd (Figs. 8.26-8.29 respectively).

Of the absorptions for which a simultaneous measurement was made of the H and K lines, a MIDAS procedure (as outlined in Section 7.3) attempted to fit the velocity of the H and K line features independently. Fig. 9.2 shows the velocities for those absorption that were fitted with a good single or good blend classification, showing the velocities did match in the H and K lines. Velocity comparisons can also be seen in Fig. 9.1 by

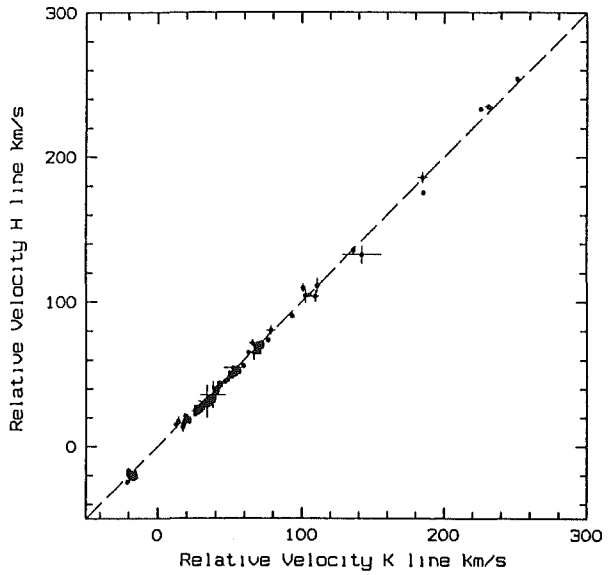

Figure 9.2: Comparison of the velocities of absorptions seen in both the H and K lines (gS and gB classifications only).

comparing filled and open symbols. Of particular interest within this figure are a number of dates where the H and K line (filled and unfilled symbols respectively) velocities do differ. The latter part of June 28th shows an interesting scenario where the velocity of the H line feature at $\sim$100 kms^{-1} is relatively stable, whereas the velocity of the simultaneous K line feature is less than that of the H line and evolving rapidly and apparently smoothly. Examination of the normalised profiles (Fig. 8.48) suggests the effect may be real, despite the slightly-poor H normalisation.A similar, although not as marked effect,

also occurs on June 13th, and at the same velocity. The fact that these velocity anomalies have clearly disappeared on June 18th indicate it is not the same absorption, but rather two separate and apparently isolated absorptions both showing the same inconsistencies. No convincing scenario appears in the opposite sense where the K line is relatively stable and the H line evolves at a lower velocity.

In nearly all of the observations made, variable absorptions were present in several velocity regimes simultaneously. This is the result of the scenario as shown in Fig. 4.3 as proposed by Lagrange-Henri *et al.* (1996)[1]. Under this scenario a further comet, not necessarily with the same perihelion, also enters our line of sight before the remnant tail of the previous comet has been dispersed. This explains the multiple structure that can be seen in most of the observations and supports the conclusions of Lagrange-Henri *et al.* as to the clumpy nature of the infalling gas.

This scenario of a stream of infalling comet-like bodies is also confirmed by the extended lifetime of the observed variable absorptions. As shown in Section 4.2, it is expected that the crossing time of a LVF should be of the order of 4 hours, whereas some of the observations made show features lasting over a period of many days. One explanation is that a succession of infalling bodies arrive before the ionic tail of the previous one has left the line of sight. The most striking of these features are the two LVFs, (one red-shifted and the other blue-shifted) observed over the period of June 25th to June 29th. It is interesting here to note the red-shifted feature appeared a day later than the blue-shifted feature, which supports the proposition that they are in fact two separate features and not one larger, broader feature spanning the circumstellar feature. A similar red-shifted feature is seen in the following observation made on July 28th. Whether this is in fact the same feature seen during June, or a new one, is impossible to tell due to the lack of coverage between those dates. Another feature lasting far longer than the crossing time of 4 hours is that between April 21st - 28th. The LVF here close to the circumstellar feature is seen to last over a period of of a week, though varying in strength. The apparent disappearance and reappearance of this feature on the 25th and 27th may in fact not be real but just a weakening. As can be seen in the normalised spectra of these dates (Figs. 8.36 and 8.38 respectively) an absorption close to the circumstellar feature can be seen, especially on June 27th, though difficulties with Gaussian fitting close to the circumstellar feature meant these features could not be Gaussian fitted.

Generally features above $\sim$60 kms^{-1} were not convincingly observed to last longer than the 4 hour crossing time. This is expected since the faster comets leave the line of sight quicker, and hence the probability of subsequent comets arriving with the same orientation and perihelion (and therefore velocity) during that time is smaller. One notable exception to this is a very high velocity ($\sim$200 kms^{-1}) K line feature apparently lasting 3 days from November 20th - 22nd. Due to an incomplete temporal coverage, this can not be definitively declared as the same absorption, though it does appear to be so. As can be seen in the corresponding normalised spectra (Figs. 8.62-8.64, and Fig. 9.1, the features are very shallow and broad making Gaussian fitting more difficult and not so reliable. (It is not surprising here that no simultaneous H line absorption was observed since it is expected to be only half as deep, and therefore too small to confidently model, if the line is optically thin). However the fact that so many were observed and at similar

velocities does go some-way in supporting the reality of these features. Assuming then these features to be real, would require the existence of a stream of ~140 comets all at the same perihelion arriving within half an hour of the previous one (based on previous observations of very high velocity absorptions only lasting the time of one exposure, or half an hour).

Two features were observed that appeared to cross the circumstellar feature, and therefore shift from being blue-shifted and moving towards us, to being red-shifted and moving away from us (June 26th and July 28th). Because of the difficulty of removing the circumstellar absorption, it is difficult to judge whether these features are real or merely inaccuracies due to the difficulties of Gaussian fitting close to the circumstellar feature.

Due to the increased instrumental stability and therefore greater sensitivity in observing broad, shallow HVFs, a number of variable feature were able to be observed at very high velocities. Two striking examples of this are of April 26th, were variable features in both the H and K lines were observed. Fig. 8.37 shows these absorptions as narrow and shallow features, lasting the duration of only one exposure (30 minutes). The reality of these features is supported by simultaneity in both the H and K lines, and any arguments of dust on the cryostat window being the cause of the variation are therefore extremely remote.

This therefore adds weight to the existence of shallow, narrow and short-lived features present at very high velocities.

9.2.2 FWHM of variable features

Fig. 9.3(a) shows the FWHM of all observed variable features as a function of the velocity. One may be surprised to see features in this figure that are narrower than the spectrograph resolution of ~10kms^{-1}, but two points should be noted. First, on nights of excellent seeing, the achieved resolution on stars may be better than that evaluated from the thorium lines, because the stellar image may be narrower than the slit. Second, when error bars are considered on Figs. 9.3(c) and (d), only very few features are clearly narrower than 10kms^{-1}. As Fig. 9.3 shows the correlation between the FWHM and velocity is very weak, even when only the best of the characterised absorptions are considered. Even though this correlation is weak, some velocity-related conclusions can still be noted from the plots:

- Absorptions of various widths can be found at any velocity.
- LVFs are more likely to be narrow absorptions.
- HVFs are more likely to be broad absorptions.

These relations can also be seen in Fig. 9.1, which again shows that the higher velocity features (represented by triangles) are generally the features with the broader FWHM.

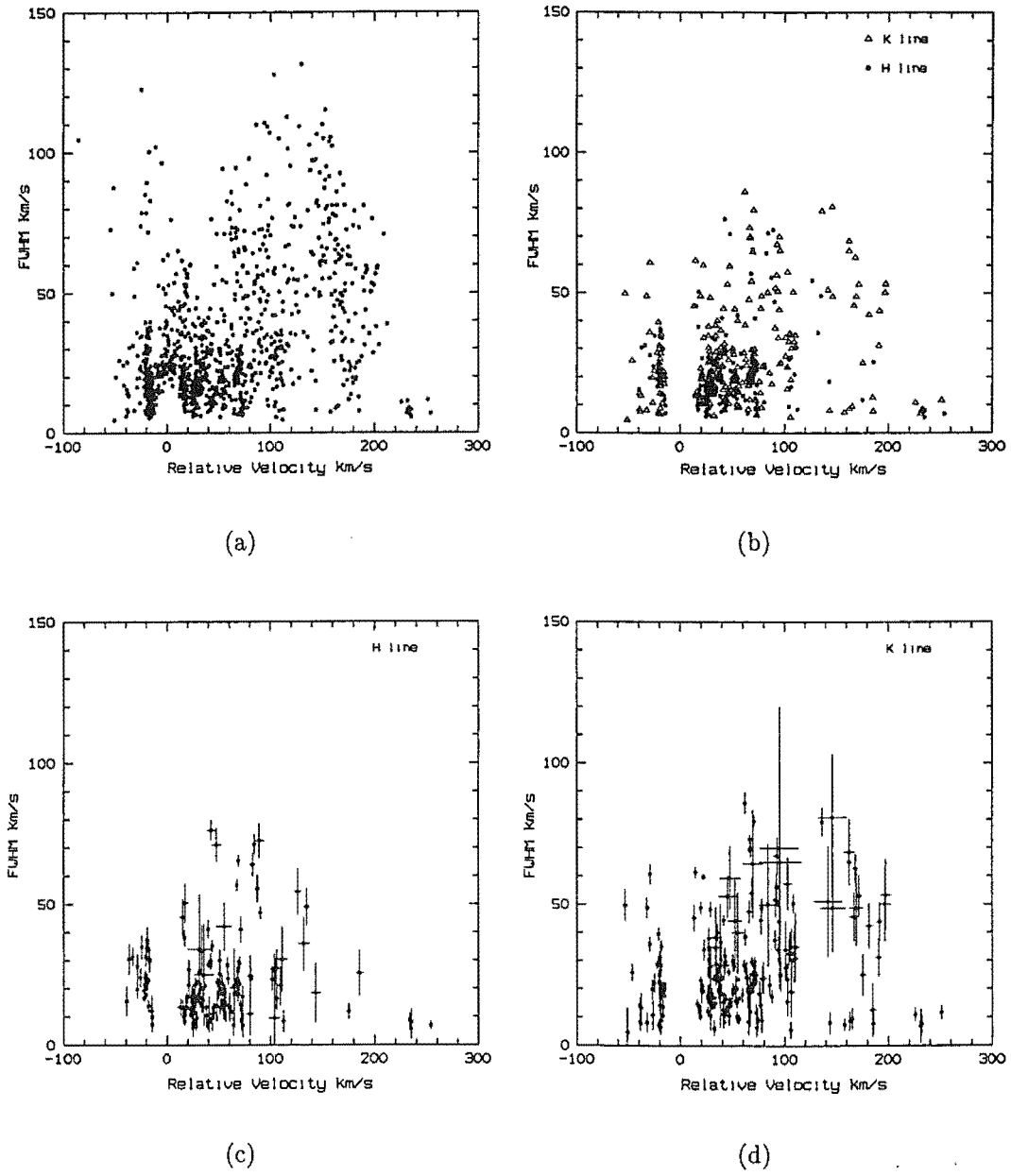

Figure 9.3: Plots of the FWHM against the relative velocity for (a), all observed features, (b) only those features classified as good singles or good blends, (c) and (d) the H and K lines respectively limited to only the good classifications also showing the associated errors of each point.

One interesting feature from Fig.9.3 is that no broad features were observed with a velocity over $\sim$200kms^{-1}. However this is perhaps due to the problems associated with identifying very shallow and broad features, since these are easily lost within the noise levels of the pseudo-continuum.

Fig. 9.1 shows the evolution of the FWHM for each of the variable absorptions observed. The HVFs showed very little indication that any sort of temporal evolution takes place with the FWHM. This is most likely due to the larger errors associated with the

shallower features observed at high velocities. The LVFs showed signs that some form of temporal evolution may be taking place. The most obvious example of this was on April 27th, where over the course of the $4\frac{1}{2}$ hours of observations, the H and K lines showed evolution similar to that expected for the equivalent width as a function of time. The equivalent width (a function of the FWHM) for the same features, also show a similar evolution, which is expected for a body crossing the stellar disk, such as in Fig. 4.8.

These type of variations in the FWHM are also seen in Fig. 9.1 on a number of other days for the LVFs such as on June 26th-28th, July 28th and October 18th.

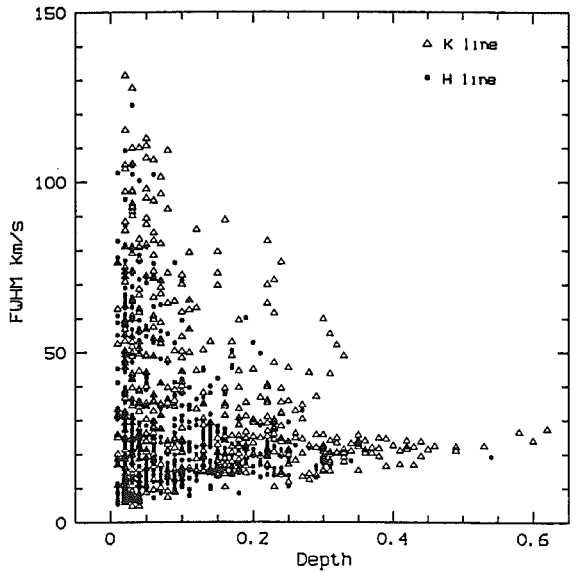

Figure 9.4: Plot of the FWHM against the depth for the observed absorptions.

Fig. 9.4 shows the relationship between the FWHM and the depth of the features. Three things can immediately be seen:

- The deepest features are always narrow features.
- The shallow features may be of any FWHM .
- The broad features are limited to only the shallow absorptions.

Another interesting feature of this plot is the gradient that can be seen as the limit to the FWHM as the depth increases. Shallower features can have a narrower FWHM than the deeper features. As the depth of the absorption increases so to does the minimum value of the FWHM the feature can have.

Fig. 9.5 shows the correlation found between the FWHM of the H and K line absorptions (limited only to those classified as good singles or blends). A strong correlation can be seen between the two, although it does appear that the FHWM of the K line is typically broader than that of the H line.

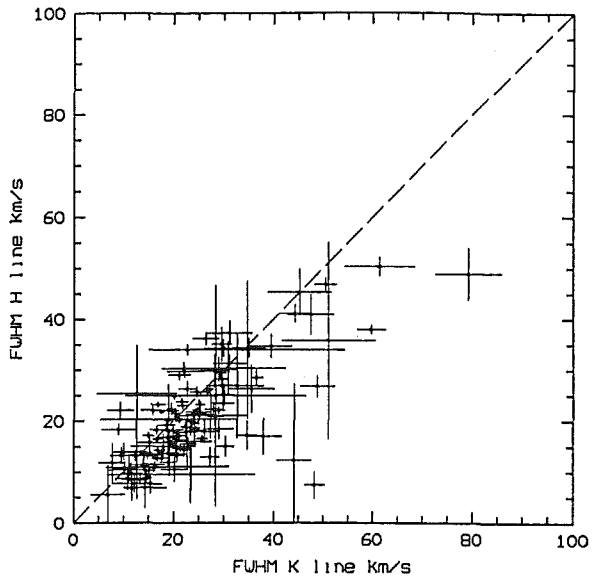

Figure 9.5: Comparison of the FWHMs in both the H and K lines (gS and gB classifications only).

9.2.3 Depth of variable features

Fig. 9.6 shows the depths of the observed absorptions as a function of their relative velocity. The cut-off as observed by Petterson [2] at $\sim 60\,\mathrm{kms}^{-1}$, thought to imply a limit in the parabolic inclination of the FEBs, while observed, was not as prominent in these observations. However the cut-off for blue-shifted features at $\sim -30\,\mathrm{kms}^{-1}$, is observed and appears to be very prominent, lending support to a definite limit in the parabolic inclinations of blue-shifted FEBs.

Figs. 9.1 and 9.6, well show the difference in the depths of the H and K lines, and hence to the following conclusions:

- The deep features are only found at low relative velocities.
- Shallow features can be found at any velocity.
- LVFs may have deep or shallow depths.
- HVFs are limited to shallow depths.

Plotting the depth of the H line against that of the simultaneous K line depth can provide information on the size of the cloud of ions occulting the stellar disk (Section 4.4). For this plot only the best absorptions were used (those classified as either good singles or good blends) to obtain greater accuracy in the calculation of the filling factors. Fig. 9.7 shows the depth of the H line against that of the K line. The lines corresponding to optically thin and thick lines refer to $p_{\mathrm{K}} \simeq 2p_{\mathrm{H}}$ and $p_{\mathrm{K}} \simeq p_{\mathrm{H}}$ respectively, where p_{H} refers to the depth of the H line and p_{K} to the depth of the K line.

Only one case is observed where the depth of the H line is greater than that of the K line (within the error bars). This point corresponds to an absorption on April 27th which can

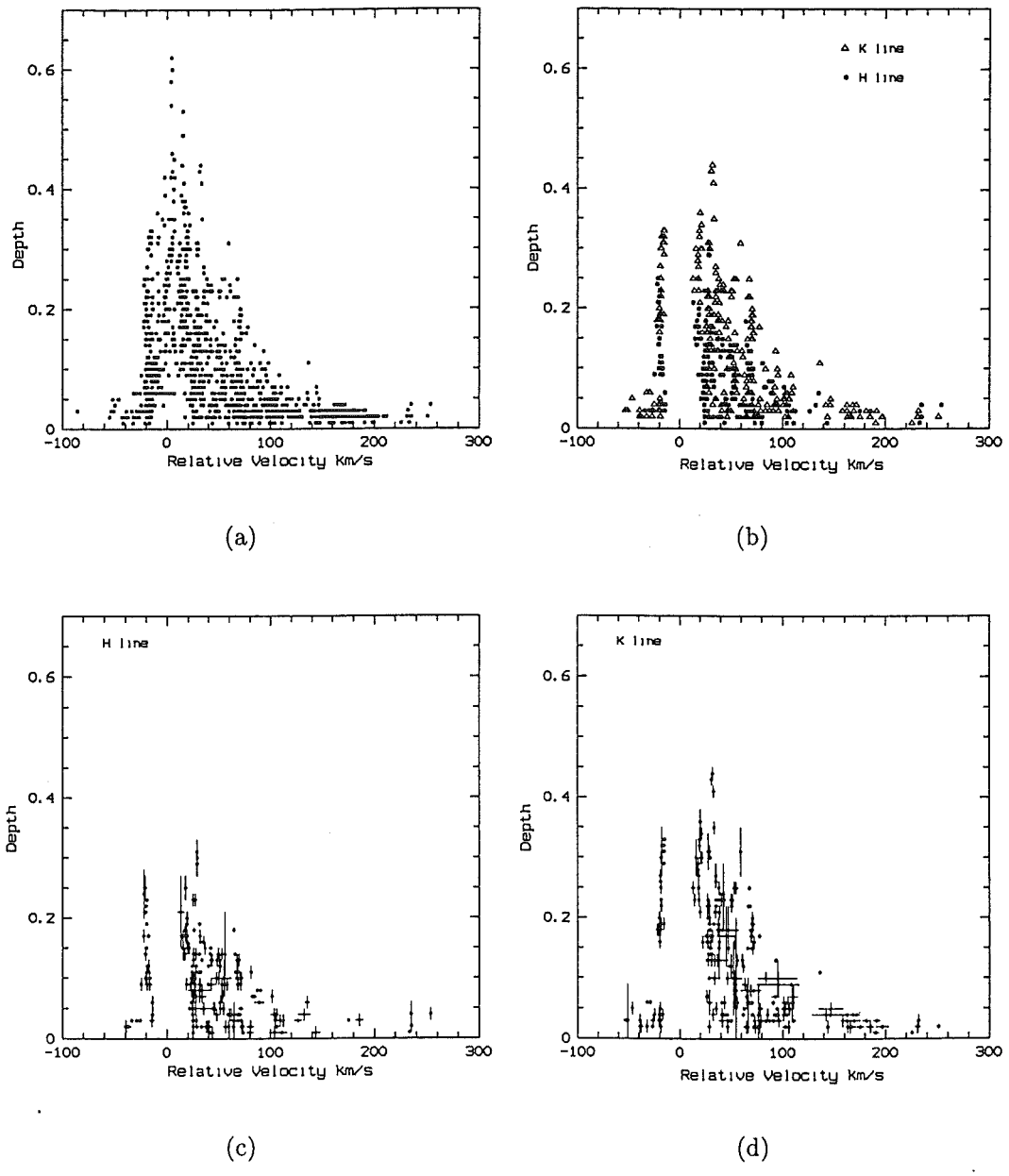

Figure 9.6: Plots of the depth against the relative velocity for (a), all observed features, (b) only those features classified as good singles or good blends, (c) and (d) the H and K lines respectively limited to only the good classifications also showing the associated errors of each point.

be seen as the last spectrum in Fig. 8.38. The Gaussians in the H line profile appear to be well fitted, but those in the K line are not so well fitted. The reality of this result is therefore questionable due to the Gaussian fitting of the K line being different to that of the H line. Therefore, even with simultaneous observations of the H and K lines, still no unequivocal cases of the H line being stronger than the K line have been observed.

As shown in Fig. 9.8, (a copy of Fig. 4.7), the difficulty arises now in determining which side of the stellar disk the cloud of ions is occulting and therefore which of the plots should

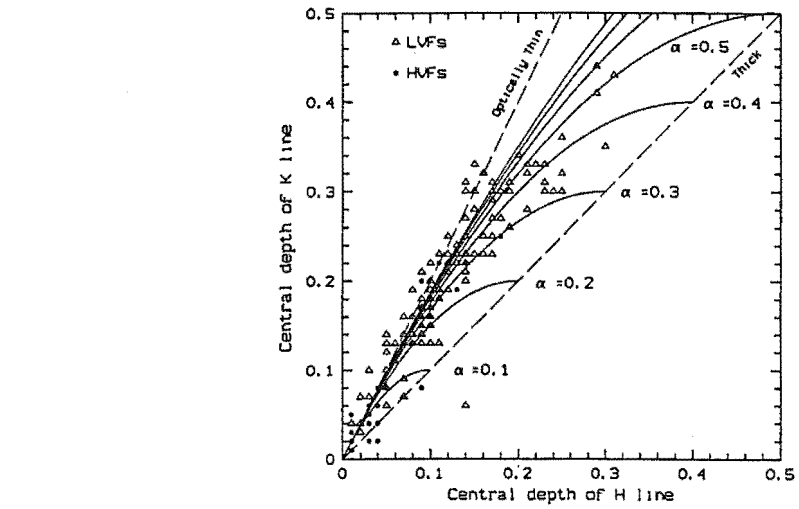

(a)

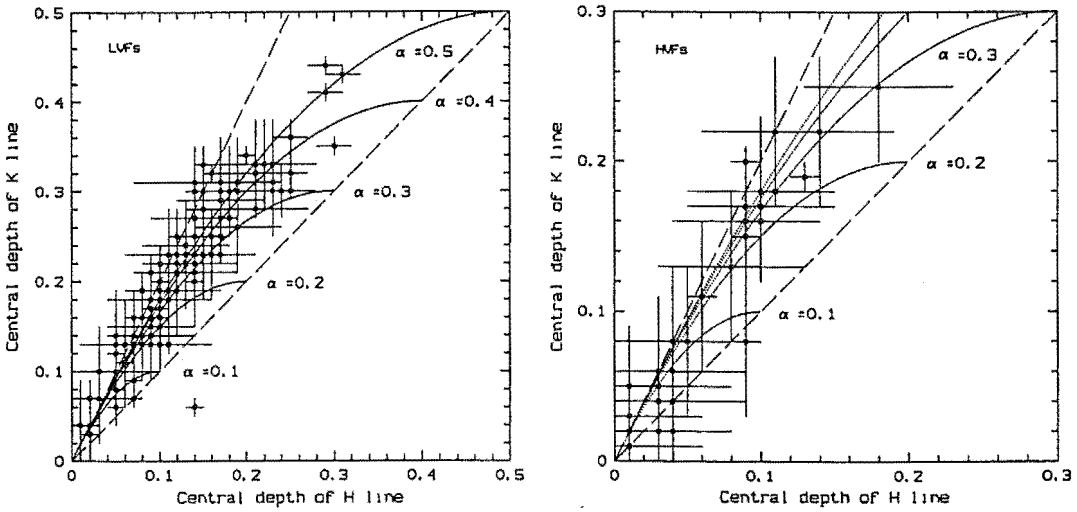

(b) (c)

Figure 9.7: Plot of the filling factors for simultaneous observations of the H and K lines (gS and gB classifications only). All plots show the iso-α lines overplotted referring to the proportion of the stellar disk being occulted by the ionic cloud. Plot (a) shows the LVFs and HVFs, with the limits of an optically thin and thick line. Plots (b) and (c) respectively show the LVFs and HVFs with error bars overplotted.

be used in determining the filling factor for a given feature. For instance, a point in the centre of the diagram could refer to a filling factor of either 0.4 or 0.8, depending whether it occults the part of the star moving towards or away from us respectively. Therefore, for simplicity sake, the situation of no stellar rotation, Fig. 4.6, has been assumed for the fitting of iso-α curves as shown in Fig. 9.7.

From this plot a number of features become apparent:

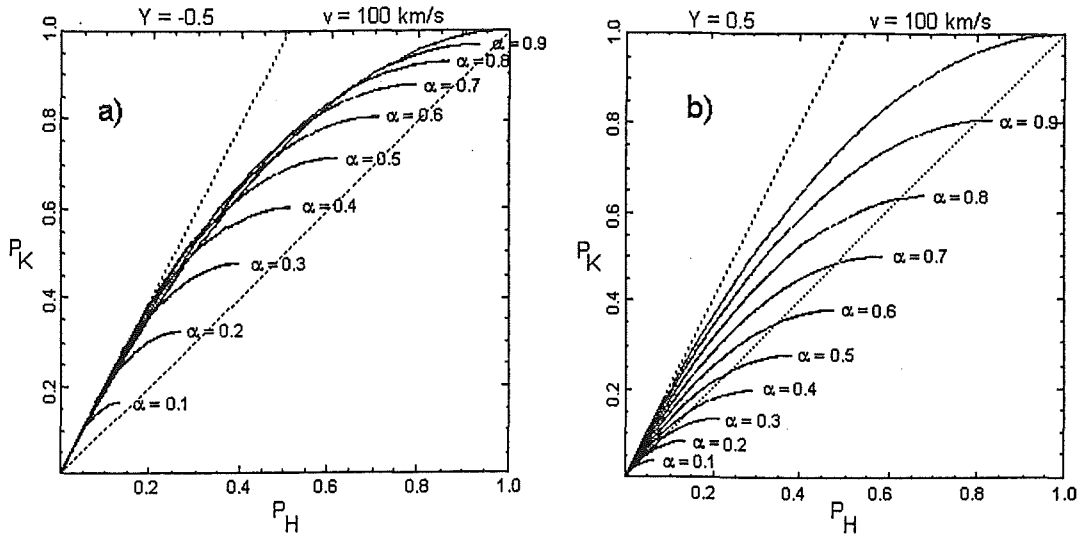

Figure 9.8: Copy of Fig. 4.7 showing the theoretical diagram of the depths of the H and K lines, for the different values of the filling factor α, when stellar rotation is considered. Plots (a) and (b) correspond respectively to Y=−0.5 (cloud masking portion of disk rotating away from us) and Y=0.5 (cloud masking portion of disk rotating toward us).

- Most of the absorptions lie near the optically thin limit, making it impossible to distinguish between weak lines arising from a cloud covering a large part of the stellar surface, from stronger lines arising from a cloud covering a small part of the star. Because the lines are not saturated it is only possible to get a lower limit on the size of the absorbing cloud.

- HVFs ($\geq$60 kms^{-1}) (shown in plots (a) and (c) of Fig. 9.7), are only found at shallow depths and therefore in the lower regions of the plot. These correspond to filling factors in a range from ~0-50%.

- LVFs ($<$60 kms^{-1}) (shown in plots (a) and (b) of Fig. 9.7), are present at a much larger range of values of α, since they have a larger range of depths than the HVFs. These are observed to cover up to ~80% of the stellar disk. Once again larger filling factors may be present, though the optically thin clouds do not allow any greater accuracy to be obtained.

Evolution of the depths of the H and K lines can be seen in Fig. 9.1. Definite evolution appears in most observations, for nearly all of the absorptions plotted. The most noticeable of these are the LVFs with the deeper absorptions, since any small fluctuations can be easily observed, unlike variations in the shallow absorptions. The H line generally tends to have a more stable depth than the K line (for example, April 25th - 26th, June 28th and October 19th). This is by no means unexpected since the strength of the lines will alter as the FEB passes across the stellar surface, in much the same way the equivalent width is expected to (see subsection 9.2.4).

9.2.4 Equivalent widths of variable features

Fig. 9.9 (copy of Fig. 4.8), shows the expected evolution of the H and K lines as an FEB crossing the stellar disk. Within Fig. 9.1 it is difficult to see such trends given the large

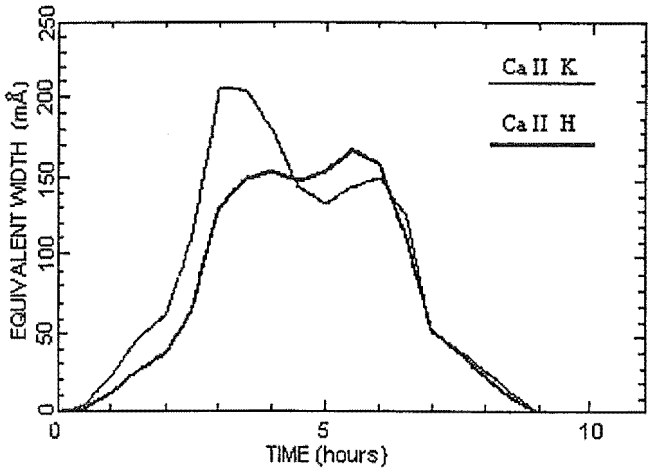

Figure 9.9: Copy of Fig. 4.8 showing the expected evolution of the H and K lines for a FEB crossing the stellar disk.

number of absorptions shown on the same plot. Despite this, trends such as those in Fig. 9.9 are still apparent in many observations. The difficulty here is that no one feature was convincingly observed from start to finish, that could possibly produce a plot such as in Fig. 9.9. A large number of long lived LVFs were observed that showed variations in the equivalent widths (such as the blue-shifted features on October 18th - 19th) but since the cloud did not disperse, the equivalent widths were never seen to drop away to zero. It would be expected though, that in the case of a long-lived feature being replenished by a stream of infalling comets, that variations representative of the top region of Fig. 9.9 should be observed without ever dropping off to zero. This is seen in many of the observations made (for example, November 20th - 22nd), with the resulting fluctuations likely to be the result of successive bodies, and the associated cloud of ions, entering our line of sight, before the previous cloud has left the line of sight or been dispersed by the radiation pressure.

9.3 Summary

This thesis contains the results of observations made with the MJUO échelle spectrograph over a period of 8 months, of the stars β Pictoris and 51 Ophiuchi. Possible broad, shallow absorptions lasting for over 2 hours appear to have been detected in 51 Oph, though no conclusive results were able to be obtained. However, β Pic continued to show large amounts of activity.

The results here confirm the findings of previous workers, but a great deal more fea-

tures, particularly broad shallow features, have been found, which is likely to be due to the addition instrumental stability achieved. These new discoveries include:

- A large number of very high velocity features, up to $254\,\mathrm{kms}^{-1}$, previously not observed. The reality of these features is largely confirmed by the simultaneous observation of the same feature in both the H and K lines.
- The existence of shallow narrow features at high velocities lasting only the duration of individual exposures.
- A large number of blue-shifted features lasting over very long timescales.
- A large number of features with a very low relative radial velocity. These absorptions are always blended with the circumstellar feature making them difficult to accurately parameterise. However in nearly all 219 spectra, a very low velocity feature was observed in conjunction with the circumstellar feature, and typically lasted days or apparently weeks on end.

The predictions of the FEB scenario seem to have well explained the variable absorptions observed in the Ca II H and K lines, with the main results of this work being:

- The observation of a large number of absorptions at a range of velocities, lending support to a stream of bodies passing the line of sight at differing perihelions and radial velocities, and the clumpy nature of the gas.
- The large number of long-lived features seen, more-so though not exclusively at low velocities, also supports the idea of a stream of infalling comets, at similar radial velocities, that produces a near continuous cloud in our line of sight, or possibly even a torus that extends the entire circumference of the star.
- The temporal evolution of both the FWHM and depth of the features that follow that expected of the equivalent width of a body passing the line of sight.
- The expected evolution of the equivalent width of the H and K lines as they cross the stellar disk was not observed in its entirety for a feature from start to finish. There is however considerable fluctuation with these lines, even in the case of long-lived features, which may be evidence of the variations predicted by Beust and Lissauer [38].
- The velocities and FWHMs of features observed are often the same in both the H and K lines.
- No confirmation was able to have been made of the proposition that the strength of the H line can exceed that of the K line, despite the newly-achieved simultaneity of the observations.

Chapter 10

Future Work

Future work on the study of β Pictoris, and other such possible protoplanetary systems, is required to continue to refine our understanding of the processes involved in the formation of planets, and to lend clues as to how our own solar system may have been formed.

Future work at MJUO should therefore include the following:

- Continual monitoring of Ca II H and K line profiles, to further refine the Falling Evaporating Bodies scenario as the cause of the variable features observed in the spectra of these and other metallic lines of β Pic.
- Improvements to the Gaussian fitting procedure of the observed absorptions. It was found that the velocities of variable features are often the same in both the H and K lines. It should therefore be considered forcing them to have the same value when trying to identify and fit Gaussians to the variable features; however, care would need to be taken not to overlook features with different velocities, such as possibly occurred on June 13th and 28th. A strong correlation also appears between the FWHM of features in the H and K lines so whether these are also forced to the same value (since the FWHM should be the same for each if it is indeed due to velocity dispersion, and hence identical for the H and K lines) should also be further considered.
- Improvements to the Gaussian fitting will allow greater accuracy in the determination of the equivalent widths of the absorptions, allowing the evolution of the H and K lines to be better followed as a FEB crosses the stellar disk.
- With improvements to the equivalent widths, stellar rotation will be able to be taken into account when the filling factors are determined. By observing differences in the equivalent widths of the H and K lines it can be determined whether the cloud is occulting the portion of the star rotating towards or away from us, and hence filling factors can be obtained for each situation.

Detailed modelling of the equivalent widths and filling factors, which is outside the scope of this thesis, would also lead to further refinements of the FEB scenario.

Chapter 11

Acknowledgements

I would like to acknowledge the assistance of the Marsden Fund of New Zealand, in providing funding for this project.

I would like to thank my supervisor William Tobin for his personal interest in this project and his continual advice, direction and support, in keeping me on task and within the various deadlines.
Thanks also to John Pritchard for bailing me out of seemingly endless computer difficulties.

I would also like to thank The Mt John University Observatory staff: Stephen Barlow and John Baker for ensuring the equipment was always set up and running satisfactorily, and Alan Gilmore and Pam Kilmartin for the meals they providing and the part they played in keeping me sane over those long winter runs.

Thanks also to the various technical staff at the University of Canterbury, who made the necessary alterations to the échelle spectrograph with the installation of the focal reducer and Series 200 CCD system.

I would also like to thank the other members of the Astronomy group: Michael, Karen, Lyndon, Orlon, Sarah, Jovan, Ljiljana and Dan for their company, and various pieces of advice and help received. Thanks also to Peter Cottrell and John Hearnshaw for their input over the past two years.

Whereas other animals hang their heads and look at the ground, he made man stand erect, bidding him look up to heaven, and lift his head to the stars.
OVID (43BC - AD17?) Roman poet.

References

[1] A.M. Lagrange-Henri, F. Plazy, H. Beust, D. Mouillet, M. Deleuil, R. Ferlet, J. Spyromilio, A. Vidal-Madjar, W. Tobin, J.B. Hearnshaw, M. Clark, and K.W. Thomas. The β Pictoris circumstellar disk - XXI Results from the December 1992 spectroscopic campaign. *A&A*, 310:547–563, 1996.

[2] O.K.L. Petterson. Ca II absorption in the circumstellar disk of β Pictoris and other A-type stars. Master's thesis, University of Canterbury, New Zealand, 1996.

[3] H.H. Aumann, F.C. Gillett, C.A. Beichman, T. DeJong, J.R. Houck, F.J. Low, G. Neugebauer, R.G. Walker, and P.R. Wesselius. Discovery of a shell around Alpha Lyrae. *Ap.J.Lett.*, 278:L23–L27, 1984.

[4] B.A. Smith and R.J. Terrile. A circumstellar disk around β Pictoris. *Science*, 226:1421–1424, 1984.

[5] F. Crifco, A. Vidal-Madjar, R. Lallement, R. Ferlet, and M. Gerbaldi. β Pictoris revisited by Hipparcos. Star properties. *A&A*, 320:L29–L32, 1997.

[6] M. Gerbaldi, J. Zorec, F. Castelli, and R. Faraggiana. Peculiar versus normal phenomena in A-type and related stars. In M.M. Dworetsky, F. Castelli, and R. Faraggiana, editors, *ASP Conference Series*, volume 44, page 413, 1993.

[7] F. Palla and S.W. Stahler. The pre-main sequence evolution of intermediate-mass stars. *Ap.J.*, 418:414–425, 1993.

[8] G. Schaller, D. Schaerer, G. Meynet, and A. Maeder. New grids of stellar models from 0.8 to 120 $M_\odot$ at Z=0.020 and Z=0.001. *A&A.S*, 96:269–331, 1992.

[9] C. Telesco and R. Knacke. Detection of silicates in the β Pictoris disk. *Ap.J.*, 372:L29–L31, 1991.

[10] D. Backman, F. Gillett, and F. Witteborn. Infrared observations and thermal models of the β Pictoris disk. *Ap.J.*, 385:670–679, 1992.

[11] P. Artymowicz. Radiation pressure forces on the β Pictoris system. *Ap.J.Lett.*, 335:L79–82, 1988.

[12] D.K. Aitken, T.J.T. Moore, P.F. Roche, C.H. Smith, and C.M. Wright. Mid-infrared spectroscopy of β Pictoris: constraints on the dust grain size. *M.N.R.A.S*, 265:L41–L43, 1993.

[13] A.M. Lagrange-Henri, A. Vidal-Madjar, and R. Ferlet. The β Pictoris circumstellar disk. *A&A*, 190:275–282, 1988.

[14] H. Beust, A. Vidal-Madjar, and R. Ferlet. The β Pictoris protoplanetary system - XII Planetary perturbations in the disk and star-grazing bodies. *A&A*, 247:505–515, 1991.

[15] A. Vidal-Madjar, A.M. Lagrange-Henri, P. Feldman, H. Beust, J. Lissauer, M. Deleuil, R. Ferlet, C. Gry, L. Hobbs, M. McGrath, J. McPhate, and H. Moos. HST-GHRS observations of β Pictoris: Additional evidence of infalling comets. *A&A*, 290:245–258, 1994.

[16] A. Boggess, F.C. Bruhweiler, C.A. Grady, D.C. Ebbets, Y. Kondo, L.M. Trafton, J.C. Brandt, and S.R. Heap. First Results From The Goddard High Resolution Spectrograph: Resolved Velocity And Density Structure In The Beta Pictoris Circumstellar Gas. *Ap.J.Lett.*, 377:L49–52, 1991.

[17] A. Vidal-Madjar, L.M. Hobbs, R. Ferlet, C. Gry, and C.E. Albert. The circumstellar gas cloud around β Pictoris. *A&A*, 167:325–332, 1986.

[18] A.M. Lagrange, H. Beust, D. Mouillet, M. Deleuil, P.D. Feldman, R. Ferlet, L. Hobbs, A. Lecavelier des Etangs, J.J. Lissauer, M.A. McGrath, J. Spyromilio, and A. Tobin, W. Vidal-Madjar. The β Pictoris circumstellar disk - XXIV Clues to the origin of the stable gas. *A&A*, 330:1091–1108, 1998.

[19] L.M. Hobbs, A. Vidal-Madjar, R. Ferlet, C.E. Albert, and C. Gry. The gaseous component of the disk around β Pictoris. *Ap.J.*, 293:L29–L33, 1985.

[20] Y. Kondo and F. Bruhweiler. *IUE* observations of β Pictoris: An *IRAS* candidate for a protoplanetary system. *Ap.J.*, 291:L1–L5, 1985.

[21] C. Burrows. Disk around star may be warped by unseen planet. Press release no: STScI-PR96-02, 1996.

[22] P. Kalas and D. Jewitt. Asymmetries in the β Pictoris dust disk. *Ap.J.*, 110:794–804, 1995.

[23] R. Villard and A. Schultz. Astronomers have found a new twist in a suspected protoplanetary disk. Press release no: STScI-PR98-03, 1998.

[24] H.F. Levison, M.J. Duncan, and G.W. Wetherill. Secular resonances and cometary orbits in the β Pictoris system. *Nature*, 372:441–444, 1994.

[25] A. Lecavelier des Etangs, M. Deleuil, R. Vidal-Madjar, A. Ferlet, C. Nitschelm, B. Nicolet, and A.M. Lagrange-Henri. β Pictoris: Evidence of light variations. *A&A*, 299:557–562, 1995.

[26] J. Coté and L.B.F.M. Waters. IRAS Observations of Be stars. *A&A*, 176:93–106, 1987.

[27] L.B.F.M. Waters, J. Coté, and T.R. Geballe. 51 Ophiuchi (B9.5Ve): A Be star in the class of β Pictoris stars? *A&A*, 203:348–354, 1988.

[28] C.A. Grady and J.M.S. Silvis. The Circumstellar Gas Surrounding 51 Ophiuchi: A Candidate proto-planetary System Similar to β Pictoris. *Ap.J.*, 402:L61–L64, 1993.

[29] A. Slettebak, G.W. Collins, and R. Truax. Physical properties of Be star envelopes from Balmer and Fe II emission lines. *Ap.J.S*, 81:335–376, 1992.

[30] S.K. Dunkin, M.J. Barlow, and S.G. Ryan. High-resolution spectroscopy of Vega-like stars - Effective temperatures, gravities and photospheric abundances. *M.N.R.A.S*, 286:604–616, 1997.

[31] H. Beust, A.M. Lagrange-Henri, A. Vidal-Madjar, and R. Ferlet. The β Pictoris circumstellar disk - IX Theoretical results on the infall velocities of Ca II, Al III and Mg II. *A&A*, 223:304–312, 1989.

[32] H. Beust, A.M. Lagrange-Henri, A. Vidal-Madjar, and R. Ferlet. The Beta Pictoris circumstellar disk - X Numerical solutions of infalling evaporating bodies. *A&A*, 236:202–216, 1990.

[33] H. Beust, A.M. Lagrange, F. Plazy, and D. Mouillet. The β Pictoris circumstellar disk - XXII Investigating the model of multiple cometary infalls. *A&A*, 310:181–198, 1996.

[34] A.M. Lagrange-Henri, E. Gosset, H. Beust, R. Ferlet, and A. Vidal-Madjar. The β Pictoris circumstellar disk - XIII Survey of the variable Ca II lines. *A&A*, 264:637–653, 1992.

[35] D.F. Gray. *The observation and analysis of stellar photospheres.* Cambridge University Press, Cambridge, 2nd edition, 1992.

[36] L.H. Aller. *The atmospheres of the sun and stars.* Ronald Press Company, New York, 2nd edition, 1963.

[37] C.E. Moore. *A Multiplet Table of astrophysical Interest.* Us Government Printing Office, Washington, 1945 edition, 1972.

[38] H. Beust and J.J. Lissauer. The effects of stellar rotation on the absorption spectra of comets orbiting β Pictoris. *A&A*, 282:804–810, 1994.

[39] O.K.L. Peterson and W. Tobin. β Pictoris: the variable Ca II H & K absorptions 1994-1996. *M.N.R.A.S*, In Press, 1998.

[40] M. Zeilik and E.v.P. Smith. *Introductory Astronomy and Astrophysics.* Saunders College Publishing, New York, 2nd edition, 1987.

[41] J.B. Hearnshaw. The cassegrain échelle spectrograph at Mt John Observatory. *Proc. Astron. Soc. Australia*, 3:102–103, 1977.

[42] J.B. Hearnshaw. An Échelle Spectrograph. *Sky Telescope*, 56:6–8, 1978.

[43] W. Tobin, J.B. Hearnshaw, G.M. Kershaw, G.R. Nankivell, S. Persson, N.J. Rumsey, and R. Thirkettle. A focal reducer for the Mt John échelle spectrograph. *Southern Stars*, In Press, 1998.

[44] European Southern Observatory. *MIDAS Volume B: Data Reduction*, Release 94NOV edition, 1994.

[45] B.A. Palmer and R. Engleman. *Atlas of the Thorium Spectrum.* Los Alamos National Laboratory, New Mexico, 1983.

[46] D. Emerson. *Interpreting Astronomical Spectra.* John Wiley and Sons, Chichester, 1996.

Appendix A

Readjustment and Alignment of the Slip Rings

A.1 Purpose of the Slip Rings

The slip rings are two wedge rings located between the spectrograph and the mounting flange for the CCD camera head. The purpose of these rings is to be able to accurately align the focal plane of the spectrograph with that of the detector, by altering the angle at which the detector is mounted and the orientation of this angle. Azimuthal adjustments can be made by a separate ring, shown as the black ring in Fig. A.1, which changes the azimuthal orientation of the camera.

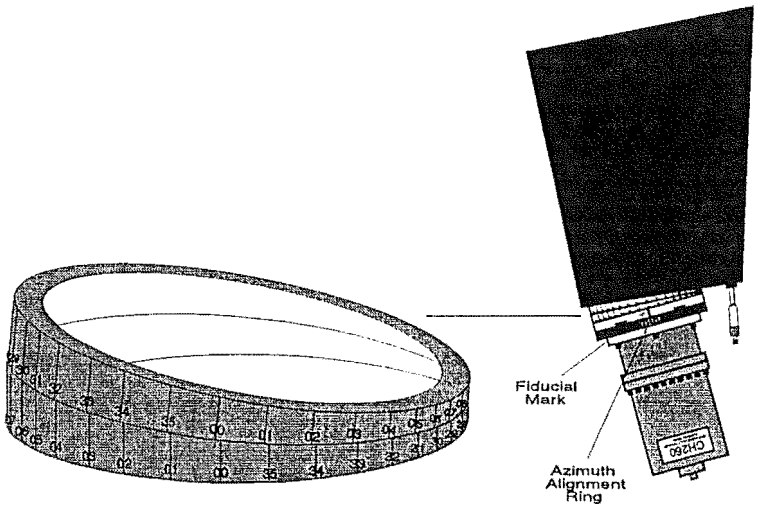

Figure A.1: Location of slip rings on the MJUO échelle spectrograph.

Fig.A.1 shows a schematic diagram of the location of the slip rings within the MJUO échelle spectrograph.

Each slip ring is circular with ten degree divisions scribed around the circumference. Since ten degree divisions are used the '0' is left off each number to avoid unnecessary cluttering. In this way '1' represents 10 degrees, '13' represents 130 degrees and so on. Both slip rings have identical

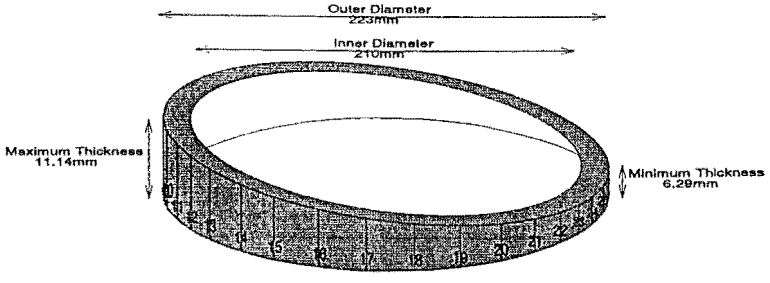

Figure A.2: Specification of the spectrograph slip rings.

dimensions with the specifications as given in Fig.A.2.

The only difference between the two rings is the direction in which the degree numbering around the circumference increases. Numbers increase clockwise on one ring, and anti-clockwise on the other. This gives us a reading of 90 degrees at the point of minimum thickness on one ring, and 270 degrees for the other. This is done in order to make the combined angle of the slip rings zero degrees, ie flat, when both rings have 90 degrees aligned. At this setting the minimum point of one ring is aligned with the maximum point of the other ring. This also implies that when the two rings are 180 degrees different, ie one at 90 and the other at 270 then we have the maximum tilt attainable since both the minimum and maximum thickness points are aligned. In simple terms the maximum tilt of the rings is obtained when the two positions add to give 360 degrees, and there is no tilt when the two positions of the rings add to give 180 degrees.

From the specifications of the slip rings in Fig.A.2 it can be found using simply trigonometry that the angle of tilt on each ring is 1.25 degrees. Therefore with the two rings together we are able to obtain any tilt between 0 and 2.5 degrees. By rotating both rings between 0 and 360 degrees we can orient this tilted plane in any direction we choose.

A.2 Adjustment of the Slip Rings

The question obviously arises regarding how the scribed positions of each ring relate to the combined orientation and tilt.

To do this it is easier to let each ring be represented by a vector. Fig.A.3 shows how this is done.

If we imagine a line perpendicular to the centre of the plane defined by the ring, and rotate the ring 360 degrees, we see that a circle is drawn by this line. The greater the wedge angle of the slip ring, the larger the radius of the circle. In this way the radius of the circle represents the tilt of our slip ring - and is therefore fixed at 1.25 degrees.

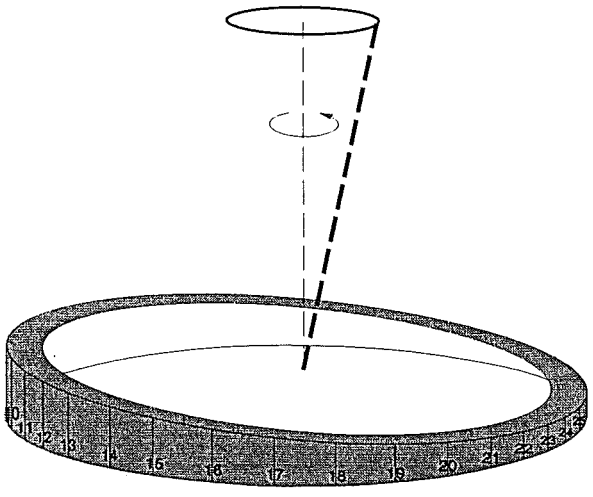

Figure A.3: Obtaining a vector for the slip ring.

The azimuth we are at in this circle represents the direction in which the inclined plane of the ring is oriented.

The two rings can then be represented as the vectors shown in Fig.A.4. Note: As men-

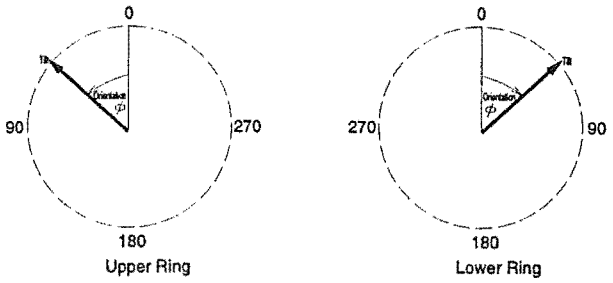

Figure A.4: Vector representation of each slip ring as viewed from above. The upper ring is the one closer to the spectrograph.

tioned earlier the numbering increases clockwise on one ring and anti-clockwise on the other, hence the reason for the orientation angle of the vectors going in opposite directions.

For simplicity sake the two rings will be labelled upper and lower, where the upper ring is that closer to the échelle and the lower is that below it, closer to the CCD.

The upper ring has the numbers increasing anti-clockwise, as seen from above.
The lower ring has the numbers increasing clockwise, as seen from above.

The rotation angles as read off the rings will be written as ϕ_u and ϕ_l, for the upper and lower rings respectively. The fiducial mark for reading these angles is located between the slip-rings and the spectrograph, as shown in Fig.A.1.

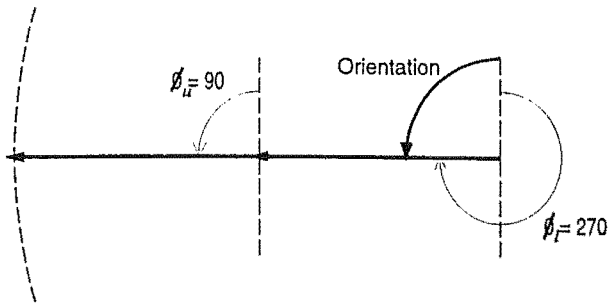

Figure A.5: Vector addition to give maximum tilt of slip rings.

The effect the two rings together have on the overall tilt and orientation can be found by adding the two vectors together. If we look at the case of maximum tilt in Fig.A.5 it is apparent that we can have the slip rings set to give their maximum tilt ($\phi_l + \phi_u = 360$), and can orient them anywhere between 0 and 360 degrees.

This is the same for any other combination of the slip rings, in that the combined tilt can be oriented in any direction.

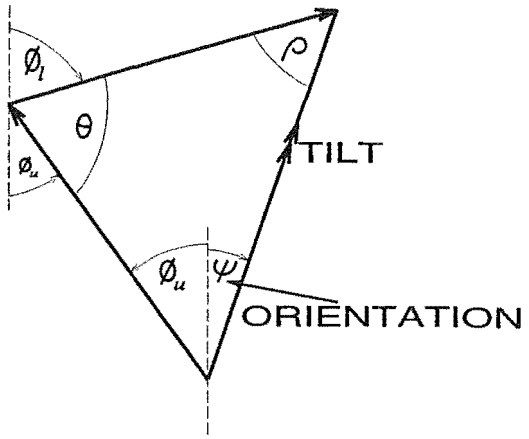

Figure A.6: Generalised addition of vectors.

Fig. A.6 shows the addition of the two vectors in an arbitrary orientation. The general formulae for the orientation and tilt of the two ring system can then be derived.
Note: In vector addition

$$\phi_u + \phi_l = \phi_l + \phi_u. \tag{A.1}$$

From Fig.A.6 we can see that:

$$\theta = 180 - (\phi_l + \phi_u). \tag{A.2}$$

Since both the vectors are the same length we have an isoceles triangle with the length of the base being the tilt of the system. Since the angles within a triangle add up to 180 degrees we can find the orientation angle as follows:

$$\rho = \frac{180 - \theta}{2} \tag{A.3}$$

$$\rho = \frac{180 - (180 - (\phi_l + \phi_u))}{2} \tag{A.4}$$

$$\rho = \frac{\phi_l + \phi_u}{2}. \tag{A.5}$$

Therefore the orientation angle, φ, is given by:

$$\varphi = \rho - \phi_u \tag{A.6}$$

$$\varphi = \frac{\phi_l + \phi_u}{2} - \phi_u \tag{A.7}$$

$$\varphi = \frac{\phi_l - \phi_u}{2}. \tag{A.8}$$

Since the length of each vector is 1.25°, (angle of each slip ring), the tilt is found to be given by:

$$\text{tilt} = 2(1.25 \cos \rho) \tag{A.9}$$

$$\text{tilt} = 2\left(1.25\left(\frac{\phi_l + \phi_u}{2}\right)\right) \tag{A.10}$$

$$\text{tilt} = 2.5\cos\left(\frac{\phi_l + \phi_u}{2}\right) \tag{A.11}$$

If we take an example using the slip ring settings prior to the installation of the focal reducer $\phi_l = 342$ and $\phi_u = 305$ we obtain:

tilt$= 2.5\cos\left(\frac{342+305}{2}\right)$ giving a tilt of 2.0°

$\varphi = \frac{342-305}{2}$ giving an orientation of 18.5°.

If we then want to retain the same orientation but change the tilt to say half its previous value, it requires the rings to moved to the values calculated below:

$\varphi = \frac{\phi_l - \phi_u}{2} = 18.5$
$\Rightarrow\ \phi_l = 37 + \phi_u$
$\Rightarrow\ \text{tilt} = \frac{2.01}{2} = 1.005 = 2.5\cos\left(\frac{2\phi_u+37}{2}\right)$

$\Rightarrow\ \phi_u = 48$ and $\phi_l = 85$

A.3 Obtaining the best alignment

The problem still remains how to match the focal plane of the spectrograph with that of the CCD.

The first step was to maximise the tilt and take a thorium spectrum with the CCD at this setting. This was then repeated with the tilt set at its minimum value. The slip rings were then returned to the setting that gave the worst range of focussed lines. By this it is meant where the lines may be well focussed in one region of the spectrum and severely out of focus in another. By looking at the worst range it was much easier to then locate regions where the focus was better. To be able to see these differences in the focus clearly the slit width needed to be narrowed down to 50μm so the lines were narrower and sharper. The focus gets worse the further apart the spectrograph and CCD focal planes are from each other.

The purpose of adjusting the slip rings is to get an even focus over the entire spectrum. Once the focus is even across the CCD chip, how well focussed the lines are is adjustable by the spectrograph camera micrometer, not by the slip rings.

Fig.A.7 shows a schematic diagram of the two focal planes with the orientation and tilt not aligned. There will however be a region of the chip read out where a good focus is obtained. This is the line where the focal planes cross. If such a line is not present the spectrograph focus will need to be adjusted. This has the effect of moving the spectrograph plane either in or out, so will overlap with the CCD focal plane at some point. By having the tilt set at the worst focus it makes this line a little easier to locate.

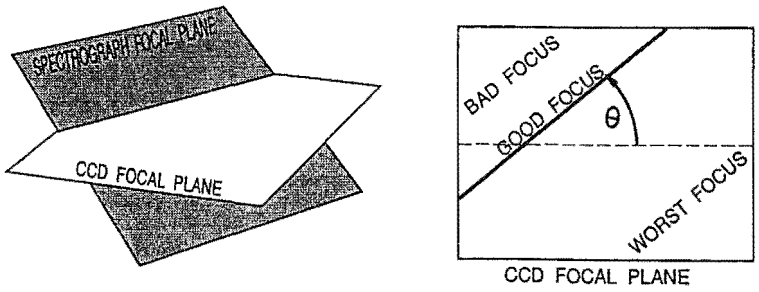

Figure A.7: Poorly aligned orientation and tilt of the focal planes.

Note: The thorium lines remain vertical, with the orders located horizontally across the chip. The line of best focus though may be oriented at any angle across the chip. It is this line that we are endeavouring to locate.

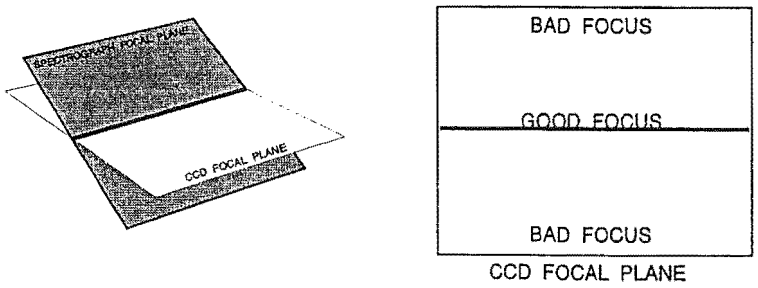

Figure A.8: Correctly aligned orientation of the focal planes.

Once found we can correctly set the orientation by rotating both rings together θ degrees so the line of best focus in now along the orders. This could also be done by rotating the rings $180 - \theta$ degrees in the opposite direction to give an orientation 180 degrees different. The correct option will be found later.

Fig.A.8 shows the focal planes having their orientation correctly aligned. By maintaining the same orientation and varying the tilt the entire chip should start to come into a more even and consistent focus, rather than some regions being in focus and others not. If the entire chip is out of focus the spectrograph may need to be focussed to obtain sharp lines.

If varying the tilt does not improve the evenness of the focus, the orientation will need to be rotated 180 degrees, and the tilt readjusted.

Fig.A.9 shows the focal planes correctly aligned. This will produce an even focus over the entire spectrum, which can then be brought into correct focus using the spectrograph camera micrometer.

While differences could be seen in the focus across the chip it was not in itself a very precise way to obtain the correct alignment. To improve this, a MIDAS procedure was

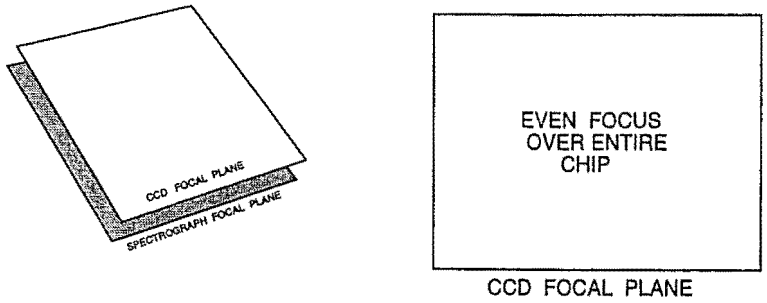

Figure A.9: Orientation and tilt correctedly aligning focal planes.

written that identifies all the thorium lines in the image and plots a circle at the same location in the graphics window, where the radius of this circle is the FWHM of the identified line. Because the line is broader where the focus is poorer, and a very narrow slit is used, regions that were in focus and out of focus could be easily distinguished.

Fig.A.10 shows two images that have had their emission lines represented graphically.

Using this method of aligning the slip-rings, the optimal settings were found to be:

$$\begin{aligned} \text{tilt} &= 1.06^\circ \\ \text{orientation} &= 0^\circ \\ \phi_l &= \phi_u = 245^\circ \end{aligned}$$

These settings are also in part confirmed in that the detector tilt has been halved as expected. With the focal reducer having a longitudinal demagnification half that of its lateral one, it was expected the tilt should be half that of the previous settings. The orientation differs by less than 20°, which is probably within the uncertainties of its determination.

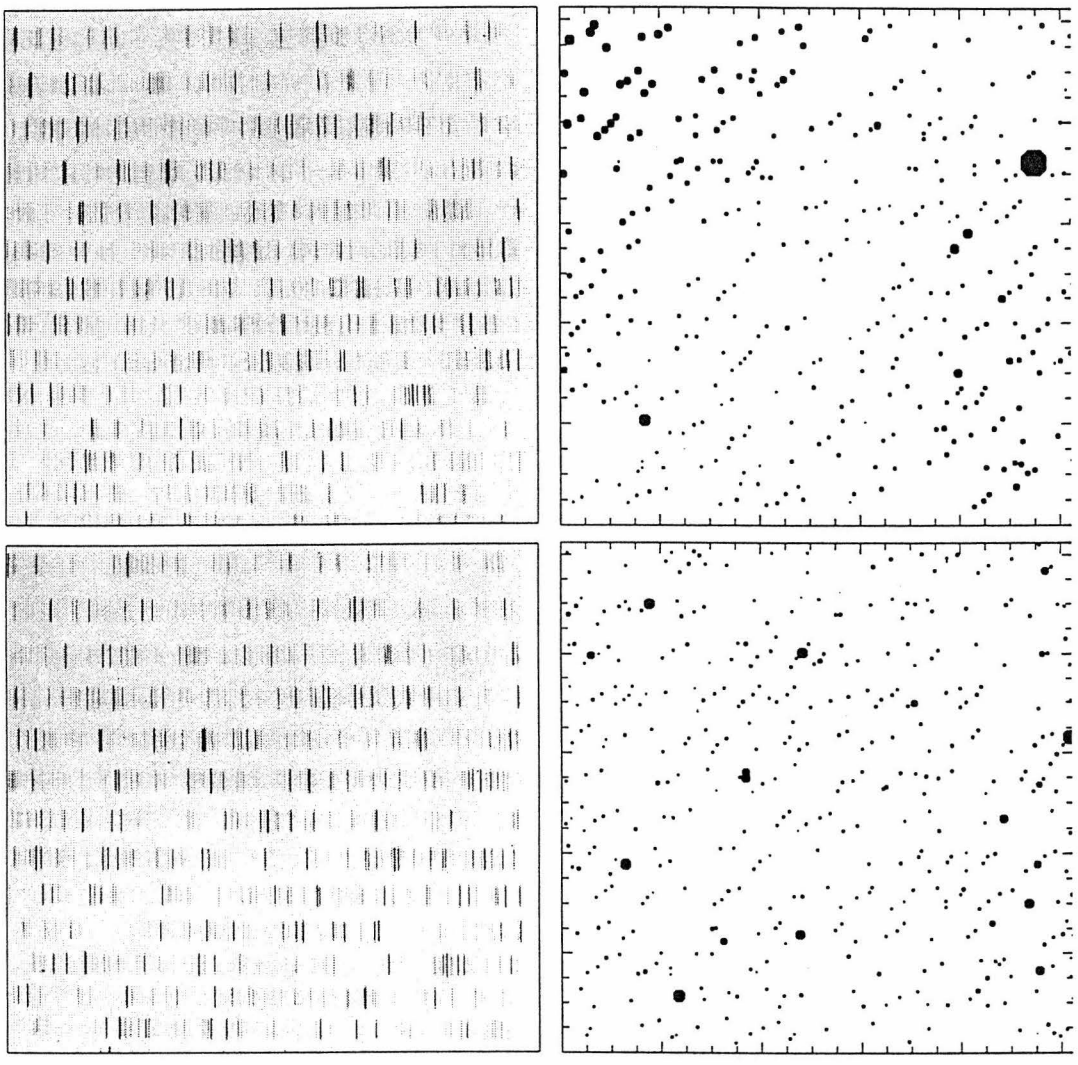

Figure A.10: *Upper left:* Thorium line image showing visually how difficult it is to evaluate the regions of best focus. *Upper right:* The same image represented graphically makes it easy to see what is a region of good focus from the lower-left to upper-right. Based on this diagram the orientation of the plane of the CCD was rotated by 45° and the tilt adjusted until the focus was even across the entire chip. *Lower left:* Thorium line image with the spectrograph correctly focussed. *Lower right:* Graphical representation of the correct focus. Spurious wide lines are the result of MIDAS being unable to separate two lines close together: the resulting points should be ignored.

Appendix B

Reduction of MJUO échelle spectra taken with the Series 200 CCD

B.1 Initialising the session

Note: All spacing shown in commands is necessary.

MIDAS> create/graphics
Makes a graphics window for displaying plots.

MIDAS> create/display 0 530,512
Makes a display window numbered "0" 530x512 pixels for displaying images.

MIDAS> load/lut pastel
This will put the image in false colour more clearly showing the orders, cosmic rays and any other features within the spectrum. Other colour options include : rainbow, backgr, color, heat, light, random, random1..4, staircase and stairs8.

MIDAS> set/context echelle
Load commands used specifically for échelle reductions.

MIDAS> init/echelle [session name]
Set the échelle parameters to those saved from a previous session, if available.

MIDAS> intape/fits [number of images to be read in] [MIDAS files prefix] [FITS files prefix]
Converts the images from file format FITS into the MIDAS format. FITS files need to be of the form `filename.mt`. At this stage it is also necessary to ensure the MIDAS filenames are not entirely numerical as this causes problems in the reduction, usually in assuming the number to be an intensity value, rather than a filename. (Since this problem was recognised, the assigned filenames at MJUO have been altered, to avoid numerical filenames, by changing the first number to the corresponding letter of the alphabet. Images obtained prior to this alteration, were changed to non-numerical filenames at this stage).
Eg. intape/fits 1-35 e056 5056
Reads in images `50560001.mt` to `50560035.mt` and converts them to `e0560001.bdf` to `e0560035.bdf`.

Note: Images must be oriented into the layout required by MIDAS. That is orders increasing from bottom to top, and wavelength increasing from left to right as the images are displayed on the screen.

B.2 Locating the Échelle Orders in the Images

This section involves the reduction of the smooth-field images to make a table `order.tbl` identifying the location of the orders within the images.

This step may be omitted once done for the first time, as images taken at the same settings will have the orders located in approximately the same position. Minor differences in the location of the orders are corrected later in the reduction process. However if the échelle spectrograph settings are changed in any way this step must be carried out again with the smooth-fields corresponding to the new settings.

MIDAS> compute/image [smooth image] = [smooth image 1]+[smooth image 2]+[smooth image 3]+.....
This creates a new image `[smooth image].bdf` which is the sum of all the smooth images, at a particular setting of the échelle spectrograph.
Eg. compute/image smooth = e0560005+e0560006+e0560007
Creates image `smooth.bdf` which is the sum of images `e0560005,6` and `7.bdf`.

MIDAS>set/echelle DEFMTD=hough DEFPOL=2,3 BKGMTD=spline BKGVISU=yes BKGRAD=6,2 BKGSTEP=10 BKGDEG=3 BKGSMO=100
Sets the échelle reduction parameters.
DEFMTD=hough. This method performs an automatic detection of the orders.
DEFPOL=2,3. Fits a polynomial of degree 2 for finding the orders (X direction), and 3 for finding the background (Y direction).
BKGMTD=spline. The background is approximated using a smoothing spline method.
BKGVISU=yes. Optional visualisation of the background.
BKGRAD=6,2. Radius of the window for the median estimate of the background.
BKGSTEP=10. Step along the X axis between background reference positions.
BKGDEG=3. Degree of the spline polynomials used to define the background values.
BKGSMO=100. Value of the smoothing factor.

MIDAS> @c necshow
Shows what the échelle reduction parameters are. A useful check to ensure the correct parameters have been set.

MIDAS> @p image smooth
Loads the image `smooth.bdf`, created previously, in the display window.
This is the same as the command `load/image smooth scale=-2 cuts=0,600` which scales the image to fit the display window, and in the intensity range 0 to 600.

MIDAS> set/graphics default
Set the graphics window to auto scaling of the X and Y axes.

MIDAS> plot/col smooth 511 1,1024
Plots row 511 of image `smooth.bdf`, between pixels 1 and 1024, ie. the entire row.

It is necessary here to note the maximum intensity in the orders.

MIDAS> copy/graphic phys809
Prints a copy of the graphics window on printer phys809.

MIDAS> define/hough smooth [number of orders] 0 DENSE 0 [DEFPOL] [hot pixel value,BKGSTEP]
This locates the orders and records all the sampling positions in a table called `order.tbl`. The two 0's are values for the half widths and threshold of the orders respectively. If set to 0 the values are measured individually for each order.
DENSE generates a hough transform based on 50 columns evenly spaced across the frame. If preceded by a minus sign (Eg. -DENSE) no median filter is applied to the frame.
The values used for DEFPOL and DEFSTEP should be the same as those set previously. The value for the hot pixel cut off should be just above the maximum intensity in the orders, recorded in the previous step.
Eg. define/hough smooth 13 0 DENSE 0 2,3 85000,10

MIDAS> read/table order
Displays the current table of order positions.
Record the 'Y-FITTED' value at X=511 in one of the central orders. This is needed later for calculation of the positional offset of the orders in the stellar image.

B.3 Setting the Offset of the Orders in the Stellar Spectrum

MIDAS> set/graphic default

MIDAS> @p select200 [stellar spectral image]
This program plots a cross section of the orders, in the stellar spectrum specified, in the graphics window. It will then prompt you for the pixel position (X axis) of the order you want to examine. This should be the same order as that chosen from the `read/table order` command previously. That is, the same order as has had its central position in the smooth-field image recorded. Ensure that sufficient background is also included in the pixel values.
The command will then replot the orders between values which the user is asked to specify.
Taking the mouse mark the background around the order by clicking either side of the profile. This will fit a Gaussian across the order. This may be repeated as many times as desired until a satisfactory fit is obtained.
All mouse cursor operations are terminated within MIDAS by clicking the right hand mouse button, and holding it down until a skull and crossbones appears.
Once terminated, note down the value of the centre of the Gaussian and the FW - twice the displayed FWHM, from the command window.

MIDAS> set/echelle SLIT=[FW] OFFSET=[calculated offset] MEDFILT=3,3,10
SLIT = the width of the order that will be examined in the reduction step, this is the FW just obtained from the Gaussian fitting.
OFFSET = the difference between the centre of the stellar spectra and those in the table

`table`.
Offset = Centre found using `select200` - Value noted from `order` table.
MEDFILT = 3,3,10. These are parameters governing the filtering between the orders. At each pixel along the rows the program takes the median value of all the pixels in a box 3×3 pixels (as set by first two parameters), then reduces to the median value any pixel that is more than 10 (third parameter) standard deviations greater than the median. This filter is applied to the entire frame outside the orders to eliminate any cosmic rays that may be present in the background.
This does not filter out cosmic rays within the orders.

B.4 Calibrating the Échelle Spectrum for Wavelength

MIDAS> plot/row [thorium arc image] [y-position] 1,1024
The value of y-position should be the centre of the order as found from the command `@p select200` in Section B.3.

From this plot record the value of the background threshold. That is the intensity at the bottom of the emission profiles. It may be necessary to change the scale of the y-axis so this can be found easily.

MIDAS> set/echelle EXTMTD=linear WIDTH2=5 THRES2=[background level]
Sets further parameters for locating the thorium emission lines.
EXTMTD = linear. Sets the method of extraction, to define the way to compute pixel values within the numerical slit, as a linear interpolation.
WIDTH2 = approximate width of the lines along the orders. 5 is the MIDAS default value.
THRES2 = the detection threshold relative to the local background. Any profiles with intensities above this threshold will be attempted to be identified.

MIDAS> extract/echelle [thorium-arc image] [name for extracted image]
Extracts the échelle orders and creates a 1-dimensional image of all the orders present in the thorium-arc spectrum.
Eg. extract/echelle e0560009 e0560009x
Creates a 1-dimensional file of `e0560009.bdf` in the file `e0560009x.bdf`.

MIDAS> search/echelle [name of extracted image]
Locates the emission lines within the extracted thorium-arc image, and indicates in the display window which lines have been identified.
The position of the detected lines are stored in the table `line.tbl`.
Eg. search/echelle e0560009x
Searches through the image `e0560009x.bdf` for the emission lines.
It may be necessary to change the value of THRES2 if good lines are missing or spurious lines are found.

MIDAS> set/graphic default

At this point it is necessary to select the method to be used to identify the lines within the thorium-arc image.

If no previous reduction has been saved then the interactive method must be chosen.

If a previous session has been saved the automatic method can be selected.

To select the automatic method, set the following parameters:

MIDAS> set/echelle WLCMTD=guess GUESS=[previous session name]

LINCAT=[name of wavelength table]

WLCMTD = wavelength calibration method. Guess refers to the automatic method.

LINCAT = name of line catalogue table providing wavelength of thorium lines.

The directory `/astro/physsip/midwork/` contains the table `thorline.tbl` for lines from 3622.2879 to 4703.9898Å.

Eg. set/echelle WLCMTD=guess LINCAT=/astro/physsip/midwork/thorline GUESS=stephen

Selects the automatic identification method by using the tables saved from the session named 'stephen'. The line catalogue table used to provide wavelengths is found in the directory `/astro/physsip/midwork/thorline.tbl`.

If the automatic identification method doesn't identify enough lines then the interactive method must be used.

To select the interactive method, set the following parameters:

MIDAS> set/echelle WLCMTD=angle LINCAT=[name of wavelength table]

It is a good idea here to have a printed copy of the thorium-arc image with lines already identified on them.

MIDAS> ident/echelle [thorium-arc image]

A mouse cursor will appear in the display window to allow the lines to be selected for which you know the wavelength. The size of this box can be changed by using the arrow keys.

At least 4 lines must be identified. It is best here to pick lines in different regions of the image to give a wider wavelength range. To select a line, position the cursor over the line and click the left-hand mouse button. A box should then be left around that line and the location given in the command window. If this is not the case click on the line again.

Clicking on the right-hand button will kill the cursor and return you to the command window.

It will then ask for the order number of the first selected line, then the wavelength of the selected lines. The lines are numbered in the display window in the order they were selected. It is in this order that they must be entered in as requested.

It will then fit a polynomial to the lines which will be recorded in a table. If a fitting rate of less than 50% is displayed, even though a good number of lines have been identified, it will be necessary to repeat the identification. The tolerance may need to be adjusted, if it is set too tight then good lines may be missed in the identification.

MIDAS> copy/graphic phys809

MIDAS> stat/table line :residual

Gives the statistics of the residuals in the table `line.tbl`.

Note the values of the mean and standard deviation of these residuals on the print-out.

MIDAS> @p fwhm [thorium-arc image]
Computes the FWHM of each of the identified lines and displays the result in the graphics window with the average FWHM in each order printed also.

MIDAS> copy/graphic phys809

B.5 Filtering the Stellar Spectrum

MIDAS> clear/channel overlay
Clears the overlaid emission line markers from the display window.

MIDAS> @p image [stellar spectral image]
Displays the stellar image to be filtered.

MIDAS> set/echelle CRFILT=15,[2×SLIT],3 CCDFILT=2.2,2.4,3
Sets the remaining echelle filtering parameters.
CRFILT = parameters for removing cosmic rays within the orders.
The first parameter refers to the inverse of the spatial slope of the orders. That is how many pixels in X the orders climb for every pixel in Y. 15 is the default value.
The second parameter is the width of the slit in the Y direction and is recommended to be twice the width of the parameter SLIT as entered in Section B.3, ie. twice the FW of the stellar orders.
The third parameter refers to the number of iterations and is typically set to 3 or 4.
CCDFILT = the parameters referring to a particular CCD detector being used.
The first parameter refers to the read-out-noise (in e^-).
The second is the inverse gain factor (e^-/ADU). The values of 2.2e− and 2.4e−/ADU refer to the Series 200 CCD system operated at a gain setting of 4, and were taken from test data provided with the system by Photometrics Ltd.
The third is the threshold for cosmic ray removal in the spectral order, in units of the standard deviation.

MIDAS> @c neckaren [stellar spectral image] [name for filtered image]
Filters the stellar image. This also produces an image recording the difference between the filtered and unfiltered images called `[spectral image]cr.bdf`. This should later be reduced to record the position of any cosmic rays within the orders.
Eg. @c neckaren e0560011 e0560011f
Will remove the background and cosmic rays both within the orders and the background from the image `e0560011.bdf`. The filtered image is called `e0560011f.bdf` and the difference image `e0560011cr.bdf`.

MIDAS> @p image midduma
Displays what MIDAS has identified to be the background.

MIDAS> @p image middumb
Displays the background subtracted image, but without the cosmic rays removed.

MIDAS> @p image [filtered spectral image]
Displays the filtered spectral image.

B.6 Preparing the Normalised Smooth-field Image

These operations are performed only once for each set of smooth-field images. They generate a normalised smooth-field image to be used in the reduction of all stellar spectra taken at those settings of the échelle spectrograph.
If the smooth-fields are changed this section must be repeated.

MIDAS> set/graphic default

MIDAS> plot/col smooth 511 1,1024
Plots the intensities of the orders in the image `smooth.bdf`.

It will be necessary here to change the scale of the axes to obtain a plot showing the maximum intensities in the orders of the H and K lines.
Eg set/graphic xaxis=300,450 yaxis=20000,25000
plot/col smooth 511 1,1024
Will replot the image `smooth.bdf` on a X axis from 300 to 450, and 20000 to 25000 on the Y axis.
Note down here the average of the intensities of the two orders.

MIDAS> compute/image [normalised smooth-field image] = smooth/[central intensity]
Normalises the smooth-field image.
Eg. compute/image smoothnorm = smooth/22000
Creates the image `smoothnorm.bdf` by divided the smooth-fields image `smooth.bdf` by the central intensity of 22000.

B.7 Reduction of the Spectra

MIDAS> set/echelle FFOPT=yes CORRECT=[normalised smooth-field image] RESPOPT=no SAMPLE=0.03 MRGMTD=concatenate MRGORD=1,13
Set parameters for the reduction of the spectra.
FFOPT = flat-field option. Identifies if a normalised smooth-field image is available.
CORRECT = name of normalised smooth-field image.
RESPOPT = response option.
SAMPLE = sample step size in Angstroms, when extracting the orders into linear wavelength steps.
MRGMTD = merge method. Concatenate merges all orders into one reduced file.
MRGORD = 1,13 merges orders 1 to 13.

MIDAS> @c necstephen [filtered spectral image] [reduced spectral image]

Reduces the image.
Eg. @c necstephen e0560011f re0560011
Reduces the filtered image `e0560011f.bdf` *and stores the result in the file* `re0560011.bdf`.

The `@c necstephen` procedure should also be carried out for the cosmic ray difference image and the thorium-arc image.
Eg. @c necstephen e0560011cr re0560011cr

MIDAS> compute/barycorr [Date] [UT-time] [RA] [Declination] [Longitude] [Latitude]
Corrects universal time and radial velocities to centre of sun.
Date = Year,Month,Day.
UT-time = Hours,Minutes,Seconds.
RA = Hours,Minutes,Seconds.
Declination = Degrees,Minutes,Seconds.
Longitude = Degrees,Minutes,Seconds.
Latitude = Degrees,Minutes,Seconds.

For β Pic:
Eg. com/bar [date] [time] 5,47,12 -51,04,03 -170,27,9 -43,59,2
For 51 Oph:
Eg. com/bar [date] [time] 17,31,25 -23,57,46 -170,27,9 -43,59,2
For Canopus:
Eg. com/bar [date] [time] 6,23,58 -52,41,44 -170,27,9 -43,59,2
It is necessary here to record the heliocentric velocity.

The radial velocity correction in wavelength space, $\delta\lambda$, can then be calculated using:

$$\frac{\delta\lambda}{\lambda} = \frac{v_r}{c} \tag{B.1}$$

λ = 3950Å for the H and K lines.
c = speed of light = 299793 kms^{-1}.
v_r = heliocentric velocity.

MIDAS> read/desc [reduced image name] start
Reads the starting wavelength value for the reduced image specified.
Note down this wavelength, and calculate the new wavelength by adding on the heliocentric wavelength correction just calculated.

MIDAS> write/desc [reduced image name] start/r/1/1 [new wavelength starting value]
This writes the new wavelength starting value for the image, so has now had the heliocentric correction performed.
Eg. write/desc re0560011 start/r/1/1 3646.57861
Changes the wavelength starting value of the reduced image `re0560011.bdf` *from its previous value to 3646.57861Å.*
Note: This correction becomes inappropriate for orders far from 58 and 59, because the

value of $\delta\lambda$ used is appropriate only for the orders containing the H and K lines.

This last step must also be performed for the reduced cosmic ray image, with the same wavelength value.
Eg. write/desc re0560011cr start/r/1/1 3646.57861

This step is **not** performed on the thorium-arc image.

MIDAS> set/graphic xaxis=3920,3985 yaxis=0,120000
Sets the graphical axes to the plot in the wavelength range 3920-3985Å which is the region containing the H and K lines.

MIDAS> plot/row [reduced thorium-arc image]
Plots the thorium lines in the wavelength range previously specified.
Eg. plot/row re0560009

MIDAS> overplot/ident line :wavec :ident
Overplots the wavelengths of the lines identified in the thorium-arc image, taken from the wavelength table `line.tbl`.

MIDAS> copy/graphic phys809

MIDAS> plot/row [reduced spectral image]
Plots the H and K absorption line profiles.
Eg. plot/row re0560011

MIDAS> overplot/row [reduced cosmic ray image]
This is the cosmic ray image corresponding to the spectral image just plotted, and will display the position and intensity of the cosmic rays that were removed.
Eg. overplot/row re0560011cr

Note: The Y axis scale may need to be changed to obtain the best plot of the profiles.

MIDAS> copy/graphic phys809

B.8 Saving the Session

Most of the settings of the échelle parameters will remain the same for all the reductions, and the interactive method of line identification can then be omitted. To do this a previous session with all the correct settings must be saved.

MIDAS> set/echelle WLCMTD=guess GUESS=[session name]
Ensures that the automatic method of line identification is used.

MIDAS> **save/echelle [session name]**

From now on the only parameters that should be needed to be changed for different images are SLIT, OFFSET, and CRFILT. All other parameters should remain the same and can be recovered by the command `init/echelle [session name]` as outlined in Section B.1.

Appendix C

MIDAS command language procedures

This appendix contains a number of the MIDAS command language procedures written for the reduction process for the spectra presented.

C.1 Reduction of the raw spectra

```
! @p reduce
!++++++++++++++++++++++++++++++++++++++++++++++++++++++++++++++
! SIP: 1997 August 13
! Used to reduce an image to a one dimensional reduced file
! once the process tables have been saved
!++++++++++++++++++++++++++++++++++++++++++++++++++++++++++++++

define/local printer/c/1/7 "phys809"
define/local  n/i/1/1 0
define/local  lambda/d/1/1 0.0d0
define/local  helio/d/1/1 0.0d0
define/local  correct/d/1/1 0.0d0

define/parameter P1 ? I "Enter stellar image to be reduced: "
write/out "Enter thorium-arc image file name, or 'null'"
write/out " if thorium image has already been reduced: "
define/parameter P2 ? ? "--> "
write/out "Enter 'p' to print out graphic windows"
write/out "Enter 'c' to continue without printing"
define/parameter P3 ? ? "--> "

set/graphic default

write/out "Printer is {printer}"

!Fits Gaussian across identified order to obtain SLIT and OFFSET
@p image {P1}
@p select200 {P1}
define/parameter P4 ? ? "Enter parameter SLIT: "
define/parameter P5 ? ? "Enter parameter OFFSET: "

compute/keyword n = 2*{P4}
set/echelle slit={P4} offset={P5} crfilt=15,{n},3

! Extracts and identifies lines in thorium-arc image
IF P2 .NE. "null" THEN
        extract/echelle {P2} {P2}x
        search/echelle {P2}x
        ident/echelle {P2}
```

```
        IF P3 .EQ. "p" THEN
                label/graph "{wlc}" 125,85,mm 0 1 1
                label/graph "Mean     = " 125,17,mm 0 0.7 1
                label/graph "Std Dev  = " 125,12,mm 0 0.7 1
                copy/graph {printer}
                write/out "Printing graphics window............."
        ENDIF

        clear/channel overlay

! Finds the FWHM of each of the identified lines
        @p fwhm {P2}

        IF P3 .EQ. "p" THEN
                label/graph "{wlc}" 125,85,mm 0 1 1
                copy/graph {printer}
                write/out "Printing graphics window............."
        ENDIF
ENDIF

@p image {P1}

write/out " "
write/out "******* Filtering stellar image {P1} *******"
write/out " "
@c neckaren {P1} {P1}f

write/out " "
write/out "******* Display shows filtered image {P1}f *******"
@p image {P1}f

        write/out " "
        write/out "******* Reducing stellar image {P1}f *******"
        write/out " "
        @c necstephen {P1}f r{P1}

        write/out " "
        write/out "******* Reducing cosmic ray image {P1}cr *******"
        write/out " "
        @c necstephen {P1}cr r{P1}cr

        IF P2 .NE. "null" THEN
                write/out " "
                write/out "******* Reducing thorium-arc image {P2} *******"
                write/out " "
                @c necstephen {P2} r{P2}
        ENDIF

        write/out " "
        write/out "Enter 1 if the image is Canopus"
        write/out "Enter 2 if the image is Beta Pic"
        write/out "Enter 3 if the image is 51 Oph"
        define/parameter P7 ? ? "--> "

! Does helicentric corrections
        IF P7 .EQ. "1" THEN
```

```
                write/out "Canopus"
                @p canopus
        ENDIF

        IF P7 .EQ. "2" THEN
                write/out "Beta Pic"
                @p betapic
        ENDIF

        IF P7 .EQ. "3" THEN
                write/out "51 Oph"
                @p 51oph
        ENDIF

        helio = {helio,:helio,1}
        lambda = {helio,:lambda,1}

set/format F10.5

        write/out " "
        read/desc r{P1} start
        write/out " "
        write/out " Corrected wavelength = Start + Delta Lambda"
        write/out " "
        define/parameter P8 ? ? "Starting Wavelength: "
        compute/keyword correct = {P8}+{lambda}
        set/format F10.5
        write/desc r{P1} start/d/1/1 {correct}
        write/desc r{P1}cr start/d/1/1 {correct}
        write/out ""
        write/out "New wavelength start value:"
        read/desc r{P1} start

! Plots thorium-arc and identified lines
        set/graphic xaxis=3920,3985 yaxis=0,120000 pmode=2
        IF P2 .NE. "null" THEN
                plot/row r{P2}
                overplot/ident line :wavec :ident
                label/graph "Start = {P8}" 125,13,mm 0 0.7 1
                IF P3 .EQ. "p" THEN
                        copy/graph {printer}
                        write/out "Printing graphics window....."
                ENDIF
        ENDIF

! Plots reduced spectrum and all parameters used
        plot/row r{P1}
        define/parameter P6 ? ? "Maximum Y axis intensity to be plotted: "
        set/graphic xaxis=3920,3985 yaxis=0,{P6} pmode=2
        plot/row r{P1}
        overplot/row r{P1}cr

        set/format f10.5
        label/graph "Th_Arc = {wlc}" 125,25,mm 0 0.7 1
        label/graph "Helio  = {helio}" 125,21,mm 0 0.7 1
        label/graph "Lambda = {lambda}" 125,17,mm 0 0.7 1
```

```
        label/graph "Start  = {correct}" 125,13,mm 0 0.7 1
        label/graph "Slit   = {P4}" 125,9,mm 0 0.7 1
        label/graph "Offset = {P5}" 125,5,mm 0 0.7 1

        IF P3 .EQ. "p" THEN
                copy/graph {printer}
                write/out "Printing graphics window..............."
        ENDIF
write/out ""
IF P2 .NE. "null" THEN
        stat/table line :residual
        write/out "*** Mean and standard deviation of residuals must be recorded ***"
ENDIF
```

C.2 Determining the instrumental profile from the Canopus spectra

```
! Procedure canopus_fit.prg
!
! Compares one night's observations of Canopus H & K to a standard profile,
! and fits the ratios with 2nd-order polynomials.  These parabolae are
! scaled to values near unity and  stored in the specified correction
! image file [P4]
!  The correction is to be applied multiplicatively.
!
!  Usage:
!    @@ canpous_fit P1 P2 P3 P4 [P5] [P6] [P7] [P8]
!
!  Expects to find following files, which should not be altered:
!        canopus_ref.bdf [if alternative not specified via P5]
!        canopus.fit
!        rebin_sample.bdf  (1D image with start=3600. step=0.05 22000 pixels)
!        h_error.bdf
!        k_error.bdf
!  hfit, kfit and middumm files can be discarded after canopus_fit has
!  been run.
!
! W Tobin & S Persson 1997 Oct 28
!
define/parameter P1 ?  I "Enter the night's 1st Canopus spectrum file:"
define/parameter P2 ?  I "Enter the night's 2nd Canopus spectrum file:"
define/parameter P3 ? I "Enter the night's 3rd Canopus spectrum file:"
define/parameter P4 ? I "Enter output file for fitted polynomials:"
define/parameter P5 canopus_ref I "Enter Canopus profile reference spectrum:"
define/parameter P6 0,3 C "Enter yaxis scale parameters:"
define/parameter P7 h_error C "Enter h_error file:"
define/parameter P8 k_error C "Enter k_error file:"

define/local fitmean/r/1/1/ 0.


define/local tempd1/d/1/1/ 1.d0
define/local tempd2/d/1/1/ 1.d0

! check rebin_sample hasn't been corrupted
```

```
copy/dk rebin_sample start/d/1/1 tempd1
compute/keyword tempd2 = {tempd1}-3600.d0
IF  M$ABS({tempd2}) .GT. 0.00001d0 THEN
  write/out "rebin_sample corrupted: start = {tempd1}"
  return
ENDIF

copy/dk rebin_sample step/d/1/1 tempd1
compute/keyword tempd2 = {tempd1}-0.050d0
IF  M$ABS({tempd2}) .GT. 0.000000000001d0 THEN
  write/out "rebin_sample corrupted: step = {tempd1}"
  return
ENDIF


rebin/linear {P1} &l rebin_sample
rebin/linear {P2} &m rebin_sample
rebin/linear {P3} &n rebin_sample
write/out "P1 descriptor"
read/descr {P1}

! compute the mean of the three Canopus spectra
compute/image &o = (&l+&m+&n)/3.
set/graph yaxis=0,100000  xaxis=3920,3985 colour=1
plot/row  &o

wait 00:05

set/fit weight=W

! compute the ratio of the canopus_ref to mean spectrum
compute/image &r = canopus_ref/&o

set/graph colour=2

over/row &r

! Extract parts of the ratio near the H and K lines
! NB it is possible that these limits will need to be edited if
! a spectrum is undefined at wavelengths at which h_error or k_error
! are small (i.e. high weight)

extract/image &h = &r [3960,@1:3985,@1]
extract/image &k = &r [3920,@1:3950,@1]

set/graph yaxis={P6} xaxis=3920,3985 colour=1 bin=on

plot/row &h
label/graph "canopus_ref/night's canopus" 3925,2.8 0 1 1
over/row &k

label/graph "Input files:" 3986,0.70 0 0.45 1
label/graph "{P1}"         3989,0.60 0 0.45 1
label/graph "{P2}"         3989,0.52 0 0.45 1
label/graph "{P3}"         3989,0.44 0 0.45 1
```

```
label/graph "Reference profile:" 3986,0.33 0 0.45 1
label/graph "{P5}"               3989,0.25 0 0.45 1
label/graph "Error files:" 3986,0.13 0 0.45 1
label/graph "{P7}"         3989,0.05 0 0.45 1
label/graph "{P8}"         3989,-0.03 0 0.45 1
set/graph yaxis={P6}  xaxis=3920,3985 colour=1
set/graph yaxis={P6}  xaxis=3920,3985 colour=1

extract/image &p = {P7} [3960,@1:3985,@1]
extract/image &q = {P8} [3920,@1:3950,@1]

set/graph colour=6 bin=off

label/graph "error (inverse of fit weight)" 3925,2.6 0 1 1

over/row &p
over/row &q


fit/image 100,0.01,-0.2  middummh,middummp canopus
compute/fit hfit
! compute/fit write STEP as single precision...correct this
write/descr hfit step/d/1/1 0.0500000d0
set/graph colour=2
labe/graph "quadratic fit" 3925,2.4 0 1 1
over/row hfit
statistics/image hfit
copy/dk hfit statistic/r/3/3 fitmean
compute/image hfit = hfit/{fitmean}


fit/image 100,0.01,-0.2  middummk,middummq canopus
compute/fit kfit
write/descr kfit step/d/1/1 0.0500000d0
over/row kfit
statistics/image kfit
copy/dk kfit statistic/r/3/3 fitmean
compute/image kfit = kfit/{fitmean}


compute/image {P4} = rebin_sample
compute/image {P4} = 0.

insert/image hfit {P4}
insert/image kfit {P4}
set/graph colour=4
label/graph "scaled fit, defined 3600-4700 A" 3925,2.2 0 1 1
over/row {p4}
label/graph "Fit file: {P4}.bdf" 3922,3.1 0 1.4 1
```

C.3 Division by reference spectrum

```
! Procedure division.prg
!
! Usage
```

```
!     @@ division P1 P2 [P3] [P4]
!            P1 = beta Pic [or 51 Oph] spectrum
!            P2 = image containing corrective factor for profile warp
!                 derived from observations of Canopus
!            P3 = output image - defaulted to {P1}d
!            P4 = reference profile defaulted to bpic_ref
!                 specify another image explicity for 51 Oph reference
!                 profile
!
!  Requires files:
!             rebin_sample.bdf
!             bpic_ref.bdf (cannot be zero anywhere)
!
!  At end, output is in {P3}
!    Following files can be discarded:
!       middumm*.bdf
!
!  Program takes a spetrum of beta Pic and
!    --> resamples onto start=3600.000000 step=0.050000;
!    --> multiplies by the profile-corrective factor {P2} calculated
!        using canopus_fit.prg and derived from observations of Canopus;
!    --> divides by the profiles of the reference spectrum bpic_ref
!        [or other image specified in P4] ( = H & K profiles showing
!        no variable cometary absorptions);
!    --> set average value of this divided spectrum to unity in each of
!        the H and K regions;
!    --> Stores result in P3 - defaulted to {P1}d.
!
!  S. Persson & W. Tobin, 1997 October 30 Thursday
!
define/parameter P1 ? I "Enter spectrum to be divided:"
define/parameter P2 ? I "Enter image containing Canopus-derived profile correction:"
define/parameter P3 {P1}d ? "Enter image name for output:"
define/parameter P4 bpic_ref I "Enter reference profile for target star:"

define/local divmean/r/1/1 1.0
define/local tempd1/d/1/1/ 1.d0
define/local tempd2/d/1/1/ 1.d0

! check rebin_sample hasn't been corrupted

copy/dk rebin_sample start/d/1/1 tempd1
compute/keyword tempd2 = {tempd1}-3600.d0
IF  M$ABS({tempd2}) .GT. 0.00001d0 THEN
  write/out "rebin_sample corrupted: start = {tempd1}"
  return
ENDIF

copy/dk rebin_sample step/d/1/1 tempd1
compute/keyword tempd2 = {tempd1}-0.050d0
IF  M$ABS({tempd2}) .GT. 0.000000000001d0 THEN
  write/out "rebin_sample corrupted: step = {tempd1}"
  return
ENDIF
```

```
! create output image {P3}
compute/image {P3} = rebin_sample

! rebin {P1}
rebin/linear {P1} &l rebin_sample

set/graph xaxis=3920,3985 yaxis=0,100000 colour=1
plot/row &l

! multiply by profile correction {P2}
compute/image &m = &l*{P2}
set/graph colour=2
over/row &m

! divide by H & K reference profile of target
compute/image &n  = &m/{P4}

! extract region centered on H line

extract/image &p = &n [3964.0,@1:3977.0,@1]
statistics/image &p
copy/dk &p statistic/r/3/3 divmean
! extract full region containing H line
extract/image &p = &n [3955.0,@1:4020.0,@1]
compute/image &r = &p/{divmean}

! extract region centered on K line

extract/image &q = &n [3928.5,@1:3940.5,@1]
statistics/image &q
copy/dk &q statistic/r/3/3 divmean
! extract full region containing K line
extract/image &q = &n [3888.0,@1:3955.0,@1]
compute/image &s = &q/{divmean}

! store in {P3}

compute/image {P3} = 0.0
insert/image &r {P3}
insert/image &s {P3}

set/graph yaxis=0,1.5 xaxis=3885,4025 colour=1
plot/row {P3}

wait 00:05

set/graph xaxis=3920,3985
plot/row {P3}
label/graph "Divided, profile-corrected spectrum: {P3}" 3920,1.55 0 1.0 1
label/graph "Profile correction:" 3987,0.2 0 0.6 1
label/graph "{P2}" 3989,0.15 0 0.6 1
label/graph "Target ref. profile" 3987,0.05 0 0.6 1
label/graph "{P4}" 3989,0.00 0 0.6 1
```

C.4 Simultaneous fitting of the Gaussians

```
!
! Procedure hkfit.prg
!   Conjointly fits multiple gaussians to  H & K absorption-line spectra.
!   Initial values for gaussians set using graphics cursor
!
! Use:
!   @@ hkfit P1 [P2]
!       where P1 = name of image file containing spectrum presumed
!                  normalised to unity.
!             P2 = Y if jump to LATE_START: wanted
!  Needs files
!       hk_cont_error.bdf
!       hk_abs_error.bdf
!
! 1997 November 12 Wednesday
!
define/parameter P1 ? I "Enter normalized spectrum file:"
define/parameter P2 N C "Jump to LATE_START:? Y or N"

define/local question/i/1/1 0
define/local N/i/1/1 0
define/local M/i/1/1 0
define/local MM/i/1/1 0
define/local length/i/1/1 0
define/local indx/i/1/1 0
define/local indx2/i/1/1 0
define/local A/r/1/1 0.
define/local B/r/1/1 0.
define/local C/r/1/1 0.
define/local D/r/1/1 0.
define/local cquestion/c/1/1 "Y"
define/local tempd1/d/1/1/ 1.d0
define/local tempd2/d/1/1/ 1.d0
define/local yhposn/r/1/1/  1.9
define/local ykposn/r/1/1/  1.15
define/local par/r/1/1 0.
define/local par_err/r/1/1/ 0.

! delete descriptor COORDS if it exists

compute/key indx = M$EXISTD("{P1}nv","coords")
read/key indx

if indx .eq. 1 then
write/out "Deleting descriptor COORDS"
delete/descr {P1}nv coords
endif

! delete keyword XVALS if it exists

compute/key indx = M$EXISTK("xvals")
read/key indx
if indx .eq. 1 then
write/out "Deleting keyword XVALS"
```

```
delete/keyword xvals
endif

if P2 .eq. "Y"  goto LATE_START

! Extract h line and error

extract/image tmp_h  = {P1}[3963.75:3973.75]
extract/image tmp_h_err  = hk_cont_error[3963.75:3973.75]

! Plot h line

set/graph xaxis=3963,3974 yaxis=0,1.5 colour=1 bin=ON
plot/row tmp_h
label/graph "H" 3964,1.30  0 2 1

! Make polynomial fit to h line

write/keyword IN_A/c/1/60 " " ALL
write/keyword OUT_A/C/1/60 " " ALL
IN_A = "hk"

INPUTI = 0

RUN APP_EXE:fittable

inquire/keyword question "What order of polynomial for h continuum? 0, 1, 2 or 3?:"

if {question} .eq. 0 then

hk_fit,:FUNCTIONS,@1 = "POLY(X;A)"
hk_fit,:PARAMETERS,@1 = "A=1."

endif

if {question} .eq. 1 then

hk_fit,:FUNCTIONS,@1 = "POLY(X;A,B)"
hk_fit,:PARAMETERS,@1 = "A=1.  B=0."

endif


if {question} .eq. 2 then

hk_fit,:FUNCTIONS,@1 = "POLY(X;A,B,C)"
hk_fit,:PARAMETERS,@1 = "A=1.  B=0.  C=0."

endif


if {question} .eq. 3 then

hk_fit,:FUNCTIONS,@1 = "POLY(X;A,B,C,D)"
hk_fit,:PARAMETERS,@1 = "A=1.  B=0.  C=0. D=0."
```

```
endif

 read/table hk_fit
! read/descr hk_fit.tbl *

write/key outputi/i/1/1 0
compute/keyword IN_A = "hk"
compute/keyword OUT_A = "hk_fit"
RUN APP_EXE:tablefit

! use MGN if on Cantua with NAG library, NR otherwise
set/fit method=NR

fit/image 40,0.001,0.2 tmp_h,tmp_h_err hk

compute/fit temp
set/graph colour=2
over/row temp

write/out "Waiting 3 seconds..."
wait/secs  3

! compute image with fully normalised 'continuum'

compute/image {P1}n = rebin_sample
compute/image {P1}n = 1.0

compute/image insert = tmp_h/temp

insert/image insert {P1}n


! Extract k line and error

extract/image tmp_k  = {P1}[3928.85:3938.85]
extract/image tmp_k_err  = hk_cont_error[3928.85:3938.85]

! Plot k line

set/graph xaxis=3928,3939 yaxis=0,1.5 colour=1 bin=ON
plot/row tmp_k
label/graph "K" 3929,1.30  0 2 1

! Make polynomial fit to k line

write/keyword IN_A/c/1/60 " " ALL
write/keyword OUT_A/C/1/60 " " ALL
IN_A = "hk"

INPUTI = 0

RUN APP_EXE:fittable

inquire/keyword question "What order of polynomial for k continuum? 0, 1, 2 or 3?:"

if {question} .eq. 0 then
```

```
hk_fit,:FUNCTIONS,@1 = "POLY(X;A)"
hk_fit,:PARAMETERS,@1 = "A=1."

endif

if {question} .eq. 1 then

hk_fit,:FUNCTIONS,@1 = "POLY(X;A,B)"
hk_fit,:PARAMETERS,@1 = "A=1.  B=0."

endif


if {question} .eq. 2 then

hk_fit,:FUNCTIONS,@1 = "POLY(X;A,B,C)"
hk_fit,:PARAMETERS,@1 = "A=1.  B=0.  C=0."

endif


if {question} .eq. 3 then

hk_fit,:FUNCTIONS,@1 = "POLY(X;A,B,C,D)"
hk_fit,:PARAMETERS,@1 = "A=1.  B=0.  C=0. D=0."

endif

 read/table hk_fit
! read/descr hk_fit.tbl *

write/key outputi/i/1/1 0
compute/keyword IN_A = "hk"
compute/keyword OUT_A = "hk_fit"
RUN APP_EXE:tablefit

! use MGN if on Cantua with NAG library, NR otherwise
set/fit method=NR

fit/image 40,0.001,0.2 tmp_k,tmp_k_err hk

compute/fit temp
set/graph colour=2
over/row temp


! compute image with fully normalised 'continuum'

compute/image insert = tmp_k/temp

insert/image insert {P1}n

inquire/keyword cquestion "Continue? Y or N:"
if cquestion .eq. "N" then
 write/out "Stopping"
```

```
 RETURN
endif
write/out "Continuing"

! convert wavelengths into velocities K at 0 km/s, H at 2000 km/s

create/image {P1}nv 1,730 -413.655,3.795
compute/image {P1}nv = 1.
set/format F20.12

! check {P1}n hasn't been corrupted

copy/dk {P1}n start/d/1/1 tempd1
compute/keyword tempd2 = {tempd1}-3600.d0
IF  M$ABS({tempd2}) .GT. 0.00001d0 THEN
  write/out "{P1}n corrupted: start = {tempd1}"
  return
ENDIF

copy/dk rebin_sample step/d/1/1 tempd1
compute/keyword tempd2 = {tempd1}-0.050d0
! less stringent test because fit/image or compute/fit only preserves STEP as
! a single-precision descriptor
IF  M$ABS({tempd2}) .GT. 0.000001d0 THEN
  write/out "{P1}n corrupted: step = {tempd1}"
  return
ENDIF

write/out "Note: insertion into velocity space: stepsizes will not match"
extract/image insert = {P1}n[@6586:@6770]
insert/image insert {p1}nv @18
extract/image insert = {P1}n[@7283:@7465]
insert/image insert {p1}nv @545

write/descriptor {P1}nv CUNIT/C/1/16  "RELATIVE TO REF."
write/descriptor {P1}nv CUNIT/C/17/16 "VELOCITY KM/S   "

! set/graph colour=1 yaxis=0,1.5 xaxis=-400,2400
! plot/row {P1}nv

LATE_START:

! Plot spectra

set/graph yaxis=0.5,2 xaxis=-350,350,100,20 bin=ON colour=1

plot/row {P1}nv
label/graph "K" 300,1.1 0 2 1
compute/image tmp_h = {P1}nv
write/descr tmp_h start/D/1/1 -2413.55
overplot/row tmp_h ? ? 0.5
label/graph "H" 300,1.6 0 2 1
! plot K again so that coords are stored in correct image
overplot/row {P1}nv
```

```
! Gaussian fitting


set/graph  ltype=1 stype=0 colour=1 bin=OFF

write/keyword IN_A/c/1/60 " " ALL
write/keyword OUT_A/C/1/60 " " ALL
IN_A = "hk"

INPUTI = 0

RUN APP_EXE:fittable

! Now get parameters from which initial values of gaussian fits can be
! estimated

write/out "Mark position of absorption features on K spectrum using cursor"
write/out " "
write/out "First mark left FWHM position, then centre, then right FWHM position"
write/out " "

get/gcurs coords,des

show/descr {P1}nv coords

read/descriptor {P1}nv coords

copy/dk {P1}nv coords xvals


read/key xvals

set/format i2
compute/key length = {outputi(3)}/7
read/key length
compute/key N = (({length}/3)*3)

if  {N} .NE. {length} then
    write/out "No of points selected not a multiple of 3"
    return
endif

! length gaussians are to be fitted

compute/keyword length = {length}/3

hk_fit,:FUNCTIONS,@1 = "POLY(X;A)"
hk_fit,:PARAMETERS,@1 = "A=1.@"

DO N = 1 {length} 1

! read/key N
compute/key M = {N}+1
compute/key MM = {M}+{length}

compute/key indx = ({N}-1)*21+9
```

```
read/key indx
compute/key A = {xvals({indx})}-1.
compute/key indx = ({N}-1)*21+8
compute/key B = {xvals({indx})}
compute/key indx = ({N}-1)*21+15
compute/key indx2 = ({N}-1)*21+1
set/format f10.4
compute/key C = 0.5*({xvals({indx})}-{xvals({indx2})})
compute/key D = {B}+2000.

hk_fit,:FUNCTIONS,@{M} = "GAUSS(X;A{M},B{M},C{M})"
hk_fit,:PARAMETERS,@{M} = "A{M}={A}  B{M}={B}  C{M}={C}"
hk_fit,:FUNCTIONS,@{MM} = "GAUSS(X;A{MM},B{MM},C{MM})"
hk_fit,:PARAMETERS,@{MM} = "A{MM}={A}  B{MM}={D}  C{MM}={C}"

ENDDO

 read/table hk_fit
 read/descr hk_fit.tbl *

write/key outputi/i/1/1 0
compute/keyword IN_A = "hk"
compute/keyword OUT_A = "hk_fit"
RUN APP_EXE:tablefit

! use MGN if on Cantua with NAG library, NR otherwise
set/fit method=NR

fit/image 90,0.0001,0.2 {P1}nv,hk_abs_error hk

save/fit temp @1
! show total fit
compute/fit temp
! k line
set/graph colour=4
over/row temp
! h line
set/graph colour=2
compute/image tmp_h = temp
write/descr tmp_h start/D/1/1 -2413.55
overplot/row tmp_h ? ? 0.5

! show individual fits
set/format F7.2
DO N = 1 {length} 1

compute/key M = {N}+1
compute/key MM = {M}+{length}
select/fun hk 1,{M},{MM}
compute/fit fit{N} = hk
! k
set/graph colour=4
over/row  fit{N} ? ? 0.25
! h
set/graph colour=2
compute/image tmp_h = fit{N}
```

```
write/descr tmp_h start/D/1/1 -2413.55
overplot/row tmp_h ? ? 0.75
! overprint the parameters
set/graph colour=1
! k fit parameters
par = m$value(temp,:A{M},@1)
par_err = m$value(temp,:A{M}_ERROR,@1)
label/graph "A{M}:" -320,{ykposn} 0 0.6 1
label/graph "{par}" -200,{ykposn} 0 0.6 2
label/graph "{par_err}" -180,{ykposn} 0 0.6 1
compute/key ykposn = ykposn-0.03
par = m$value(temp,:B{M},@1)
par_err = m$value(temp,:B{M}_ERROR,@1)
label/graph "B{M}:" -320,{ykposn} 0 0.6 1
label/graph "{par}" -200,{ykposn} 0 0.6 2
label/graph "{par_err}" -180,{ykposn} 0 0.6 1
compute/key ykposn = ykposn-0.03
par = m$value(temp,:C{M},@1)
par_err = m$value(temp,:C{M}_ERROR,@1)
label/graph "C{M}:" -320,{ykposn} 0 0.6 1
label/graph "{par}" -200,{ykposn} 0 0.6 2
label/graph "{par_err}" -180,{ykposn} 0 0.6 1
compute/key ykposn = ykposn-0.06
! h fit parameters
par = m$value(temp,:A{MM},@1)
par_err = m$value(temp,:A{MM}_ERROR,@1)
label/graph "A{MM}:" -320,{yhposn} 0 0.6 1
label/graph "{par}" -200,{yhposn} 0 0.6 2
label/graph "{par_err}" -180,{yhposn} 0 0.6 1
compute/key yhposn = yhposn-0.03
par = m$value(temp,:B{MM},@1)
compute/key par = par-2001.6
par_err = m$value(temp,:B{MM}_ERROR,@1)
label/graph "B{MM}:" -320,{yhposn} 0 0.6 1
label/graph "{par}" -200,{yhposn} 0 0.6 2
label/graph "{par_err}" -180,{yhposn} 0 0.6 1
compute/key yhposn = yhposn-0.03
par = m$value(temp,:C{MM},@1)
par_err = m$value(temp,:C{MM}_ERROR,@1)
label/graph "C{MM}:" -320,{yhposn} 0 0.6 1
label/graph "{par}" -200,{yhposn} 0 0.6 2
label/graph "{par_err}" -180,{yhposn} 0 0.6 1
compute/key yhposn = yhposn-0.06

ENDDO

!save total profile fit of h & k lines
compute/image {P1}hk = temp

set/graph default

! then do
!     assign/print phys809
!     print/fit hk
!     copy/graph phys809
      $ mv hk.fit {P1}.fit
```

Appendix D

Variable absorption parameters

Contained in the two tables below are the complete set of parameters (velocity, depth, FWHM and equivalent width) of the variable Ca II H and K lines observed in 51 Ophiuchi (Table 1) and β Pictoris (Table 2).

Table 1. Gaussian fits to observed 51 Ophiuchi variable Ca II absorptions. The centre of the circumstellar feature is taken as the zero point of the velocity scale.

Date/Time (mid exposure)	CaII	Velocity $km\,s^{-1}$	FWHM $km\,s^{-1}$	Depth	Eq. Wdth mÅ	Classification
1997 May 29						
10:56:04	K	138.0	37.6	0.03	15.83	UD
		±1.1	±2.6	±0.01	±2.86	
11:59:37	K	135.8	38.5	0.02	10.78	UD
		±1.4	±3.4	±0.01	±2.86	
13:07:01	K	144.4	37.9	0.02	10.62	UD
		±1.4	±3.3	±0.01	±2.81	
1997 September 15						
09:12:32	K	166.1	54.3	0.02	15.23	UD
		±2.6	±6.1	±0.01	±4.17	
10:26:00	K	170.8	63.9	0.02	17.91	UD
		±3.4	±8.0	±0.01	±5.01	
1997 September 19						
07:42:06	K	131.0	32.4	0.02	9.09	UD
		±2.7	±6.8	±0.01	±2.97	
08:46:01	K	123.8	14.0	0.01	1.96	UD
		±2.8	±6.7	±0.01	±1.36	

Table 2. Gaussian fits to observed β Pictoris variable Ca II absorptions. The centre of the circumstellar feature is taken as the zero point of the velocity scale.

Date/Time (mid exposure)	CaII	Velocity $km\,s^{-1}$	FWHM $km\,s^{-1}$	Depth	Eq. Wdth mÅ	Classification
1997 April 21						
09:00:00	K	13.5	16.4	0.39	89.45	C
		±4.0	±3.7	±0.14	±37.92	
09:00:00	H	12.1	13.1	0.29	53.34	C
		±6.4	±5.7	±0.22	±46.61	
09:32:00	K	14.8	21.0	0.49	143.92	C
		±1.2	±1.3	±0.03	±12.74	
09:32:00	H	12.5	15.8	0.22	48.73	C
		±5.6	±5.5	±0.10	±27.90	
09:32:00	K	82.1	20.6	0.05	14.45	pB
		±1.3	±3.7	±0.01	±3.86	
09:32:00	H	70.5	7.2	0.02	2.02	pB
		±1.6	±3.5	±0.01	±1.40	
09:32:00	K	147.6	92.7	0.03	38.99	pB
		±6.1	±15.6	±0.01	±6.55	
09:32:00	H	144.9	82.7	0.01	11.60	pB
		±10.7	±26.2	±0.01	±3.67	
10:09:00	K	15.0	22.3	0.53	165.48	C
		±1.1	±1.3	±0.03	±13.46	
10:09:00	H	12.5	15.7	0.23	50.50	C
		±6.8	±6.7	±0.12	±34.03	
10:09:00	K	72.9	6.3	0.03	2.67	gB
		±1.3	±3.2	±0.01	±1.62	
10:09:00	K	102.8	57.4	0.06	48.25	gB
		±3.8	±9.3	±0.01	±7.79	
10:09:00	H	99.4	26.8	0.02	7.51	pB
		±5.6	±13.8	±0.01	±5.39	
10:09:00	K	169.3	48.7	0.03	20.50	gB
		±6.2	±13.4	±0.01	±5.66	
10:09:00	H	149.5	61.3	0.02	17.19	pB
		±12.3	±30.0	±0.01	±8.40	
10:42:00	K	14.3	19.3	0.44	118.93	C
		±7.6	±8.2	±0.20	±73.87	
10:42:00	H	13.5	17.4	0.14	34.17	C
		±23.1	±25.9	±0.20	±70.51	
10:42:00	K	81.8	18.6	0.01	2.61	pB
		±16.7	±45.4	±0.03	±10.10	
10:42:00	K	152.8	115.1	0.02	32.29	pS
		±32.7	±84.7	±0.01	±28.71	
10:42:00	H	150.2	54.9	0.02	15.39	pS
		±19.9	±49.0	±0.02	±20.62	
11:16:00	K	15.3	22.0	0.49	151.41	C
		±1.2	±1.4	±0.03	±13.41	
11:16:00	H	13.2	17.5	0.18	44.06	C
		±5.4	±5.9	±0.06	±21.00	
11:16:00	K	100.8	34.0	0.05	23.83	gB
		±2.4	±9.9	±0.02	±11.78	
11:16:00	H	110.9	25.3	0.03	10.63	pB
		±2.9	±7.3	±0.01	±4.69	
11:16:00	K	146.5	80.8	0.04	45.31	gB
		±13.6	±22.5	±0.01	±12.59	
11:16:00	H	157.2	55.1	0.01	7.72	pB
		±13.1	±32.0	±0.01	±4.49	
1997 April 23						
07:17:00	K	17.3	40.4	0.22	124.58	C
		±0.5	±0.8	±0.01	±2.56	
07:17:00	H	13.2	26.9	0.13	49.01	C
		±1.3	±1.6	±0.01	±4.80	
07:17:00	K	67.9	20.8	0.25	72.97	gS
		±0.2	±0.4	±0.01	±1.47	
07:17:00	H	64.7	21.0	0.18	52.95	gS
		±0.2	±0.6	±0.01	±1.39	

Table 2 (continued)

Date/Time (mid exposure)	CaII	Velocity $km\,s^{-1}$	FWHM $km\,s^{-1}$	Depth	Eq. Wdth mÅ	Classification
07:17:00	K	157.7	70.7	0.02	19.84	pS
		±3.9	±9.4	±0.01	±2.64	
07:17:00	H	157.0	76.2	0.01	10.69	pS
		±5.8	±13.9	±0.01	±1.95	
08:52:00	K	15.3	39.7	0.22	122.45	C
		±0.4	±0.8	±0.01	±6.04	
08:52:00	H	13.4	26.3	0.14	51.64	C
		±1.3	±1.6	±0.01	±4.88	
08:52:00	K	68.3	19.1	0.22	58.94	gS
		±0.2	±0.5	±0.01	±1.42	
08:52:00	H	65.7	18.0	0.14	35.23	gS
		±0.3	±0.6	±0.01	±1.26	
08:52:00	K	154.4	65.7	0.03	27.62	UD
		±2.4	±5.7	±0.01	±2.41	
08:52:00	H	149.4	66.2	0.02	18.57	UD
		±3.8	±9.1	±0.01	±2.54	
09:25:00	K	17.4	34.3	0.27	130.03	C
		±0.5	±0.7	±0.01	±5.52	
09:25:00	H	15.0	27.3	0.14	53.62	C
		±1.4	±1.9	±0.01	±5.40	
09:25:00	K	68.6	19.9	0.22	61.32	gS
		±0.2	±0.5	±0.01	±1.51	
09:25:00	H	66.1	21.9	0.11	33.77	gS
		±0.4	±0.9	±0.01	±1.39	
09:25:00	K	152.9	90.1	0.03	37.90	UD
		±3.0	±7.8	±0.01	±3.28	
09:25:00	H	169.6	65.0	0.02	18.23	UD
		±3.3	±7.8	±0.01	±2.18	
09:58:00	K	20.3	35.5	0.25	124.53	C
		±0.7	±1.2	±0.01	±6.54	
09:58:00	H	16.4	27.3	0.14	53.58	C
		±2.0	±2.9	±0.01	±6.86	
09:58:00	K	70.3	22.4	0.19	59.75	gS
		±0.3	±0.9	±0.01	±3.94	
09:58:00	H	67.5	18.9	0.13	34.37	gS
		±0.4	±1.0	±0.01	±3.22	
09:58:00	K	150.0	109.9	0.03	46.24	UD
		±5.8	±15.3	±0.01	±6.42	
09:58:00	H	152.3	87.2	0.02	24.46	UD
		±5.3	±13.3	±0.01	±3.72	
10:30:00	K	14.8	19.2	0.38	102.34	C
		±4.0	±9.3	±0.17	±67.58	
10:30:00	H	13.5	15.8	0.24	53.26	C
		±6.7	±11.0	±0.12	±45.57	
10:30:00	K	38.1	28.4	0.13	51.73	gB
		±8.7	±21.7	±0.03	±41.31	
10:30:00	H	35.5	24.9	0.05	17.46	gB
		±9.2	±18.1	±0.01	±13.15	
10:30:00	K	71.6	24.3	0.19	64.68	gS
		±1.6	±3.2	±0.01	±9.15	
10:30:00	H	69.4	18.1	0.13	32.97	gS
		±0.7	±1.7	±0.01	±4.06	
10:30:00	K	106.0	19.0	0.05	13.35	gB
		±3.6	±8.7	±0.01	±6.65	
10:30:00	H	106.0	16.4	0.04	9.22	gB
		±1.7	±4.1	±0.01	±3.24	
10:30:00	K	127.9	19.6	0.03	8.24	pB
		±6.2	±14.7	±0.02	±8.26	
10:30:00	H	141.3	29.3	0.04	16.44	UD
		±2.7	±7.7	±0.01	±5.98	

Table 2 (continued)

Date/Time (mid exposure)	CaII	Velocity $km\,s^{-1}$	FWHM $km\,s^{-1}$	Depth	Eq. Wdth mÅ	Classification
10:30:00	K	165.1	66.9	0.04	37.51	UD
		±8.7	±18.1	±0.01	±10.15	
10:30:00	H	189.4	37.4	0.02	10.49	UD
		±5.1	±13.1	±0.01	±6.41	
11:03:00	K	18.0	15.2	0.30	63.93	C
		±1.5	±4.6	±0.03	±20.46	
11:03:00	H	17.5	7.7	0.11	11.89	C
		±2.5	±5.7	±0.02	±9.01	
11:03:00	K	37.1	19.0	0.13	34.65	gB
		±2.3	±4.3	±0.01	±8.21	
11:03:00	H	33.5	33.3	0.07	32.69	gB
		±3.9	±9.1	±0.01	±10.04	
11:03:00	K	69.5	22.1	0.17	52.72	gS
		±0.5	±1.3	±0.01	±4.38	
11:03:00	H	71.2	14.3	0.09	18.06	gS
		±0.7	±1.6	±0.01	±2.86	
11:03:00	K	143.7	97.5	0.03	41.00	UD
		±5.0	±13.2	±0.01	±5.56	
11:03:00	H	153.4	79.8	0.03	33.56	UD
		±4.0	±9.9	±0.01	±4.16	
11:35:00	K	16.1	13.8	0.24	46.30	C
		±4.9	±8.4	±0.14	±39.14	
11:35:00	H	15.3	12.3	0.10	17.22	C
		±13.2	±22.7	±0.16	±42.08	
11:35:00	K	33.9	34.7	0.13	63.23	gB
		±5.8	±13.5	±0.01	±25.15	
11:35:00	H	31.1	33.9	0.08	38.06	gB
		±11.2	±19.6	±0.02	±23.97	
11:35:00	K	71.2	22.6	0.15	47.46	gS
		±1.0	±1.9	±0.01	±5.11	
11:35:00	H	68.4	17.7	0.09	22.35	gS
		±1.1	±2.3	±0.01	±3.80	
11:35:00	K	156.9	91.3	0.03	38.41	UD
		±4.7	±12.2	±0.01	±5.11	
11:35:00	H	146.8	69.3	0.03	29.16	UD
		±4.3	±10.5	±0.01	±4.41	
1997 April 24						
07:15:00	K	22.9	33.2	0.12	55.79	C
		±2.0	±4.5	±0.01	±8.90	
07:15:00	H	22.0	24.2	0.04	13.58	C
		±4.5	±10.0	±0.01	±6.56	
07:15:00	K	70.6	28.3	0.18	71.47	gS
		±0.6	±1.4	±0.01	±5.33	
07:15:00	H	68.1	20.8	0.11	32.03	gS
		±0.7	±1.6	±0.01	±3.82	
07:15:00	K	171.8	53.1	0.04	29.77	gS
		±3.1	±7.2	±0.01	±4.05	
07:15:00	H	162.1	56.7	0.03	23.86	pS
		±4.5	±10.7	±0.01	±4.48	
07:48:00	K	22.3	34.0	0.16	76.18	gB
		±1.6	±3.6	±0.01	±9.39	
07:48:00	H	16.9	18.3	0.06	15.36	C
		±6.7	±10.5	±0.01	±9.22	
07:48:00	K	70.8	29.8	0.20	83.67	gS
		±0.6	±1.5	±0.01	±5.83	
07:48:00	H	68.3	23.4	0.09	29.49	gS
		±0.9	±2.2	±0.01	±4.26	
07:48:00	K	171.6	81.2	0.04	45.51	UD
		±3.7	±9.1	±0.01	±5.13	
07:48:00	H	174.6	63.2	0.03	26.57	UD
		±5.2	±12.2	±0.01	±5.15	

Table 2 (continued)

Date/Time (mid exposure)	CaII	Velocity $km\,s^{-1}$	FWHM $km\,s^{-1}$	Depth	Eq. Wdth mÅ	Classification
08:26:00	K	27.2	30.4	0.13	55.39	gB
		±0.6	±2.0	±0.01	±3.57	
08:26:00	H	23.8	15.0	0.06	12.59	gB
		±0.6	±1.7	±0.01	±1.42	
08:26:00	K	69.3	25.3	0.18	63.80	gS
		±0.3	±0.7	±0.01	±1.79	
08:26:00	H	67.3	23.1	0.10	32.41	gS
		±0.4	±0.9	±0.01	±1.30	
08:26:00	K	165.8	63.6	0.02	17.84	UD
		±2.9	±6.9	±0.01	±1.93	
08:26:00	H	153.2	60.9	0.02	17.07	UD
		±4.0	±9.6	±0.01	±2.68	
08:58:00	K	28.1	29.1	0.14	57.08	gB
		±0.6	±2.0	±0.01	±4.02	
08:58:00	H	24.4	18.4	0.05	12.90	gB
		±1.1	±2.9	±0.01	±3.28	
08:58:00	K	70.4	25.3	0.17	60.23	gS
		±0.4	±0.9	±0.01	±2.17	
08:58:00	H	68.8	21.5	0.10	30.09	gS
		±0.5	±1.1	±0.01	±1.61	
08:58:00	K	162.5	65.0	0.03	27.32	gS
		±2.4	±5.8	±0.01	±2.43	
08:58:00	H	147.1	49.9	0.02	14.00	UD
		±3.0	±7.2	±0.01	±2.01	
09:32:00	K	26.8	34.7	0.13	63.24	gB
		±1.0	±2.8	±0.01	±5.12	
09:32:00	H	27.1	17.1	0.05	11.99	gB
		±0.9	±2.3	±0.01	±2.89	
09:32:00	K	71.6	23.9	0.16	53.50	gS
		±0.4	±0.9	±0.01	±2.06	
09:32:00	H	69.0	19.7	0.09	24.91	gS
		±0.5	±1.2	±0.01	±1.49	
09:32:00	K	168.4	62.7	0.04	35.16	gS
		±2.2	±5.1	±0.01	±2.87	
09:32:00	H	163.6	68.9	0.02	19.33	UD
		±3.7	±8.8	±0.01	±2.47	
10:04:00	K	27.1	38.0	0.13	69.26	gB
		±1.2	±3.5	±0.01	±6.47	
10:04:00	H	23.8	16.9	0.05	11.87	gB
		±1.4	±3.7	±0.01	±3.51	
10:04:00	K	72.6	25.1	0.16	56.30	gS
		±0.5	±1.2	±0.01	±4.46	
10:04:00	H	70.6	21.6	0.10	30.28	gS
		±0.6	±1.4	±0.01	±3.63	
10:04:00	K	167.2	92.4	0.03	38.86	UD
		±3.6	±9.1	±0.01	±3.84	
10:04:00	H	153.9	94.9	0.02	26.60	UD
		±6.7	±17.3	±0.01	±4.85	
1997 April 25						
11:00:00	K	55.1	70.9	0.07	69.63	pB
		±2.0	±7.1	±0.01	±12.16	
11:00:00	H	77.6	57.1	0.04	32.00	pB
		±5.7	±9.5	±0.01	±5.35	
11:00:00	K	53.8	20.0	0.16	44.75	gB
		±0.4	±1.3	±0.01	±3.98	
11:00:00	H	49.7	18.2	0.10	25.49	gB
		±0.6	±2.1	±0.01	±3.89	
11:32:00	K	55.0	23.5	0.25	82.26	gS
		±2.0	±0.7	±0.01	±4.15	
11:32:00	H	51.5	19.9	0.12	33.50	gS
		±0.4	±1.1	±0.01	±3.31	

Table 2 (continued)

Date/Time (mid exposure)	CaII	Velocity $km\,s^{-1}$	FWHM $km\,s^{-1}$	Depth	Eq. Wdth mÅ	Classification
12:04:00	K	59.3	18.0	0.31	78.23	gB
		±1.4	±2.6	±0.04	±15.06	
12:04:00	H	55.8	15.0	0.14	29.42	gB
		±1.7	±6.4	±0.07	±19.41	
12:04:00	K	82.7	35.7	0.09	45.03	pB
		±7.2	±19.1	±0.03	±28.43	
12:04:00	H	77.1	36.3	0.08	40.73	pB
		±12.2	±22.9	±0.02	±27.59	
1997 April 26						
06:43:00	K	13.8	19.7	0.24	66.32	C
		±3.2	±4.1	±0.05	±19.41	
06:43:00	H	14.1	18.2	0.11	28.04	C
		±5.4	±6.5	±0.03	±12.66	
06:43:00	K	56.8	53.7	0.07	52.73	pB
		±2.3	±12.0	±0.01	±11.81	
06:43:00	H	56.5	14.3	0.02	4.02	gB
		±2.3	±5.9	±0.01	±2.61	
06:43:00	K	106.7	30.2	0.05	21.16	gB
		±2.4	±6.0	±0.01	±5.99	
06:43:00	H	114.0	66.3	0.03	27.90	UD
		±3.7	±11.8	±0.01	±4.98	
06:43:00	K	162.6	68.5	0.04	38.44	gB
		±4.9	±11.8	±0.01	±6.59	
06:43:00	H	177.1	23.5	0.03	9.88	pB
		±2.4	±5.9	±0.01	±4.12	
07:15:00	K	15.2	23.1	0.20	64.72	C
		±2.5	±4.0	±0.03	±14.75	
07:15:00	H	15.5	18.2	0.11	28.05	C
		±4.1	±5.8	±0.02	±10.31	
07:15:00	K	62.4	73.2	0.08	82.16	UD
		±3.7	±12.8	±0.01	±17.64	
07:15:00	K	158.1	105.3	0.03	44.29	UD
		±14.7	±27.0	±0.01	±11.34	
07:15:00	H	127.7	109.2	0.02	30.63	UD
		±8.0	±18.1	±0.01	±5.08	
07:47:00	K	−20.5	7.0	0.04	3.93	gS
		±0.8	±2.0	±0.01	±1.50	
07:47:00	H	−21.2	8.1	0.01	1.13	pS
		±3.9	±8.5	±0.01	±1.64	
07:47:00	K	14.6	16.4	0.22	50.71	C
		±3.5	±5.4	±0.08	±24.83	
07:47:00	H	13.9	26.0	0.13	47.44	C
		±3.5	±5.1	±0.02	±11.80	
07:47:00	K	33.8	38.3	0.10	53.68	gB
		±5.5	±10.6	±0.01	±15.84	
07:47:00	H	59.6	30.7	0.01	4.31	pB
		±9.9	±25.1	±0.01	±3.52	
07:47:00	K	92.7	67.2	0.07	65.94	gB
		±3.3	±6.7	±0.01	±6.58	
07:47:00	H	96.7	34.9	0.04	19.56	UD
		±4.3	±8.2	±0.01	±4.62	
08:18:00	K	15.8	14.5	0.24	48.69	C
		±4.8	±6.7	±0.10	±30.33	
08:18:00	H	15.1	18.9	0.15	39.79	C
		±3.4	±6.5	±0.03	±15.78	
08:18:00	K	35.6	39.5	0.08	44.35	pB
		±5.2	±10.6	±0.01	±13.10	
08:18:00	K	96.2	91.9	0.08	103.10	UD
		±4.3	±8.0	±0.01	±8.94	
08:18:00	H	101.7	76.6	0.04	42.95	UD
		±4.8	±10.6	±0.01	±5.93	

Table 2 (continued)

Date/Time (mid exposure)	CaII	Velocity $km\,s^{-1}$	FWHM $km\,s^{-1}$	Depth	Eq. Wdth mÅ	Classification
08:52:00	K	12.2	23.8	0.31	103.53	C
		±4.0	±5.2	±0.06	±30.30	
08:52:00	H	14.9	16.8	0.17	40.04	C
		±3.8	±5.2	±0.03	±14.16	
08:52:00	K	52.9	54.5	0.10	76.42	pB
		±3.9	±9.5	±0.01	±15.38	
08:52:00	H	75.4	65.2	0.03	27.41	UD
		±6.1	±20.5	±0.01	±8.61	
08:52:00	K	119.2	95.2	0.05	66.73	UD
		±9.8	±16.6	±0.01	±17.71	
08:52:00	H	135.9	34.1	0.05	23.92	pB
		±2.9	±6.4	±0.01	±6.58	
08:52:00	K	231.0	6.8	0.02	1.92	gS
		±2.7	±5.9	±0.01	±1.91	
08:52:00	H	234.9	5.5	0.04	3.11	gS
		±1.1	±3.4	±0.02	±2.47	
09:28:00	K	14.8	19.3	0.30	81.30	C
		±3.5	±5.3	±0.06	±27.49	
09:28:00	H	13.7	16.2	0.18	40.78	C
		±6.0	±6.9	±0.07	±23.59	
09:28:00	K	48.2	39.5	0.08	44.36	pB
		±3.7	±14.2	±0.02	±19.41	
09:28:00	H	60.3	13.3	0.04	7.48	gB
		±1.8	±5.1	±0.01	±3.40	
09:28:00	K	97.0	109.1	0.08	122.40	UD
		±13.0	±19.5	±0.01	±26.71	
09:28:00	H	107.7	105.0	0.03	44.16	UD
		±7.8	±17.5	±0.01	±7.36	
10:00:00	K	16.4	16.4	0.22	50.68	C
		±3.4	±5.2	±0.05	±19.87	
10:00:00	H	14.5	17.3	0.14	34.02	C
		±5.2	±6.9	±0.04	±16.65	
10:00:00	K	52.3	44.2	0.10	61.91	gB
		±6.6	±14.9	±0.06	±42.63	
10:00:00	H	54.4	12.3	0.05	8.59	gB
		±1.1	±3.5	±0.01	±2.98	
10:00:00	K	95.6	65.0	0.09	81.99	gB
		±20.4	±33.6	±0.02	±46.17	
10:00:00	H	90.2	81.0	0.05	56.77	UD
		±4.5	±11.5	±0.01	±8.03	
10:00:00	K	178.9	53.0	0.03	22.31	UD
		±8.4	±16.8	±0.01	±7.05	
10:00:00	H	171.4	22.2	0.02	6.22	UD
		±3.8	±9.3	±0.01	±4.06	
10:33:00	K	16.2	21.5	0.22	66.22	C
		±2.7	±4.7	±0.03	±16.95	
10:33:00	H	13.8	18.5	0.19	49.15	C
		±4.2	±5.0	±0.04	±16.93	
10:33:00	K	94.9	69.9	0.10	98.07	gB
		±18.7	±50.0	±0.03	±76.09	
10:33:00	K	54.9	40.0	0.10	56.09	gB
		±5.5	±14.4	±0.10	±59.59	
10:33:00	H	50.9	5.7	0.02	1.61	UD
		±1.7	±3.6	±0.01	±1.29	
10:33:00	K	234.2	6.3	0.02	1.78	pS
		±2.4	±6.0	±0.01	±1.90	
10:33:00	H	235.1	8.1	0.02	2.27	gS
		±1.8	±4.3	±0.01	±1.66	
11:06:00	K	16.3	18.2	0.18	45.98	C
		±3.7	±5.4	±0.03	±15.61	

Table 2 (continued)

Date/Time (mid exposure)	CaII	Velocity $km\,s^{-1}$	FWHM $km\,s^{-1}$	Depth	Eq. Wdth mÅ	Classification
11:06:00	H	12.1	13.7	0.17	32.72	C
		±16.5	±13.9	±0.31	±68.25	
11:06:00	K	65.0	63.0	0.12	105.96	pB
		±5.2	±10.9	±0.05	±47.82	
11:06:00	H	73.5	48.0	0.07	47.12	pB
		±3.1	±6.5	±0.01	±9.28	
11:06:00	K	116.3	101.3	0.07	99.46	pB
		±29.2	±32.3	±0.02	±42.58	
11:06:00	H	134.4	55.7	0.04	31.25	UD
		±5.7	±12.0	±0.01	±6.74	
11:38:00	K	76.3	88.7	0.16	199.02	pB
		±1.9	±5.2	±0.01	±11.57	
11:38:00	H	48.1	13.9	0.04	7.82	gB
		±1.7	±5.4	±0.01	±3.61	
11:38:00	H	71.9	12.5	0.10	17.55	gB
		±0.7	±1.9	±0.01	±3.20	
11:38:00	H	101.6	23.3	0.07	22.87	gB
		±1.4	±4.3	±0.01	±5.34	
11:38:00	K	166.6	61.7	0.04	34.61	pB
		±6.5	±13.2	±0.01	±11.38	
11:38:00	H	171.3	43.0	0.03	18.06	UD
		±5.4	±12.5	±0.01	±8.00	
1997 April 27						
06:49:00	K	50.1	18.5	0.12	31.16	gB
		±0.6	±2.0	±0.02	±6.18	
06:49:00	H	50.2	13.9	0.06	11.69	pB
		±0.8	±2.6	±0.01	±2.95	
06:49:00	K	77.8	48.8	0.17	116.33	gB
		±1.7	±3.1	±0.01	±7.39	
06:49:00	H	77.6	44.4	0.10	62.19	pB
		±1.7	±3.7	±0.01	±5.16	
06:49:00	K	−19.1	6.6	0.02	1.85	gS
		±1.4	±2.8	±0.01	±1.22	
07:21:00	K	54.3	15.3	0.09	19.29	gB
		±0.6	±1.6	±0.01	±2.96	
07:21:00	H	52.6	15.7	0.07	15.45	gB
		±0.7	±2.3	±0.01	±3.19	
07:21:00	K	70.2	79.4	0.15	167.06	gB
		±1.0	±2.2	±0.01	±4.52	
07:21:00	H	87.2	55.4	0.08	62.17	gB
		±2.1	±4.8	±0.01	±5.38	
07:53:00	K	52.8	15.8	0.11	24.43	gB
		±0.3	±0.9	±0.01	±1.34	
07:53:00	H	51.1	22.0	0.06	18.55	gB
		±0.6	±2.4	±0.01	±3.71	
07:53:00	K	66.6	69.5	0.15	146.22	gB
		±0.6	±1.3	±0.01	±2.73	
07:53:00	H	82.6	64.1	0.07	62.86	gB
		±2.5	±4.1	±0.01	±4.06	
07:53:00	K	−20.8	7.4	0.03	3.13	gS
		±0.7	±1.7	±0.01	±1.27	
08:24:00	K	−19.7	6.7	0.03	2.83	pS
		±0.9	±2.0	±0.01	±1.26	
08:24:00	K	56.1	16.7	0.13	30.47	gB
		±0.3	±0.9	±0.01	±2.83	
08:24:00	H	52.8	18.2	0.09	22.99	gB
		±0.4	±1.3	±0.01	±3.05	
08:24:00	K	66.4	73.1	0.15	153.79	gB
		±0.6	±1.7	±0.01	±3.53	
08:24:00	H	84.2	71.2	0.07	69.92	gB
		±2.0	±3.5	±0.01	±3.46	

Table 2 (continued)

Date/Time (mid exposure)	CaII	Velocity $km\,s^{-1}$	FWHM $km\,s^{-1}$	Depth	Eq. Wdth mÅ	Classification
08:57:00	K	61.0	28.5	0.13	51.96	gB
		±0.5	±1.8	±0.01	±5.11	
08:57:00	H	58.0	28.3	0.09	35.73	gB
		±0.7	±2.8	±0.01	±5.27	
08:57:00	K	61.9	86.0	0.12	144.65	gB
		±1.0	±3.7	±0.01	±13.55	
08:57:00	H	88.9	72.5	0.06	60.95	gB
		±4.8	±6.2	±0.01	±5.21	
09:29:00	K	−19.2	8.9	0.03	3.72	gB
		±1.3	±3.0	±0.01	±1.77	
09:29:00	K	64.6	64.3	0.22	198.39	pB
		±0.5	±1.3	±0.01	±3.95	
09:29:00	H	73.0	59.3	0.10	83.18	pB
		±1.4	±2.6	±0.01	±3.69	
09:29:00	K	54.2	10.1	0.07	9.88	gB
		±0.6	±1.7	±0.01	±2.17	
09:29:00	H	53.3	13.9	0.07	13.62	gB
		±0.7	±2.0	±0.01	±2.79	
10:02:00	K	55.0	9.0	0.08	10.14	gB
		±0.4	±1.1	±0.01	±1.76	
10:02:00	H	54.6	18.3	0.05	12.82	gB
		±1.1	±3.4	±0.01	±3.52	
10:02:00	K	61.1	71.1	0.23	229.37	pB
		±0.4	±1.2	±0.01	±3.97	
10:02:00	H	67.6	56.8	0.11	87.67	gB
		±1.3	±2.2	±0.01	±8.66	
10:33:00	K	56.1	9.6	0.06	8.06	gB
		±0.6	±1.5	±0.01	±1.87	
10:33:00	H	51.3	13.2	0.05	9.26	gB
		±0.8	±2.2	±0.01	±2.43	
10:33:00	K	60.6	76.4	0.24	256.94	pB
		±0.4	±1.2	±0.01	±3.94	
10:33:00	H	69.3	65.4	0.11	100.84	gB
		±1.1	±2.0	±0.01	±3.08	
11:06:00	K	12.8	41.1	0.10	57.66	C
		±2.5	±4.2	±0.01	±8.24	
11:06:00	H	22.0	14.4	0.05	10.12	pB
		±1.0	±3.0	±0.01	±2.92	
11:06:00	K	53.3	8.8	0.09	11.07	pB
		±0.3	±1.0	±0.01	±1.78	
11:06:00	H	57.6	33.0	0.11	50.94	pB
		±1.4	±4.6	±0.04	±19.81	
11:06:00	K	66.9	69.8	0.22	215.20	gB
		±1.9	±2.9	±0.01	±9.04	
11:06:00	H	87.7	56.2	0.07	55.12	UD
		±11.2	±13.2	±0.01	±15.18	
11:37:00	K	32.4	6.1	0.04	3.44	gB
		±0.6	±2.6	±0.01	±1.68	
11:37:00	H	26.0	17.3	0.08	19.37	gB
		±0.9	±2.6	±0.01	±3.79	
11:37:00	K	55.9	9.3	0.06	7.81	gB
		±0.6	±1.6	±0.01	±1.86	
11:37:00	H	52.8	22.0	0.14	43.24	gB
		±0.8	±2.7	±0.01	±6.10	
11:37:00	K	57.5	82.6	0.22	254.86	UD
		±0.7	±1.6	±0.01	±4.90	
11:37:00	H	80.9	23.4	0.11	36.01	gB
		±1.2	±4.3	±0.01	±7.38	
11:37:00	K	111.4	4.7	0.04	2.65	pB
		±1.0	±4.1	±0.03	±3.05	

Table 2 (continued)

Date/Time (mid exposure)	CaII	Velocity $km\,s^{-1}$	FWHM $km\,s^{-1}$	Depth	Eq. Wdth mÅ	Classification
11:37:00	H	109.9	30.0	0.06	25.24	pB
		±3.5	±6.2	±0.01	±6.72	
1997 April 28						
09:59:00	K	16.8	24.6	0.38	131.17	C
		±1.3	±2.6	±0.02	±15.29	
09:59:00	H	13.7	18.7	0.25	65.44	C
		±4.2	±5.3	±0.05	±22.75	
09:59:00	K	50.1	30.1	0.23	97.00	gB
		±1.0	±2.1	±0.01	±8.06	
09:59:00	H	50.7	25.1	0.13	45.75	gB
		±0.8	±2.0	±0.01	±5.03	
09:59:00	K	136.3	79.2	0.11	122.22	gB
		±1.8	±5.1	±0.01	±7.80	
09:59:00	H	135.3	48.9	0.06	41.14	gB
		±2.5	±6.6	±0.01	±8.83	
09:59:00	K	185.0	12.6	0.02	3.53	gB
		±3.4	±9.4	±0.01	±3.18	
09:59:00	H	185.7	25.4	0.03	10.67	gB
		±3.4	±8.0	±0.01	±4.89	
10:31:00	K	16.5	21.8	0.37	112.83	C
		±2.4	±4.2	±0.03	±23.63	
10:31:00	H	14.6	19.2	0.22	59.16	C
		±4.9	±6.8	±0.05	±25.02	
10:31:00	K	50.6	29.0	0.22	89.39	gB
		±1.0	±2.4	±0.01	±8.44	
10:31:00	H	50.7	30.0	0.12	50.51	gB
		±1.4	±3.7	±0.01	±7.46	
10:31:00	K	144.3	81.9	0.07	80.40	UD
		±3.0	±8.2	±0.01	±14.02	
10:31:00	H	124.9	50.0	0.04	28.06	UD
		±16.3	±24.7	±0.02	±19.70	
10:31:00	H	177.7	59.9	0.03	25.19	UD
		±26.3	±39.8	±0.01	±18.71	
11:03:00	K	15.7	23.8	0.36	120.12	C
		±1.3	±2.0	±0.02	±12.27	
11:03:00	H	13.9	19.7	0.21	58.06	C
		±4.0	±5.3	±0.04	±19.20	
11:03:00	K	51.3	27.9	0.23	90.03	gB
		±0.6	±1.4	±0.01	±6.07	
11:03:00	H	48.2	22.2	0.13	40.48	gB
		±0.7	±1.7	±0.01	±4.44	
11:03:00	K	144.5	106.4	0.06	89.53	UD
		±3.1	±8.2	±0.01	±6.88	
11:03:00	H	159.4	102.2	0.03	42.99	UD
		±6.2	±15.2	±0.01	±6.39	
11:35:00	K	16.8	23.0	0.34	109.64	C
		±1.6	±2.4	±0.02	±13.05	
11:35:00	H	12.1	20.0	0.21	58.94	C
		±3.8	±5.1	±0.04	±18.70	
11:35:00	K	53.1	19.6	0.25	68.66	gB
		±0.3	±0.8	±0.01	±3.93	
11:35:00	H	49.5	22.0	0.14	43.08	gB
		±0.6	±1.5	±0.01	±4.25	
11:35:00	K	105.2	29.5	0.06	24.82	pB
		±1.8	±4.9	±0.01	±5.83	
11:35:00	H	112.3	17.1	0.03	7.19	pB
		±2.3	±5.7	±0.01	±3.39	
11:35:00	K	163.2	77.3	0.04	43.33	UD
		±5.4	±13.0	±0.01	±7.31	
11:35:00	H	174.8	66.1	0.03	27.82	UD
		±6.4	±16.5	±0.01	±6.94	

Table 2 (continued)

Date/Time (mid exposure)	CaII	Velocity km s^{-1}	FWHM km s^{-1}	Depth	Eq. Wdth mÅ	Classification
1997 May 28						
07:53:16	K	4.4	36.8	0.29	149.74	C
		±1.0	±2.1	±0.02	±13.45	
07:53:16	H	−1.0	38.2	0.16	85.76	C
		±2.4	±3.3	±0.02	±13.00	
07:53:16	K	33.0	16.9	0.41	97.32	gB
		±0.2	±0.6	±0.01	±4.09	
07:53:16	H	29.0	16.5	0.29	67.04	gB
		±0.4	±1.0	±0.02	±6.10	
08:30:00	K	−14.4	17.4	0.15	36.63	C
		±1.0	±2.2	±0.01	±5.29	
08:30:00	H	−2.2	37.5	0.16	84.21	C
		±3.2	±4.2	±0.02	±14.13	
08:30:00	K	32.0	23.6	0.44	145.34	gS
		±0.2	±0.5	±0.01	±4.56	
08:30:00	H	28.4	15.5	0.29	62.86	gS
		±0.5	±1.2	±0.02	±6.44	
09:01:50	K	−0.5	39.2	0.24	132.00	C
		±1.1	±1.6	±0.01	±7.60	
09:01:50	H	−1.4	39.9	0.14	78.36	C
		±2.5	±3.2	±0.01	±8.38	
09:01:50	K	31.0	16.7	0.43	100.80	gS
		±0.2	±0.5	±0.01	±3.63	
09:01:50	H	28.5	16.4	0.31	71.28	gS
		±0.3	±0.8	±0.02	±5.69	
09:33:30	K	33.5	15.1	0.35	73.95	gS
		±0.2	±0.6	±0.01	±3.62	
09:33:30	H	28.7	17.1	0.30	71.84	gS
		±0.4	±1.2	±0.02	±6.84	
09:33:30	K	5.1	43.6	0.31	189.36	C
		±0.8	±1.6	±0.01	±9.39	
09:33:30	H	−1.6	45.3	0.13	82.55	C
		±4.0	±4.7	±0.02	±15.34	
1997 May 29						
06:51:30	K	19.3	48.8	0.33	225.87	gB
		±1.9	±2.1	±0.02	±16.79	
06:51:30	H	21.0	26.7	0.15	56.19	gB
		±1.2	±3.4	±0.01	±8.15	
06:51:30	K	69.2	64.4	0.08	72.29	gB
		±9.8	±19.0	±0.01	±23.16	
06:51:30	H	47.6	71.0	0.10	99.54	gB
		±4.6	±6.1	±0.01	±13.16	
06:51:30	K	164.2	81.0	0.02	22.72	UD
		±12.4	±26.7	±0.01	±7.48	
06:51:30	H	137.6	102.7	0.01	14.39	UD
		±28.9	±52.3	±0.01	±7.34	
07:33:02	K	21.9	59.7	0.30	251.22	gS
		±0.3	±0.9	±0.01	±3.83	
07:33:02	H	17.0	37.9	0.14	74.47	gB
		±1.1	±2.9	±0.01	±7.80	
07:33:02	H	42.7	76.2	0.09	96.21	gB
		±3.8	±3.5	±0.01	±11.55	
07:59:08	K	11.0	46.8	0.23	150.88	C
		±4.9	±4.4	±0.06	±41.80	
07:59:08	H	17.0	46.0	0.17	109.64	C
		±5.3	±5.7	±0.02	±18.77	
07:59:08	K	45.2	53.0	0.17	126.22	gB
		±8.8	±7.6	±0.05	±41.33	
07:59:08	H	54.9	42.0	0.10	58.95	gB
		±7.0	±8.5	±0.03	±21.35	

Table 2 (continued)

Date/Time (mid exposure)	CaII	Velocity $km\,s^{-1}$	FWHM $km\,s^{-1}$	Depth	Eq. Wdth mÅ	Classification
07:59:08	K	171.6	50.5	0.02	14.17	UD
		±4.4	±11.1	±0.01	±3.10	
07:59:08	H	147.7	60.8	0.01	8.52	UD
		±9.8	±25.6	±0.01	±3.59	
08:37:22	K	18.1	52.1	0.32	233.70	C
		±1.9	±2.3	±0.01	±12.72	
08:37:22	H	18.0	52.8	0.20	147.97	C
		±2.7	±4.0	±0.01	±13.44	
08:37:22	K	53.1	20.6	0.08	23.16	gB
		±0.9	±3.9	±0.03	±9.74	
08:37:22	H	56.2	31.6	0.07	30.99	pB
		±2.7	±8.7	±0.04	±19.65	
08:37:22	K	71.2	52.4	0.07	51.44	pB
		±12.7	±15.1	±0.02	±20.84	
08:37:22	H	86.6	59.4	0.03	24.98	pB
		±30.4	±39.9	±0.01	±18.73	
08:37:22	K	176.3	62.7	0.01	8.80	UD
		±5.4	±13.8	±0.01	±1.93	
08:37:22	H	172.1	33.5	0.01	4.69	UD
		±7.2	±17.5	±0.01	±2.45	
09:14:54	K	11.8	43.9	0.28	172.37	C
		±3.0	±3.6	±0.07	±45.38	
09:14:54	H	18.5	49.6	0.21	145.94	C
		±2.2	±3.2	±0.01	±9.27	
09:14:54	K	47.3	59.4	0.18	149.80	gB
		±9.9	±11.4	±0.04	±43.92	
09:14:54	H	62.1	37.4	0.09	47.19	pB
		±2.8	±4.9	±0.01	±8.16	
09:14:54	K	151.1	105.0	0.02	29.44	UD
		±8.8	±19.9	±0.01	±5.57	
09:14:54	H	124.9	45.5	0.02	12.76	UD
		±3.6	±9.2	±0.01	±2.58	
09:51:36	K	19.2	55.4	0.31	240.87	C
		±1.8	±2.9	±0.01	±14.70	
09:51:36	H	22.1	60.1	0.19	159.99	C
		±1.9	±3.3	±0.01	±12.19	
09:51:36	K	63.5	34.9	0.08	39.18	pB
		±9.2	±6.2	±0.02	±12.01	
09:51:36	H	66.6	27.7	0.07	27.19	pB
		±1.6	±4.4	±0.01	±5.83	
1997 June 13						
06:15:20	K	5.1	22.0	0.43	132.63	C
		±0.6	±2.3	±0.13	±42.49	
06:15:20	H	−0.2	21.6	0.16	48.41	C
		±1.4	±4.0	±0.09	±28.68	
06:15:20	K	42.3	28.1	0.24	94.69	gS
		±0.6	±3.2	±0.05	±22.47	
06:15:20	H	42.3	29.7	0.13	54.13	gS
		±0.9	±3.0	±0.01	±6.83	
06:15:20	K	73.2	59.6	0.06	50.17	pB
		±15.7	±30.6	±0.01	±27.10	
06:48:18	K	4.7	22.2	0.46	143.30	C
		±0.5	±2.3	±0.11	±37.37	
06:48:18	H	−2.8	22.3	0.13	40.72	C
		±2.1	±2.9	±0.04	±13.60	
06:48:18	K	42.5	29.6	0.23	95.38	gS
		±0.7	±3.4	±0.05	±23.43	
06:48:18	H	43.7	35.0	0.13	63.85	gS
		±0.7	±2.0	±0.01	±6.11	
06:48:18	K	74.7	66.1	0.06	55.64	pB
		±22.5	±42.6	±0.02	±40.33	

Table 2 (continued)

Date/Time (mid exposure)	CaII	Velocity $km\,s^{-1}$	FWHM $km\,s^{-1}$	Depth	Eq. Wdth mÅ	Classification
06:48:18	H	104.5	28.2	0.02	7.90	pS
		±3.8	±9.2	±0.01	±4.72	
06:48:18	K	170.4	88.3	0.02	24.76	UD
		±14.3	±27.6	±0.01	±7.73	
07:21:31	K	42.7	29.2	0.23	94.22	gS
		±0.4	±1.1	±0.01	±5.48	
07:21:31	H	41.7	29.4	0.14	57.63	gS
		±0.5	±1.2	±0.01	±2.41	
07:21:31	K	2.0	25.5	0.29	103.84	C
		±0.5	±1.6	±0.04	±15.76	
07:21:31	H	−13.0	10.3	0.10	14.45	C
		±1.7	±3.0	±0.01	±4.46	
07:21:31	K	103.2	127.6	0.03	53.67	UD
		±9.4	±18.9	±0.01	±7.95	
07:21:31	H	122.6	73.4	0.02	20.59	UD
		±5.1	±13.0	±0.01	±3.65	
07:54:50	K	43.4	29.6	0.23	95.58	gS
		±0.6	±1.7	±0.01	±6.80	
07:54:50	H	42.1	28.2	0.15	59.22	gS
		±0.5	±1.1	±0.01	±2.38	
07:54:50	K	1.7	23.9	0.35	117.23	C
		±0.5	±1.4	±0.05	±18.01	
07:54:50	H	−12.6	12.1	0.12	20.39	C
		±1.8	±3.0	±0.01	±5.29	
07:54:50	K	83.9	49.9	0.03	20.98	gB
		±8.9	±21.7	±0.01	±9.14	
07:54:50	H	121.0	58.3	0.02	16.35	UD
		±5.7	±15.5	±0.01	±4.34	
07:54:50	K	173.2	72.3	0.02	20.27	UD
		±5.5	±14.1	±0.01	±3.96	
07:54:50	H	187.9	27.0	0.02	7.58	UD
		±3.2	±7.8	±0.01	±2.17	
08:27:58	K	38.7	36.6	0.21	107.70	gS
		±0.5	±1.6	±0.01	±6.88	
08:27:58	H	39.9	28.4	0.12	47.85	gS
		±0.5	±1.3	±0.01	±2.14	
08:27:58	K	−10.9	10.2	0.16	22.86	C
		±1.9	±3.9	±0.01	±8.84	
08:27:58	H	−8.6	17.0	0.21	50.05	C
		±4.4	±4.9	±0.06	±20.31	
08:27:58	K	−26.5	10.8	0.03	4.53	gB
		±2.2	±5.0	±0.01	±2.60	
08:27:58	K	98.0	73.9	0.03	31.10	UD
		±7.9	±25.9	±0.01	±10.91	
08:27:58	H	117.3	30.9	0.02	8.66	UD
		±3.6	±8.4	±0.01	±2.36	
08:27:58	K	181.5	42.3	0.03	17.80	gS
		±3.5	±8.1	±0.01	±3.39	
08:27:58	H	198.8	28.4	0.02	7.97	UD
		±3.0	±6.9	±0.01	±1.95	
09:03:01	K	3.9	23.8	0.42	140.38	C
		±0.9	±3.7	±0.15	±54.74	
09:03:01	H	−1.8	23.6	0.22	72.88	C
		±2.4	±4.1	±0.09	±32.36	
09:03:01	K	42.4	31.7	0.24	106.80	gB
		±1.1	±2.7	±0.01	±10.06	
09:03:01	H	38.5	29.3	0.11	45.22	pB
		±1.9	±4.9	±0.01	±8.66	
09:03:01	K	109.3	30.6	0.03	12.87	UD
		±4.7	±11.3	±0.01	±6.40	

Table 2 (continued)

Date/Time (mid exposure)	CaII	Velocity $km\,s^{-1}$	FWHM $km\,s^{-1}$	Depth	Eq. Wdth mÅ	Classification
09:03:01	K	168.8	35.5	0.04	19.89	UD
		±4.7	±11.4	±0.01	±8.09	
18:46:33	K	−9.7	21.1	0.36	106.65	C
		±1.4	±1.9	±0.02	±11.19	
18:46:33	H	−14.7	17.5	0.25	61.48	C
		±0.8	±1.5	±0.01	±5.74	
18:46:33	K	41.5	44.3	0.18	111.85	gS
		±0.7	±1.7	±0.01	±4.39	
18:46:33	H	39.8	41.1	0.09	51.85	gS
		±1.2	±3.2	±0.01	±3.97	
1997 June 14						
06:27:15	K	4.8	23.8	0.60	200.54	C
		±0.5	±1.5	±0.10	±35.82	
06:27:15	H	0.3	29.3	0.25	102.66	C
		±0.6	±2.1	±0.03	±14.37	
06:27:15	K	36.6	22.8	0.13	41.57	gB
		±1.5	±5.4	±0.01	±10.38	
06:27:15	H	35.0	15.9	0.05	11.16	gB
		±1.8	±4.8	±0.01	±4.04	
06:27:15	K	63.5	24.1	0.09	30.41	gB
		±2.7	±5.6	±0.01	±7.84	
06:27:15	H	62.8	29.0	0.04	16.29	pB
		±3.1	±7.9	±0.01	±6.02	
06:27:15	K	102.4	23.4	0.05	16.43	gS
		±1.8	±5.6	±0.01	±5.13	
06:27:15	H	104.0	9.5	0.01	1.33	gS
		±5.1	±12.9	±0.01	±2.24	
06:27:15	K	155.0	80.8	0.03	33.98	UD
		±7.1	±16.8	±0.01	±7.08	
06:27:15	H	151.2	63.0	0.02	17.67	UD
		±5.9	±15.4	±0.01	±4.33	
07:00:35	K	3.7	26.4	0.58	215.00	C
		±1.0	±1.5	±0.06	±25.25	
07:00:35	H	−2.7	28.2	0.21	83.17	C
		±4.6	±4.5	±0.11	±45.50	
07:00:35	K	37.1	39.2	0.16	87.98	pB
		±2.8	±16.1	±0.01	±36.55	
07:00:35	H	30.5	41.0	0.07	40.29	pB
		±17.7	±53.1	±0.01	±52.43	
07:00:35	K	66.6	18.9	0.06	15.92	gB
		±2.5	±6.8	±0.04	±12.07	
07:00:35	H	64.8	20.3	0.03	8.54	gB
		±4.9	±13.6	±0.03	±10.29	
07:00:35	K	106.5	34.9	0.05	24.49	gB
		±2.5	±6.8	±0.01	±6.81	
07:00:35	H	124.2	34.9	0.03	14.69	UD
		±5.7	±10.4	±0.01	±6.58	
07:00:35	K	163.0	60.8	0.03	25.56	UD
		±5.4	±12.6	±0.01	±5.31	
07:00:35	H	168.8	46.5	0.02	13.03	UD
		±9.8	±19.6	±0.01	±5.49	
07:34:20	K	4.2	27.2	0.62	236.69	C
		±0.7	±1.4	±0.05	±22.59	
07:34:20	H	0.9	32.8	0.27	124.08	C
		±0.6	±1.9	±0.02	±11.69	
07:34:20	K	38.7	30.5	0.18	76.94	gB
		±1.3	±6.1	±0.01	±15.95	
07:34:20	H	33.8	15.3	0.06	12.88	pB
		±1.5	±4.3	±0.01	±4.24	
07:34:20	K	65.2	16.9	0.07	16.61	gB
		±1.9	±4.5	±0.02	±6.49	

Table 2 (continued)

Date/Time (mid exposure)	CaII	Velocity $km\,s^{-1}$	FWHM $km\,s^{-1}$	Depth	Eq. Wdth mÅ	Classification
07:34:20	H	56.3	19.0	0.05	13.32	pB
		±1.8	±4.3	±0.01	±4.02	
07:34:20	K	103.7	56.7	0.05	39.73	UD
		±4.7	±19.5	±0.01	±13.68	
07:34:20	H	119.8	22.5	0.03	9.46	pB
		±3.0	±7.1	±0.01	±4.33	
07:34:20	K	174.2	59.8	0.03	25.17	UD
		±8.8	±17.1	±0.01	±7.19	
07:34:20	H	164.6	47.1	0.03	19.82	UD
		±5.0	±12.9	±0.01	±5.42	
1997 June 18						
06:40:34	K	62.0	69.0	0.07	67.73	pB
		±2.6	±7.3	±0.01	±7.18	
06:40:34	H	62.3	11.8	0.04	6.60	gS
		±1.1	±2.6	±0.01	±2.19	
06:40:34	K	156.2	75.0	0.02	21.02	UD
		±7.4	±17.2	±0.01	±4.81	
06:40:34	H	160.0	77.9	0.01	10.92	UD
		±9.1	±23.5	±0.01	±3.30	
07:13:32	K	43.2	12.5	0.06	10.52	gB
		±1.1	±2.6	±0.01	±2.80	
07:13:32	K	68.9	27.5	0.06	23.11	pB
		±2.2	±6.9	±0.01	±7.00	
07:13:32	H	69.9	23.8	0.03	10.02	pB
		±2.5	±6.4	±0.01	±4.30	
07:13:32	K	111.7	43.4	0.03	18.25	UD
		±4.8	±11.5	±0.01	±7.77	
07:13:32	H	115.7	31.6	0.03	13.30	UD
		±3.5	±8.9	±0.01	±5.80	
07:13:32	K	182.5	19.6	0.03	8.25	pS
		±2.3	±5.4	±0.01	±3.58	
07:13:32	H	181.3	23.0	0.02	6.45	pS
		±3.3	±7.8	±0.01	±3.89	
07:46:22	K	43.5	16.5	0.06	13.85	gS
		±0.8	±1.8	±0.01	±2.77	
07:46:22	H	42.5	9.8	0.04	5.48	pS
		±0.9	±2.1	±0.01	±1.79	
07:46:22	K	73.6	10.6	0.05	7.43	pS
		±0.7	±1.6	±0.01	±1.88	
07:46:22	H	71.5	8.7	0.04	4.86	pS
		±0.7	±1.7	±0.01	±1.54	
07:46:22	K	99.8	22.0	0.04	12.31	pS
		±1.5	±3.7	±0.01	±3.71	
07:46:22	H	101.5	21.4	0.03	9.01	pS
		±1.7	±4.1	±0.01	±3.46	
07:46:22	K	163.1	37.7	0.02	10.57	UD
		±2.7	±6.4	±0.01	±1.79	
07:46:22	H	160.1	32.5	0.02	9.10	UD
		±2.6	±6.2	±0.01	±1.73	
08:21:39	K	−17.2	10.7	0.04	5.98	gS
		±1.0	±2.5	±0.01	±2.05	
08:21:39	K	47.2	25.9	0.05	18.16	pS
		±1.0	±2.4	±0.01	±1.69	
17:25:00	K	−17.6	29.2	0.03	12.28	UD
		±3.2	±7.3	±0.01	±3.07	
17:25:00	K	47.7	16.3	0.15	34.34	gS
		±0.2	±0.6	±0.01	±1.22	
17:25:00	H	45.8	13.9	0.06	11.70	pS
		±0.5	±1.2	±0.01	±1.02	
17:59:16	K	48.3	15.4	0.12	25.86	gS
		±0.3	±0.7	±0.01	±1.19	

Table 2 (continued)

Date/Time (mid exposure)	CaII	Velocity $km\,s^{-1}$	FWHM $km\,s^{-1}$	Depth	Eq. Wdth mÅ	Classification
17:59:16	H	45.9	13.6	0.05	9.53	gS
		±0.6	±1.5	±0.01	±2.17	
17:59:16	K	165.3	9.4	0.02	2.65	gS
		±1.6	±3.7	±0.01	±1.68	
18:32:02	K	46.3	14.0	0.10	19.60	gS
		±0.5	±1.2	±0.01	±2.57	
18:32:02	H	45.0	11.4	0.05	7.97	gS
		±0.9	±2.1	±0.01	±2.17	
19:04:46	K	46.5	14.8	0.10	20.78	gS
		±0.3	±0.8	±0.01	±1.08	
19:04:46	H	44.6	13.3	0.05	9.30	gS
		±0.7	±1.6	±0.01	±1.11	
19:04:46	K	−32.2	8.1	0.02	2.27	gS
		±1.5	±3.5	±0.01	±1.51	
1997 June 25						
06:20:53	K	−13.3	14.0	0.08	15.70	C
		±1.1	±2.3	±0.01	±3.28	
06:20:53	H	−23.1	25.8	0.03	10.86	C
		±2.6	±6.9	±0.01	±2.90	
06:20:53	K	175.5	25.0	0.02	7.00	gS
		±3.1	±7.3	±0.01	±2.04	
06:20:53	H	158.4	31.9	0.01	4.48	UD
		±4.9	±11.4	±0.01	±1.61	
06:54:43	K	−14.3	13.1	0.08	14.69	C
		±0.8	±1.9	±0.01	±2.78	
06:54:43	H	−18.9	11.9	0.06	9.98	C
		±0.6	±1.5	±0.01	±2.07	
06:54:43	K	164.6	9.2	0.03	3.89	pS
		±1.1	±2.6	±0.01	±1.69	
06:54:43	H	161.5	45.2	0.01	6.33	UD
		±5.5	±13.0	±0.01	±1.83	
07:27:35	K	−10.1	24.1	0.10	33.77	C
		±3.0	±4.3	±0.01	±6.86	
07:27:35	H	−19.2	15.8	0.05	11.08	C
		±1.0	±2.6	±0.01	±2.88	
08:00:42	K	−12.9	12.6	0.10	17.68	C
		±1.1	±2.4	±0.01	±3.83	
08:00:42	H	−18.4	21.2	0.05	14.88	C
		±1.9	±4.6	±0.01	±4.39	
1997 June 26						
06:00:08	K	−9.4	15.6	0.18	39.39	C
		±1.5	±2.0	±0.01	±5.59	
06:00:08	H	−15.9	12.5	0.10	17.50	C
		±0.5	±1.2	±0.01	±1.64	
06:00:08	K	33.3	24.6	0.19	65.64	gS
		±0.2	±0.6	±0.01	±1.54	
06:00:08	H	30.9	22.1	0.11	34.04	gS
		±0.4	±0.9	±0.01	±1.43	
06:32:52	K	−0.9	27.5	0.23	88.55	C
		±0.8	±1.1	±0.02	±8.49	
06:32:52	H	−15.6	10.0	0.09	12.66	C
		±0.4	±1.1	±0.01	±1.96	
06:32:52	K	35.4	24.3	0.23	78.23	gS
		±0.3	±0.8	±0.01	±2.45	
06:32:52	H	32.2	21.5	0.11	33.22	gS
		±0.3	±0.9	±0.01	±1.31	
06:32:52	K	64.6	19.2	0.02	5.40	gS
		±2.4	±5.8	±0.01	±1.64	
07:06:23	K	−0.1	29.1	0.20	81.74	C
		±0.8	±1.2	±0.01	±5.38	

Table 2 (continued)

Date/Time (mid exposure)	CaII	Velocity $km\,s^{-1}$	FWHM $km\,s^{-1}$	Depth	Eq. Wdth mÅ	Classification
07:06:23	H	−15.9	10.9	0.10	15.35	C
		±0.3	±0.9	±0.01	±1.32	
07:06:23	K	35.4	26.7	0.22	82.42	gB
		±0.4	±0.9	±0.01	±2.65	
07:06:23	H	31.1	25.7	0.14	50.50	gS
		±0.3	±0.8	±0.01	±1.55	
07:06:23	K	178.6	32.6	0.02	9.14	UD
		±2.9	±6.7	±0.01	±1.89	
07:06:23	H	181.9	18.9	0.02	5.31	pS
		±1.6	±3.8	±0.01	±1.07	
07:39:48	K	1.5	32.2	0.24	108.21	C
		±0.7	±1.4	±0.01	±6.47	
07:39:48	H	−14.7	18.7	0.07	18.36	C
		±1.6	±3.0	±0.01	±2.96	
07:39:48	K	37.5	27.2	0.23	87.68	gB
		±0.5	±0.9	±0.01	±2.97	
07:39:48	H	32.1	26.1	0.16	58.59	gS
		±0.3	±0.8	±0.01	±1.70	
08:19:56	K	6.9	44.8	0.20	125.70	C
		±1.5	±3.0	±0.01	±10.39	
08:19:56	H	2.6	44.5	0.13	81.14	C
		±1.7	±3.7	±0.01	±9.23	
08:19:56	K	40.4	24.0	0.23	77.52	gB
		±0.5	±1.0	±0.01	±4.73	
08:19:56	H	36.8	21.0	0.15	44.16	gB
		±0.6	±1.4	±0.01	±4.15	
16:00:55	K	−8.8	52.6	0.07	51.64	C
		±7.4	±10.1	±0.01	±12.38	
16:00:55	H	−3.8	51.5	0.04	28.91	C
		±14.8	±19.4	±0.01	±13.06	
16:00:55	K	27.1	25.1	0.22	77.48	gB
		±0.6	±1.4	±0.02	±8.29	
16:00:55	H	27.1	21.2	0.10	29.75	gB
		±1.4	±2.6	±0.02	±7.00	
16:00:55	K	83.8	29.2	0.02	8.18	UD
		±2.5	±6.1	±0.01	±1.71	
16:00:55	H	64.4	7.0	0.02	1.95	gS
		±1.4	±3.7	±0.01	±1.42	
16:38:43	K	27.7	25.8	0.23	83.03	gS
		±0.3	±0.8	±0.01	±2.48	
16:38:43	H	23.8	16.5	0.12	27.73	gS
		±0.4	±1.1	±0.01	±1.82	
16:38:43	K	−12.8	7.2	0.08	8.11	C
		±0.5	±1.6	±0.01	±2.09	
16:38:43	H	−15.6	6.0	0.04	3.36	C
		±1.0	±3.8	±0.01	±2.27	
16:38:43	K	−39.1	14.2	0.03	5.97	gS
		±1.1	±2.7	±0.01	±2.29	
17:11:12	K	29.2	19.8	0.20	55.38	gB
		±0.3	±0.7	±0.01	±3.33	
17:11:12	H	27.5	15.6	0.14	30.56	gB
		±0.3	±0.7	±0.01	±2.58	
17:11:12	K	−11.9	15.2	0.08	17.00	C
		±1.9	±3.8	±0.01	±4.73	
17:11:12	H	−15.5	14.8	0.05	10.37	C
		±1.8	±4.5	±0.01	±3.75	
17:11:12	K	−37.8	13.3	0.02	3.73	gB
		±2.0	±5.0	±0.01	±2.34	
17:11:12	H	−42.2	17.0	0.01	2.39	pB
		±4.3	±11.0	±0.01	±2.84	

Table 2 (continued)

Date/Time (mid exposure)	CaII	Velocity $km\,s^{-1}$	FWHM $km\,s^{-1}$	Depth	Eq. Wdth mÅ	Classification
17:11:12	K	77.7	9.1	0.02	2.54	gB
		±1.8	±4.3	±0.01	±1.74	
17:11:12	K	105.7	5.7	0.02	1.59	gB
		±1.7	±2.9	±0.01	±1.13	
17:11:12	H	108.3	7.9	0.02	2.22	pS
		±2.1	±5.3	±0.01	±1.85	
17:44:16	K	−14.7	21.2	0.05	14.90	C
		±1.5	±3.4	±0.01	±2.40	
17:44:16	H	−19.3	13.4	0.04	7.54	C
		±0.8	±2.1	±0.01	±2.21	
17:44:16	K	27.6	19.9	0.20	55.88	gB
		±0.2	±0.6	±0.01	±1.68	
17:44:16	H	25.1	15.1	0.14	29.56	gS
		±0.2	±0.7	±0.01	±2.48	
17:44:16	K	163.0	8.7	0.02	2.43	gS
		±1.4	±3.2	±0.01	±1.50	
17:44:16	K	231.5	8.0	0.02	2.25	gS
		±1.2	±2.6	±0.01	±1.35	
18:16:56	K	−14.7	21.4	0.04	11.97	C
		±1.5	±3.4	±0.01	±1.92	
18:16:56	H	−16.9	6.8	0.03	2.85	C
		±0.8	±1.5	±0.01	±1.15	
18:16:56	K	32.0	13.8	0.17	32.96	gS
		±0.3	±0.9	±0.01	±2.84	
18:16:56	H	25.2	16.7	0.13	30.44	gS
		±0.3	±0.8	±0.01	±1.44	
18:49:32	K	28.4	19.2	0.22	59.31	gS
		±0.2	±0.6	±0.01	±1.79	
18:49:32	H	24.8	15.9	0.13	28.94	gS
		±0.3	±0.8	±0.01	±2.68	
18:49:32	K	−10.6	20.0	0.06	16.82	C
		±3.1	±5.2	±0.01	±5.22	
18:49:32	H	−16.6	7.7	0.02	2.16	C
		±1.3	±3.2	±0.01	±1.40	
19:23:51	K	−39.1	8.4	0.02	2.36	gS
		±1.3	±3.1	±0.01	±1.46	
19:23:51	H	−40.1	6.0	0.02	1.69	pS
		±1.7	±3.2	±0.01	±1.23	
19:23:51	K	−14.1	18.0	0.06	15.16	C
		±2.0	±4.4	±0.01	±4.49	
19:23:51	H	−19.6	13.2	0.02	3.71	C
		±2.4	±6.4	±0.01	±2.58	
19:23:51	K	29.0	16.9	0.22	52.16	gS
		±0.2	±0.5	±0.01	±2.88	
19:23:51	H	25.1	14.3	0.14	28.03	gS
		±0.3	±0.8	±0.01	±2.52	
1997 June 27						
06:14:09	K	−15.5	15.9	0.10	22.35	C
		±0.5	±1.3	±0.01	±1.84	
06:14:09	H	−19.3	9.4	0.05	6.60	C
		±0.4	±1.1	±0.01	±1.51	
06:14:09	K	29.7	18.1	0.30	76.17	gS
		±0.1	±0.3	±0.01	±1.26	
06:14:09	H	25.7	14.3	0.18	36.06	gS
		±0.2	±0.4	±0.01	±1.06	
06:14:09	K	73.8	8.6	0.02	2.40	gS
		±1.4	±3.3	±0.01	±1.51	
06:47:21	K	−15.1	12.4	0.09	15.65	C
		±0.5	±1.3	±0.01	±2.42	
06:47:21	H	−18.0	10.1	0.05	7.07	C
		±0.6	±1.6	±0.01	±1.79	

Table 2 (continued)

Date/Time (mid exposure)	CaII	Velocity $km\,s^{-1}$	FWHM $km\,s^{-1}$	Depth	Eq. Wdth mÅ	Classification
06:47:21	K	29.3	17.9	0.30	75.12	gS
		±0.1	±0.3	±0.01	±1.47	
06:47:21	H	27.0	14.2	0.23	45.92	gS
		±0.2	±0.4	±0.01	±2.34	
06:47:21	K	89.3	24.9	0.01	3.49	UD
		±3.9	±9.1	±0.01	±1.28	
06:47:21	K	168.1	27.1	0.02	7.60	UD
		±2.6	±6.1	±0.01	±1.71	
06:47:21	H	169.9	44.2	0.02	12.40	UD
		±3.7	±8.8	±0.01	±2.46	
07:21:06	K	−14.4	15.5	0.10	21.75	C
		±1.0	±2.2	±0.01	±3.76	
07:21:06	H	−15.7	15.7	0.05	11.03	C
		±1.8	±4.0	±0.01	±3.59	
07:21:06	K	29.0	17.4	0.31	75.49	gS
		±0.2	±0.4	±0.01	±2.97	
07:21:06	H	26.7	13.6	0.23	43.98	gS
		±0.2	±0.4	±0.01	±2.34	
07:21:06	K	84.3	21.2	0.02	5.96	UD
		±2.8	±6.6	±0.01	±1.84	
07:21:06	H	139.8	22.0	0.02	6.16	UD
		±2.6	±6.3	±0.01	±3.55	
07:21:06	H	183.0	24.7	0.02	6.93	UD
		±3.7	±8.8	±0.01	±4.25	
08:02:25	K	−15.0	14.6	0.10	19.92	C
		±0.5	±1.7	±0.01	±2.67	
08:02:25	H	−17.7	11.7	0.05	8.23	C
		±0.9	±2.3	±0.01	±2.30	
08:02:25	K	27.8	19.8	0.31	86.14	gS
		±0.4	±1.1	±0.03	±9.68	
08:02:25	H	24.4	15.6	0.23	50.30	gS
		±0.2	±0.6	±0.01	±2.92	
08:02:25	K	88.2	32.0	0.02	8.96	UD
		±3.0	±7.3	±0.01	±2.06	
08:02:25	K	159.0	49.2	0.02	13.79	UD
		±3.5	±8.8	±0.01	±2.48	
08:02:25	H	167.8	49.6	0.02	13.90	UD
		±9.8	±9.5	±0.01	±2.68	
16:00:48	K	−16.7	15.4	0.15	31.41	C
		±0.3	±0.8	±0.01	±1.55	
16:00:48	H	−21.5	13.6	0.07	14.41	C
		±0.4	±1.0	±0.01	±1.11	
16:00:48	K	29.5	17.0	0.18	42.92	gS
		±0.2	±0.5	±0.01	±1.23	
16:00:48	H	24.5	12.9	0.10	18.86	gS
		±0.3	±0.7	±0.01	±1.84	
16:00:48	K	88.3	39.5	0.03	14.62	UD
		±2.5	±5.2	±0.01	±1.81	
16:43:54	K	−17.1	15.7	0.14	30.74	C
		±0.3	±0.7	±0.01	±1.45	
16:43:54	H	−21.6	14.0	0.07	13.73	C
		±0.4	±1.0	±0.01	±1.01	
16:43:54	K	28.9	16.4	0.19	43.63	gS
		±0.2	±0.4	±0.01	±1.17	
16:43:54	H	23.8	13.0	0.11	20.06	gS
		±0.3	±0.7	±0.01	±1.14	
16:43:54	K	91.2	42.3	0.03	17.81	UD
		±1.7	±4.1	±0.01	±1.71	
16:43:54	K	169.8	32.4	0.02	9.10	UD
		±2.3	±5.6	±0.01	±1.56	

Table 2 (continued)

Date/Time (mid exposure)	CaII	Velocity $km\,s^{-1}$	FWHM $km\,s^{-1}$	Depth	Eq. Wdth mÅ	Classification
16:43:54	H	160.9	41.1	0.01	5.76	UD
		±3.8	±9.4	±0.01	±1.32	
17:17:03	K	−16.3	15.1	0.15	31.82	C
		±0.3	±0.8	±0.01	±1.66	
17:17:03	H	−21.3	13.2	0.08	14.85	C
		±0.4	±1.0	±0.01	±1.17	
17:17:03	K	30.1	17.7	0.17	42.14	gS
		±0.2	±0.6	±0.01	±1.31	
17:17:03	H	25.2	12.7	0.10	17.81	gS
		±0.3	±0.8	±0.01	±2.10	
17:17:03	K	86.2	36.5	0.02	10.23	UD
		±2.6	±6.6	±0.01	±1.84	
17:50:34	K	−16.1	16.0	0.15	33.58	C
		±0.3	±0.9	±0.01	±1.81	
17:50:34	H	−20.0	15.3	0.07	15.02	C
		±0.5	±1.4	±0.01	±1.32	
17:50:34	K	30.0	14.1	0.16	31.52	gS
		±0.2	±0.5	±0.01	±1.10	
17:50:34	H	26.2	11.3	0.10	15.79	gS
		±0.3	±0.7	±0.01	±1.85	
17:50:34	K	75.5	18.4	0.02	5.16	gS
		±1.9	±4.4	±0.01	±1.24	
17:50:34	H	143.5	18.4	0.01	2.58	gS
		±4.4	±10.6	±0.01	±2.97	
17:50:34	H	112.3	8.4	0.03	3.51	gS
		±1.7	±3.9	±0.01	±2.01	
17:50:34	H	195.1	35.2	0.02	9.88	UD
		±6.1	±14.6	±0.01	±6.41	
17:50:34	K	169.0	25.8	0.01	3.61	UD
		±7.1	±16.9	±0.01	±4.32	
18:23:28	K	−16.3	14.8	0.16	33.18	C
		±0.3	±0.7	±0.01	±1.50	
18:23:28	H	−20.5	15.9	0.08	17.82	C
		±0.5	±1.2	±0.01	±1.38	
18:23:28	K	29.7	14.5	0.17	34.51	gS
		±0.2	±0.4	±0.01	±1.05	
18:23:28	H	24.4	10.2	0.10	14.34	gS
		±0.3	±0.7	±0.01	±1.71	
18:56:44	K	−15.3	16.8	0.16	37.78	C
		±0.3	±0.7	±0.01	±1.50	
18:56:44	H	−19.9	14.4	0.08	16.14	C
		±0.3	±0.8	±0.01	±0.94	
18:56:44	K	30.1	13.5	0.15	28.41	gS
		±0.2	±0.4	±0.01	±0.76	
18:56:44	H	25.8	13.9	0.10	19.43	gS
		±0.4	±1.1	±0.01	±2.51	
18:56:44	K	90.7	30.7	0.02	8.62	UD
		±1.6	±3.7	±0.01	±1.03	
19:28:29	K	−14.2	18.1	0.15	37.98	C
		±0.6	±1.2	±0.01	±2.50	
19:28:29	H	−18.9	15.7	0.07	15.40	C
		±0.6	±1.5	±0.01	±1.46	
19:28:29	K	30.2	14.2	0.14	27.85	gS
		±0.2	±0.6	±0.01	±1.08	
19:28:29	H	26.2	11.3	0.08	12.71	gS
		±0.3	±0.8	±0.01	±1.83	
19:28:29	K	96.4	46.8	0.02	13.13	UD
		±2.8	±6.5	±0.01	±1.83	
19:28:29	H	111.0	18.4	0.02	5.17	UD
		±1.8	±4.3	±0.01	±1.20	

Table 2 (continued)

Date/Time (mid exposure)	CaII	Velocity $km\,s^{-1}$	FWHM $km\,s^{-1}$	Depth	Eq. Wdth mÅ	Classification
1997 June 28						
06:05:01	K	−8.5	20.2	0.32	90.45	C
		±0.8	±1.0	±0.01	±5.49	
06:05:01	H	−14.1	14.5	0.20	40.57	C
		±0.4	±0.7	±0.01	±1.99	
06:05:01	K	29.8	14.0	0.15	29.42	gS
		±0.2	±0.4	±0.01	±0.80	
06:05:01	H	26.8	11.4	0.09	14.36	gS
		±0.2	±0.6	±0.01	±0.69	
06:05:01	K	76.7	14.3	0.02	4.02	gB
		±1.5	±4.0	±0.07	±14.10	
06:05:01	H	73.5	6.9	0.01	0.97	gB
		±1.8	±4.3	±0.01	±0.60	
06:05:01	K	105.0	35.5	0.06	29.90	gB
		±1.4	±4.7	±0.01	±6.37	
06:05:01	H	104.5	26.2	0.03	11.03	gB
		±1.2	±4.6	±0.01	±4.15	
06:05:01	K	148.0	59.7	0.02	16.73	UD
		±12.4	±19.2	±0.01	±5.38	
06:05:01	H	141.2	63.5	0.03	26.70	UD
		±6.7	±11.8	±0.01	±4.97	
06:37:53	K	−9.4	14.9	0.31	64.89	C
		±0.7	±1.0	±0.01	±4.71	
06:37:53	H	−14.4	13.9	0.22	42.87	C
		±0.3	±0.6	±0.01	±1.94	
06:37:53	K	30.7	14.8	0.14	28.97	gS
		±0.2	±0.4	±0.01	±0.86	
06:37:53	H	26.8	11.2	0.09	14.18	gS
		±0.2	±0.6	±0.01	±0.72	
06:37:53	K	72.3	11.6	0.02	3.26	gB
		±1.1	±3.2	±0.01	±0.91	
06:37:53	H	71.8	8.5	0.03	3.58	gB
		±0.7	±1.9	±0.01	±0.79	
06:37:53	K	108.2	50.3	0.09	63.48	gB
		±1.0	±3.3	±0.01	±4.21	
06:37:53	H	117.6	54.7	0.05	38.34	pB
		±1.1	±3.2	±0.01	±2.26	
06:37:53	K	167.0	45.5	0.02	12.77	gB
		±4.3	±8.6	±0.01	±2.42	
06:37:53	H	176.4	22.1	0.02	6.19	UD
		±1.8	±4.2	±0.01	±1.19	
07:10:54	K	−2.4	22.1	0.42	130.19	C
		±0.5	±0.6	±0.02	±7.02	
07:10:54	H	−14.7	13.2	0.21	38.83	C
		±0.3	±0.7	±0.01	±2.09	
07:10:54	K	31.1	14.4	0.14	28.24	gS
		±0.3	±0.7	±0.01	±1.32	
07:10:54	H	25.7	8.5	0.07	8.32	gS
		±0.3	±0.8	±0.01	±1.40	
07:10:54	K	79.1	24.0	0.03	10.09	gB
		±3.6	±5.5	±0.01	±4.07	
07:10:54	H	69.3	6.6	0.02	1.84	pS
		±0.9	±2.2	±0.01	±1.10	
07:10:54	K	109.2	32.6	0.06	27.44	gB
		±2.8	±10.2	±0.03	±16.20	
07:10:54	H	103.6	26.8	0.04	15.03	gB
		±3.8	±5.4	±0.01	±4.82	
07:10:54	K	142.3	51.1	0.04	28.65	gB
		±13.7	±19.4	±0.01	±13.02	
07:10:54	H	132.4	35.8	0.04	20.08	gB
		±5.8	±9.4	±0.01	±7.30	

Table 2 (continued)

Date/Time (mid exposure)	CaII	Velocity $km\,s^{-1}$	FWHM $km\,s^{-1}$	Depth	Eq. Wdth mÅ	Classification
07:10:54	K	185.5	7.8	0.02	2.18	gB
		±1.5	±3.8	±0.01	±1.53	
07:10:54	H	175.4	11.8	0.03	4.95	gS
		±1.1	±2.7	±0.01	±1.13	
07:43:59	K	−2.2	24.4	0.39	133.25	C
		±0.6	±0.7	±0.02	±7.91	
07:43:59	H	−8.6	22.3	0.23	71.84	C
		±1.7	±1.9	±0.02	±8.84	
07:43:59	K	30.9	14.7	0.13	26.74	gB
		±0.4	±1.0	±0.01	±2.75	
07:43:59	H	27.8	8.8	0.07	8.64	gS
		±0.4	±1.0	±0.01	±1.58	
07:43:59	K	78.5	23.5	0.05	16.50	gB
		±2.9	±4.7	±0.01	±4.68	
07:43:59	H	80.2	11.0	0.01	1.55	gB
		±3.1	±7.5	±0.01	±1.87	
07:43:59	K	110.4	34.9	0.07	34.21	gB
		±3.7	±12.1	±0.02	±15.39	
07:43:59	H	127.1	43.1	0.05	30.20	UD
		±1.4	±3.4	±0.01	±2.40	
07:43:59	K	146.9	48.7	0.05	34.16	gB
		±11.8	±15.4	±0.01	±12.79	
08:21:41	K	−4.8	25.5	0.35	125.13	C
		±1.6	±1.8	±0.03	±13.77	
08:21:41	H	−9.5	22.5	0.26	81.98	C
		±2.3	±2.9	±0.02	±12.34	
08:21:41	K	30.1	18.4	0.16	41.23	gB
		±0.8	±1.7	±0.01	±4.53	
08:21:41	H	25.7	13.0	0.09	16.44	pB
		±0.6	±1.5	±0.01	±2.62	
08:21:41	K	72.8	6.6	0.03	2.75	pB
		±1.2	±2.9	±0.01	±1.54	
08:21:41	K	104.3	58.7	0.07	57.59	UD
		±1.9	±5.3	±0.01	±5.22	
08:21:41	H	110.1	36.4	0.03	15.31	UD
		±4.6	±11.5	±0.01	±4.83	
08:21:41	K	161.6	25.4	0.04	14.24	UD
		±2.0	±4.8	±0.01	±4.46	
16:03:48	K	−9.2	14.8	0.12	24.82	C
		±2.9	±3.8	±0.02	±7.54	
16:03:48	H	−14.9	9.5	0.11	14.71	C
		±0.4	±1.2	±0.01	±2.26	
16:03:48	K	26.8	16.1	0.17	38.35	gS
		±0.2	±0.7	±0.01	±2.75	
16:03:48	H	22.8	10.7	0.10	15.06	gS
		±0.3	±0.8	±0.01	±1.90	
16:03:48	K	141.6	97.0	0.03	40.79	UD
		±9.0	±16.3	±0.01	±6.85	
16:03:48	H	185.3	73.2	0.03	30.77	UD
		±4.9	±10.8	±0.01	±4.55	
16:03:48	K	89.1	33.1	0.01	4.64	UD
		±4.0	±15.7	±0.01	±5.14	
16:03:48	H	107.1	24.6	0.02	6.90	UD
		±3.0	±9.3	±0.01	±4.32	
16:41:30	K	−9.3	15.2	0.12	25.59	C
		±2.5	±3.3	±0.02	±6.96	
16:41:30	H	−14.5	9.5	0.09	11.95	C
		±0.6	±1.4	±0.01	±2.18	
16:41:30	K	26.0	17.7	0.17	42.11	gS
		±0.3	±0.7	±0.01	±1.76	

Table 2 (continued)

Date/Time (mid exposure)	CaII	Velocity $km\,s^{-1}$	FWHM $km\,s^{-1}$	Depth	Eq. Wdth mÅ	Classification
16:41:30	H	22.1	12.7	0.09	16.04	gS
		±0.4	±1.1	±0.01	±2.30	
16:41:30	K	66.6	11.9	0.02	3.34	gS
		±1.9	±5.0	±0.01	±2.18	
16:41:30	K	129.9	131.3	0.02	36.81	UD
		±6.3	±15.3	±0.01	±4.29	
16:41:30	H	151.2	74.4	0.02	20.86	UD
		±3.1	±7.5	±0.01	±2.11	
17:14:44	K	−0.8	24.6	0.26	89.85	C
		±1.4	±1.4	±0.03	±11.60	
17:14:44	H	−1.5	24.2	0.16	54.31	C
		±2.0	±2.2	±0.03	±11.32	
17:14:44	K	27.5	16.3	0.16	36.61	gB
		±0.7	±1.3	±0.01	±3.67	
17:14:44	H	24.1	11.4	0.07	11.24	gB
		±1.1	±2.0	±0.01	±2.54	
17:14:44	K	75.9	39.0	0.04	21.88	UD
		±1.8	±5.8	±0.01	±6.36	
17:14:44	H	105.9	27.1	0.02	7.60	gB
		±2.1	±6.5	±0.01	±1.83	
17:14:44	K	140.2	97.1	0.02	27.22	UD
		±8.8	±18.4	±0.01	±5.16	
17:14:44	H	159.9	81.1	0.02	22.74	UD
		±7.3	±16.6	±0.01	±4.67	
17:47:45	K	−8.3	14.4	0.19	38.23	C
		±2.4	±2.7	±0.03	±9.41	
17:47:45	H	−13.7	15.0	0.11	23.16	C
		±1.1	±2.0	±0.01	±3.67	
17:47:45	K	26.6	16.8	0.16	37.78	gS
		±0.2	±0.7	±0.01	±1.55	
17:47:45	H	23.0	12.6	0.08	14.14	gS
		±0.4	±1.1	±0.01	±2.14	
17:47:45	K	92.1	56.4	0.04	31.62	gS
		±1.7	±4.6	±0.01	±2.60	
17:47:45	H	109.8	19.4	0.03	8.16	UD
		±1.6	±4.2	±0.01	±3.25	
17:47:45	K	159.0	36.1	0.03	15.20	UD
		±2.4	±5.7	±0.01	±2.41	
17:47:45	H	148.1	48.9	0.02	13.70	UD
		±5.7	±13.9	±0.01	±3.90	
18:20:28	K	−0.3	24.4	0.24	82.17	C
		±1.2	±1.3	±0.03	±11.16	
18:20:28	H	−12.9	15.4	0.11	23.70	C
		±1.3	±2.1	±0.01	±3.90	
18:20:28	K	27.8	15.1	0.13	27.59	gB
		±0.6	±1.3	±0.01	±3.15	
18:20:28	H	23.6	10.2	0.10	14.31	gS
		±0.3	±0.6	±0.01	±1.69	
18:20:28	K	99.1	107.0	0.05	75.02	UD
		±2.2	±5.8	±0.01	±4.03	
18:20:28	H	117.4	67.0	0.02	18.79	UD
		±2.8	±6.5	±0.01	±1.83	
18:53:10	K	−10.2	15.0	0.12	25.17	C
		±1.5	±2.2	±0.01	±4.27	
18:53:10	H	−3.7	22.5	0.19	59.80	C
		±2.0	±1.8	±0.03	±10.60	
18:53:10	K	26.8	19.0	0.13	34.61	gS
		±0.3	±0.9	±0.01	±1.60	
18:53:10	H	24.4	11.9	0.07	11.65	gS
		±0.8	±1.6	±0.01	±2.32	

Table 2 (continued)

Date/Time (mid exposure)	CaII	Velocity $km\,s^{-1}$	FWHM $km\,s^{-1}$	Depth	Eq. Wdth mÅ	Classification
18:53:10	K	94.2	110.6	0.05	77.50	UD
		±2.4	±6.0	±0.01	±4.21	
18:53:10	H	118.0	81.7	0.02	22.89	UD
		±3.1	±7.3	±0.01	±2.05	
19:25:35	K	−38.3	7.6	0.02	2.13	gS
		±0.9	±2.1	±0.01	±0.58	
19:25:35	K	−7.8	20.6	0.10	28.92	C
		±3.3	±4.1	±0.02	±8.15	
19:25:35	H	−15.3	11.3	0.08	12.64	C
		±0.5	±1.3	±0.01	±1.41	
19:25:35	K	27.7	20.9	0.13	38.00	gS
		±0.3	±1.0	±0.01	±1.77	
19:25:35	H	22.8	17.0	0.06	14.33	gS
		±0.7	±1.8	±0.01	±1.52	
19:25:35	K	86.1	110.0	0.04	61.68	UD
		±3.2	±7.4	±0.01	±4.16	
19:25:35	H	120.4	73.7	0.03	31.00	UD
		±2.2	±5.3	±0.01	±2.23	
1997 June 29						
06:16:05	K	−7.0	24.5	0.15	51.63	C
		±3.9	±4.6	±0.03	±14.15	
06:16:05	H	−8.8	15.5	0.15	32.68	C
		±6.2	±6.6	±0.07	±20.59	
06:16:05	K	28.9	27.8	0.06	23.40	gB
		±2.7	±7.6	±0.02	±10.09	
06:16:05	K	62.6	81.7	0.05	57.24	pB
		±11.9	±17.8	±0.01	±16.91	
06:16:05	H	72.9	9.3	0.02	2.62	gS
		±1.8	±4.6	±0.01	±1.84	
06:48:48	K	−7.0	20.4	0.15	42.82	C
		±3.5	±4.1	±0.03	±12.14	
06:48:48	H	−11.0	12.7	0.11	19.65	C
		±2.9	±4.1	±0.02	±7.24	
06:48:48	K	26.9	28.1	0.06	23.68	pB
		±1.4	±4.0	±0.01	±5.19	
06:48:48	H	17.0	58.2	0.02	16.32	pB
		±6.1	±14.3	±0.01	±9.09	
06:48:48	K	66.6	94.6	0.06	79.54	UD
		±5.2	±8.4	±0.01	±7.08	
07:22:34	K	−5.1	24.1	0.18	60.79	C
		±2.6	±3.0	±0.03	±12.62	
07:22:34	H	−2.3	30.0	0.18	75.76	C
		±0.7	±1.3	±0.01	±5.35	
07:22:34	K	26.3	12.2	0.07	11.94	gB
		±0.8	±1.8	±0.01	±2.46	
07:22:34	H	24.8	7.7	0.02	2.16	gB
		±1.8	±4.5	±0.01	±1.66	
07:22:34	K	53.2	94.3	0.06	79.29	UD
		±3.7	±9.4	±0.01	±7.95	
07:22:34	H	58.7	23.5	0.04	13.18	gS
		±0.9	±2.1	±0.01	±1.20	
07:22:34	H	121.8	17.5	0.02	4.90	UD
		±1.5	±3.6	±0.01	±1.00	
08:00:25	K	−5.0	14.9	0.18	37.73	C
		±9.6	±7.0	±0.30	±65.32	
08:00:25	H	−13.6	9.5	0.11	14.67	C
		±2.0	±4.1	±0.02	±6.89	
08:00:25	K	27.3	20.3	0.17	48.36	pS
		±1.4	±3.1	±0.01	±7.89	
08:00:25	H	21.6	7.9	0.11	12.15	pS
		±0.6	±1.3	±0.02	±3.01	

Table 2 (continued)

Date/Time (mid exposure)	CaII	Velocity km s^{-1}	FWHM km s^{-1}	Depth	Eq. Wdth mÅ	Classification
08:00:25	K	79.8	40.8	0.07	40.05	UD
		±2.1	±5.2	±0.01	±7.66	
08:00:25	H	71.7	28.4	0.05	19.90	UD
		±2.6	±6.1	±0.01	±5.82	
1997 July 28						
14:20:18	K	−4.2	61.8	0.10	86.62	C
		±3.6	±5.5	±0.01	±11.63	
14:20:18	H	−11.4	102.1	0.06	85.92	C
		±6.9	±6.6	±0.01	±5.54	
14:20:18	K	37.1	20.0	0.18	50.60	gS
		±0.4	±1.5	±0.01	±4.76	
14:20:18	H	28.8	24.9	0.07	24.45	pS
		±21.0	±19.9	±0.14	±52.64	
14:20:18	K	71.1	13.0	0.03	5.46	pS
		±1.6	±3.9	±0.01	±2.45	
14:54:26	K	−1.7	49.8	0.11	76.76	C
		±1.4	±2.3	±0.01	±3.52	
14:54:26	H	1.4	52.8	0.09	66.59	C
		±1.2	±2.5	±0.01	±3.09	
14:54:26	K	37.7	21.4	0.19	57.03	gS
		±0.3	±0.8	±0.01	±3.73	
14:54:26	H	33.5	14.6	0.08	16.42	gB
		±0.4	±1.2	±0.01	±2.48	
14:54:26	K	77.0	44.4	0.04	24.91	gB
		±2.0	±4.9	±0.01	±2.76	
15:27:21	K	38.5	18.8	0.16	42.26	gB
		±0.4	±1.5	±0.01	±4.21	
15:27:21	H	31.3	16.7	0.09	21.10	gB
		±0.6	±2.1	±0.01	±3.53	
15:27:21	K	8.7	56.7	0.11	87.46	C
		±2.9	±5.1	±0.01	±11.23	
15:27:21	H	0.6	63.5	0.06	53.41	C
		±3.6	±5.0	±0.01	±9.84	
15:27:21	K	89.5	47.7	0.02	13.36	UD
		±5.3	±12.3	±0.01	±3.46	
15:27:21	H	72.2	9.0	0.02	2.53	gS
		±1.5	±3.8	±0.01	±1.65	
15:27:21	K	143.9	8.0	0.02	2.25	gS
		±1.7	±3.9	±0.01	±1.57	
16:00:06	K	10.6	64.9	0.09	81.88	C
		±2.8	±3.8	±0.01	±10.26	
16:00:06	H	6.8	53.6	0.06	45.11	C
		±2.4	±4.5	±0.01	±8.41	
16:00:06	K	38.1	20.4	0.15	42.88	gB
		±0.3	±1.5	±0.01	±4.21	
16:00:06	H	31.7	14.8	0.09	18.65	gB
		±0.4	±1.5	±0.01	±2.77	
16:00:06	K	75.3	11.7	0.02	3.29	pS
		±1.6	±4.2	±0.01	±2.02	
16:00:06	H	75.5	11.5	0.01	1.61	pS
		±2.8	±6.8	±0.01	±1.87	
16:00:06	K	102.3	15.6	0.02	4.38	gS
		±2.1	±5.1	±0.01	±1.43	
16:32:46	K	36.6	19.5	0.13	35.52	gS
		±0.4	±1.2	±0.01	±3.53	
16:32:46	H	29.0	22.3	0.11	34.33	gS
		±0.4	±1.0	±0.01	±1.53	
17:12:01	K	34.4	29.0	0.21	85.26	gS
		±0.3	±0.7	±0.01	±2.06	
17:12:01	H	27.9	22.0	0.12	37.05	gS
		±0.4	±1.2	±0.01	±2.04	

Table 2 (continued)

Date/Time (mid exposure)	CaII	Velocity km s^{-1}	FWHM km s^{-1}	Depth	Eq. Wdth mÅ	Classification
17:12:01	K	−26.2	34.2	0.03	14.39	UD
		±2.6	±6.7	±0.01	±2.83	
17:54:31	K	−25.0	22.1	0.04	12.42	gS
		±1.3	±3.4	±0.01	±3.63	
17:54:31	H	−26.8	23.0	0.03	9.66	pS
		±1.7	±4.2	±0.01	±3.68	
17:54:31	K	38.1	21.2	0.25	74.31	gS
		±0.2	±0.6	±0.01	±3.54	
17:54:31	H	35.2	20.1	0.16	45.09	gS
		±0.3	±0.7	±0.01	±3.26	
17:54:31	K	65.1	8.4	0.02	2.35	gB
		±1.9	±4.5	±0.01	±1.72	
18:27:25	K	−16.3	23.9	0.05	16.72	C
		±1.7	±3.9	±0.01	±2.73	
18:27:25	H	−29.1	27.7	0.03	11.66	gS
		±1.8	±4.6	±0.01	±1.93	
18:27:25	K	39.1	23.5	0.24	78.97	gS
		±0.2	±0.5	±0.01	±1.55	
18:27:25	H	33.4	20.0	0.13	36.45	gS
		±0.3	±0.7	±0.01	±1.33	
18:27:25	K	76.0	20.5	0.03	8.63	pB
		±1.6	±3.9	±0.01	±1.65	
18:27:25	H	67.7	6.7	0.01	0.94	pB
		±1.9	±4.5	±0.01	±1.13	
18:27:25	K	204.0	31.2	0.02	8.76	UD
		±2.5	±5.9	±0.01	±1.66	
1997 July 30						
13:59:30	K	−43.1	24.2	0.02	6.79	UD
		±2.2	±5.5	±0.01	±1.54	
13:59:30	K	−15.6	8.6	0.05	6.06	C
		±0.5	±1.2	±0.01	±1.49	
13:59:30	H	−15.6	9.7	0.02	2.72	C
		±1.9	±5.3	±0.01	±2.01	
13:59:30	K	35.1	24.6	0.26	89.67	gS
		±0.2	±0.6	±0.01	±2.00	
13:59:30	H	31.1	18.4	0.19	48.88	gS
		±0.3	±0.7	±0.01	±1.86	
13:59:30	K	75.4	34.8	0.04	19.49	UD
		±1.7	±4.3	±0.01	±2.41	
13:59:30	H	56.7	23.5	0.04	13.18	UD
		±2.0	±4.5	±0.01	±2.55	
14:33:45	K	−51.2	4.6	0.03	1.95	gS
		±0.7	±8.7	±0.06	±5.34	
14:33:45	H	−39.6	15.5	0.02	4.35	gS
		±2.2	±5.2	±0.01	±2.62	
14:33:45	K	−19.6	14.2	0.04	7.95	gS
		±1.3	±3.3	±0.01	±2.71	
14:33:45	H	−17.7	7.8	0.04	4.40	C
		±1.0	±2.5	±0.01	±1.77	
14:33:45	K	35.2	24.3	0.27	91.87	gS
		±0.4	±1.2	±0.02	±8.25	
14:33:45	H	31.5	19.5	0.17	46.50	gS
		±0.4	±1.0	±0.01	±3.58	
14:33:45	K	65.6	49.5	0.04	27.73	UD
		±9.1	±15.0	±0.01	±10.91	
14:33:45	H	59.9	16.9	0.03	7.10	UD
		±1.9	±4.7	±0.01	±3.09	
15:06:35	K	−29.4	16.4	0.02	4.59	pS
		±2.1	±6.5	±0.01	±2.92	
15:06:35	H	−17.2	5.3	0.01	0.75	pS
		±2.3	±3.7	±0.01	±0.91	

Table 2 (continued)

Date/Time (mid exposure)	CaII	Velocity $km\,s^{-1}$	FWHM $km\,s^{-1}$	Depth	Eq. Wdth mÅ	Classification
15:06:35	K	34.9	24.6	0.21	72.57	gS
		±0.3	±1.0	±0.01	±4.58	
15:06:35	H	30.6	25.6	0.14	50.25	gS
		±0.4	±1.4	±0.01	±2.79	
1997 August 28						
13:15:26	K	−16.0	7.4	0.03	3.11	C
		±0.9	±2.1	±0.01	±1.37	
13:15:26	K	17.5	20.2	0.37	104.73	C
		±0.9	±1.3	±0.01	±7.31	
13:15:26	H	14.3	22.5	0.22	69.40	C
		±2.0	±3.1	±0.02	±11.53	
13:15:26	K	83.8	25.9	0.04	14.52	pS
		±1.6	±3.7	±0.01	±2.09	
13:15:26	H	69.1	19.1	0.03	8.05	pS
		±1.7	±4.9	±0.01	±3.39	
13:50:33	K	20.0	20.2	0.36	102.11	gS
		±1.3	±2.4	±0.02	±13.24	
13:50:33	H	17.5	10.5	0.25	36.66	gS
		±1.5	±2.7	±0.02	±9.84	
14:46:44	K	−19.6	19.0	0.05	13.29	gS
		±1.2	±3.1	±0.01	±3.43	
14:46:44	K	15.9	20.9	0.41	120.25	C
		±1.1	±1.4	±0.02	±10.10	
14:46:44	H	16.3	13.6	0.25	47.84	C
		±1.0	±1.5	±0.01	±5.56	
14:46:44	K	82.4	20.1	0.03	8.45	UD
		±1.5	±3.6	±0.01	±1.53	
1997 September 15						
14:16:04	K	−53.3	49.7	0.03	20.91	gB
		±2.2	±5.7	±0.01	±2.41	
14:16:04	H	−54.7	72.6	0.02	20.36	UD
		±3.8	±9.8	±0.01	±2.73	
14:16:04	K	−17.1	13.7	0.04	7.71	gB
		±0.9	±2.8	±0.01	±2.49	
14:16:04	K	29.7	19.2	0.02	5.39	pS
		±1.8	±4.5	±0.01	±1.26	
14:16:04	H	24.6	5.9	0.01	0.82	gS
		±1.6	±3.0	±0.01	±0.92	
14:16:04	K	87.6	17.5	0.03	7.35	gS
		±1.0	±2.3	±0.01	±0.98	
14:16:04	H	73.3	17.1	0.02	4.80	gS
		±1.6	±3.8	±0.01	±1.07	
14:50:23	K	−3.8	35.2	0.06	29.57	C
		±2.3	±3.3	±0.01	±5.65	
14:50:23	H	−12.1	23.9	0.04	13.43	C
		±7.3	±9.8	±0.01	±6.42	
14:50:23	K	84.4	15.4	0.03	6.49	pS
		±1.3	±3.1	±0.01	±2.52	
14:50:23	H	81.3	12.7	0.02	3.57	pS
		±1.6	±3.7	±0.01	±2.07	
15:56:08	K	−46.6	25.8	0.05	18.06	gS
		±1.3	±3.0	±0.01	±4.17	
15:56:08	H	−49.8	20.0	0.04	11.19	UD
		±1.2	±2.8	±0.01	±3.22	
15:56:08	K	44.4	15.9	0.02	4.44	UD
		±3.0	±7.2	±0.01	±2.99	
15:56:08	K	90.5	21.3	0.03	8.98	UD
		±1.9	±4.4	±0.01	±3.53	
15:56:08	H	97.0	11.8	0.02	3.31	UD
		±2.6	±6.2	±0.01	±2.39	

Table 2 (continued)

Date/Time (mid exposure)	CaII	Velocity $km\,s^{-1}$	FWHM $km\,s^{-1}$	Depth	Eq. Wdth mÅ	Classification
15:56:08	K	173.8	18.7	0.02	5.25	UD
		±3.2	±7.6	±0.01	±3.37	
15:56:08	H	179.3	17.6	0.01	2.47	UD
		±4.0	±9.5	±0.01	±2.81	
15:56:08	K	232.1	7.7	0.03	3.22	gS
		±1.4	±3.1	±0.01	±1.70	
15:56:08	H	231.5	11.2	0.02	3.13	UD
		±2.1	±5.0	±0.01	±2.10	
16:29:18	K	−51.6	87.6	0.05	61.38	UD
		±2.0	±5.1	±0.01	±3.60	
16:29:18	H	−85.6	104.7	0.03	44.02	UD
		±3.0	±7.5	±0.01	±3.17	
16:29:18	K	75.9	48.8	0.03	20.53	UD
		±2.4	±5.7	±0.01	±2.38	
1997 September 17						
11:57:52	K	−5.2	27.5	0.10	38.60	C
		±1.5	±1.9	±0.01	±4.69	
11:57:52	H	−14.4	7.1	0.06	6.01	gS
		±0.7	±2.5	±0.01	±2.29	
11:57:52	K	158.1	7.4	0.03	3.11	gS
		±0.9	±2.1	±0.01	±1.37	
11:57:52	H	162.3	50.3	0.02	14.12	UD
		±3.8	±8.9	±0.01	±2.51	
12:31:09	K	−6.0	27.6	0.10	38.65	C
		±2.7	±3.2	±0.01	±5.92	
12:31:09	H	−14.9	12.1	0.03	5.09	gS
		±2.3	±5.3	±0.01	±2.80	
12:31:09	K	28.8	10.5	0.02	2.94	gS
		±2.0	±5.0	±0.01	±2.03	
13:03:42	K	−4.0	23.4	0.10	32.83	C
		±1.6	±1.7	±0.01	±4.09	
13:03:42	H	−7.2	37.4	0.06	31.43	C
		±1.4	±3.0	±0.01	±5.81	
13:03:42	K	30.4	9.1	0.02	2.55	UD
		±0.9	±2.3	±0.01	±0.64	
13:38:36	K	−9.4	23.6	0.08	26.51	C
		±3.2	±4.4	±0.01	±5.98	
13:38:36	H	−14.3	9.9	0.04	5.57	gS
		±1.6	±3.8	±0.01	±2.53	
13:38:36	K	31.0	14.4	0.02	4.03	UD
		±1.6	±3.9	±0.01	±1.09	
14:11:02	K	−11.1	24.7	0.09	31.20	C
		±2.5	±3.9	±0.01	±6.05	
14:11:02	H	−12.1	19.9	0.08	22.36	C
		±2.9	±4.3	±0.01	±5.57	
14:11:02	K	32.0	15.7	0.05	11.03	pS
		±0.7	±1.6	±0.01	±1.13	
14:11:02	H	27.9	6.6	0.03	2.76	gS
		±0.7	±1.6	±0.01	±1.14	
14:43:33	K	−8.0	21.8	0.09	27.44	C
		±2.8	±3.5	±0.01	±5.35	
14:43:33	H	−2.9	21.9	0.22	67.58	C
		±0.5	±0.7	±0.02	±6.53	
14:43:33	K	33.7	18.5	0.04	10.37	pS
		±0.6	±1.6	±0.01	±0.90	
14:43:33	H	28.7	9.6	0.02	2.68	gS
		±1.0	±2.4	±0.01	±0.68	
15:16:04	K	−5.1	20.3	0.10	28.49	C
		±4.1	±4.1	±0.03	±10.26	
15:16:04	H	−13.7	8.5	0.09	10.74	C
		±0.6	±1.5	±0.01	±2.23	

Table 2 (continued)

Date/Time (mid exposure)	CaII	Velocity $km\,s^{-1}$	FWHM $km\,s^{-1}$	Depth	Eq. Wdth mÅ	Classification
15:16:04	K	35.1	22.8	0.04	12.77	pS
		±1.1	±2.9	±0.01	±1.63	
15:16:04	H	26.5	15.8	0.02	4.44	pS
		±1.5	±3.8	±0.01	±1.07	
1997 September 18						
12:28:38	K	42.0	13.5	0.04	7.56	gS
		±0.7	±1.6	±0.01	±0.92	
12:28:38	H	41.7	8.3	0.01	1.86	gS
		±1.4	±3.3	±0.01	±1.35	
13:01:08	K	41.0	15.4	0.04	8.66	gS
		±0.8	±1.9	±0.01	±1.04	
13:01:08	H	39.4	7.6	0.02	2.14	gS
		±1.0	±2.3	±0.01	±1.24	
13:33:38	K	43.0	11.0	0.04	6.17	gS
		±0.6	±1.4	±0.01	±0.78	
13:33:38	H	43.7	9.4	0.01	1.32	gS
		±1.8	±4.3	±0.01	±1.46	
15:19:36	K	44.0	12.2	0.04	6.86	gS
		±0.6	±1.4	±0.01	±0.78	
15:19:36	H	33.3	14.5	0.02	4.07	gS
		±1.3	±3.1	±0.01	±0.88	
15:52:16	K	46.5	14.1	0.03	5.93	gS
		±0.6	±1.5	±0.01	±0.62	
16:24:38	K	46.3	26.1	0.04	14.65	gS
		±0.5	±1.2	±0.01	±0.67	
16:57:03	K	48.0	14.1	0.03	5.93	gS
		±0.4	±1.0	±0.01	±0.42	
16:57:03	K	225.8	10.8	0.01	1.52	gS
		±1.0	±2.3	±0.01	±0.33	
16:57:03	H	233.3	8.7	0.01	1.22	gS
		±1.0	±2.4	±0.01	±0.33	
17:29:30	K	−26.9	19.8	0.02	5.54	gS
		±1.4	±3.5	±0.01	±0.98	
17:29:30	H	−32.5	58.8	0.01	8.24	UD
		±5.7	±12.9	±0.01	±1.81	
17:29:30	K	50.2	19.8	0.03	8.31	gB
		±1.0	±2.3	±0.01	±0.98	
18:01:56	K	46.6	10.5	0.02	2.95	gS
		±1.4	±3.3	±0.01	±1.74	
1997 September 19						
10:41:03	K	−29.4	35.8	0.06	30.13	gB
		±1.1	±2.4	±0.01	±2.01	
10:41:03	K	28.7	48.2	0.10	67.65	gB
		±1.3	±2.7	±0.01	±3.76	
10:41:03	H	24.8	7.4	0.03	3.12	gB
		±0.8	±2.1	±0.01	±1.35	
10:41:03	K	251.1	11.7	0.02	3.27	gS
		±1.0	±2.4	±0.01	±0.68	
10:41:03	H	253.9	6.8	0.04	3.83	gS
		±0.6	±1.4	±0.01	±1.25	
11:13:46	K	−5.6	96.4	0.07	94.63	C
		±2.7	±3.7	±0.01	±3.62	
11:13:46	H	−25.8	23.8	0.03	10.01	gS
		±1.3	±3.4	±0.01	±1.44	
11:13:46	K	33.4	31.4	0.07	30.78	pB
		±0.8	±2.6	±0.01	±5.09	
11:13:46	H	21.0	21.1	0.05	14.81	gB
		±1.7	±3.7	±0.01	±2.57	
11:59:18	K	−32.2	48.8	0.06	410.42	gB
		±1.7	±3.7	±0.01	±30.79	

Table 2 (continued)

Date/Time (mid exposure)	CaII	Velocity $km\,s^{-1}$	FWHM $km\,s^{-1}$	Depth	Eq. Wdth mÅ	Classification
11:59:18	H	−39.1	25.2	0.02	7.07	UD
		±2.8	±6.5	±0.01	±1.81	
11:59:18	K	27.4	44.5	0.12	74.83	pB
		±1.2	±2.3	±0.01	±3.80	
11:59:18	H	16.8	52.8	0.06	44.45	C
		±2.0	±3.4	±0.01	±2.89	
12:31:57	K	−16.5	82.8	0.06	69.68	C
		±5.5	±8.2	±0.01	±6.91	
12:31:57	H	−29.3	19.6	0.03	8.26	gS
		±1.4	±3.3	±0.01	±1.37	
12:31:57	K	32.5	38.9	0.09	49.03	pB
		±0.9	±3.1	±0.01	±6.68	
12:31:57	H	20.9	43.9	0.05	30.77	UD
		±2.8	±4.9	±0.01	±3.46	
13:23:26	K	−20.2	78.5	0.06	66.03	C
		±3.6	±6.3	±0.01	±5.29	
13:23:26	H	−33.8	31.2	0.03	13.14	gS
		±1.3	±3.2	±0.01	±1.32	
13:23:26	K	36.6	34.0	0.09	42.93	pB
		±0.8	±2.0	±0.01	±5.38	
13:23:26	H	24.7	38.9	0.05	27.29	UD
		±2.0	±4.1	±0.01	±2.89	
13:56:22	K	−21.2	85.1	0.06	71.59	C
		±3.3	±5.8	±0.01	±4.92	
13:56:22	H	−37.3	30.4	0.02	8.53	gS
		±2.6	±5.4	±0.01	±1.50	
13:56:22	K	40.1	36.1	0.08	40.49	pB
		±0.8	±2.1	±0.01	±5.60	
13:56:22	H	19.2	56.8	0.05	39.82	UD
		±3.2	±5.3	±0.01	±3.73	
14:31:29	K	−19.7	89.3	0.05	62.62	C
		±4.2	±6.9	±0.01	±4.87	
14:31:29	K	35.6	34.2	0.07	33.59	pB
		±0.8	±2.7	±0.01	±5.49	
14:31:29	H	3.7	76.1	0.06	64.00	C
		±1.4	±5.4	±0.01	±11.61	
15:04:10	K	−18.5	71.6	0.06	60.24	C
		±3.4	±5.6	±0.01	±4.70	
15:04:10	H	−17.3	100.3	0.04	562.76	C
		±1.9	±3.4	±0.01	±19.18	
15:04:10	K	35.5	40.0	0.05	28.04	gB
		±1.5	±3.0	±0.01	±5.99	
15:04:10	H	24.2	10.2	0.04	5.72	gB
		±0.5	±1.2	±0.01	±0.68	
15:37:04	K	−25.7	73.8	0.06	62.12	C
		±2.2	±4.4	±0.01	±3.70	
15:37:04	H	−24.6	78.6	0.04	44.10	C
		±2.5	±4.6	±0.01	±2.56	
15:37:04	K	30.3	24.8	0.06	20.90	pB
		±0.7	±2.1	±0.01	±1.73	
15:37:04	H	24.2	11.4	0.04	6.40	gB
		±0.5	±1.5	±0.01	±0.82	
16:09:42	K	−29.1	60.7	0.06	51.04	gS
		±1.5	±3.4	±0.01	±2.86	
16:09:42	H	−25.0	122.6	0.03	51.55	UD
		±2.4	±4.5	±0.01	±1.89	
16:09:42	K	27.4	27.3	0.07	26.76	gS
		±0.8	±1.8	±0.01	±1.76	
16:09:42	H	24.5	12.9	0.03	5.42	gS
		±0.7	±1.9	±0.01	±0.80	

Table 2 (continued)

Date/Time (mid exposure)	CaII	Velocity $km\,s^{-1}$	FWHM $km\,s^{-1}$	Depth	Eq. Wdth mÅ	Classification
1997 October 16						
08:56:53	K	1.2	31.4	0.16	70.37	C
		±0.5	±1.6	±0.02	±9.54	
08:56:53	H	−3.0	18.0	0.34	85.85	C
		±1.1	±1.1	±0.07	±18.38	
08:56:53	K	93.3	50.5	0.13	92.13	gS
		±0.5	±1.3	±0.01	±2.33	
08:56:53	H	90.1	46.8	0.08	52.55	gS
		±0.9	±2.2	±0.01	±2.45	
09:29:32	K	2.6	25.9	0.26	94.45	C
		±0.3	±1.3	±0.03	±11.93	
09:29:32	H	−2.9	21.2	0.24	71.47	C
		±0.8	±1.1	±0.04	±12.46	
09:29:32	K	97.9	62.5	0.11	96.31	pS
		±0.8	±1.8	±0.01	±2.76	
09:29:32	H	97.4	57.8	0.05	40.52	pS
		±1.4	±3.4	±0.01	±2.37	
10:04:21	K	2.1	25.6	0.30	107.55	C
		±0.3	±1.0	±0.03	±11.49	
10:04:21	H	−0.9	21.1	0.25	74.06	C
		±0.5	±1.2	±0.04	±12.55	
10:04:21	H	59.8	13.2	0.02	3.72	gB
		±1.4	±3.9	±0.01	±2.16	
10:04:21	K	91.7	72.6	0.10	101.81	pS
		±0.8	±2.1	±0.01	±2.99	
10:04:21	H	99.8	70.5	0.05	49.41	pB
		±2.0	±4.5	±0.01	±3.18	
10:40:55	K	0.9	33.3	0.18	83.93	C
		±0.4	±1.3	±0.01	±5.72	
10:40:55	H	−0.5	21.6	0.28	84.83	C
		±0.4	±1.2	±0.05	±15.88	
10:40:55	K	83.7	50.1	0.10	70.30	gB
		±1.3	±3.9	±0.01	±8.94	
10:40:55	H	73.5	21.1	0.06	17.75	pB
		±0.9	±2.6	±0.01	±3.69	
10:40:55	K	138.5	93.6	0.03	39.35	UD
		±17.3	±24.9	±0.01	±10.49	
10:40:55	H	113.3	59.5	0.04	33.35	UD
		±3.4	±7.6	±0.01	±4.23	
11:13:40	K	3.7	22.8	0.35	112.08	C
		±0.3	±1.4	±0.03	±11.81	
11:13:40	H	−1.7	21.3	0.20	59.84	C
		±0.9	±1.8	±0.05	±15.74	
11:13:40	K	89.8	65.3	0.11	100.66	pS
		±0.9	±2.1	±0.01	±3.25	
11:13:40	H	97.4	72.0	0.05	50.49	UD
		±1.9	±4.4	±0.01	±3.10	
11:50:38	K	0.0	34.7	0.16	77.79	C
		±0.7	±2.0	±0.02	±10.69	
11:50:38	H	−6.7	21.8	0.13	39.77	C
		±3.2	±3.2	±0.03	±10.92	
11:50:38	K	84.4	53.0	0.14	104.03	pS
		±0.7	±1.6	±0.01	±3.24	
11:50:38	H	84.6	54.1	0.07	53.05	pS
		±1.5	±3.5	±0.01	±3.40	
1997 October 18						
09:21:40	K	−21.0	39.5	0.18	99.66	gS
		±1.0	±2.3	±0.01	±8.02	
09:21:40	H	−24.6	34.7	0.09	43.76	gS
		±1.7	±4.2	±0.01	±7.20	

Table 2 (continued)

Date/Time (mid exposure)	CaII	Velocity $km\,s^{-1}$	FWHM $km\,s^{-1}$	Depth	Eq. Wdth mÅ	Classification
09:54:22	K	−19.9	31.1	0.16	69.88	gS
		±1.0	±2.4	±0.01	±6.88	
09:54:22	H	−19.2	37.2	0.09	46.95	gS
		±2.3	±4.5	±0.01	±7.71	
10:27:20	K	−20.2	30.0	0.20	84.01	gS
		±0.7	±1.7	±0.01	±6.33	
10:27:20	H	−19.6	34.2	0.10	48.02	gS
		±1.9	±3.9	±0.01	±7.28	
11:00:00	K	−22.4	28.6	0.18	72.25	gS
		±0.6	±1.5	±0.01	±5.50	
11:00:00	H	−16.6	39.6	0.11	61.09	pS
		±1.8	±3.0	±0.01	±7.27	
11:33:10	K	−18.5	35.1	0.19	93.42	gS
		±0.9	±1.9	±0.01	±7.06	
11:33:10	H	−19.5	34.3	0.11	52.94	gS
		±1.6	±3.3	±0.01	±6.97	
12:05:51	K	−19.6	31.0	0.19	82.71	gS
		±0.7	±1.7	±0.01	±6.36	
12:05:51	H	−20.5	31.2	0.10	43.74	gS
		±1.5	±3.3	±0.01	±6.39	
12:41:14	K	−19.0	28.4	0.18	71.57	gS
		±0.8	±1.8	±0.01	±6.07	
12:41:14	H	−16.1	36.7	0.13	66.80	pS
		±1.5	±2.6	±0.01	±6.99	
13:13:46	K	−19.5	26.4	0.19	70.43	gS
		±0.5	±1.2	±0.01	±3.17	
13:13:46	H	−19.1	36.1	0.12	60.79	gS
		±1.3	±2.6	±0.01	±4.37	
13:13:46	K	191.5	43.7	0.03	18.39	gS
		±3.0	±7.1	±0.01	±2.97	
13:46:54	K	−20.4	25.0	0.20	70.02	gS
		±0.4	±1.2	±0.01	±4.80	
13:46:54	H	−16.9	37.7	0.10	52.88	pS
		±1.8	±3.1	±0.01	±6.88	
13:46:54	K	202.3	58.6	0.02	16.42	pS
		±4.1	±9.7	±0.01	±2.72	
13:46:54	H	178.9	19.5	0.02	5.48	UD
		±3.5	±8.3	±0.01	±3.60	
14:19:20	K	−20.3	22.8	0.18	57.49	gS
		±0.4	±1.1	±0.01	±4.22	
14:19:20	H	−17.7	34.0	0.11	52.36	gS
		±1.6	±3.0	±0.01	±4.61	
14:19:20	K	191.7	57.0	0.02	15.97	pS
		±3.7	±8.7	±0.01	±2.44	
14:19:20	H	175.0	39.6	0.02	11.11	pS
		±4.8	±11.4	±0.01	±3.19	
14:53:07	K	−19.4	22.2	0.18	56.00	gS
		±0.4	±1.2	±0.01	±4.29	
14:53:07	H	−16.9	29.7	0.10	41.61	gS
		±1.9	±3.6	±0.01	±6.52	
14:53:07	K	71.1	12.2	0.02	3.42	pS
		±1.9	±4.4	±0.01	±2.11	
14:53:07	K	208.7	70.7	0.02	19.82	UD
		±5.0	±11.7	±0.01	±3.28	
15:25:49	K	−20.3	22.0	0.18	55.49	gS
		±0.5	±1.2	±0.01	±4.41	
15:25:49	H	−17.0	30.2	0.09	38.13	gS
		±2.2	±4.3	±0.01	±6.91	
15:25:49	K	156.8	103.8	0.02	29.10	pS
		±6.7	±15.7	±0.01	±4.40	

Table 2 (continued)

Date/Time (mid exposure)	CaII	Velocity km s^{-1}	FWHM km s^{-1}	Depth	Eq. Wdth mÅ	Classification
1997 October 19						
10:27:58	K	−19.2	18.0	0.26	68.63	gS
		±0.2	±0.6	±0.01	±3.42	
10:27:58	H	−20.8	23.9	0.14	46.52	gS
		±0.6	±1.5	±0.01	±3.62	
11:00:54	K	−19.4	20.1	0.27	76.12	gS
		±0.2	±0.6	±0.01	±3.64	
11:00:54	H	−20.8	24.8	0.14	48.68	gS
		±0.6	±1.5	±0.01	±2.94	
11:33:38	K	−18.9	16.9	0.25	59.13	gS
		±0.2	±0.6	±0.01	±3.07	
11:33:38	H	−20.7	23.2	0.14	45.54	gS
		±0.6	±1.5	±0.01	±4.36	
12:06:00	K	−18.6	20.5	0.23	66.20	gS
		±0.3	±0.7	±0.01	±2.32	
12:06:00	H	−19.9	20.4	0.15	42.96	gS
		±0.4	±1.2	±0.01	±2.44	
12:06:00	K	163.9	85.8	0.02	24.07	pS
		±5.2	±12.3	±0.01	±3.44	
12:06:00	H	139.4	64.4	0.02	18.06	UD
		±3.7	±8.8	±0.01	±2.45	
12:38:32	K	−18.6	20.7	0.22	63.85	gS
		±0.4	±1.0	±0.01	±4.30	
12:38:32	H	−20.5	26.5	0.15	55.81	pS
		±0.8	±2.0	±0.01	±5.66	
12:38:32	K	104.7	10.8	0.04	6.07	pS
		±1.2	±2.8	±0.01	±2.17	
12:38:32	H	115.9	53.6	0.04	30.04	UD
		±2.7	±6.4	±0.01	±3.58	
13:17:22	K	−16.0	19.0	0.19	50.53	gS
		±0.8	±2.0	±0.01	±5.91	
13:17:22	H	−18.0	13.7	0.12	23.05	gS
		±0.8	±2.2	±0.01	±4.16	
13:17:22	K	122.4	54.7	0.03	23.00	pS
		±4.9	±11.5	±0.01	±9.07	
13:17:22	H	120.6	42.3	0.05	29.65	pS
		±3.0	±7.0	±0.01	±7.68	
1997 October 21						
09:46:33	K	−15.8	21.8	0.29	88.59	gS
		±0.3	±0.7	±0.01	±2.76	
09:46:33	H	−18.0	22.9	0.17	54.63	gS
		±0.5	±1.1	±0.01	±2.69	
09:46:33	K	18.7	10.2	0.23	33.05	gS
		±0.6	±1.1	±0.01	±3.83	
09:46:33	H	16.4	10.5	0.14	20.65	gS
		±1.5	±2.3	±0.01	±4.69	
09:46:33	K	62.8	26.2	0.05	18.38	gS
		±1.0	±2.3	±0.01	±1.58	
09:46:33	H	65.0	17.9	0.03	7.52	gS
		±1.3	±3.0	±0.01	±1.27	
10:20:44	K	−16.7	20.3	0.31	88.40	gS
		±0.2	±0.5	±0.01	±2.09	
10:20:44	H	−22.4	16.6	0.17	39.54	gS
		±0.6	±1.0	±0.01	±3.33	
10:20:44	K	15.9	14.8	0.30	62.25	gS
		±1.4	±1.7	±0.03	±9.35	
10:20:44	H	3.7	22.6	0.35	110.85	C
		±0.6	±1.2	±0.05	±16.88	
10:20:44	K	68.4	29.6	0.06	24.94	gS
		±0.7	±1.7	±0.01	±1.45	
10:20:44	H	68.6	26.9	0.03	11.31	gS
		±1.4	±3.3	±0.01	±1.38	

Table 2 (continued)

Date/Time (mid exposure)	CaII	Velocity $km\,s^{-1}$	FWHM $km\,s^{-1}$	Depth	Eq. Wdth mÅ	Classification
10:53:27	K	−15.7	20.5	0.31	89.27	gS
		±0.2	±0.5	±0.01	±2.35	
10:53:27	H	−19.9	20.8	0.19	55.51	gS
		±0.3	±0.7	±0.01	±1.92	
10:53:27	K	18.4	11.7	0.25	40.94	gS
		±0.6	±1.0	±0.01	±4.03	
10:53:27	H	16.4	9.7	0.14	19.08	gS
		±1.5	±2.2	±0.01	±4.58	
10:53:27	K	62.0	38.5	0.04	21.59	gS
		±1.1	±2.9	±0.01	±1.62	
10:53:27	H	72.2	28.3	0.02	7.94	pS
		±1.8	±4.2	±0.01	±1.18	
12:05:51	K	−15.7	20.4	0.32	91.61	gS
		±0.2	±0.5	±0.01	±2.29	
12:05:51	H	−20.3	17.8	0.21	52.41	gS
		±0.2	±0.5	±0.01	±1.53	
12:05:51	K	18.3	13.3	0.27	50.42	gS
		±0.6	±1.0	±0.01	±4.09	
12:05:51	H	17.1	8.4	0.18	21.20	gS
		±0.9	±1.4	±0.01	±3.82	
12:05:51	K	70.2	26.1	0.06	21.96	gS
		±0.7	±1.7	±0.01	±1.44	
12:05:51	H	71.7	30.9	0.03	13.01	pS
		±1.7	±4.0	±0.01	±1.68	
12:39:07	K	−16.0	19.0	0.33	87.81	gS
		±0.2	±0.5	±0.01	±2.27	
12:39:07	H	−20.3	20.0	0.22	61.78	gS
		±0.2	±0.6	±0.01	±1.91	
12:39:07	K	18.0	12.4	0.28	48.48	gS
		±0.7	±1.1	±0.01	±4.62	
12:39:07	H	15.1	13.2	0.15	27.72	gS
		±2.3	±2.9	±0.02	±7.08	
12:39:07	K	70.9	25.0	0.04	14.04	gS
		±1.0	±2.3	±0.01	±1.32	
12:39:07	H	68.5	21.7	0.04	12.17	gS
		±1.1	±2.5	±0.01	±1.43	
13:12:04	K	−15.1	20.2	0.33	93.36	gS
		±0.2	±0.5	±0.01	±2.22	
13:12:04	H	−21.5	16.7	0.21	49.14	gS
		±0.4	±0.8	±0.01	±2.30	
13:12:04	K	18.0	13.7	0.29	55.54	gS
		±0.6	±0.9	±0.01	±4.13	
13:12:04	H	3.9	19.2	0.54	145.51	C
		±0.5	±0.9	±0.08	±22.59	
13:12:04	K	70.4	23.5	0.06	19.78	gS
		±0.6	±1.5	±0.01	±1.28	
13:12:04	H	65.1	18.6	0.04	10.46	gS
		±0.8	±1.9	±0.01	±1.04	
13:12:04	K	170.3	16.9	0.01	2.36	pS
		±2.1	±5.0	±0.01	±0.70	
13:44:40	K	−15.5	17.6	0.33	81.47	gS
		±0.2	±0.3	±0.01	±1.62	
13:44:40	H	−19.6	21.8	0.23	70.14	gS
		±0.2	±0.5	±0.01	±1.64	
13:44:40	K	17.4	14.2	0.28	55.59	gS
		±0.7	±1.0	±0.01	±4.26	
13:44:40	H	13.2	13.3	0.21	39.07	gS
		±3.1	±3.0	±0.06	±14.27	
13:44:40	K	69.0	21.1	0.08	23.67	gS
		±0.4	±0.9	±0.01	±1.02	

Table 2 (continued)

Date/Time (mid exposure)	CaII	Velocity $km\,s^{-1}$	FWHM $km\,s^{-1}$	Depth	Eq. Wdth mÅ	Classification
13:44:40	H	70.4	28.9	0.04	16.22	gS
		±0.9	±2.2	±0.01	±1.26	
13:44:40	K	190.7	31.1	0.01	4.37	gS
		±2.8	±6.6	±0.01	±0.92	
1997 October 22						
11:28:31	K	−18.8	21.6	0.30	90.93	gB
		±0.2	±0.8	±0.01	±4.37	
11:28:31	H	−21.1	23.7	0.25	83.10	gB
		±0.6	±1.2	±0.02	±7.87	
11:28:31	K	14.3	61.4	0.23	198.12	gB
		±1.2	±1.9	±0.01	±10.51	
11:28:31	H	17.3	50.4	0.17	120.15	gB
		±3.1	±7.1	±0.01	±18.38	
11:28:31	K	72.2	22.8	0.08	25.52	gB
		±0.6	±1.5	±0.01	±1.67	
11:28:31	H	68.7	26.2	0.09	33.06	gB
		±0.9	±1.8	±0.01	±4.29	
11:28:31	K	211.7	38.7	0.02	10.84	pS
		±3.0	±7.1	±0.01	±2.00	
12:01:28	K	−18.0	20.3	0.32	91.16	gB
		±0.4	±1.0	±0.03	±9.74	
12:01:28	H	−21.6	21.4	0.25	75.04	gB
		±0.6	±1.0	±0.02	±7.02	
12:01:28	K	12.9	45.3	0.25	158.71	gB
		±2.2	±4.6	±0.01	±17.36	
12:01:28	H	15.0	45.3	0.17	107.97	gB
		±2.8	±6.4	±0.01	±16.61	
12:01:28	K	65.7	47.5	0.08	53.31	gB
		±2.6	±4.0	±0.01	±4.43	
12:01:28	H	71.3	40.9	0.05	28.69	gB
		±2.3	±4.6	±0.01	±3.25	
12:01:28	K	201.3	37.8	0.02	10.59	pS
		±2.8	±6.5	±0.01	±1.83	
12:34:54	K	−18.1	18.7	0.30	78.53	gB
		±0.3	±1.1	±0.03	±9.20	
12:34:54	H	−22.2	19.2	0.24	64.50	gB
		±0.7	±1.7	±0.04	±12.21	
12:34:54	K	10.0	43.8	0.28	171.78	C
		±2.0	±3.0	±0.02	±17.12	
12:34:54	H	7.0	42.2	0.15	88.68	C
		±4.7	±6.9	±0.02	±18.73	
12:34:54	K	68.1	54.0	0.06	45.46	gB
		±2.8	±5.3	±0.01	±4.47	
12:34:54	H	66.3	71.4	0.04	40.07	pB
		±5.8	±10.4	±0.01	±5.82	
12:34:54	K	199.5	52.5	0.01	7.35	pS
		±4.2	±9.9	±0.01	±1.39	
1997 November 20						
09:54:11	K	21.1	20.7	0.30	87.19	gS
		±0.5	±1.0	±0.01	±5.25	
09:54:11	H	19.3	13.2	0.15	27.68	gS
		±0.6	±1.4	±0.01	±3.42	
09:54:11	K	90.7	37.4	0.06	31.44	gS
		±1.4	±3.3	±0.01	±2.82	
09:54:11	H	102.3	41.9	0.03	17.61	pS
		±3.6	±8.5	±0.01	±3.57	
09:27:11	H	18.8	15.5	0.16	34.70	gS
		±0.8	±1.7	±0.01	±4.31	
09:27:11	K	19.3	23.1	0.32	103.55	gS
		±0.8	±1.3	±0.01	±6.59	

Table 2 (continued)

Date/Time (mid exposure)	CaII	Velocity kms^{-1}	FWHM kms^{-1}	Depth	Eq. Wdth mÅ	Classification
09:27:11	H	73.1	10.8	0.02	3.03	gS
		±1.8	±4.2	±0.01	±1.92	
09:27:11	K	94.6	44.0	0.05	30.81	gS
		±1.7	±4.1	±0.01	±2.86	
09:27:11	H	126.5	54.4	0.03	22.89	gB
		±3.3	±8.2	±0.01	±3.47	
09:27:11	K	179.9	73.8	0.02	20.68	pB
		±5.2	±13.6	±0.01	±3.80	
10:00:56	K	21.9	19.1	0.30	80.38	gS
		±0.4	±0.9	±0.01	±4.78	
10:00:56	H	19.0	15.7	0.17	37.51	gS
		±0.8	±1.7	±0.01	±4.53	
10:00:56	K	93.8	33.9	0.04	18.99	gS
		±2.1	±5.0	±0.01	±2.79	
10:00:56	H	91.5	28.8	0.02	8.08	pS
		±3.1	±7.7	±0.01	±4.58	
10:00:56	K	181.8	58.4	0.02	16.36	pS
		±4.5	±10.8	±0.01	±3.03	
10:34:03	K	20.7	21.3	0.30	89.42	gS
		±0.7	±1.2	±0.01	±6.04	
10:34:03	H	18.8	17.1	0.19	45.44	gS
		±0.9	±1.7	±0.01	±5.10	
10:34:03	K	73.7	9.4	0.02	2.64	gB
		±1.6	±4.0	±0.01	±1.74	
10:34:03	K	103.9	32.6	0.04	18.26	gB
		±2.0	±5.2	±0.01	±2.92	
10:34:03	H	113.6	29.0	0.03	12.18	pS
		±2.5	±6.0	±0.01	±2.52	
10:34:03	K	192.2	59.4	0.02	16.64	pS
		±4.1	±10.3	±0.01	±2.89	
11:09:22	K	21.3	20.8	0.34	99.01	gS
		±0.6	±1.1	±0.01	±6.17	
11:09:22	H	18.9	16.3	0.20	45.59	gS
		±0.9	±1.8	±0.01	±5.46	
11:09:22	K	104.4	41.9	0.03	17.63	pS
		±3.5	±8.4	±0.01	±3.53	
11:09:22	H	111.6	46.6	0.02	13.08	pS
		±4.9	±11.7	±0.01	±3.28	
11:09:22	K	189.1	55.2	0.02	15.47	pS
		±4.8	±11.8	±0.01	±3.30	
11:09:22	H	177.4	13.5	0.03	5.67	UD
		±2.0	±4.8	±0.01	±2.76	
1997 November 21						
09:29:02	K	5.1	24.7	0.32	110.64	C
		±0.4	±1.5	±0.05	±18.52	
09:29:02	H	2.4	19.3	0.20	54.03	C
		±0.8	±4.4	±0.17	±47.53	
09:29:02	K	99.0	20.0	0.01	2.80	pS
		±4.5	±10.6	±0.01	±3.18	
09:29:02	K	200.9	56.7	0.02	15.88	pS
		±6.1	±14.3	±0.01	±4.02	
10:02:36	K	6.8	21.3	0.45	134.45	C
		±0.5	±1.1	±0.07	±22.02	
10:02:36	K	100.9	31.5	0.01	4.41	pS
		±5.4	±12.6	±0.01	±4.75	
10:02:36	K	197.4	53.3	0.02	14.95	gS
		±5.3	±12.6	±0.01	±3.53	
10:35:07	K	6.4	22.4	0.40	125.73	C
		±0.4	±1.1	±0.06	±19.91	
10:35:07	K	96.1	25.1	0.03	10.57	gS
		±2.5	±5.9	±0.01	±4.31	

Table 2 (continued)

Date/Time (mid exposure)	CaII	Velocity $km\,s^{-1}$	FWHM $km\,s^{-1}$	Depth	Eq. Wdth mÅ	Classification
10:35:07	K	197.9	76.3	0.01	10.70	pS
		±8.2	±19.6	±0.01	±2.75	
11:09:05	K	7.0	23.3	0.35	114.14	C
		±0.5	±1.2	±0.05	±17.32	
11:09:05	K	95.4	24.6	0.04	13.82	gS
		±1.9	±4.4	±0.01	±4.25	
11:09:05	H	96.3	29.5	0.02	8.27	pS
		±4.2	±10.7	±0.01	±5.10	
11:09:05	K	202.6	59.2	0.02	16.61	UD
		±5.6	±13.2	±0.01	±3.69	
11:45:24	K	6.5	22.1	0.35	108.30	C
		±0.6	±1.5	±0.07	±22.88	
11:45:24	H	5.3	16.8	0.17	40.11	C
		±2.9	±4.9	±0.22	±53.21	
11:45:24	K	100.8	27.4	0.04	15.35	gS
		±1.9	±4.4	±0.01	±4.56	
11:45:24	H	109.4	21.0	0.03	8.82	gS
		±2.9	±6.9	±0.01	±4.13	
11:45:24	K	196.6	50.2	0.02	14.07	gS
		±5.6	±13.2	±0.01	±3.70	
12:18:50	K	6.3	21.5	0.38	114.76	C
		±0.5	±1.3	±0.07	±22.26	
12:18:50	K	110.4	30.9	0.03	12.98	gS
		±2.2	±5.2	±0.01	±2.20	
12:18:50	H	119.3	35.4	0.02	9.94	pS
		±3.8	±9.0	±0.01	±2.52	
12:18:50	K	193.2	58.1	0.02	16.29	pS
		±5.5	±13.4	±0.01	±3.77	
13:23:51	K	7.0	21.3	0.33	98.36	C
		±1.1	±2.6	±0.13	±40.52	
13:56:21	K	7.4	21.4	0.42	125.95	C
		±0.7	±1.5	±0.09	±28.31	
14:30:51	K	5.0	22.2	0.30	93.21	C
		±0.5	±2.0	±0.08	±26.19	
14:30:51	H	2.2	22.9	0.06	19.23	C
		±2.0	±9.6	±0.08	±26.87	
14:30:51	K	98.1	9.8	0.02	2.74	pS
		±2.5	±5.9	±0.01	±2.15	
14:30:51	K	190.2	50.5	0.02	14.15	pS
		±6.3	±14.8	±0.01	±4.14	
15:03:30	K	4.3	22.5	0.30	94.55	C
		±0.4	±2.1	±0.08	±26.69	
15:36:06	K	4.0	22.4	0.28	87.85	C
		±0.4	±2.0	±0.08	±26.30	
15:36:06	H	−0.5	24.6	0.06	20.68	C
		±2.2	±6.4	±0.04	±14.81	
15:36:06	K	85.4	21.4	0.04	12.01	gS
		±1.5	±3.7	±0.01	±3.64	
15:36:06	H	110.9	30.3	0.01	4.25	gS
		±4.9	±11.5	±0.01	±1.62	
1997 November 22						
09:27:42	K	14.6	35.1	0.22	108.14	C
		±0.7	±1.1	±0.01	±5.90	
09:27:42	H	7.2	27.9	0.14	54.72	C
		±1.1	±2.1	±0.02	±8.86	
10:01:01	K	12.8	35.2	0.24	118.37	C
		±0.7	±1.4	±0.01	±6.75	
10:01:01	H	7.4	29.2	0.14	57.33	C
		±0.9	±1.7	±0.02	±8.86	
10:01:01	K	68.4	72.4	0.05	50.79	pB
		±4.8	±13.6	±0.01	±9.54	

Table 2 (continued)

Date/Time (mid exposure)	CaII	Velocity $km\,s^{-1}$	FWHM $km\,s^{-1}$	Depth	Eq. Wdth mÅ	Classification
10:01:01	H	72.3	11.0	0.02	3.07	pB
		±1.9	±4.9	±0.01	±2.07	
10:01:01	K	180.8	79.1	0.03	33.27	UD
		±4.5	±11.4	±0.01	±4.77	
10:01:01	H	129.6	73.6	0.02	20.63	UD
		±5.4	±13.8	±0.01	±3.87	
10:38:07	K	14.2	35.7	0.22	110.24	C
		±0.8	±1.4	±0.01	±6.70	
10:38:07	H	7.0	31.7	0.14	62.16	C
		±0.9	±2.0	±0.02	±9.71	
10:38:07	K	74.8	72.0	0.06	60.57	pB
		±3.6	±10.9	±0.01	±9.13	
10:38:07	K	189.9	81.1	0.03	34.10	pS
		±5.1	±12.9	±0.01	±5.43	
11:14:50	K	10.6	32.6	0.26	118.98	C
		±0.6	±1.4	±0.01	±6.88	
11:14:50	H	5.9	27.7	0.14	54.35	C
		±1.0	±2.4	±0.03	±12.56	
11:14:50	K	79.0	97.9	0.05	68.62	UD
		±4.8	±11.2	±0.01	±7.85	
11:14:50	H	80.4	24.5	0.02	6.87	gS
		±3.1	±7.3	±0.01	±3.99	
11:48:06	K	10.0	36.6	0.21	107.70	C
		±0.5	±1.5	±0.01	±6.75	
11:48:06	H	4.9	26.4	0.15	55.58	C
		±0.7	±2.4	±0.03	±12.23	
11:48:06	K	40.8	18.2	0.06	15.32	gB
		±1.0	±2.6	±0.01	±3.06	
11:48:06	H	38.2	13.3	0.02	3.43	gB
		±1.3	±4.3	±0.01	±2.92	
11:48:06	K	92.6	56.2	0.04	31.54	gS
		±2.8	±7.3	±0.01	±3.62	
12:22:02	K	9.9	30.2	0.27	114.43	C
		±0.5	±1.2	±0.02	±9.58	
12:22:02	H	6.3	27.3	0.16	61.17	C
		±0.9	±2.2	±0.03	±12.50	
12:22:02	K	40.9	11.1	0.04	6.23	gB
		±1.0	±2.5	±0.01	±2.08	
12:22:02	H	37.8	10.4	0.02	2.91	gB
		±1.8	±4.2	±0.01	±1.88	
12:22:02	K	91.1	51.7	0.03	21.73	gS
		±2.4	±6.2	±0.01	±2.59	
12:55:23	K	19.9	19.2	0.21	56.65	gB
		±1.4	±4.2	±0.01	±12.71	
12:55:23	H	18.4	13.5	0.09	16.98	gB
		±1.6	±3.4	±0.01	±4.71	
12:55:23	K	41.2	12.6	0.03	5.32	gB
		±3.0	±6.2	±0.01	±3.15	
12:55:23	H	40.8	10.9	0.02	3.05	gB
		±2.5	±6.2	±0.01	±2.32	
12:55:23	K	97.7	83.2	0.04	46.68	UD
		±3.3	±8.6	±0.01	±4.81	
13:29:55	K	12.5	30.9	0.22	95.15	C
		±0.6	±0.9	±0.01	±5.21	
13:29:55	H	9.5	27.7	0.11	42.77	C
		±1.4	±2.1	±0.02	±8.41	
13:29:55	K	97.7	49.1	0.05	34.45	pS
		±1.5	±3.7	±0.01	±2.59	
13:29:55	H	123.7	76.9	0.02	21.55	UD
		±4.7	±11.1	±0.01	±3.11	

Table 2 (continued)

Date/Time (mid exposure)	CaII	Velocity $km\,s^{-1}$	FWHM $km\,s^{-1}$	Depth	Eq. Wdth mÅ	Classification
14:03:08	K	13.4	26.6	0.22	82.20	C
		±1.1	±1.4	±0.02	±8.57	
14:03:08	H	7.9	24.4	0.13	44.40	C
		±1.5	±2.3	±0.03	±11.08	
14:03:08	K	115.4	112.7	0.05	78.97	UD
		±3.0	±7.9	±0.01	±5.54	
14:03:08	H	116.9	81.3	0.03	34.19	UD
		±4.4	±10.4	±0.01	±4.38	